Imaging cardio-vascular infection

The work presented in this thesis has been performed at the University of Pisa, where most of the clinical work have been carried. Part of the research have been made in collaboration with, "Sapienza" University of Roma, Arcispedale S. Maria Nuova – IRCCS, Reggio Emilia and University Medical Center Groningen.

ISBN 978-90-367-6648-7 (book version)

ISBN 978-90-367-6649-4 (digital version)

Cover Page: Jean-Michel Folon

Printed-by Dedalo, Pisa - Italy

rijksuniversiteit groningen

Imaging cardio-vascular infection

Proefschrift

ter verkrijging van het doctoraat in de
Medische Wetenschappen
aan de Rijksuniversiteit Groningen
op gezag van de
Rector Magnificus, dr. E. Sterken,
in het openbaar te verdedigen op
maandag 25 november 2013
om 09:00 uur

door

Paola Anna Erba
geboren op 12 juni 1973
te Gallarate, Italië

Promotores:	Prof. dr. A. Signore Prof. dr. G. Mariani Prof. dr. R.A.J.O. Dierckx
Beoordelingscommissie:	Prof. dr. R. Sinatra Prof. dr. G. Habib Prof. dr. M. Mariani

Paranimfen: Elena Lazzeri
Adrianus Waltherus Johannes Maria Glaudemans

To my family

Index of chapters

Chapter 1

Introduction

Taken from:

Paola A. Erba. **Infective Endocarditis and Cardiovascular Implantable Electronic Device Infection,** *in: Radionuclide Imaging of Infection and Inflammation. A Pictorial Case-Based Atlas. Eds: Elena Lazzeri, Alberto Signore, Paola Anna Erba, Napoleone Prandini, Annibale Versari, Giovanni D'Errico, Giuliano Mariani. Springer 2013 (ISBN: 978-88-470-2762-6 / 978-88-470-2763-3)*

Paola A. Erba, Martina Sollini, Elena Lazzeri and Giuliano Mariani. **[^{18}F]FDG PET in Cardiac Infections**, *Seminar Nuclear Medicine 2013, Spt; 43(5):377-395*

Paola A. Erba, Gaurav Malviya, Martina Sollini, L.Kelly Anzola, Elena Lazzeri, Alberto Signore. **Current status of molecular imaging in infectious disorders**, *submitted to Current Opinions in Infections*

During the past decades, molecular imaging of infectious processes has enormously contributed to new insights in clinical practice, for diagnostic purpose as well as for prognostic loading and treatment decision making. Such strengthening relies on the ability of molecular imaging to pinpoint singular phase of disease onset besides the pure morphological anomalies, generally depicted by the majority of radiological imaging procedures. In fact, morphologic techniques (i.e. computed tomography, CT and ultrasonography, US) are extremely useful for treatment management once macroscopic changes are present. However, they may suffer from limitations in the early phase of infectious processes, when indistinctive sings of disease are manifested and when foreign bodies, implants, prosthesis are present.

Cardiac infections

Cardiac infections can occur in different tissues like the heart muscle, the pericardium or the endocardial surface of the heart. Infections can extend to prosthetic material or the electrocatether (leads) in case of the implantation of devices. Despite their relative low incidence, these infections, that are associated with high morbidity and mortality, involve a relevant burden of diagnostic workup. Moreover, the number of patients with suspected cardiac infections is progressively rising because of the increased use of prosthetic valve and cardiovascular electronic device implants. Early diagnosis is crucial for adequate patient treatment management, as early treatment improves the prognosis. Unfortunately, the clinical manifestations are often nonspecific.

Accurate diagnosis typically requires the correlation of imaging data with laboratory data. Echocardiography is always performed as a first line test, primarily to evaluate heart structures, wall thickness, wall motion, and cardiac function. Computed tomography (CT) and magnetic resonance imaging (MRI) are also being increasingly employed because of their possibility for tissue characterization.

Positron emission tomography with fluorine-18-fluorodeoxyglucose ([^{18}F]FDG PET) is a well-established imaging modality for the diagnosis and management of malignancies[1], and evidence is also increasing regarding its value for assessing infectious and inflammatory diseases[2]. This introduction summarizes published evidence on the usefulness of [^{18}F]FDG PET and radiolbelled leukocytes for the diagnosis of cardiac infections and vascular graft infections. Since the majority of such reports deal with endocarditis and cardiovascular device infections, these two conditions constitute the main

topic of this introduction. Nevertheless, the diagnostic potential of [^{18}F]FDG PET in patients with pericarditis and myocarditis is also briefly reviewed, considering the most likely future advances and new perspectives that the use of PET/MR would provide in the diagnosis of such conditions.

Infective Endocarditis

Infective endocarditis (IE) is an infection of the endocardial surface of the heart that can involve prosthetic material in case of valve replacements[3]. The incidence of IE is approximately 2-4 cases per 100,000 persons per year[4]. Although this overall value has not changed in the past 50 years, it is increasing in elderly subjects. At present, 25%-50% of the cases occur in patients older than 60 years[5]. An age-related pattern that implies several diagnostic and therapeutic challenges. Additionally, the clinical patterns of IE have changed significantly since the 1960s[6]. In particular, the increasing diffusion in the population of substance addiction (with intravenous self-administration), growing and wider applications of invasive vascular procedures and massive use of antibiotics have multiplied the cases of IE linked to intravenous drug abuse[7], prosthetic valve endocarditis[8], and nosocomial IE[9]. The underlying valvular pathology in IE has also changed from rheumatic disease (that was predominant until about 30 years ago) to calcific aortic stenosis (now accounting for 50% of the cases in elderly patients)[10]. On the other hand, mitral valve prolapse is currently the most common predisposing condition for native valve endocarditis in young patients (about 30% of the cases)[11]. Less commonly, IE arises from artero-venous fistulas used for hemodialysis[12], central venous and pulmonary artery catheters, peritoneal-venous shunts for ascites, and ventriculo-atrial shunts for hydrocephalus, or as a complication of liver, heart, and heart-lung transplants[13]. IE may present itself as an acute, rapidly progressive infection, or else as a sub-acute or chronic disease with low grade fever and non-specific symptoms which may prevent or confound initial assessment. Therefore, patients may be referred to a variety of specialists who may consider a range of alternative diagnoses.

The diagnosis of IE is essentially clinical[14] and should be suspected in all patients presenting with fever of unknown origin, particularly when fever (up to 90% of the cases) is associated with laboratory signs of infection, anemia, and microscopic haematuria, and when septic embolic manifestations are present (brain, lung or spleen, in about 30% of the cases)[15,16]. The main cardiac signs include heart murmur (up to 85% of the cases) and progressive

heart failure. Systemic signs, typically represented by spleen enlargement, glomerulonephritis, and peripheral stigmata, occur when IE remains undiagnosed for a long period. Vascular and immunological phenomena such as splinter haemorrhages and Roth spots are common. However, atypical symptoms may occur in elderly or immunocompromised patients[17].

Microbiological tests for germ characterization along with positive echocardiographic findings are necessary to establish a diagnosis according to the modified Dukes criteria[18,19] (Table 1.1). Overall sensitivity of the Duke criteria is 80%[20]. However, in several instances blood culture and/or echocardiography are inconclusive, thus leading to a high proportion of unconfirmed cases of suspected IE. Indeed, up to 24% of the patients with pathologically proven endocarditis can be misclassified as "possible" IE based on Duke criteria alone[20]. The main reasons for the relatively low diagnostic accuracy of the Duke criteria are represented by either a negative blood culture or the failure to demonstrate vegetation at echocardiography.

Negative blood cultures occur in 2.5-31% of IE patients, more commonly because of prior antibiotic administration[21,22]. Sub-acute right side endocarditis and mural endocarditis[23], slow-growing and fastidious organisms as *Coxiella burnetii*, *Brucella* spp., *Abiotrophia* spp., HACEK group endocarditis, *Listeria monocytogenes* and fungi accounts for other causes of culture-negative endocarditis. A negative blood culture results in delayed diagnosis and therefore negatively impacts on treatment outcome[22].

Both transthoracic echocardiography (TTE) and transoesophageal echocardiography (TEE) may be used for detecting vegetations, with sensitivities ranging 40-63% and 90-100%, respectively. Three echocardiographic findings are major criteria in the diagnosis of IE: vegetation, abscess, and new dehiscence of a prosthetic valve. A negative TEE has a very high negative-predictive value for IE (86-97%)[24]. However, identification of vegetations may be difficult in the presence of pre-existing severe anatomic changes, especially in the early phases when vegetations are very small. Furthermore, several conditions may mimic vegetations, as occurs in degenerative valve disease, rheumatic disorders, valvular thrombus, chordal rupture, and with small intracardiac tumors[3]. Besides representing a crucial diagnostic aid for IE, echocardiography parameters are also useful for predicting the potential embolic burden, even though CT and MRI are generally necessary for detecting septic embolism[25].

Table 1.1: modifies Duke criteria[18,19].

Major criteria:

A) Positive blood culture with typical IE microorganism, defined as one of the following:

- Typical microorganism consistent with IE from 2 separate blood cultures, as noted below:
  - Viridans-group streptococci, or
  - *S. bovis* including nutritional variant strains, or
  - HACEK group, or
  - *S. aureus*, or
  - Community-acquired enterococci, in the absence of a primary focus
- Microorganisms consistent with IE from persistently positive blood cultures defined as:
  - Two positive cultures of blood samples drawn >12 hours apart, or
  - All of 3 or a majority of 4 separate cultures of blood (with first and last sample drawn 1 hour apart)
  - *Coxiella burnetii* detected by at least one positive blood culture or antiphase I IgG antibody titer >1:800

2. Evidence of endocardial involvement

   Echocardiographic findings positive for IE (TEE recommended in patients with prosthetic valves, rated at least possible IE by clinical criteria or complicated IE [paravalvular abscess]; TTE as first test in other patients), defined as follows:
   - Oscillating intracardiac mass on valve or supporting structures, in the path of regurgitant jets, or on implanted material in the absence of an alternative anatomic explanation, or
   - Abscess, or
   - New partial dehiscence of prosthetic valve or new valvular regurgitation (worsening or changing of pre-existing murmur not sufficient)

Minor criteria:

- Predisposition, predisposing heart condition, or intravenous drug use
- Fever, temperature >38°C
- Vascular phenomena, major arterial emboli, septic pulmonary infarcts, mycotic aneurysm, intracranial hemorrhage, conjunctival hemorrhages, and Janeway lesions
- Immunologic phenomena: glomerulonephritis, Osler nodes, Roth spots, and rheumatoid factor
- Positive blood culture (that doesn't meet a major criterion) or serologic evidence of infection with organism consistent with IE but not satisfying major criterion
- Positive echocardiogram (that doesn't meet a major criterion)*

Although attempts have been made to improve the diagnostic performance of the Duke criteria by proposing several additional clinical and microbiological parameters[18], molecular imaging techniques (i.e., radionuclide imaging) could in principle be useful to integrate such traditional diagnostic criteria. Therefore, molecular imaging techniques might

fill uncertain gaps with information on the biochemical burden of the endocardial vegetations. However, during the last decades the use of radionuclide imaging for IE has been rather limited in daily clinical routine, because of the general perception of their relatively low diagnostic value. The introduction of hybrid equipment for both conventional nuclear medicine (e.g., SPECT/CT) and PET (e.g., PET/CT) has notably changed this scenario. In fact, thanks to a technology that allows the three-dimensional reconstruction of small regions of interest and precise localization of the site(s) of abnormal radiopharmaceutical accumulation, evidence is growing that SPECT and PET, performed with suitable infection imaging agents and co-registered with CT, improve the diagnosis of IE. SPECT/CT imaging relies on the use of autologous radiolabeled leukocytes that accumulate in a time-dependent fashion at the site of infection (difference between delayed images acquired at 3 hrs versus late image acquired at 20-24 hrs)[26]. PET/CT is generally performed using a single acquisition time-point (generally at 1 hour) after administration of [^{18}F]FDG, which is actively incorporated by activated leukocytes[27], monocyte-macrophages[28], and $CD4^+$ T-lymphocytes[29] present at the site of infection. Less common PET/CT applications involve the use of autologous leukocytes labeled by in-vitro incubation with [^{18}F]FDG, a more cumbersome procedure that is still in the phase of clinical validation[30].

The majority of the reports available in literature are based on the use of suboptimal radiopharmaceuticals for imaging infection (mostly [^{67}Ga]-citrate and ^{99m}Tc-labeled anti-granulocyte antibodies and just more recently [^{18}F]FDG), combined with planar and/or stand-alone SPECT acquisitions. Scintigraphy with [^{67}Ga]-citrate and ^{111}In-labeled leukocytes has been used mainly for the detection of myocardial abscess[31-34]. Scintigraphy with ^{99m}Tc-labeled anti-granulocyte monoclonal antibodies, alone or associated with echocardiography is the technique with the highest accuracy for the detection of IE (100% sensitivity, 86% specificity, 92.2% overall accuracy, 89% positive predictive value) [35,36]. However, these data have been produced before the introduction of SPECT/CT and PET/CT equipment, therefore limiting the correct evaluation of the heart region. Leukocyte scintigraphy can detect IE of native (Figure 1.1) and prosthetic valve infection origin (Figure 1.2). In the latter circumstance, both the attenuation-corrected images and the non-corrected CT images should be always inspected side by side, to minimize metal-related artefacts. It is reasonable to expect that, similarly as demonstrated for other infectious conditions[37,38], the use of suitable infection-specific agents and hybrid SPECT/CT or PET/CT equipment would

strengthen the diagnostic performance of molecular imaging of IE. In fact, SPECT/CT with ^{99m}Tc-HMPAO-WBC can accurately diagnose cardiac and additional unsuspected extra-cardiac sites of infection in up to 30% of IE patients and 23% of patients with CIED-related sepsis[39], with limitations to be considered in case of small central nervous system embolism. Similarly, the use of ^{99m}Tc-HMPAO-WBC images allows to detect perivalvular abscess with 100% positive predictive value, impacting on patients management in 29% of patients[40]. Furthermore, whole-body images followed by additional planar imaging and SPECT/CT may allow to identify distant sites of septic embolism. Figure 1.3 represent some examples of the use of radiolabelled white blood cell (WBC) scans to detect septic embolisms. Table 1.2 summarized all the studies with [^{67}Ga]-citrate and ^{111}In-labeled leukocytes and ^{99m}Tc-HMPAO-WBCs in patients with IE.

Most of the published evidence concerning the use of [^{18}F]FDG PET/CT in patients with suspected IE is represented by case reports or small series reports. The main findings of such reports are summarized in Table 1.3. In particular, [^{18}F]FDG PET/CT has been used to confirm the presence of IE involving either native valves IE (9 patients) or prosthetic valves IE (18 patients). Suspicion of IE was based on clinical signs, laboratory tests and positive blood culture/serology (n=24), while echocardiography was negative or inconclusive in 17/24 cases (6/9 native valves and 11/18 prosthetic valve). In the remaining 3 patients negative blood culture was associated with either a negative echocardiography (n=2) or with the echocardiographic finding of paravalvular leak (n=1). Of interest, after a positive PET/CT a repeat echocardiography detected vegetations in 3 patients. [^{18}F]FDG PET/CT confirmed the presence of IE in 8/9 patients with native valve infection and in 16/18 patients with prosthetic valve. In two patients with complex prosthesis of the aortic valve, the aortic root and the ascending aorta (Bentall's procedure), IE was excluded by [^{18}F]FDG PET/CT, that localized infection at the aortic portion of the graft. Out of the 27 [^{18}F]FDG PET/CT scans, one was false negative, in a patient with native valve IE sustained by *Bartonella henselae* that also exhibited a negative echocardiography.

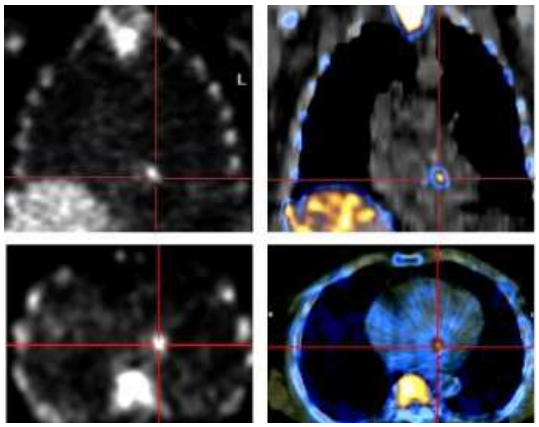

Figure 1.1 - Example of radiolabelled leukocyte scintigraphy in a patient with native valve endocarditis (coronal images at upper panel and transaxial images at lower panel, SPECT at left and superimposed SPECT/CT at right panel

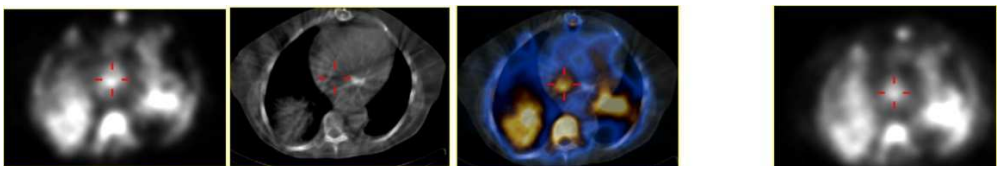

Figure 1.2 - Example of radiolabelled leukocyte scintigraphy in a patient with prosthetic mitral valve endocarditis (From left to right: transaxial SPECT, transaxial CT, SPECT/CT and transaxial non attenuated corrected SPECT images). The CT uncorrected CT image should always be inspected next to the corrected image to exclude artifacts due to metal implants.

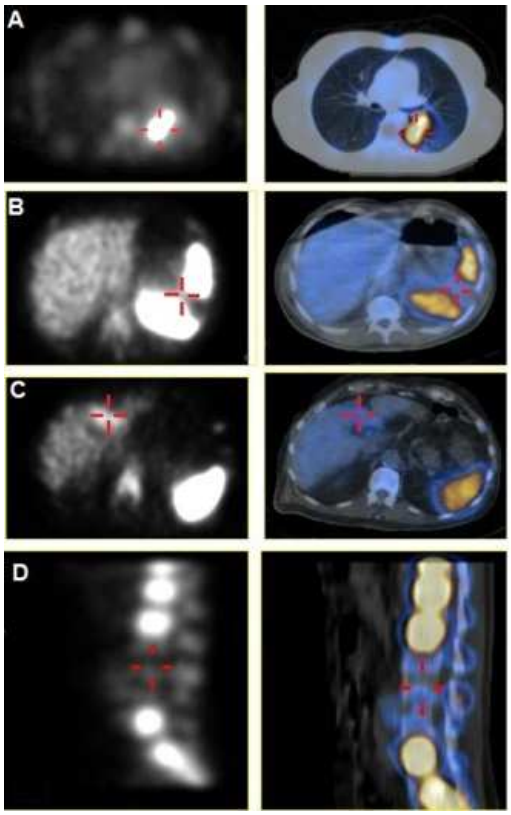

Figure 1.3 - Examples of the use of radiolabelled WBC scans to detect septic embolisms and metastatic sites of infection in patients with endocarditis. Lung embolisms (A), spleen embolisms (B), cholecystitis (C) as well as vertebral (D) embolisms were detected.. (left column SPECT images and right column SPECT/CT images). Images demonstrate the focal area of uptake at left upper lung lobe (A, and at cholecystis (C) while for spleen and vertebral embolisms the typical finding at WBC scan is represented by a fotopenic area.

Table 1.2: Published evidence concerning the use of [^{67}Ga]-citrate, ^{99m}Tc-labelled antibodies and ^{111}In-labeled leukocytes and ^{99m}Tc-HMPAO-WBCs in IE

[^{67}Ga]-citrate							
Patients	***Clinical presentation***	***Site of IE***	***Microbiology***	***Radiopharmaceutical and acquisition***	***Scintigraphic finding***	***Echocardiography***	***Reference***
11	Unknown	unknown	Unknown	[^{67}Ga]-citrate	63% sensitivity	Unknown	Wiseman J et al. Radiology 1976[152]
33	Unknown	Mixed	Unknown	[^{67}Ga]-citrate	2/33 pts positive	80% sensitivity	Melvin ET et al. Am J Cardiol 1981[153]
80 y, M	Pirexya after knee infective injury	Mitral, native	*Staphylococcus aureus*	[^{67}Ga]-citrate, Planar, SPECT	Pericardium, mitral valve and knee	Negative	Martin P, et al. 1982 Eur J Nucl Med Mol Imaging[154]
66 y, M	Sepsis after urinary retention	Aortic	*Escherichia coli*	[^{67}Ga]-citrate, Planar, SPECT	Right side of the heart	Negative	Miller SW et al. J Nucl Med, 1987[155]
3 mths, M	Fever and thrombophlebitis post pyloric myotomy	Mitral, native	*Staphylococcus aureus*	[^{67}Ga]-citrate, Planar, SPECT	Knee, hip, hearth	Vegetation at mitral valve	Hardoff R et al. Eur J Nucle Med. 1989[156]
52 y, M	Abdominal pain, fever and diarrhea 3 weeks after insertion of ureteric stent	Aortic, biological prosthesis	*Staphylococcus aureus*	[^{67}Ga]-citrate, Planar, SPECT	Site of aortic valve	No vegetation; mitral and aortic insufficiency	O'Brian K, et al. J Nucl Med 1991[32]
62 y, F	Persisten fever in IE after extensive dental work	Aortic, native	*Enterococcus spp*	[^{67}Ga]-citrate, Planar, SPECT	Abscess aortic valve, pericarditis	Vegetation on aortic valve	Desai SP et al. J Nucl Med. 1993[157]

61 y, F	Fever and neutrophilia after AMI, aneurismectomy, positioning of Teflon patch	Ventricular patchl	*Propinibacterium acnes*	[^{67}Ga]-citrate, Planar, SPECT	Lf ventricle, patch	Negatibe (TTE, TEE)	Vandenbos F et al. J Infect 2001[158]
28 y, M	Fever	Aortic, prosthesis	*Staphylococcus* spp	[^{67}Ga]-citrate, Planar, SPECT	Site of aortic valve	Vegetation (TEE)	Pena FJ, Clin Nucl med 2002[159]
44 y, M	Fever lasting for 3 wks	Aortic, prosthesis	Unknown	[^{67}Ga]-citrate + ^{99m}Tc-SestaMibi SPECT	Periaortic valve abscess	Negative (TTE, TEE)	Salem R. et al. Clin Nucl Med 2004[33]
70 y, M	Fever, sweating, weight loss and worsening of back pain. CABG, valve prosthesis, PM	Aortic, prosthesis	*Enterococcus spp*	[^{67}Ga]-citrate, Planar, SPECT	Aortic root, spine	Perivalvular aortic root abscess (TEE)	Thomson LE, et al. ClinNucl Med 2005[34]
70 y, M	Pirexya, confusion. CABG, valve prosthesis, PM	Aortic, prosthesis	*Coagulase negative Staphylococcus*	[^{67}Ga]-citrate, Planar, SPECT and co-registration with CT	Aortic prosthesis disappearing at FU scan	Negative (TEE)	Yavari A et al. Circ Cardiovasc Imaging 2009[160]
67 y,F	Fever, chest pain after aortic valve replacement	Aortic, prosthesis	Unknown	[^{67}Ga]-citrate, Planar, SPECT and co-registration with CT	Aortic, prosthesis	No vegetation, suspicious of abscess (TEE)	McWilliams ET, et al. J Cardiovascu Comput Tomogr 2011[161]

^{99m}Tc-labelled antibodies							
54 y, F	Clinical signs of IE	Aortic and mitral prosthesis	Unknown	BW 250/130/^{111}In-oxine WBCs	Valve	No vegetation	Bair HJ, et al. Nuklearmedizin 1991[162]
38	Persistent fever, suspected IE	Prosthetic valve	Unknown	BW 250/130, SPECT 20-24 hrs	Valve (Sensitivity=78 %, Specificity=85 %)	TTE+TEE (Sensitivity=89%, Specificity=95%)	Morguet AJ, et al. Dtsch Med Wochenschr. 1995[35]
24	FUO and predisposing heart disease	Aortic, mitral (native and prosthesis)	*Streptococcus spp, Bacillus fastidiousus, Staphylococcus aureus*	LeukoScan®, planar 4 and 24 hrs, SPECT 17-26 hrs	Valve (Sensitivity=71. 5%, Specificity=94 %)	TTE (Sensitivity=40%, Specificity=76%) TEE (Sensitivity=80%, Specificity=79%)	Gratz S, et al. J Cardiol. 2000[36].
^{111}In-oxine/99mTc-HMPAO WBCs							
52 y, F	Elevetaed WBCs post mitral replacement+ tricuspid valvoplasty	Mitral prosthesis	*Staphylococcus aureus*	^{111}In-oxine WBCs + ^{99m}Tc-colloids	Spleen abscesses	Unknown	O'Doherty et al. Eur J Nucl Med 1985[163]

	Mitral calcification	Mitral, native		^{111}In-oxine WBCs	Valve	Positive	Oated E et al. Clin Nucl Med 1988[164]
59 y, F	unknown	Mitral	*Staphylococcus aureus*	^{111}In-oxine WBCs	Valve	Unknown	Cerqueira MD, J Nucl Med 1989[31]
30	unknown	Unknown	Unknown	^{111}In-oxine/^{99m}Tc-HMPAO WBCs	Sensitivity=67% , specificity=95%	Unknown	Borst U, et al. Z Kardiol. 1992[165]
72 y, M	Septicaemia, suspected recurrent IE; previous IMA and PM infection	EC	*Staphylococcus aureus*	^{99m}Tc-HMPAO WBCs, planar and SPECT 3 hrs	Right atrium , PM pocket	Vegetation in right atrium at EC	Ramackers JM, et al. Eur J Nucl Med. 1995[166]
56 y, M	unknown	Unknown	*Staphylococcus aureus*	^{99m}Tc-HMPAO WBCs, planar and SPECT 3/24 hrs	Myocardial abscess, spleen infartcs	Unknown	Adams BK. Clin Nucl Med 1995[167]
49 y, M	Renal failure, sepsis, dyspnea	Aortic, native	*Staphylococcus aureus*	^{111}In-oxine WBCs	Peristernal, hearth region	TTE: aortic sclerosis. Subsequent TEE: aortic perivalvular abscess	Campeau RJ, et al. Clin Nucl Med 1998[168]
6	Suspected IE	Unknown	Unknown	^{99m}Tc-HMPAO WBCs, planar and SPECT/CT 30 min,	All negative scans	6/6 positive TTE or TEE	Ellemann A, et a. Cardiovasc J S Afr 2003[169]

				4-24 hrs			
7	Fever,	Aortic native and prosthisis, mitral native	*Staphylococcus spp, Serratia, Streptococcus pneumoniae*	^{111}In-oxine WBCs	All negative scans	Vegetations (5-15mm)	McDermott BP, et al. Am J Med 2004[170]
42	Fever infectious syndrome and/or TEE indicating perivalvular infection	aortic and mitral, prosthesis	mixed	^{99m}Tc-HMPAO WBCs, planar and SPECT/CT 4-24 hrs	Valve-perivalvular, impact on pts' management in 29%	TEE semsitivity 67% for abscess detection	Hyafil F et al. Eur Heart J Cardiovascular Imaging 2013[40]

AMI=acute myocardial infarction, CABG=coronary artery bypass graft, TTE= transthoracic echography, TEE=transesophageal echography, PM=Pacemaker, IE=infectious endocarditis, FUO=fever of unknown origin

Native valve						
Patients	***Clinical presentation***	***Site of IE***	***Microbiology***	***[^{18}F]FDG PET/CT findings***	***Echocardiography***	***Reference***
n=4	Prior ischemic stroke with left hemiparesis	Aortic (1)	*Staphylococcus epidermidis*	Valve	Perivalvular mass	Yen RF et al. Acad Radiol 2004[171]
	Anemia, severe tricuspid regurgitation, dilated right ventricle	Tricuspid (1)	*Staphylococcus aureus*		Vegetation	
	Rheumatic heart disease, mitral stenosis, mitral+/- aortic regurgitation, anemia	Mitral (2)	*Escherichia coli* (1) Negative culture (1)		Thrombus	
40 y, F	FUO (6 w), severe thrombocytopenia erythematous swelling on right foot	Mitral	Negative culture	Base of left ventricle, cardiac fibrous ring near aortic root ***Spleen embolism***	Negative	Ho HH et al. Eur Heart J 2006[172]
47 y F	Fever >40°C (1 w), productive cough, pain in left side of chest, aortic stenosis, systolic murmur	Aortic	*Haemophilus infuenzae* + *Staphylococcus* spp.	Valve	No vegetation (stenosis); repeat TEE post PET/CT: pseudoaneurysm	Vind SH et al. J Nucl Cardiol 2010 [173]
64 y, M	Persistent fever, suspected IE	Aortic (bicuspid valve)	Negative culture (final diagnosis: *Bartonella henselae*)	Sigmoid diverticulosis (FN)	Negative, repeat TTE (1 m) after positive serology: vegetation	Sankatsing SU et al. J Heart Valve Dis 201 [174]
87 y, F	Fever (39.6°C)	Mitral	*Pseudomonas*	Valve	Negative	Yeh CL et al.

			aeruginosa	***Spleen embolism***	(calcification) Repeat post PET/CT: vegetation	Kaohsiung J Med Sci 2011[175]
59 y, F	Persistent MRSA sepsis following removal of Hickman catheter	Mitral	*Staphylococcus aureus*	Valve ***Lung embolisms***, ***Spleen embolism, Bone and muscle infections***	Vegetation	Gheysens O et al. Eur J Nucl Med Mol Imaging 2012 [176]

Table 1.3: Published evidence concerning the use of[18F]FDGPET/CT in patients with suspected infective endocarditis

Prosthetic valve						
Patients	***Clinical presentation***	***Site of IE***	***Microbiology***	***[^{18}F]FDG PET/CT findings***	***Echocardiography (TTE/TEE)***	***Reference***
unknown	Chronic fever post total knee replacement	Aortic biological	*Staphylococcus aureus*	Valve ***Left knee***	unknown	Belohlavek O et al. Eur J Nucl Med Mol Imaging 2005 [177]
unknown	Persistent bacteremia, mitral valve replacement	Mitral (unknown)	Positive culture (organism unknown)	Intracardiac uptake	Valvular vegetations and mitral annular abscess	Love C et al. Radiographics 2005[178]
77 y, M	FUO	Unknown	*Enterococcus* spp.	Valve ***Lung embolism***	unknown	Klingensmith WC et al. Mol Imaging Biol 2007[179]
82 y, M	Fever, malaise (10 d)	Aortic mechanical	*Streptococcus viridans*	Right lateral atrial wall and left atrial appendage/pulmonary outflow tract. ***Lumbar embolism***	No vegetation, mild aortic regurgitation, aortic leaflet thickening	Moghadam Kia S, et al. Hell J Nucl Med 2009[180]
71 y, M	Ischemic occipital stroke, FUO	Aortic biological	Oxacillin resistant *Staphylococcus epidermidis*	Valve ***Mediastinal lns***	Negative	Huyge V et al. Am J Med 2010 [181]
35 y, M	Fever 38-39°C >14 d; (tetralogy of Fallot, pulmonary atresia repaired)	Pulmonary mechanical	*Streptococcus viridans*	Artificial blood vessel site of right ventricular outflow tract	Negative	Kenzaka T et al. J Nucl Cardiol 2011 [182]

63 y, M	Dyspnea, elevated CRP and WBC.	Mitral biological	Negative culture	Valve	Inconclusive	Plank F et al. Interact Cardiovasc Thorac Surg 2012[183]
24 y, M	Fever, cough, vomiting. (Kono repair)	Pulmonary biological	*Haemophilus parainfluenzae*	Pulmonic stent	Negative	Yedidya I et al. Ann Thorac Surg 2011[184]
75 y, M	Fungal sepsis	Aortic biological	*Candida parapsilosis*	Valve	Negative	Wallner M et al. Herz 2012[185]
74 y, M	TIA	Aortic mechanical	Negative culture	Valve	Paravalvular leak	Feuchtner G et al. Eur Heart J Cardiovasc Imaging 2012[186]
64 y, M	Fever > 2 mths	Aortic mechanical	Unknown	Valve, decreased after antibiotic therapy	Negative	Klaipetch A et al. Clin Nucl Med 2012[187]
30 y, F	Asthenia, fever episodes >39°C (1 m)	Aortic mechanical	*Streptococcus sanguinis*	Valve	No vegetations, thickened area at noncoronary sinus of Valsalva	Pons J et al. Rev Esp Cardiol 2012 [188]
84 y, F	Right femur osteosynthesis, infection of total knee prosthesis	Mitral biological + PM	*Morganella morganii* + *Enterococcus fecalis*	Valve + lead	Mitral regurgitation + prolapsing cusp	Gouriet F et al. Scand J Infect Dis 2013[189]
24 y,	Fever, vomiting	Pulmonar mechanical + pumonic stent	*Staphylococcus aureus*	Pulmonic stent	Echogenic mass within the pulmonic stent	Yedidya I et al. Ann Thorac Surg 2011[184]
84 y, M*	FUO, weight loss	Aortic	Streptococcus bovis	Valve	Negative	Dumarey N et al. J

		biological				Nucl Med 2006[54]
Septic embolism detection						
n=25	IE definite according to Duke's criteria	Native unknown (15) Prosthetic unknown (10)	*Staphylococcus aureus* (4) *Streptococcus* spp. (10) *Enterococcus faecalis* (9) *Escherichia coli* (1) Negative culture (1)	12% IE 44% septic embolism of metastatic infection	25 positive, unspecified	Van Riet J et al. Eur J Nucl Med Mol Imaging 2010[52]
Prosthesis of aortic valve, aortic root and ascending aorta (Bentall's procedure)						
n=2	Fever	Aortic	*Staphylococcus* spp. *Salmonella* spp.	Aortic valve + aortic root	Inconclusive	Yen RF et al. Acad Radiol 2004[171]
61 y, F	Fever and chills (1 d)	Aortic	*Staphylococcus aureus*	Aortic arch	Unknown	Vos FJ et al. Q J Nucl Med Mol Imaging 2008[191]
47 y, F	Fever >40°C + chills (6 d)	Aortic	*Staphylococcus aureus*	Valve + base of ascending aorta/ aortic wall/graft + aorta (atherosclerotic changes, FP)	Negative	Vind SH et al. J Nucl Cardiol 2010[173]
56 y, M	Fever, chills, night sweats (3 w)	Aortic	*Cardiobacterium hominis*	Aortic graft	No vegetations, non-specific thickening of aortic root	El Hajjaji I et al. Int J Cardiol 2012[190]

FUO, fever of unknown origin; lns = lymph nodes; CRP, c-reactive protein; FN, false negative; MRSA, methicillin-resistant Staphylococcus aureus; TIA, transient ischemic attack; PM, pacemaker; FP, false positive, WBC, white blood cell; * [^{18}F]FDG-radiolabelled leukocytes

Taken altogether, these data support the use of [^{18}F]FDG PET/CT in association with echocardiography, to confirm or rule out IE in equivocal and/or difficult-to-explore situations, such as those due to artifacts caused by mechanical prosthesis or catheters. However, it should be noted that all the cases that have been reported so far investigated with [^{18}F]FDG PET/CT represent patients with a high pre-test probability of IE. Therefore, the false positive rate of [^{18}F]FDG PET/CT can be underestimated. In fact, some drawbacks in the use of [^{18}F]FDG for the diagnosis of IE should be considered when interpreting the scan, avoiding false-positive findings in PET studies. Variable focal of diffuse physiologic [^{18}F]FDG uptake is often observed in the normal myocardium of fasting nondiabetic patients (6-12 hours to overnight) with normal glucose levels[41]. Accumulation of [^{18}F]FDG is most notable in the left ventricular myocardium, which has a greater muscle mass than other cardiac chambers. Uptake in the wall of the right ventricle is typically equal to or less intense than that in the left ventricular myocardium; uptake in the wall of the right and left atria is usually not detected. Factors possibly influencing myocardial uptake of [^{18}F]FDG include blood glucose levels, and a low-carbohydrate diet. In particular, while age and fasting time do not affect [^{18}F]FDG uptake in the myocardium, blood glucose levels may have a nonlinear effect on myocardial uptake[42]. A low-carbohydrate diet[43] and a very high-fat, low-carbohydrate, protein-permitted meal followed by fasting for 3-6 hours[44] before [^{18}F]FDG injection might be adopted to decrease myocardial uptake. However, no specific protocol has yet been standardized and/or recommended to reduce the nonspecific myocardial uptake when assessing cardiac infection with [^{18}F]FDG PET/CT. Another potential confounding factor for [^{18}F]FDG PET/CT is represented by increased metabolic activity along the posterior aspect of the heart, where lipomatous hypertrophy of the interatrial septum may appear as a fat-containing mass with increased [^{18}F]FDG uptake[45]. Furthermore, a number of pathological conditions can mimic the pattern of focally increased [^{18}F]FDG uptake that is typically observed in IE, such as active thrombi[41], soft atherosclerotic plaques[46], vasculitis[47], primary cardiac tumors[48], cardiac metastasis from a non-cardiac tumor[49], post-surgical inflammation[50] and foreign body reactions (such as BioGlue, a surgical adhesive used to repair the aortic root) [51]. Indeed, high specificity for IE using [^{18}F]FDG can be achieved only by adopting accurate patient selection and inclusion criteria. On the contrary, the use of [^{18}F]FDG PET/CT in patients with lower pre-test probability will rely on the high negative predictive value of this imaging procedure. Figure 1.4 shows examples of positive [^{18}F]FDG

PET/CT scans in patients with IE. Figure1.5 shows an example of the use of [^{18}F]FDG PET/CT to exclude the presence of IE in a patient with doubtful echocardiographic finding and fever.

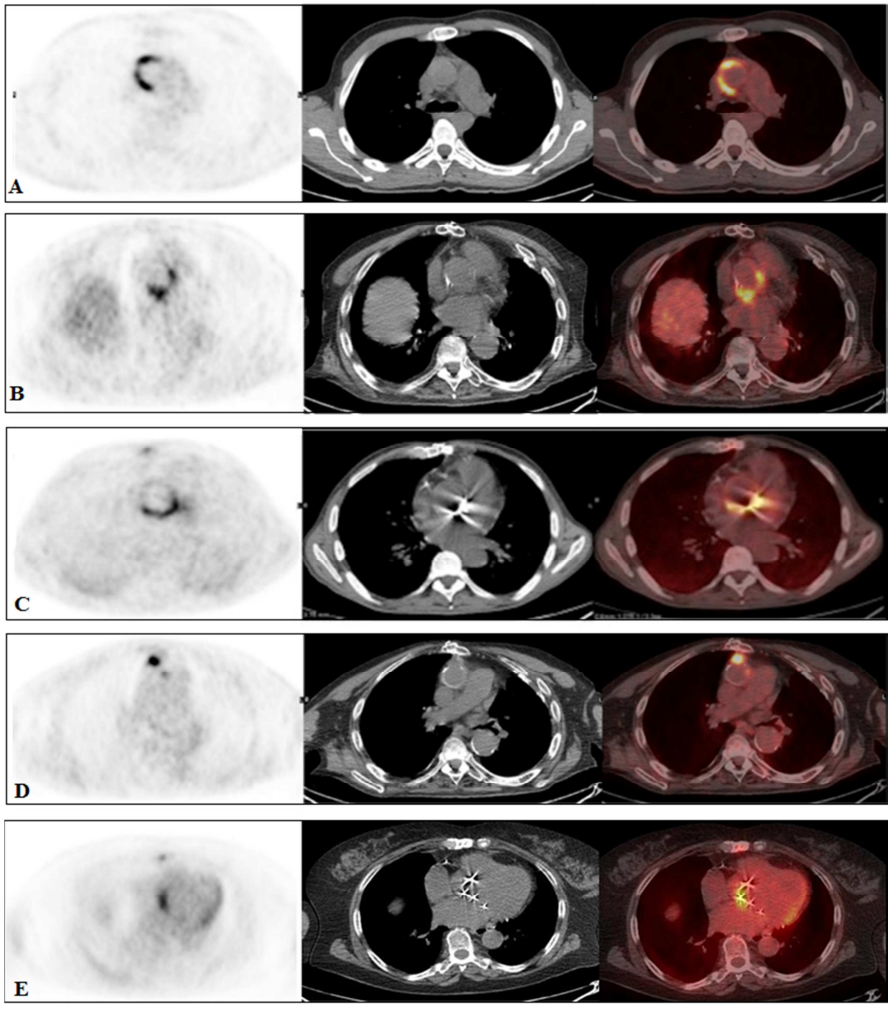

Figure 1.4: Examples of [^{18}F]FDG uptake in patients with IE. *A)* Biological aortic prosthesis with linear focal uptake in the anteromedial portion. *B)* Mechanical aortic prosthesis with predominant uptake at the posterior and medial region of the aortic valve. *C)* Mechanical aortic prosthesis with predominant uptake at the posterior region of the valve. *D)* Mechanical aortic prosthesis with perivalvular abscess. *E)* Mechanical mitral valve IE with prevalent uptake at the posterolateral region of the valve.
Left column: SPECT emission transaxial images, middle column: CT transaxial images, right column transaxial superimposed PET/CT images.

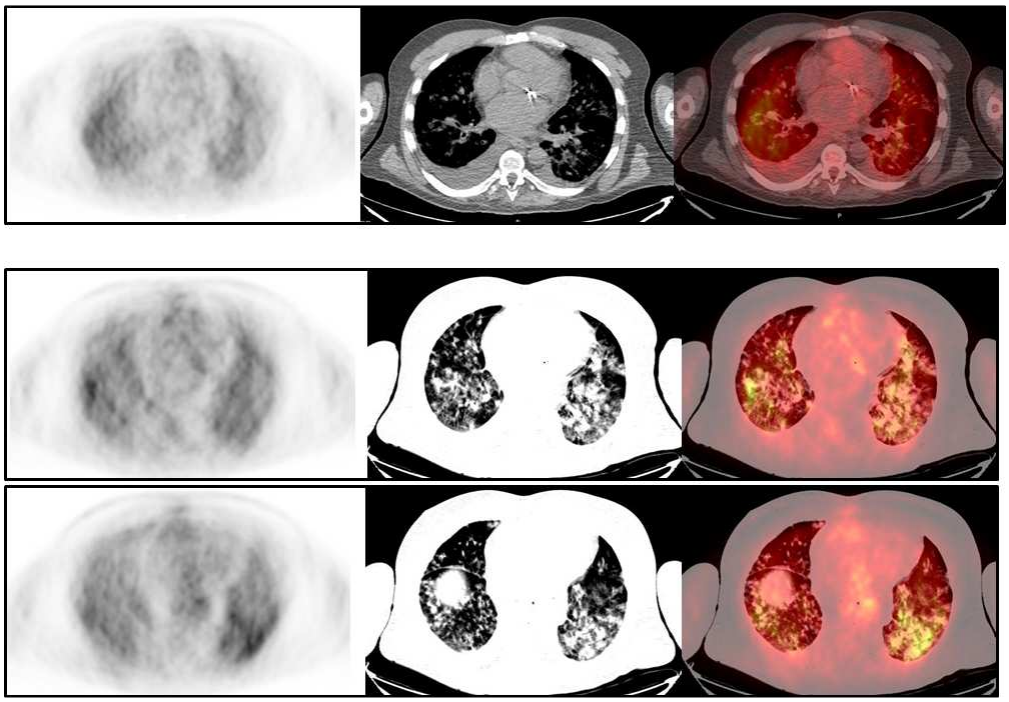

Figure 1.5: [^{18}F]FDG PET/CT excluding the presence of IE in a patient with fever and a doubtful echocardiographic positive finding. Images (left column: SPECT emission transaxial images, middle column: CT transaxial images, right column: transaxial superimposed PET/CT images) show absence of significant uptake at the region of the mitral mechanical valve. Transaxial images of the thorax at different levels (upper panel with mediastinal window, middle and lower panel using lung parenchyma window) show multiple sites of [^{18}F]FDG uptake in both lungs, appearing to show the site of infection (pneumonia by Aspergillus).

An additional advantage of [^{18}F]FDG PET/CT imaging is its ability to reveal the concomitant presence of extra-cardiac infection sites as the consequence of septic embolisms, resulting from "metastatic" infections which originate from IE. According to literature reports, such embolisms were detected in a total of 11/27 patients evaluated for suspected IE. The sites of septic embolism were mainly localized at the lungs, bones, and spleen. Similarly, in a prospective study carried out in patients with definite IE, according to the modified Duke criteria prior to surgery, [^{18}F]FDG PET/CT was able to detect at least one focus of peripheral embolization and/or metastatic infection in 11/24 patients (44%)[52]. These complications were detected even in patients without prior clinical suspicion and in patients without the typical echocardiographic findings considered as predictors of systemic embolism[53]. This unique whole-body exploring ability of PET/CT to detect multiple sites of disease with a single examination, can guide treatment management considering the optimal time window for surgical intervention. A limitation to the use of [^{18}F]FDG PET/CT is localization of septic embolisms in the brain, due to the high physiological uptake of this tracer in the brain cortex and to the fact that metastatic infections are generally smaller than 5 mm, which is the spatial resolution threshold of the current PET/CT scanner. Figure 1.6 show examples of septic embolism and metastatic infections in patients with IE detected by [^{18}F]FDG PET/CT.

Finally, an additional promising role of [^{18}F]FDG PET/CT considers patients with established IE, in whom it can be used to monitor response to antimicrobial treatment. In fact, considering the difficulties in the choice of the proper type, dose and duration of antimicrobial treatment, the possibility to distinguish patients who respond favorably to treatment from those who require intensified administration or alternative treatment options with PET/CT imaging is extremely attractive. Figure 1.7 shows an example of the use of [^{18}F]FDG PET/CT to monitor response to antimicrobial treatment in a patient with IE.

The possibility of efficient radiolabelling of autologous leukocytes with positron emitting radionuclides can be expected to change the whole scenario of PET imaging for patients with suspected IE. In this regard, intense [^{18}F]FDG-WBC uptake at the site of valve infection has been described only for one patient with IE, reported up to now[54]. Unfortunately, the physical half-life of ^{18}F is too short to encompass the whole kinetics of leukocyte migration into sites of infection, thus making the use of this procedure suboptimal for this purpose.

A new interesting radiopharmaceutical for PET imaging(^{64}Cu-DTPA-ProT) has been developed to tag prothrombin and therefore track its deposition to the fibrin-rich vegetations in *Staphylococcus aureus'* experimental IE in rats[55]. This interesting approach is certainly worthy of further investigation.

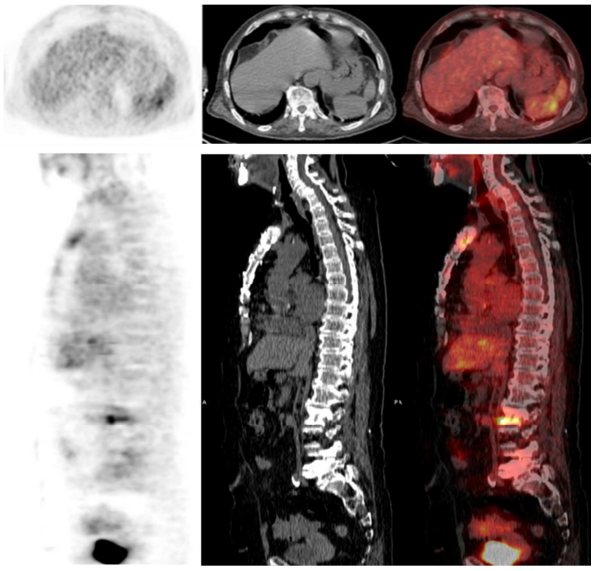

Figure 1.6: Examples of septic embolism detection using [^{18}F]FDG PET/CT. *Upper* panel: [^{18}F]FDG PET/CT uptake in the lower posterior portion of the spleen in patients with aortic IE (left column: SPECT emission, middle column: CT, right column: PET/CT) . *Lower panel*: [^{18}F]FDG PET/CT uptake in the spine, involving the inferior portion of the vertebral body of L3 and the superior portion of the vertebral body of L4 in patients with aortic IE, identifying spondylodiscitis(left column: SPECT, middle column: CT, right column: SPECT/CT).

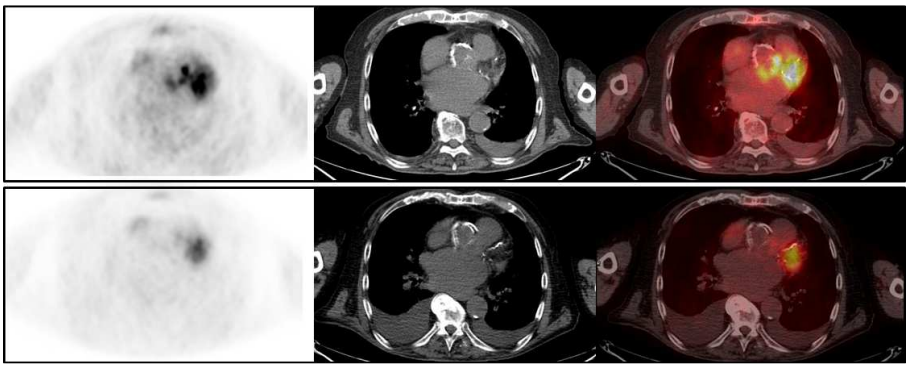

Figure 1.7: Example of the use of [^{18}F]FDG PET/CT to monitor response to antimicrobial therapy. *Upper panel*: PET/CT images in a patient with IE at the mechanical aortic prosthesis at baseline condition show intense [^{18}F]FDG uptake at the posterior part of the aortic prosthesis. Concomitant uptake at the left ventricle wall is also evident, making it difficult to interpret the images. Mild pleural effusion is evident in the CT images.
Lower panel: A PET/CT performed 4 months after initiation of antimicrobial therapy shows normalization of the [^{18}F]FDG uptake at the site of the mechanical valve. Increased pleural effusion is detected at the CT component of the scan, consistent with the worsening of the valve regurgitation as indicated by echocardiography. Therefore, prosthetic valve substitution was performed at this stage based on the PET/CT finding of significant reduction in infective burden. Left column: SPECT, middle column: CT, right column: PET/CT.

Cardiovascular implantable electronic devices infections

In the past few decades there has been an increase in the use of cardiovascular implantable electronic devices (CIED), mostly related to an increasing elderly population, both in the developed and in the developing countries. Worldwide there are approximately 3.25 million functioning pacemakers and 180,000 functioning implantable cardioverter defibrillators[56]. Infection rates for these devices range from 1% to 7%[57-60]. The majority of CIED infections are caused by either *Staphylococcus aureus* or coagulase-negative staphylococci; a variety of other bacteria and fungi are less commonly identified as causes of CIED infection[56,61,62]. CIED-associated infections cause significant morbidity and high death rate, particularly regarding endovascular infection (20%)[62]. The incremental cost for managing CIED infection has been estimated to be about $ 28,676 to $ 53,349[63,64]. Nearly half of this amount being due to intensive care procedures[65]. Furthermore, device replacement procedures that are periodically necessary for battery depletion or for upgrading, are associated with infection rates higher than those occurring after initial implantation[66,67].

The interval between CIED implant or revision and the onset of infection varies widely, from days to years. The clinical presentation of CIED

infection depends on several factors, including the site of infection (e.g., generator's pocket *versus* intravascular leads or epicardial leads), the type of microorganism, and the origin of the infection (e.g., pocket erosion, localized infection of the generator's pocket, bacteremia from a remote site). Early infections, i.e. those occurring within a few months after implantation, manifest as acute or sub-acute infections of the pulse-generator's pocket. Bacteremia may occur even without clinical signs and symptoms. Fever is the most common finding and is the only sign in approximately 33% of the patients. Although some cases of CIED infection occur without obvious inflammatory changes of the skin, the diagnosis is most often (about 70% of cases) based on findings at the generator's pocket site, including local pain, swelling, redness, drainage, and skin and soft-tissue ulceration. The first sign of infection may be erosion through the skin at the site of the generator's pocket, with external exposure of the generator or the leads, with or without local inflammatory changes. Late infections occur up to several years after implantation or reimplantation and have much more subtle manifestations. Most often the transvenous or epicardial leads are involved. In the latter circumstance, complications such as pericarditis, mediastinitis and right-sided endocarditis are often present.

The diagnostic workup of CIED infections is problematic, since patients can present with a variety of manifestations including subtle signs of systemic or local infection. Final diagnosis of CIED infection is generally based on microbiological tests (blood cultures and culture of material from exposed sites of the device) and ultrasound evaluation of the cardiac region (either TTE or TEE) and of the venous pathway of the device. The above tests constitute the basis for defining the patients' likelihood to have CIED infection according to the Duke criteria[68]. However, in case of CIED infections the Duke criteria, originally developed for the diagnosis of IE, may be inadequate. Even with the addition of clinical parameters[69,70] the possibility remains high of missing the presence and/or underestimating the extent of infection[71].

Blood cultures are recommended in all suspected cases of CIED infection, regardless of whether the patient is febrile or has other signs or symptoms of systemic infection. However, blood cultures may be negative despite CIED infection, particularly in patients with pocket-site infection and in those receiving antibiotics shortly before blood samples are drawn for culture. Moreover, positive blood cultures may be due to a source other than an infected CIED. The likelihood of CIED infection when blood cultures are positive varies according to the pathogen detected, the number and duration

of positive blood cultures, and the presence of other findings that suggest device-related infections[72-77].

TEE is recommended for patients with bacteremia, especially if the bloodstream infection is due to staphylococcal species or if the source is not identified. Also for patients with signs of systemic infection, regardless of the results of blood-culture TEE is recommended[78]. The main purpose of TEE is to identify complications such as valvular vegetations or myocardial or perivalvular abscesses. In adults, TEE is more sensitive than TTE for detecting signs of an intracardiac infection[79,80]. Vegetations on a lead are consistent with, but not diagnostic of, lead-related endocarditis. Bland (uninfected) clots on leads have been found on echocardiographic examination in 5% to 10% of patients with CIED despite the absence of infection[81,82] and these mass lesions usually cannot be distinguished from infected vegetations. A negative TEE result does not rule out the possibility of lead infection[83]. Fever and/or a positive blood culture without identification of a primary source in patients with a CIED, represent device-associated IE until proven otherwise.

Several nuclear medicine imaging techniques have been applied to evaluate patients with suspected or ascertained CIED infection. In particular [^{67}Ga]-citrate scintigraphy has been successfully employed in small series of patients with CIED infection[84,85]. The role of scintigraphy with ^{111}In-oxime-leukocytes or ^{99m}Tc-HMPAO-leukocytes has been tested in this clinical setting as well, demonstrating that this technique in some cases can define the presence of CIED infection and to evaluate its extension[86,87], also in patients with implantation of left-ventricular-assist device (LVAD)[88]. In this study, leukocyte SPECT/CT was able to identify and define the precise anatomic location and extent of a suspected infection, improving patients' treatment management[88,89]. Additionally, ^{99m}Tc-HMPAO-leukocyte SPECT/CT allows the detection of additional unsuspected extra-cardiac sites of infection in up to 23% of patients of device-related sepsis[89], although with some limitations in case of small SNC embolism. Similar results have been published in one case of lead-associated infection using SPECT/CT with ^{99m}Tc-sulesomab[90]. Figure 1.8, Figure 1.9 and Figure 1.10 represent typical patterns of radiolabelled leukocyte scintigraphy in presence of CIED infections. Table 1.4 summarized all the published evidence on the use of [^{67}Ga]-citrate scintigraphy, ^{111}In-oxime-leukocytes or ^{99m}Tc-HMPAO-leukocytes and ^{99m}Tc-sulesomab.

The use of [^{18}F]FDG PET/CT in CIED infections has been implemented to respond to specific clinical needs: i) confirming/excluding

the presence of infection in patients with equivocal echocardiographic findings or during febrile episodes without evidence of a primary source; ii) defining the extent of device involvement; iii) assisting in the decision whether to treat medically or to remove the device; iv) evaluating the response to antimicrobial therapy; v) selecting the optimal time to re-implant. Although the earliest reports on the use of [^{18}F]FDG PET/CT for diagnosing CIED infection date back to 2006, original retrospective studies were published only in 2011 (Table 1.5). Overall, a total of 159 patients have been evaluated so far, including 54 controls. Based on these data, [^{18}F]FDG PET/CT appears to provide useful information when added in the diagnostic workup of CIED infection, mostly because of its ability to confirm the presence of infection (70/78 total confirmed CIED-associated infections), to define the extent of device involvement, and to detect associated complications such as infectious endocarditis and septic embolism (occurring in more than 20% of the patients).

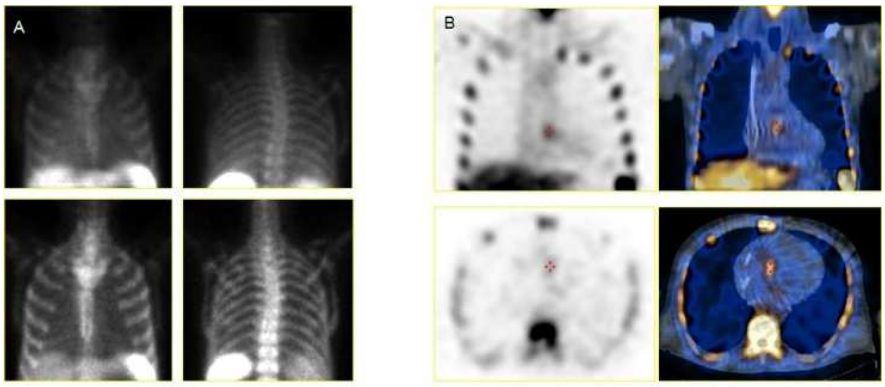

Figure 1.8 - Typical pattern of radiolabelled leukocyte scintigraphy in presence of CIED infections limited at the intracardiac portion of the lead. Planar images at both early and delayed time points seem negative (A upper panel, 30 minutes and lower panel 6 hrs.) while only using SPECT/CT (B upper panel coronal images and lower panel transaxial images, left column SPECT and right column SPECT/CT) it's possible to demonstrate and localize a focal area of increased radiopharmaceutical uptake at the distal part of the intracardiac portion of the lead, without any involvement of the other portion of the lead and the pocket.

Figure 1.9 - Typical pattern of radiolabelled leukocyte scintigraphy in presence of CIED infections. SPECT/CT (transaxial SPECT left column, CT central column and SPECT/CT right column) demonstrate and localize a focal area of increased radiopharmaceutical uptake at the intravascular portion of the lead just behind the sternum, without any involvement of the other portion of the lead. However, in this patient the pocket is also infected (see below Figure 1.10 upper panel).

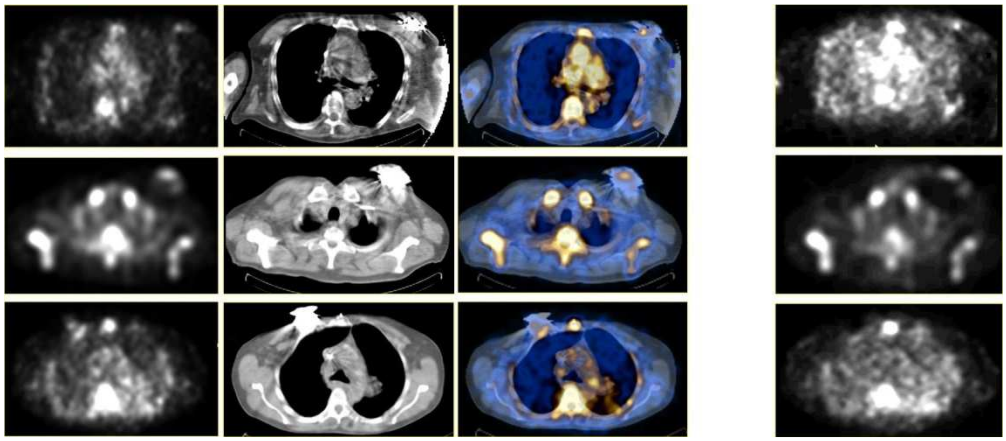

Figure 1.10 - Examples of SPECT/CT images acquired 6 hrs. after ^{99m}Tc-HMPAO administration (left panel: transaxial images of the attenuated corrected SPECT (left column), CT (central column) and SPECT/CT (right column)) demonstrate and localize a focal area of increased radiopharmaceutical uptake at the pocket site that is confirmed at non attenuated corrected images (right panel, transaxial image) in the first two cases (upper and middle panel) while in the last case (lower panel) the disappearance of uptake at the corresponding non-attenuated corrected images is a consequence of metal artifact.

Table 1.4: Published evidence concerning the use of scintigraphy with ^{111}In/^{99m}Tc-HMPAOradiolabelled leukocyte and ^{99m}Tc-sulesomab in Cardiovascular Implantable Electronic Device infections.

Cardiovascular implantable electronic device							
Patients	***Clinical presentation***	***Site of IE***	***Microbiolgy***	***Radiopharmaceutical and acquisition***	***Scintigraphic finding***	***Echocardiography***	***References***
74 y, F	Fever after CABG and ICD positioning	ICD	*Staphylococcus aureus*	^{111}In-oxine WBCs, planar	Patches, EC and pocket	unknown	Bhadelia RA et al. Ann Thorac Surg 1997[86]
57 y, M	Fever, anorexia and weight loss 15 mths post cardiac transplant	LVAD	*unknown*	^{111}In-oxine WBCs, planar and SPECT	Uptake at the LVAD tubular remnant	CT: rindlike thickening around the LVAD tubing	Roman CD et al. Clin Nucl Med 2005[88]
8	FUO	LVAD	*Staphylococcus aureus, Corynebacterium, Klebsiella oxytocagy*	^{99m}Tc-HMPAO WBCs, plana and SPECT/CT at 4 and 24 hrs	Treatment modification in 23% pts	na	Litzler PY et al. J Nucl Med 2010[89]
57 y, M	Suspected IE 20 mths after positioning ICD	ICD	*Staphylococcus aureus*	^{99m}Tc-sulesomab plana and SPECT co-registered with CT	EC in superioir caval course	inconclusive	Schiavo R et al. J Cardiovasc Med (Hagerstown) 2009[90]

CABG= coronary artery bypass graft, ICD= implantable cardia defribillator, LVAD= left-ventricular-assist device, CT=computed tomography, FUO=fever of unknown origin; EC=eletrocatheter

Table 1.5: Published evidence concerning the use of[18F]FDG PET/CT in Cardiovascular Implantable Electronic Device infections

Cardiovascular implantable electronic device						
Patients	***Clinical presentation***	***Site of IE***	***Microbiology***	***[^{18}F]FDG PET/CT findings***	***Echocardiography***	***Reference***
40 y, F	Fever,tenderness at PM pocket after tricuspid valvuloplasty replacement & PM battery change (3 w previous)	PM, prosthetic tricuspid valve	*Staphylococcus aureus*	PM pocket + Leads + IE.	Initial TEE no vegetations/valvular dysfunction; repeated TEE: valvular insufficiency.	Vos FJ et al. Eur J Nucl Med Mol Imaging 2006[191]
80 y, M	Fever after PM replacement for infection (3 y previous)	PM	Negative culture	PM + leads	Negative	Miura T et al. J Arrhythmia 2006[192]
55 y F	Fever, axillary wire of PM removed and replaced (3 m previous)	AICD, PM	*Pseudomonas spp.*	Old wire track in left axilla + lead + tip of lead at coronary sinus	Unknown	Khamaisi M et al. J Cardiovasc Electrophysiol 2008[193]
8 y, F	FUO, PM for congenital atrioventricular block progressing to complete heart block (1 y previous)	PM/lead infection	*Staphylococcus aureus*	PM pocket +leads ***Lung embolism***	Initial TTE no vegetations. TEE post PET/CT: vegetations on PM lead + tricuspid valve annulus	Abikhzer G et al. J Nucl Cardiol 2010[194]

9 y, M	Low-grade fever,induration in the epigastric region	Epicardial dual chamber PM tunneled to the left upper abdominal quadrant	Unknown	Around PM, along the tunnelized wires, intra-abdominal leads	Abdominal US: negative	Turpin S et al. Eur J Nucl Med Mol Imaging 2010[195]
n=50 (40 controls)	PM implanted >3 m previously	PM	*Staphylococcus aureus* (2) *Staphylococcus epidermidis* (4)	Sensitivity=100% Specificity=93% PPV=66% NPV=100%	TTE and TTE negative	Ploux S et al. Heart Rhythm 2011[91]
n=35 (14 controls)	Suspected CIED infection (21) and asymptomatic (14)	PM, ICD	*Staphylococcus spp.* (4) *Streptococcus spp.* (2) *Klebsiella pneumoniae* (1) *Corynebacterium jeikeium* (1) *Pseudomonas aeruginosa* (1) *Escherichia coli* (1)	Sensitivity=80% Specificity=100% PPV=100% NPV=84.6%	31.25% TEE positive for vegetations	Bensimhon L et al. Clin Microbiol Infect 2011[196]
59 y, M	Swelling over PM box (5 months previous), rigors & sweats (1 m). Prior heart block after BPAC+mitral valve substitution	PM, mechanical mitral valve	*Staphylococcus epidermidis, Candida albicans*	PM pocket	Negative	Mehta PA et al. Heart 2012[197]
n=2	Severe sepsis/septic shock of unknown origin	PM	Unknown	PM (unspecified)	Positive	Kluge S et al. J Crit Care 2012[198]

75 y, M	FUO (1 w); PM (8 y previous) with septic episode (7 y previous)	PM	*Mycobacterium peregrinum*	Atrial lead	Negative	Amraoui S et al. Arch Cardiovasc Dis 2012[199]
60 y, M	Bacteremia of unknown origin PM dependent for 30 y with 7 leads	ICD	*Staphylococcus epidermidis*	Intravascular lead	Unk	van Oostrom AJ et al. Europace 2012[200]
n=42	Suspected CIED infections (35/42 confirmed)	PM	*Staphylococcus spp.* (18) *Streptococcus spp.* (4) Others n=5	Qualitative analysis: Sensitivity=88.6% Specificity=85.7% PPV=96.9% NPV=63.7% Semiquantitative analysis*: Sensitivity=88.7% Specificity=100% PPV= 100%	54.5% TEE positive	Sarrazin JF et al. J Am Coll Cardiol 2012[201]
n=21	CIED infection	PM	*Staphylococcus spp.* (10) *Streptococcus spp.* (3) *Propionibacterium acnes* (3)	For pocket infection Sensitivity=86.7% Specificity=100% PPV=100% NPV=75% For cardiac device related EI sensitivity=30.8%, specificity=62.5% PPV=57% NPV=36%	77% positivity (either TTE or TEE)	Cautela J et al. Europace 2013[94]

60 y, M	Infection at the percutaneous retroauricular skull-mounted pedestal	Left ventricle assistance device	Unk	Left cutaneous retroauricular pedestal, thoracic internal cable, Left lung, normalized after treatment	Unk	Costo S et al. Clin Nucl Med 2011[202]

FUO, fever of unknown origin; lns, lymph nodes; PM, pacemaker; US, ultrasound. AICD = Automatic C; PPV = positive predictive value; NPV = negative predictive value; ICD = implantable cardioverter-defibrillator; CABG = coronary artery bypass graft *Using maximum count rate device/mean count rate between right and left lung parenchyma >1.87

[^{18}F]FDG PET/CT enabled to discriminate patients with isolated pocket infections (Figure 1.11) from patients with more severe and extended infection, involving the pocket and leads (Figure 1.12 and Figure 1.13). This also accounts for early device infection. In case of pocket infection [^{18}F]FDG PET/CT sensitivity ranges from 86.7%-100% and specificity from 85-100%. However, in case of CIED infections, [^{18}F]FDG specificity becomes particularly relevant when classifying patients with undetermined echocardiographic findings, e.g., bland clots adherent on leads detected on echocardiography without clear signs of infection. Therefore, in this circumstance and considering the high rate of false positive findings (up to 8%) reported in asymptomatic patients with pacing systems [91], [^{18}F]FDG PET/CT is of clinical value mostly because of its high negative predictive value.

High diagnostic accuracy of [^{18}F]FDG PET/CT was also reported for ruling out the involvement of devices during febrile episodes and for defining the embolic burden in patients with ascertained infection. A negative scan (negative predictive value from 75% to 100%) has consistently been associated with a favorable clinical outcome when antimicrobial therapy alone is initiated.

A strong correlation between sites of infection identified by [^{18}F]FDG PET/CT and outcome following various treatment regimens was also demonstrated. Therefore, [^{18}F]FDG PET/CT has been suggested as a guide to clinicians for choosing the most suitable treatment, i.e., conservative treatment (antimicrobial agents alone, or removal of just the generator) *versus* full hardware extraction. This would be especially relevant considering the ongoing debate arising from the observation that novel antimicrobial agents can penetrate the bacteria-produced biofilm[92], thus potentially decreasing the need of hardware removal in CIED infection[93]. However, the diagnostic accuracy of [^{18}F]FDG PET/CT for cardiac device related IE has been recently questioned, based on the very low sensitivity (30.8%) and specificity (62.5%) reported by Cautela et al[94]. Previous antimicrobial therapy (that was ongoing in 9/13 patients with cardiac device related IE) and/or vegetation size could account for the poor sensitivity of [^{18}F]FDG PET/CT in such report. Furthermore, [^{18}F]FDG uptake in normal heart tissue may explain why low-intensity lesions were undetected. Considering that the differential diagnosis between an infection limited at the skin/pocket and a more severe infection that involves the device over the pocket, remains the most important issue, which translates into a different patients' management[95] (from medical to surgical treatment). This issue requires further investigation before the

technique can be introduced in the routine diagnostic work-up of CIED infection.

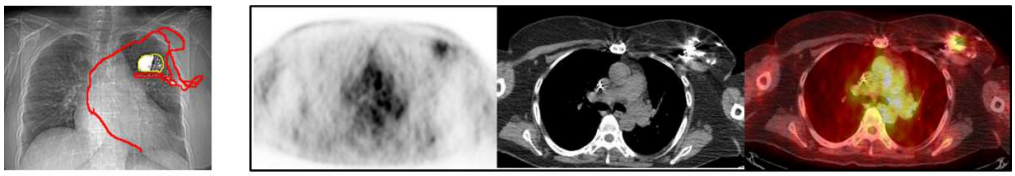

Figure 1.11: [^{18}F]FDG PET/CT in patients with suspected infection of a pacemaker. Left column: chest X-ray with delineation of the generator site (yellow) and the leads course (red). Right column: PET/CT (from left to right: SPECT image, CT l image and PET/CT image) showing intense [^{18}F]FDG uptake at the pocket site.

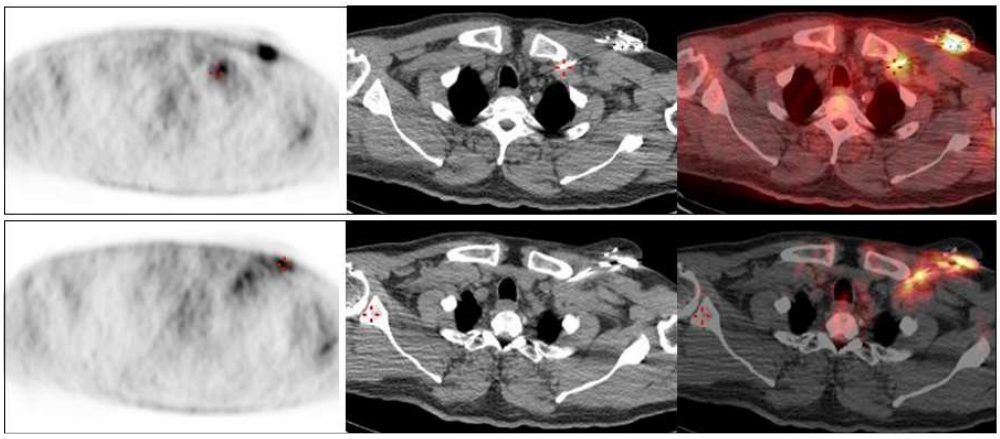

Figure 1.12: [^{18}F]FDG PET/CT in patients with suspected infection of a pacemaker. Transaxial PET/CT images at different levels (: SPECT image, CT image and PET/CT image) show intense [^{18}F]FDG uptake at the pocket site (upper panel) and all along the intravascular portion of the lead (lower panel).

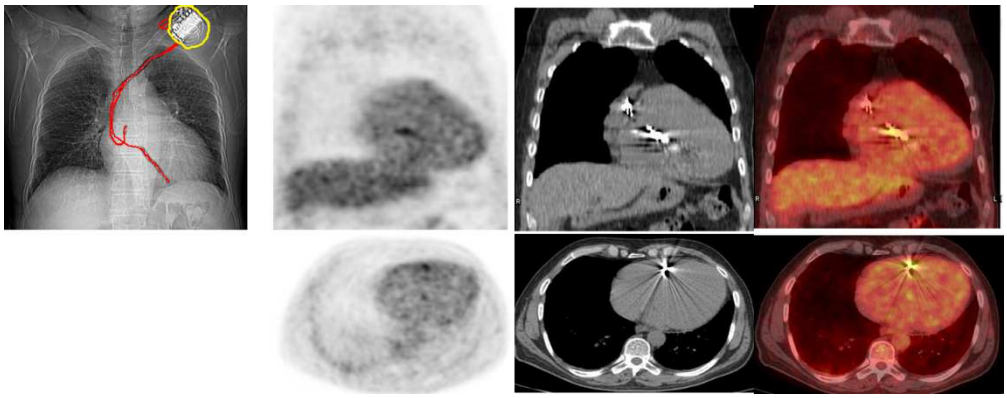

Figure 1.13: [^{18}F]FDG PET/CT in patients with suspected infection of a pacemaker. Left upper panel: chest X-ray with delineation of the generator site (yellow) and the leads course (red). PET/CT images (from left to right: emission images, CT images and superimposed PET/CT) in coronal views (right upper column) and transaxial views (lower panel) show intense [^{18}F]FDG uptake at the intracardiac portion of the PM lead.

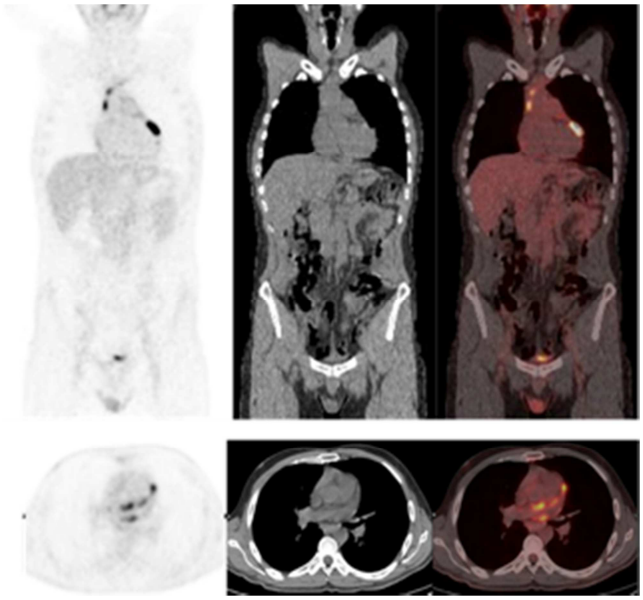

Figure 1.14: [^{18}F]FDG PET/CT images of patients with infection of unknown origin demonstrating sites of increased [^{18}F]FDG uptake at the pericardium, finally diagnosed as CMV-related pericarditis. Upper panel: coronal PET/CT images (left column emission images, middle column CT images and right column superimposed PET/CT). Lower panel: transaxial PET/CT images (left column emission images, middle column CT images and right column superimposed PET/CT).

Acute Pericarditis

Pericarditis is an inflammatory process that can be caused by localized or systemic diseases, including infection, connective tissue disorders, and uremia, or can occur after radiation therapy. Although dyspnea and pleuritic chest pain that changes with patient's position are the typical signs of the disease, clinical manifestations can be more variable, depending on the extent of pericardial disease, the rate at which it develops, and its effect on cardiac function[96]. Additional signs include pericardial friction rub at physical examination and nonspecific S-T segment and T-wave changes on ECG.

Discriminating pericarditis from myocardial disease or pulmonary infarction can be difficult on the basis of physical examination alone. Imaging may instead be helpful for distinguishing these different conditions.

Echocardiography, CT, and MRI are frequently employed to identify and characterize the pericardium and pericardial space, their typical findings including pericardial thickening, pericardial enhancement and pericardial effusions[97]. However, echocardiographic assessment of pericardial thickening can be difficult, and the entire pericardium often cannot be fully evaluated because of the poor acoustic window. CT and MRI allow clearer characterization of the pericardium and pericardial space and can therefore help to distinguish between pericardial fluid effusion and thickening[98].

[^{18}F]FDG PET/CT is generally employed as a complement to other imaging modalities, since the different pattern of [^{18}F]FDG accumulation in the pericardium or in the pericardial fluid might help in distinguishing infectious/inflammatory conditions from neoplastic pericardial involvement. In fact, noninfectious and inflammatory processes involving the pericardium or pericardial space generally present a mild to moderate increase or no increase in [^{18}F]FDG uptake, whereas neoplastic conditions generally present intense metabolic activity often associated with a focal soft-tissue mass. Incidental reports of cardiac infection or inflammation with increased [^{18}F]FDG activity have been described in patients evaluated with [^{18}F]FDG PET/CT for fever of unknown origin[99]. In patients with meningococcal sepsis and AIDS, intense pericardial uptake at [^{18}F]FDG PET allowed to recognize infectious pericarditis[100,101]. Three cases of tuberculous pericarditis were diagnosed using [^{18}F]FDG PET/CT, that identified either tuberculous pericardial involvement alone[102,103] or associated with disease dissemination throughout the body[103]. A recent study exploited the ability of [^{18}F]FDG PET/CT to distinguish acute tuberculous from idiopathic pericarditis[104]. Patients with acute tuberculous pericarditis showed a diffuse or multifocal

pattern of [^{18}F]FDG uptake in the pericardium associated with mediastinal and supraclavicular lymph nodes with increased uptake. Significantly higher mean pericardial thickness (5.1 mm) and SUV_{max} at both pericardium and lymph-nodes was observed in tuberculous pericarditis (13.5 and 5.3, respectively) as compared with patients with acute idiopathic pericarditis (3.4 mm, 3.0 and 2.8) who showed diffuse or regional [^{18}F]FDG uptake. On the contrary, constrictive or effusive constrictive pericarditis, an uncommon complication of chemotherapy, can present with mild and diffuse pericardial [^{18}F]FDG uptake[105]. Similarly, the lack of [^{18}F]FDG accumulation in the pericardial space in a patient presenting with idiopathic pericarditis associated with striking hypermetabolism of the thoracic and abdominal aortic wall (highly suggestive of large vessel vasculitis) is consistent with pericarditis as the initial manifestation of giant cell arteritis[106]. Figure 1.14 shows an example of [^{18}F]FDG PET/CT in a patient with infective pericarditis.

Myocarditis

Myocarditis, or inflammation of the heart muscle, may present as an acute, sub-acute, or chronic illness. A large proportion of afflicted individuals may be asymptomatic. Because of such insidious nature of the disease, its epidemiology has been defined through post-mortem studies. Prospective and retrospective studies have identified myocardial inflammation in 1-9% of routine post-mortem examinations[107-109]. Myocarditis is a major cause of sudden, unexpected death (up to 20% of cases) in adults younger than 40 years[110]. The causes of myocarditis include a variety of infectious or systemic diseases, toxins, and drugs. Viruses, especially enteroviruses, are the most important causes of myocarditis in developed countries. The enterovirus genome has been identified in the myocardium of patients with myocarditis or with dilated cardiomyopathy[111-113]. Since the early 1980s, endomyocardial biopsy has been used to evaluate patients with suspected myocarditis. In 1986, the Dallas criteria for the histologic diagnosis of myocarditis were defined[114], based on the identification of infiltrating lymphocytes and of myocytolysis. Patients with lymphocytic infiltration but without myocytolysis were classified as having sub-clinical or ongoing myocarditis. However, less than 10% of the patients with suspected myocarditis had positive biopsies when assessed by the Dallas criteria[115], thus raising the issue of low sensitivity and high inter-observer variability. A second clinical

classification system was proposed in 1999[116], but has not been widely accepted.

Although there have not been major advances in the identification of the etiology of myocarditis in recent years, new molecular techniques such as polymerase chain reaction and genomic hybridization have allowed confirmation of the etiology in some cases which would have otherwise remained undiagnosed. The serum level of creatine kinase-MB (CK-MB) has high specificity, but limited sensitivity for the diagnosis of myocarditis. On the other hand, serum troponin I is more often elevated than CK-MB in patients with myocarditis[117,118]. Echocardiography performed in the setting of acute myocarditis may demonstrate either normal heart function, global hypokinesis or regional left ventricular hypokinesis, with an overall low reported sensitivity[119]. MRI allows discrimination of myocarditis from myocardial infarction by depicting scattered areas of hyper-enhancement with a nonvascular distribution (in midmyocardial or subepicardial locations) in case of myocarditis. These areas of hyper-enhancement correspond to inflammation and cell necrosis, and are most commonly seen in inferior and inferiolateral myocardial segments[119-121].

Diffuse, increased metabolic activity in the left wall with mild heterogeneity suggesting the occurrence of myocarditis have been observed at [^{18}F]FDG PET/CT in a patient with chronic active EBV infection presenting with fever, dyspnea on exertion, general malaise, hepatosplenomegaly. The patient subsequently developed heart failure and myocarditis was confirmed by endomyocardial biopsy[122]. This condition must be discriminated from congestive heart failure, right ventricular strain, and hypertrophy due to elevated pulmonary artery pressure, which can also lead to increased [^{18}F]FDG uptake in the right ventricular myocardium[123].

Vascular graft infection

Vascular prosthetic infection (VPI) is a severe, late and most unwelcome complication following vascular surgery. It has a low frequency (between 0.4% and 3.0%)[124,125] but it is one of the most challenging issues for both diagnosis and treatment, and has a high morbidity and mortality rates (around 50% and 25%-75%, respectively). Its severity depends also on the location of the graft, with 13% rate of infection in the inguinal region followed by aorto-bifemoral bypass and femoro-popliteal bypass. Management of infected vascular grafts depends on several factors, including the position of the infected prosthesis, the extent of infection, and the underlying

microorganism[126]. Diagnosis is difficult, as there is no single diagnostic procedure that has 100% of accuracy. Therefore, a combination of physical examination, laboratory tests, and several imaging techniques is mandatory. In fact, patients may have a variety of clinically equivocal complaints and assessment of the extent of graft infection (one of the most difficult challenges) can be difficult. Furthermore, blood chemistry parameters can only show moderately elevated WBC counts, erythrocyte sedimentation rate and/or C-reactive-protein values, a common, non-specific finding. When clinical signs are minimal or absent because of low-grade infection, the diagnosis of vascular graft infection is uncertain. Nevertheless, it is critically important to avoid complications such as sepsis, aneurismatic ruptures, gastrointestinal bleeding and suture line disruption. Since risk factors for infection include removal of infected material by an aggressive surgical treatment, once a vascular graft infection is suspected, early and accurate detection is required for the correct choice of therapeutic procedures. Delay in treatment can lead to life-threatening sepsis and/or bleeding.

The majority of VPI cases are due to *Staphylococcus aureus*, *Escherichia coli* and *S. epidermidis* whereas, *Klebsiella* spp, P*seudomonas* spp, *Enterobacter* spp and *Proteu*s spp account for most of the remaining infections[127]. Patients with suspected graft infection usually present with local pain, redness, a palpable lump, and/or secretion in the area of the surgical wound, associated with blood chemistry values consistent with infection. Microbiological cultures (obtained by a CT-guided needle aspiration, if technically feasible) may confirm the diagnosis. Success of surgical intervention is dependent on an early diagnosis and generally CT angiography is the technique of choice for both infection confirmation and complication detection.

In case of a potentially infected vascular graft, the diagnostic approach can begin with imaging studies readily available in all healthcare institutions (mainly angio-CT and US) and radionuclide imaging studies are usually complementary to radiologic imaging

Ultrasonography with color flow doppler is the first-line imaging procedure for diagnosing an infected prosthetic vascular graft. This non-invasive technique does not involve any risk of contrast allergy and nephrotoxicity, does not expose the patient to ionizing radiation, and is in general highly cost-effective[128]. Unfortunately, especially in case of aortic grafts, its predictive value is limited both because of air content in the intestinal lumen and, sometimes, because of abundant subcutaneous fat of the patient. Computed Tomography (CT), is considered the gold standard

radiologic imaging technique. It has 94% sensitivity and 85% specificity[129]. Unfortunately, detection of gas bubbles around the graft, a diagnostic sign for infection, has good specificity but rather low sensitivity (about 50%). Despite several advantages (high specificity, guidance for needle aspiration, microbiological analysis, and speed of execution), CT imaging suffers from some limitations, such as low sensitivity in detecting low-grade and early post-surgical infections, and a significant radiation burden to patients[130].

The diagnostic role of Magnetic Resonance Imaging (MRI) in patients with suspected vascular graft infection is still unclear[131,132].In particular, its sensitivity in the detection of peri-graft infection has not been thoroughly investigated, and is probably similar to that of CT. Furthermore, MRI suffers from the same limitations as CT imaging for the differential diagnosis of peri-prosthetic fluid accumulation in the first weeks after surgery. Nevertheless, this non-invasive imaging modality provides multiparametric information which is especially useful for tissue characterization.

Nuclear medicine techniques are in general characterized by high accuracy in detecting graft infection in patients with aortic grafts and without specific signs of infection (low-grade phases), while in processes localized close to the prosthesis false positive results have occurred[133,134]. However, nuclear medicine procedures and MRI are limited to doubtful cases in which CT sensitivity is low (as in the cases of low-grade infection and early after surgery). Treatment of VPI is controversial: antimicrobial therapy may be the only option in high-risk patients. However, surgery and antimicrobial therapy remain the treatments of choice based on the patients' clinical condition. The appropriate duration of antibiotic therapy both for patients treated with or without surgery is questioned[135,136] and the decision to discontinue is clinically guided (absence of symptoms, fever and negative inflammatory markers)[137].

Radiolabeled autologous leukocytes (either with ^{99m}Tc or ^{111}In) are most frequently used for scintigraphy imaging in VPI, but ^{67}Ga-citrate, radiolabeled HIG and labeled anti-granulocyte antibodies have also been evaluated. A meta-analysis of the performance of nuclear medicine techniques for the diagnosis of prosthetic graft infection (37 papers published from 1980 to 2003)[138] have shown a clear superiority of ^{99m}Tc-labeled autologous leukocytes (82-100% sensitivity and, 85-100% specificity) over the other methods including CT (specificity 56.6% and sensitivity 75%). When the abdominal region is included in the study and ^{99m}Tc-HMPAO WBC is used, methodological efforts are necessary to decrease false positive findings (i.e. adequate image acquisition time). This superiority over other

methods has increased with the introduction of SPECT/CT. In fact, fused images allow exclusion of false positive results (i.e. abdominal aspecific accumulation), accurate characterization of pathological foci site and extension, confirmation or rejection of graft involvement even in presence of post-surgical distortions and in complex anatomical sites[139-141]. High specificity is even maintained when scintigraphy is performed during the first month after surgery [142]. A comparative study between MRI and ^{111}In-WBC reported a similar performance of the two methods (positive and negative predictive value of 95% and 80% for MRI and 80% and 82% for ^{111}In-WBC)[143]. WBC scintigraphy may be used to determine the response to treatment, preventing the risk of adverse drug reactions related to long-lasting regimens as well as the acquisition of resistance in patients treated with long-term suppressive antibiotic treatment[144]. Figure 1.15 show an example of ^{99m}Tc-HMPAO WBC in VPI.

^{99m}Tc-Fanolesomab was shown to diagnose prosthetic vascular graft infection with an accuracy of 95%[145]. Table 1.6 summarized the published evidence concerning the use of ^{67}Ga-citrate, ^{111}In-oxine WBCs, ^{99m}Tc-HMPAO WBC and ^{99m}Tc-Fanolesomab in VPI.

[^{18}F]FDG-PET and PET/CT may be considered an alternative valuable method for the evaluation of suspected vascular graft infections[146]. Sensitivity of 91% (versus 64% of CT) and specificity of 64% (versus 86% of CT) have been reported with significant improvement (sensitivity up to 95%) when appropriate interpretation criteria are used (presence of focal [^{18}F]FDG)[147]. In fact, inhomogeneous [^{18}F]FDG uptake represents unspecific uptake, possibly related to very low grade infection, weak immune reaction, inflammation (i.e. vasculitis, atherosclerosis) or chronic aseptic inflammation and post-surgical scar tissue, which may persist for years after the implantation of the prosthesis[148]. More recently, the use of PET/CT allowed to increase sensitivity to 93% and specificity to 70-91%, with positive and negative predictive values of 82-88% and 88-96%[149], mainly as a consequence of the better anatomical localization. Despite those favorable results, a high false positive rates may be an issue, as reported in a small series of patients using both semiquantitative [^{18}F]FDG uptake and CT features (graft wall thickening, oedema, gas surrounding the graft or any other sights)[150]. Nevertheless, Spacek et al.[151] identified the presence of focal [^{18}F]FDG uptake and irregular graft boundary at CT images as an independent significant predictor of low-grade VPI with erroneous classification occurring in less than 5% in the majority of patients (75%). Table 1.7 summarized the published evidence concerning the use of[^{18}F]FDG

PET and PET/CT in VPI. Figure 1.16 shows an example of [^{18}F]FDG PET/CT imaging in patients with VPI.

In conclusion, radiolabeled autologous leukocytes are considered the 'gold standard' for vascular graft infection diagnosis and treatment monitoring, since the high sensitivity and specificity of the method. The introduction of SPECT/CT increases the diagnostic accuracy. [^{18}F]FDG-PET and PET/CT with appropriate criteria for imaging interpretation may provide a valid substitute. Still, no data on its use in the early phase after surgeryor for treatment evaluation are currently available.

Figure 1.15 ^{99m}Tc-HMPAO WBC transaxial images of patients with suspected VPI showing very high uptake at the site of the vascular aotoiliac graft (left panel emission, middle panle CT at right panel fused SPECT-CT).

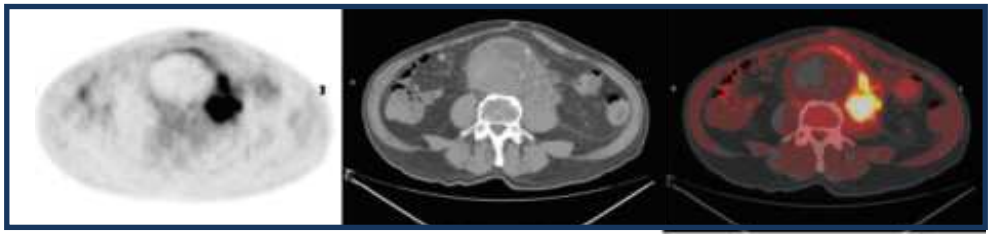

Figure 1.16: [^{18}F]FDG PET/CT images of patients with suspected aneurysmatic dilatation of the abdominal aorta. Transaxial images (left panel emission, middle panle CT at right panel fused PET-CT) show high metabolic activity around the posteolateral aspect of the aneurysm.

Table 1.6: Published evidence concerning the use of ^{67}Ga-citrate, ^{111}In-oxine WBCs, ^{99m}Tc-HMPAO WBC and ^{99m}Tc-Fanolesomab in VPI

Patients	***Clinical presentation***	***Microbiology***	***Radiopharmaceutical andacuisition***	***Main findings***	***Other imaging modalities***	***Reference***
5	Suspected VPI	*Gram -, Enterococcus spp, Staphylococcus aureus, Escherichia coli*	^{67}Ga-citrate, planar	Sensitivity 70-100% and specificity 94-100%	Upper GE series, CT, endoscophy following scintigraphy	Causey DA et al. AJR Am J Roentgenol 1980[203]
21	Unknown	*Unknown*	^{111}In-oxine WBCs	Sensitivity 100%, Specificity 87%	Unknown	Lawrence P et al. J Vasc Surg 1985[204]
21	Fever, suspected VPI	*Unknown*	^{111}In-oxine WBCs, planar 4 and 24 hrs	Sensitivity 100%, Specificity 88%	CT (10): Sensitivity 75%, Specificity 100%	Williamson MR et al. AJR Am J Roentgenol 1986[205]
70	Suspected VPI	*Unknown*	^{111}In-oxine WBCs	Sensitivity 100%, Specificity 85%	Unknown	Brunner MC et al. J Vasc Surg 1986[206]
30	Sequential evaluation after surgery	*Unknown*	^{111}In-oxine WBCs	Abnormal scan for mean 114 daysa after surgery, rare in abdomen and most frequent in the groin. For wound infection after surgery: sensitivity 100%, specificity 50%, accuracy 53%	na	Sedwitz M et al. J Vasc Surg 1987[207]
11	Suspected VPI	*Unknown*	^{67}Ga-citrate and ^{99m}Tc-HMPAO WBC, planar and SPECT	For ^{67}Ga: Sensitivity 100%, Specificity 90% For WBCs:	na	Vorne M et al. J Nucl Med 1989[208]

				Sensitivity 100%, Specificity 100%		
32	Suspected VPI (23) and controls (9)	*Unknown*	^{111}In-oxine WBCs	Sensitivity 82%, Specificity 83%	Unknown	Reilly DT et al. Eur J Vasc Surg. 1989[209]
16	Suspected infection	*Unknown*	^{67}Ga-citrate, planar and SPECT	Sensitivity 78%, Specificity 94%	CT: Sensitivity 100%, Specificity 82%	Johnson K, et al. AJR Am J Roentgenol 1990[210]
106	Unknown	*Unknown*	^{111}In-oxine WBCs (enriched garnulocytes)	Sensitivity 67%, Specificity 97%	Unknown	Thomas P et al. Clin Nucle Med 1994[211]
37	High (10) and low (18) suspiscion VPI and anastomotic aneurysms infections (9).	*Staphylococcus spp, Escherichia coli,*	^{99m}Tc-HMPAO WBC	High suspicion of VPI: Sensitivity and Specificity 100%. Low suspiscion of VPI: sensitivity 100%, specificity 94.4%, In anastomotic aneurysms infections: sensitivity 100%, specificity 89%,	CT: High suspicion of VPI: sensitivity and Specificity 100%. Low suspiscion of VPI: sensitivity 100%, specificity 55.5%. In anastomotic aneurysms infections: sensitivity and specificity 100%.	Fiorani P et al. J Vasc Surg 1993[212]
61	Suspected VPI (36) and controls (25)	*Staphylococcus spp, Staphylococcus aureus Corynrcacterium spp, Pseudomonas*	^{99m}Tc-HMPAO WBC, dynamic and planar 5-30 min and 3-24 hrs	Sensitivity and specificity 100%	CT (12) Sensitivity 67%, Specificity 100%	Prats E et al. J Nucl Med 1994[213]

		aeuruginosa, Enterocuccus spp Enterobacter spp Actinobacter spp, Escherichia coli, Kblebsiella pneumoniae				
21		*Unknown*	^{99m}Tc-HMPAO WBC	Sensitivity 53% Specificity 100%	Unknown	Krznaric E et al. Nucl Med Commun 1994[214]
75	Suspected aortofemoral graft infection, high and low suspiscion and in anastomotic aneurism	*Unknown*	^{99m}Tc-HMPAO WBC, planar 2 hrs	Sensitivity 100%, Specificity 92%	na	Liberatore M et al. Eur J Vacs Endovasc Surgery 1997[215]
129	Aortofemoral and peripheral grafts with high and low clinical suspicion of infection	*Staphylococcus spp, Staphylococcus aureus Enterobacter spp Pseudomonas spp Escherichia coli Serratia marcescens Klebsiella oxytoca Corynrcacteriumspp Citrobacter*	^{99m}Tc-HMPAO WBC, dynamic and planar at 2 hrs	Aortofemoral high suspicion: sensitivity 100% and specificity 92.5% low suspicion: sensitivity 100% and specificity 92.3% Peripheral grafts: sensitivity/specificiy 100%	na	Liberatore M et al. J Nucl Med 1998[216]
24	Suspeceted infection	*Mixed*	^{99m}Tc-HMPAO WBC SPECT/CT	SPECT/CT contributory in 67% cases	Unknown	Bar-Shalom R et al. J Nucl Med. 2006[140]

23	Serial scan 1 wk before and 1 wk and 1 mth after surgery	*Unknown*	^{99m}Tc-HMPAO WBC SPECT	No FP < 1 mth from surgery	na	Liberatore M et al. Med Sci Monit. 2006[142]
40	Suspected infection	*Mixed*	111In-oxine WBCs, planar	Sensitivity = 73%, Specificity = 87%	MRI: Sensitivity = 68%, Specificity = 97%	Shahidi S et al. Ann Vasc Surg. 2007[143]
18	Suspected VPI	*Unknown*	^{99m}Tc-Fanolesomab, 2-5 and 18-30 hrs	At 18-30 hrs images accuracy 95%	na	Tronco GG et al. Nucl Med Commun. 2007[145]
73 y, F	Fever and tenderness of right axilla in axillofemoral graft	*Staphylococcus aureus*	^{99m}Tc-HMPAO WBC SPECT/CT	Uptake around the vascular graft in the lateral chest wall	CT: graft patency, small fluid collection around the graft at right axilla, saccular aneurysm of the aortic arch	Lee A. et al. Clin Nucl Med. 2008[217]
11	Suspected VPI	*Mixed*	^{99m}Tc-HMPAO WBC SPECT/CT	Sensitivity = 86%, Specificity = 100%		Lou L et al. Nucl Med Commun. 2010[141]
20	Suspected VPI	*Staphylococcus aureus, Candida glarata, Pseudomonas, polymicrobial infections*	^{99m}Tc-HMPAO WBC SPECT	Sensitivity 75%, Specificity 100% after CT software coregistration Sensitivity 94%, Specificity 50	CT: Sensitivity 88%, Specificity 50%	Khaja MS et al. Clin Imaging 2013[218]

VPI=vascular prosthesis infection, na=not assessed, GE=gastroenteric, CT=computed tomography, MRI=magnetic resonance imaging.

Table 1.7: Published evidence concerning the use of[18F]FDG PET and PET/CT in VPI

.

Patients	***Clinical presentation***	***Microbiology***	***Criteria of positivity***	***Main findings***	***Comparison with other imaging modalities***	***Reference***
70 y, M	Low grade fever and malaise 2 yrs after graft replacement of abdominal aorta aneurysm; melena	*Eikenella corrodens*	Linear uptake	Aortic graft uptake, confirmed at surgery	CT: abnormal stranding in the retroperitoneal region, suggesting infection	Krupnick AS et al. Vasc Endovascular Surg 2003[219]
54 y, M	Fever 6 mts after femoropopliteal PTFE distal bypass	*Staphylococcus aureus*	abnormal FDG uptake linear + focal	na	US: reduced flow in the bypass, no exudate around the graft. MRI walll thrombi + superficial femoral artery obliteration. CT: faint, partially developed, nonspecific hypodense rim around some parts of the graft	Stadler P et al. J Vasc Surg 2004[220]
75 y, M	Spiking fever and malaise 15 yrs after	Anaerobic gram positive bacilli	Focal uptake at both limbs of the	na	CT: unconclusive,	Tsunekawa T et al. Eur J Vasc

	aorto-biexternal iliac bypass grafting		prosthesis highest at the distal portion			Endovasc Surg 2007[221]
5	Suspected VPI	*Escherichia coli*+ *Pseudomonas aeruginosa Staphylococcus aureus Staphylococcus epidermidis*	Increased uptake	All positive: 3/4 confirmed at surgery; 1/4 superficial infection confirmed at surgery; 1/4 only moderate uptake (postoperative period)	CT: localized superficial infection	Lauwers P et al. Angiology 2007[222]
79 y, M	Recurrent fever, chills 6 yrs after vascular grafting	*Unknown*	Shaped uptake at proximal anastomosis	na	CT negative	Balink H et al. Vasc Endovascular Surg 2007[223]
60 y, M	Fever, shivering	Polymcrobial (*Escherichia coli, Enterococcus faecium, Klebsiella pneumonia*)	Increased uptake at bifurcation	na	CT: small bubbles	Tegler G et al. J Vasc Surg 2007[224]
72 y, M	Infected pus secreting surgical woung 1 mth after PTFE femoro-post tibial bypass	*Pseudomonas spp + Staphylococcus spp*	Increased uptake	Vascular graft + soft tissue abscess	na	Keidar Z et al. Mol Imaging Biol 2003[225]
33	Suspected advanced aortic graft infection (9), low-grade aortic graft infection with	*Unknown*	Positivity: focal uptake grade 3 (<physiologic uptake by the bladder) or 4	sensitivity 91%, specificity 95%, PPV 91%, NPV 93%, and accuracy 73%	CT: sensitivity 64%, specificity 86%, PPV 70%, NPV	Fukuchi K et al. J Vasc Surg 2005[147]

	nonspecific manifestations (17), asymptomatic controls (7)		(= physiologic urinary uptake by the bladder		83%, and accuracy 79%,	
124	FUO (94) and post-surgical infection (30)	unspecified	Unspecified	7 confirmed VPI	na	Jaruskova M et al. Eur J Nucl Med Mol Imaging 2006[226]
39	Clinical signs (local pain, swelling, cellulitis, pus-secreting surgical wound or abscess at the site of surgical scarring, bacteremia, fever	Unspecified	Positivity: focal uptake with intensity > surrounding tissues	sensitivity 93%, specificity 91%, PPV 88%, NPV 96%.	na	Keidar Z et al. J Nucl Med 2007[137]
58 y, M	Long term relapsing fevers, malaise, weight loss, inflammatory laboratory abnormalities 6 mths after aortic prosthestic grafting	Coxiella burnetii	Increased uptake	Uptake at vascular graft (99mTc-WBCs negative) negative after treatment	TEE, US, CT negative	Van Assen S et al. J Vasc Surg 2007[227]
16	Out of 2,045 pts examined by PET/CT for oncological indications	unspecified	3-grade scale for high, low, or no uptake; SUVmean and TBR. CT: graft wall thickening, edema, or	All pts positive, but very high SUVmax and TBR seems to be more specific for graft infection	na	Wassélius J et al. J Nucl Med. 2008[150]

			gas surrounding the graft or any other signs of graft infection.			
unk	Abdominal pain, GE beelding Increased inflammatory markers 7 wks after proximal type I endoleak repair	na	Increased uptake	Uptake resulting FP at laparotomy	na	Zimmerman PM et al. Vascular 2008[228]
76	suspected VPI based on clinical signs of infection (e.g. local pain, cellulitis, secreting surgical wound, sonographic finding of periprosthetic fluid, FUO, positive blood culture) not requiring urgent surgical treatment	unspecified	Positivity: inhomogeneous FDG uptake; irregular boundary of the prosthesis	sensitivity 98.2%, specificity 75.6%, PPV 84.4%, NPV 96.6 and accuracy 88.5%	irregular graft boundary at CT : sensitivity 72.7%, specificity 85.7%, , PPV 88.9%, NPV 88.9%, accuracy 77.8%	Spacek M et al. Eur J Nucl Med Mol Imaging. 2009 [151]
				irregular boundary of the prosthesis + intense focal FDG uptake = probability of VPI >96%		
75 y, M	Swelling, pain and patchy erythema of the lf leg 5 mths after femoral-popliteal bypass	*Mycobacterium abscessus*	Increased uptake	Uptake at bypass graft	US: negative MRI: edema, myositis	Marion MD et al. J Vasc Surg 2009[229]
83 y, M	Asyntomatic	*Unknown*	Increased uptake	Uptake at aorto-iliac graft + fistula into bone causing osteomyelitis	na	Makis W et al. Clin Nucl Med. 2010[230]

25	Suspected VPI: fever and/or pain	*Unknown*	Positivity: focal uptake grade 3 (<physiologic uptake by the bladder) or 4 (= physiologic urinary uptake by the bladder SUVmax and TBR	sensitivity 93%, specificity 70%, PPV 82%, NPV 88%	CT: sensitivity 56%, specificity 57%, PPV 60%, NPV 58%,	Bruggink JL et al. Eur J Vasc Endovasc Surg. 2010[149]
47 y, M	Sepsis 6 mths after bypass betwenn thoracic descendent aorta and both femoral arteries	*Staphylococcus aureus*	Increased uptake	Uptake all along the vascular graft (99mTc-WBCs negatve)	CT negative	Gardet E et al. Interact Cardiovasc Thorsc Surg 2010[231]
70 y, M	Abdominal and pelvic pain 2 yrs after aortobiiliac endoprosthesis positioning	*Coxiella burnetii*	Increased uptake	Uptake at prosthesis, along the lt psoas, L2-L4	CT: extensive periaortic fibrosis, large collection in lf psoas muscle, small cysts at L4	Merhej V et al. Comp Immunol Microbiol Infect Dis 2012[232]
57y M	Intermittent pain for microemboli in claves, finger and feet 1 yrs after aortic arch prosthesis	*Candida albicans*	Increased uptake	Focus of uptake at aortic prosthetic graft, negative after antifungal therapy	CT/MRI: thrombotic material adherent to the aortic prosthesis TEE: intraortic lesion with floating parts	Motloch L et al. Tex Heart Insti J 2011[233]

PTFE=polytetrafluoroethylene, na=not assessed; US=ultrasonography, CT=computed tomography, MRI=magnetic resonance imaging, VPI=vascular prosthesis infection; GE=gastroenteric; FUO=fever of unknown origin; PPV=positive predictive value; NPV=negative predictive value; FP=false positive

References

1. Hillner BE, Siegel BA, Shields AF, et al. Impact of positron emission tomography/computed tomography and positron emission tomography (PET) alone on expected management of patients with cancer: initial results from the National Oncologic PET Registry. J Clin Oncol 2008; 26:2155–2161
2. Basu S, Chryssikos T, Moghadam-Kia S, et al. Positron emission tomogra¬phy as a diagnostic tool in infection: present role and future possibilities. Semin Nucl Med 2009; 39: 36–51
3. Habib G, Hoen B, Tornos P, et al. Guidelines on the prevention, diagnosis, and treatment of infective endocarditis (new version 2009). Eur Heart J 2009; 30:2369-2413
4. Tleyjeh IM, Steckelberg JM, Murad HS, et al. Temporal trends in infective endocarditis: a population-based study in Olmsted Country, Minnesota. JAMA 2005; 293:3022-3028
5. Durante-Mangoni E, Bradley S, Selton-Suty C, et al. Current features of infective endocarditis in elderly patients: results of the International Collaboration on Endocarditis Prospective Cohort Study. Arch Intern Med 2008; 168:2095-2103
6. Murdoch DR, Corey GR, Hoen B, et al. Clinical presentation, etiology, and outcome of infective endocarditis in the 21st century: the International Collaboration on Endocarditis-Prospective Cohort Study. Arch Intern Med 2009; 169:463-473
7. Graves MK, Soto L. Left-sided endocarditis in parenteral drug abusers: recent experience at a large community hospital. South Med J 1992; 85:378-380
8. Grover FL Cohen DJ, Oprian C, et al. Determinants of the occurrence of and survival from prosthetic valve endocarditis. Experience of the Veterans Affairs Cooperative Study on Valvular Heart Disease. J Thorac Cardiovasc Surg 1994; 108:207-214
9. Berlin JA Abrutyn E, Strom BL, et al. Incidence of infective endocarditis in the Delaware Valley, 1988-1990. Am J Cardiol 1995; 76:933-936
10. Michel PL, Acar J. Native cardiac disease predisposing to infective endocarditis. Eur Heart J 1995; 16 (supplB):2-6
11. Steckelberg JM, Wilson WR. Risck factors for infective endocarditis. Infect Dis Clin North Am 1993; 7:9-19
12. McCarthy JT, Steckelberg JM. Infective endocarditis in patients receiving long-term hemodialysis. Mayo Clin Proc 2000; 75:1008-1014
13. Fowler VG, Durack DT. Infective endocarditis. Curr Opin Cardiol 1994; 9:389-400
14. Bayer AS, Bolger AF, Taubert KA, et al. Diagnosis and management of infective endocarditis and its complications. Circulation 1998; 98:2936-2948
15. Horstkotte D, Follath F, Gutschik E, et al. Guidelines on prevention, diagnosis and treatment of infective endocarditis executive summary; the task force on infective endocarditis of the European society of cardiology. Eur Heart J 2004; 25:267-276
16. Thuny F, Di Salvo G, Belliard O, et al. Risk of embolism and death in infective endocarditis: prognostic value of echocardiography: a prospective multicenter study. Circulation 2005;112:69-75
17. Perez de Isla L, Zamorano J, Lennie V, et al. Negative blood culture infective endocarditis in the elderly: long-term follow-up. Gerontology 2007; 53:245–249
18. Li JS, Sexton DJ, Mick N, et al. Proposed modifications to the Duke criteria for the diagnosis of infective endocarditis. Clin Infect Dis 2000; 30:633-638

19. Fournier PE, Casalta JP, Habib G, et al. Modification of the diagnostic criteria proposed by the Duke Endocarditis Service to permit improved diagnosis of Q fever endocarditis. Am J Med 1996;100:629-633
20. Habib G, Derumeaux G, Avierinos JF, et al. Value and limitations of the Duke criteria for the diagnosis of infective endocarditis. J Am Coll Cardiol. 1999; 33:2023-2029
21. Lamas CC, Eykyn SJ. Blood culture negative endocarditis: analysis of 63 cases presenting over 25 years. Heart 2003; 89:258-262
22. Werner M, Andersson R, Olaison L, et al. A clinical study of culture-negative endocarditis. Medicine (Baltimore) 2003; 82:263-273
23. Brouqui P, Raoult D. Endocarditis due to rare and fastidious bacteria. Clin Microbiol Rev 2001; 14:177-207
24. Vegas a, Jariani M: Aortic Valve and Aortic Root, in Oxorn DC (eds): Intraoperative Echocardiography. (1 st ed). Philadelphia, PA, Elsevier Saunders, 2011
25. Nkomo VT. Epidemiology and prevention of valvular heart diseases and infective endocarditis in Africa. Heart 2007; 93:1510-9
26. Palestro CJ, Brown ML, Forstrom LA, et al. Society of Nuclear Medicine Procedure Guideline for 99mTc-exametazime (HMPAO)-labeled leukocyte scintigraphy for suspected infection/ inflammation, version 3.0, 2004, http://interactive.snm.org/docs/ HMPAO_v3.pdf.
27. Ishimori T, Saga T, Mamede M, et al. Increased (18)F-FDG uptake in a model of inflammation: concanavalin A-mediated lymphocyte activation. J Nucl Med 2002; 43:658-663
28. Kubota R, Yamada S, Kubota K, et al. Intratumoral distribution of fluorine-18-fluorodeoxyglucose in vivo: high accumulation in macrophages and granulation tissues studied by microautoradio- graphy. J Nucl Med 1992; 33:1972–1980
29. Brewer S, McPherson M, Fujiwara D, et al. Molecular imaging of murine intestinal inflammation with 2-deoxy-2-[18F]fluoro-D- glucose and positron emission tomography. Gastroenterology 2008; 135:744–755
30. Forstrom LA, Mullan BP, Hung JC, et al. 18F-FDG labelling of human leukocytes. Nucl Med Commun 2000; 21:691-694
31. Cerqueira MD, Jacobson AF. Indium-111 leukocyte scintigraphic detection of myocardial abscess formation in patients with endocarditis J Nucl Med 1989;30:703-706
32. O'Brian K, et al Gallium SPECT in the detection of prosthetic valve endocarditis and aortic ring abscess. J Nucl Med 1991;32:1791-1793.
33. Salem R, Boucher L, Laflamme L (2004) Dual Tc-99m sestamibi and Gallium-67 SPECT localize a myocardial abscess around a bioprosthetic aortic valve. ClinNucl Med 29:799-800.
34. Thomson LE, Goodman MP, Naqvi TZ et al (2005) Aortic root infection in a prosthetic valve demonstrated by gallium-67 citrate SPECT. ClinNucl Med 30:265-268
35. Morguet AJ, et al. [The clinical importance of scintigraphy with the murine monoclonal antigranulocyte antibody BW 250/183 for the diagnosis of prosthesis-related endocarditis]. Dtsch Med Wochenschr. 1995;120:861-6.
36. Gratz S, Raddatz D, Hagenah G et al (2000) 99mTc-labelled antigranulocyte monoclonal antibody FAB' fragments versus echocardiography in the diagnosis of subacute infective endocarditis.Int J Cardiol 75:75-84

37. Filippi L, Uccioli L, Giurato L, Schillaci O. Diabetic foot infection: usefulness of SPECT/CT for 99mTc-HMPAO-labeled leukocyte imaging. J Nucl Med. 2009 Jul;50(7)
38. Jasper N, Däbritz J, Frosch M, Loeffler M, Weckesser M, Foell D. Diagnostic value of [(18)F]-FDG PET/CT in children with fever of unknown origin or unexplained signs of inflammation. Eur J Nucl Med Mol Imaging. 2010 Jan;37(1):136-4532.
39. Litzler PY, Manrique A, Etienne M (2010) Leukocyte SPECT/CT for detecting infection of left-ventricular-assist devices: preliminary results. J Nucl Med 51:1044-1048.
40. Hyafil F et al. Role of radiolabeled leukocyte scintigraphy in patients with a suspicion of prosthetic valve endocarditis and inconclusive echocardiography Eur Heart J Cardiovascular Imaging 2013, 14(6):586-594.
41. Shreve PD, Anzai Y, Wahl RL. Pitfalls in oncologic diagnosis with FDG PET imaging: physiologic and benign variants. RadioGraphics 1999; 19:61–77
42. de Groot M, Meeuwis AP, Kok PJ, et al. Influence of blood glucose level, age and fasting period on non-pathological FDG uptake in heart and gut. Eur J Nucl Med Mol Imaging 2005; 32:98–101
43. Lum D, Wandell S, Ko J, et al. Positron emission tomography of thoracic malignancies: reduction of myocardial fluorodeoxyglucose uptake artifacts with a carbohydrate restricted diet. Clin Positron Imaging 2000; 3:155
44. Williams G, Kolodny GM. Suppression of Myocardial 18F-FDG Uptake by Preparing Patients with a High-Fat, Low-Carbohydrate Diet AJR Am J Roentgenol 2008; 190:W151-156
45. Fan CM, Fischman AJ, Kwek BH, et al. Lipomatous hypertrophy of the inter¬atrial septum: increased uptake on FDG PET. AJR Am J Roentgenol 2005; 184:339–342
46. Williams G, KolodnyGM. Retrospective study of coronary uptake of 18F-fluorodeoxyglucose in association with calcification and coronary artery disease: a preliminary study. Nucl Med Commun 2009; 30:287-291
47. Kobayashi Y, Ishii K, Oda K, et al. Aortic wall inflammation due to Takayasu arteritis imaged with 18F-FDG PET coregistered with enhanced CT. J Nucl Med 2005; 46:917-922
48. Kaderli AA, Baran I, Aydin O, et al. Diffuse involvement of the heart and great vessels in primary cardiac lymphoma. Eur J Echocardiogr 2010; 11:74-76
49. García JR, Simo M, Huguet M, et al. Usefulnessof 18-fluorodeoxyglucose positron emission tomography in the evaluation of tumor cardiac thrombus from renal cell carcinoma.Clin Transl Oncol 2006; 8:124-8
50. Abidov A, D'agnolo A, Hayes SW, et al. Uptake of FDG in the area of a recently implanted bioprosthetic mitral valve. Clin Nucl Med 2004; 29:848
51. Schouten LR, Verberne HJ, Bouma BJ et al. Surgical glue for repair of the aortic root as a possible explanation for increased F-18 FDG uptake. J Nucl Cardiol 2008; 15:146–147
52. Van Riet J, Hill EE, Gheysens O, et al. 18F-FDG PET/CT for early detection of embolism and metastatic infection in patients with infective endocarditis. Eur J Nucl Med Mol Imaging 2010; 37:1189–1197
53. Di Salvo G, Habib G, Pergola V, et al. Echocardiography predicts embolic events in infective endocarditis. J Am Coll Cardiol 2001; 37:1069-1076

54. Dumarey N, Egrise D, Blocklet D, et al. Imaging infection with 18F-FDG-labeled leukocyte PET/CT: initial experience in 21 patients. J Nucl Med 2006; 47:625–632
55. Panizzi P, Nahrendorf M, Figueiredo JL, et al. In vivo detection of Staphylococcus aureus endocarditis by targeting pathogen-specific prothrombin activation. Nat Med 2011; 17:1142–1146
56. Chua JC, Wilkoff BL, Lee I, et al. Diagnosis and management of infections involving implantable electrophysiologic cardiac devices. Ann Intern Med 2000; 133:604–608
57. Vaudaux P, Francois P, Lew PD. Role of plasma and extracellular matrix proteins, in the physiopathology of foreign body infection. Ann Vasc Surg 1998; 12:34–40
58. Vandecasteele SJ, Van Wijngaerden E, Van Elene J, et al. New insights in the pathogenesis of foreign body infections with coagulase negative staphylococci. Acta Clinica Belgica 2000; 55:148–153
59. Janatova J. Activation and control of complement, inflammation, and infection associated with the use of biomedical polymers. ASAIO J 2000; 46:S53–62
60. Frame R, Brodman RF, Furman S, et al. Surgical removal of infected transvenous pacemaker leads. Pacing Clin Eletrophysiol 1993; 16:2343–2348
61. Sohail MR, Uslan DZ, Khan AH, et al. Management and outcome of permanent pacemaker and implantable cardioverter-defibrillator infections. J Am Coll Cardiol 2007; 49:1851-1859
62. Sohail MR, Uslan DZ, Khan AH, et al. Infective endocarditis complicating permanent pacemaker and implantable cardioverter-defibrillator infection. Mayo Clin Proc 2008; 83:46-53
63. Darouiche RO. Treatment of infections associated with surgical implants. N Engl J Med 2004; 350:1422-1429
64. Ferguson TB Jr, Ferguson CL, Crites K, et al. The additional hospital costs generated in the management of complications of pacemaker and defibrillator implantations. J Thorac Cardiovasc Surg 1996; 111:742-751
65. Sohail MR, Henrikson CA, Braid-Forbes MJ, et al. Mortality and cost associated with cardiovascular implantable electronic device infections. Arch Intern Med 2011; 171:1821-1828
66. Klug D, Balde M, Pavin D, et al. Risk factors related to infections of implanted pacemakers and cardioverter-defibrillators: results of a large prospective study. Circulation 2007; 116:1349-1355
67. Johansen JB, Jørgensen OD, Møller M, et al. Infection after pacemaker implantation: infection rates and risk factors associated with infection in a population-based cohort study of 46299 consecutive patients. Eur Heart J 2011; 32:991-998
68. Durack DT, Lukes AS, Bright DK. New criteria for diagnosis of infective endocarditis: utilization of specific echocardiographic findings. Duke endocarditis service. Am J Med 1994; 96:200-209
69. Cacoub P, Leprince P, Nataf P, et al. Pacemaker infective endocarditis. Am J Cardiol 1998; 82:480-484
70. Lamas CC, Eykyn SJ. Suggested modifications to the Duke criteria for the clinical diagnosis of native valve and prosthetic valve endocarditis: analysis of 118 pathologically proven cases. Clin Infect Dis 1997; 25:713-719
71. Gandhi T, Crawford T, Riddell J 4th. Cardiovascular implantable electronic device associated infections. Infect Dis Clin North Am 2012; 26:57-76

72. Camus C, Leport C, Raffi F, et al. Sustained bacteremia in 26 patients with a permanent endocardial pacemaker: assessment of wire removal. Clin Infect Dis 1993; 17:46-55
73. Chamis AL, Peterson GE, Cabell CH, et al. Staphylococcus aureus bacteremia in patients with permanent pacemakers or implantable cardioverter-defibrillators. Circulation 2001; 104:1029-1033
74. Uslan DZ, Dowsley T, Sohail MR, et al. Cardiovascular implantable electronic device infection in patients with Staphylococcus aureus bacteremia. Pacing Clin Electrophysiol 2010; 33:407-413
75. Sopena B, Crespo M, Beiras X, et al. Individualized management of bacteremia in patients with a permanent endocardial pacemaker. Clin Microbiol Infect 2010; 16:274-280
76. Uslan DZ, Sohail MR, Friedman PA, et al. Frequency of permanent pacemaker or implantable cardioverter-defibrillator infection in patients with gram-negative bacteremia. Clin Infect Dis 2006; 43:731-736
77. Madhavan M, Sohail MR, Friedman PA, et al. Outcomes in patients with cardiovascular implantable electronic devices and bacteremia caused by Gram-positive cocci other than Staphylococcus aureus. Circ Arrhythm Electrophysiol 2010; 3:639-645
78. Tarakji KG, Chan EJ, Cantillon DJ, et al. Cardiovascular implantable electronic device infections: presentation, management, and patient outcomes. Heart Rhythm 2010; 7:1043-1047
79. Shapiro SM, Young E, De Guzman S, et al. Transesophageal echocardiography in diagnosis of infective endocarditis. Chest 1994; 105:377-382
80. Chirillo F, Bruni A, Giujusa T, et al. Echocardiography in infective endocarditis: reassessment of the diagnostic criteria of vegetation as evaluated from the precordial and transesophageal approach. Am J Card Imaging 1995; 9:174-179
81. Lo R, D'Anca M, Cohen T, et al. Incidence and prognosis of pacemaker lead-associated masses: a study of 1,569 transesophageal echocardiograms. J Invasive Cardiol 2006; 18:599-601
82. Downey BC, Juselius WE, Pandian NG, et al. Incidence and significance of pacemaker and implantable cardioverter-defibrillator lead masses discovered during transesophageal echocardiography. Pacing Clin Electrophysiol 2011; 34:679-683
83. Baddour LM, Cha YM, Wilson WR. Clinical practice. Infections of cardiovascular implantable electronic devices. N Engl J Med 2012; 367:842-829
84. Kelly PA, Wallace S, Tucker B et al (1988) Postoperative infection with the automatic implantable cardioverter defibrillator: clinical presentation and use of the gallium scan in diagnosis. Pacing Clin Electrophysiol 11:1220-1225.
85. Matsushita K, Tsuboi N, Nanasato M et al (2002) [Intravenous vegetation of methicillin-resistant Staphylococcus aureus induced by central venous catheter in a patient with implantable cardioverter-defibrillator: a case report]. J Cardiol 40:31-35.
86. Bhadelia RA, Oates E (1997) Early cardioverter defibrillator infection: value of indium-111 leukocyte imaging. Ann Thorac Surg 63:236-238.
87. Almirante B, Miró JM (2008) [Infections associated with prosthetic heart valves, vascular prostheses, and cardiac pacemakers and defibrillators]. Enferm Infecc Microbiol Clin 26:647-664.

88. Roman CD, Habibian MR, Martin WH (2005)Identification of an infected left ventricular assist device after cardiac transplant by indium-111 WBC scintigraphy. Clin Nucl Med 30:16-17.
89. Litzler PY, Manrique A, Etienne M (2010) Leukocyte SPECT/CT for detecting infection of left-ventricular-assist devices: preliminary results. J Nucl Med 51:1044-1048.
90. Schiavo R, Ricci A, Pontillo D et al (2009) Implantable cardioverter-defibrillator lead infection detected by 99mTc-sulesomab single-photon emission computed tomography/computed tomography 'fusion' imaging. J Cardiovasc Med (Hagerstown) 10:883-884.
91. Ploux S, Riviere A, Amraoui S, et al. Positron emission tomography in patients with suspected pacing system infections may play a critical role in difficult cases. Heart Rhythm 2011;8:1478-1481
92. Costerton JW, Stewart PS, Greenberg EP. Bacterial biofilms: A common cause of persistent infections. Science 1999; 284:1318-1322
93. Hansen LK, Berg K, Johnson D, et al. Efficacy of local rifampin/minocycline delivery AIGIS(RX)®) to eliminate biofilm formation on implanted pacing devices in a rabbit model. Int J Artif Organs 2010; 33:627-635
94. Cautela J, Alessandrini S, Cammilleri S, et al. Diagnostic yield of FDG positron-emission tomography/computed tomography in patients with CEID infection: a pilot study. Europace 2013; 15:252-257
95. Durante-Mangoni E, Mattucci I, Agrusta F, et al: Current trends in the management of cardiac implantable electronic device (CIED) infections. Intern Emerg Med 2013; 8:465-476.
96. Wang ZJ, Reddy GP, Gotway MB, et al. CT and MR imaging of pericar¬dial disease. RadioGraphics 2003; 23(Spec No):S167–S180.
97. Alter P, Figiel JH, Rupp TP, et al. MR, CT, and PET imaging in pericardial disease. Heart Fail Rev (in press)
98. Blockmans D, Stroobants S, Vanderschueren S, et al. FDG-PET scan in the diagnosis of postmeningococcal pericarditis. Clin Nucl Med 2002; 27:59
99. Pointon O, Scott AM, Berlangieri S, McKay WJ, Goldstein D. F-18 fluorodeoxyglucose PET and Ga-67 citrate scintigraphy in a case of AIDS lymphoma and pericarditis. Clin Nucl Med 1999; 24:817-818
100. Testempassi E, Kubota K, Morooka M, et al. Constrictive tuberculous pericarditis diagnosed using 18F-fluorodeoxyglucose positron emission tomography: a report of two cases. Ann Nucl Med 2010; 24:421-425
101. Lee VY, Wong JT, Fan HC, et al. Tuberculous pericarditis presenting as massive haemorrhagic pericardial effusion. BMJ Case Rep 2012; 2012:bcr0320125967
102. Dong A, Dong H, Wang Y, et al. 18F-FDG PET/CT in Differentiating Acute Tuberculous From Idiopathic Pericarditis: Preliminary Study. Clin Nucl Med 2013; 38:e160-165
103. Losik SB, Studentsova Y, Margouleff D. Chemotherapy-induced pericarditis on F-18 FDG positron emission tomography scan. Clin Nucl Med 2003; 28:913-915
104. Couturier B, Huyge V, Soyfoo MS. pericarditis revealing large vessel vasculitis. ISRN Rheumatol 2011; 2011:648703.
105. Saphir, O. Myocarditis: A general review with an analysis of two hundred and forty cases. Arch Pathol 1941; 32:1000–1051

106. Gore I, Saphir O. Myocarditis: a classification of 1402 cases. Am Heart J 1947; 34:827–830
107. Blankenhorn MA, Gall EA. Myocarditis and myocardosis: A clinicopathologic approach. Circulation 1956; 13:217-223
108. McCaffrey FM, Braden DS, Strong WB. Sudden cardiac death in young athletes: A review. Am J Dis Child 1991; 145:177–183
109. Bowles NE, Richardson PJ, Olsen EGJ, et al. Detection of Coxsackie-B virus specific RNA sequences in myocardial biopsy samples from patients with myocarditis and dilated cardiomyopathy. Lancet 1986; 1:1120–1123
110. Jin O, Sole MJ, Buttany JW, et al. Detection of enterovirus RNA in myocardial biopsies from patients with myocarditis and cardiomyopathy using gene amplification by polymerase chain reaction. Circulation 1990; 82:8–16
111. Schwaiger A, Umlauft F, Weyner K, et al. Detection of enteroviral ribonucleic acid in myocardial biopsies from patients with idiopathic dilated cardiomyopathy by polymerase chain reaction. Am Heart J 1993; 126:406–410
112. Aretz HT, Billingham ME, Edwards WD, et al. Myocarditis: a histopathologic definition and classification. Am J Cardiovasc Pathol 1987; 1:3–14
113. Mason JW, O'Connell JB, Herskowitz A, et al. A clinical trial of immunosuppressive therapy for myocarditis. N Engl J Med 1995; 308:12–18
114. Lieberman EB, Hutchins GM, Herskowitz A, et al. Clinico-pathologic description of myocarditis. J Am Coll Cardiol 1991;18:1617–1626
115. Magnani JW, Dec GW. Myocarditis: current trends in diagnosis and treatment. Circulation 2006; 113:876–890
116. Smith SC, Ladenson JH, Mason JW, et al. Elevations of cardiac troponin I associated with myocarditis: experimental and clinical correlates. Circulation 1997; 95:163–168
117. Goitein O, Matetzky S, Beinart R, et al. Acute myocarditis: noninvasive evaluation with cardiac MRI and transthoracic echocardiography. AJR Am J Roentgenol 2009; 192:254–258
118. Laissy JP, Hyafil F, Feldman LJ, et al. Differentiating acute myocardial infarction from myocarditis: diag¬nostic value of early- and delayed-perfusion cardiac MR imaging. Radiology 2005; 237:75–82
119. Takano H, Nakagawa K, Ishio N, et al. Active myocarditis in a patient with chronic active Epstein–Barr virus infection. Int J Cardiol 2008; 130:e11-13
120. Oikawa M, Kagaya Y, Otani H, et al. Increased [18F]fluorodeoxyglucose accumulation in right ventricular free wall in patients with pulmonary hy¬pertension and the effect of epoprostenol. J Am Coll Cardiol 2005; 45:1849–1855
121. Laissy JP, Hyafil F, Feldman LJ, et al. Differentiating acute myocardial infarction from myocarditis: diag¬nostic value of early- and delayed-perfusion cardiac MR imaging. Radiology 2005; 237:75–82
122. Takano H, Nakagawa K, Ishio N, et al. Active myocarditis in a patient with chronic active Epstein–Barr virus infection. Int J Cardiol 2008; 130:e11-13
123. Oikawa M, Kagaya Y, Otani H, et al. Increased [18F]fluorodeoxyglucose accumulation in right ventricular free wall in patients with pulmonary hypertension and the effect of epoprostenol. J Am Coll Cardiol 2005; 45:1849–1855
124. O'Connor S, Andrew P, Batt M, Becquemin JP (2006) A systematic rewiew and meta-analysis of treatments for aortic graft infection. J Vasc Surg 44: 38-45

125. Vogel TR, Symon R, Flum DR (2008) The incidence and factors associated with graft infection after aorti aneurysm repair. J Vasc Surg 2008; 47: 264-9
126. Seeger JM (2000) Management of patients with prosthetic vascular graft infection. Am Surg 66:166-177.
127. FitzGerald SF, Kelly C, Humphreys H. Diagnosis and treatment of prosthetic aortic graft infections: confusion and inconsistency in the absence of evidence or consensus. J Antimicrob Chemother. 2005;56(6):996–9.
128. Chaer RA, Gushchin A, Rhee R, et al (2009) Duplex ultrasound as the sole long-term surveillance method post-endovascular aneurysm repair: a safe alternative for stable aneurysms. J Vasc Surg 49: 845-849; discussion 849-50.
129. Low RN, Wall SD, Jeffrey RB Jr, et al (1999) Aortoenteric fistula and perigraft infection: evaluation with CT. Radiology 175: 157-162.
130. Qvarfordt PG, Reilly LM, Mark AS, Goldstone J, Wall SD, Ehrenfeld WK, et al. Computerized tomographic assessment of graft incorporation after aortic reconstruction. Am J Surg 1985;150(2):227-31
131. Orton DF, LeVeen RF, Saigh JA, et al (2000) Aortic prosthetic graft infections: radiologic manifestations and implications for management. Radiographics 20(4): 977-93.
132. Insall RL, Jones NA, Chamberlain J, et al (1990) New isotopic technique for detecting prosthetic arterial graft infection: 99mTc-hexametazime-labelled leucocyte imaging. Br J Surg 77: 1295-1298.
133. Liberatore M, Iurilli AP, Ponzo F, et al (1998) Clinical usefulness of technetium-99m-HMPAO-labeled leukocyte scan in prosthetic vascular graft infection. J Nucl Med 39: 875-879.
134. Palestro CJ, Love C, Bhargava KK (2009) Labeled leukocyte imaging: current status and future directions. Q J Nucl Med Mol Imaging 53: 105-123.
135. Homer-Vanniasinkam S. Surgical site and vascular infections: treatment and prophylaxis. Int J Infect Dis. 2007 May;11 Suppl 1:S17-22
136. Setacci C, De Donato G, Setacci F, Chisci E, Perulli A, Galzerano G, Siringano P. Management of abdominal endograft infection. J Cardiovasc Surg (Torino). 2010 Feb;51(1):33-41
137. Roy D, Grove DI. Efficacy of long-term antibiotic suppressive therapy in proven or suspected infected abdominal aortic grafts. J Infect. 2000 Mar;40(2):184-204
138. Annovazzi A, Bagni B, Burroni L, D'Alessandria C, Signore A.)Nuclear medicine imaging of inflammatory/infective disorders of the abdomen. Nucl Med Commun. 2005 Jul;26(7):657-64
139. Quirce R, Carril JM, Gutiérrez-Mendiguchía C, Serrano J, Rabasa JM, Bernal JM. Assessment of the diagnostic capacity of planar scintigraphy and SPECT with 99mTc-HMPAO-labelled leukocytes in superficial and deep sternal infections after median sternotomy. Nucl Med Commun. 2002 May;23(5):453-9
140. Bar-Shalom R et al. SPECT/CT using 67Ga and 111In-labeled leukocyte scintigraphy for diagnosis of infection. J Nucl Med. 2006; 47:587-594
141. Lou L, Alibhai KN, Winkelaar GB, Turnbull RG, Hoskinson ME, Warshawski R, Jen H, Abele JT. 99mTc-WBC scintigraphy with SPECT/CT in the evaluation of arterial graft infection. Nucl Med Commun. 2010 May;31(5):411-6
142. Liberatore M, Misuraca M, Calandri E, Rizzo L, Speziale F, Iurilli AP, Anagnostou C. White blood cell scintigraphy in the diagnosis of infection of endovascular

prostheses within the first month after implantation. Med Sci Monit. 2006 Mar;12(3):MT5-9
143. Shahidi S, Eskil A, Lundof E, Klaerke A, Jensen BS. Detection of abdominal aortic graft infection: comparison of magnetic resonance imaging and indium-labeled white blood cell scanning. Ann Vasc Surg. 2007 Sep;21(5):586-92
144. FitzGerald SF, Kelly C, Humphreys H. Diagnosis and treatment of prosthetic aortic graft infections: confusion and inconsistency in the absence of evidence or consensus. J Antimicrob Chemother. 2005 Dec;56(6):996-9
145. Tronco GG, Love C, Rini JN, Yu AK, Bhargava KK, Nichols KJ, Pugliese PV, Palestro CJ. Diagnosing prosthetic vascular graft infection with the antigranulocyte antibody 99mTc-fanolesomab. Nucl Med Commun. 2007 Apr;28(4):297-300
146. Burroni L, D'Alessandria C, Signore A. Diagnosis of vascular prosthesis infection: PET or SPECT? J Nucl Med. 2007 Aug;48(8):1227-9
147. Fukuchi K, Ishida Y, Higashi M, Tsunekawa T, Ogino H, Minatoya K, Kiso K, Naito H. Detection of aortic graft infection by fluorodeoxyglucose positron emission tomography: comparison with computed tomographic findings. J Vasc Surg. 2005 Nov;42(5):919-25
148. Keidar Z, Nitecki S.FDG-PET for the detection of infected vascular grafts. Q J Nucl Med Mol Imaging. 2009 Feb;53(1):35-40
149. Bruggink JL, Glaudemans AW, Saleem BR, Meerwaldt R, Alkefaji H, Prins TR, Slart RH, Zeebregts CJ. Accuracy of FDG-PET-CT in the Diagnostic Work-up of Vascular Prosthetic Graft Infection. Eur J Vasc Endovasc Surg. 2010 Jun 22;
150. Wassélius J, Malmstedt J, Kalin B, Larsson S, Sundin A, Hedin U, Jacobsson H. High 18F-FDG Uptake in synthetic aortic vascular grafts on PET/CT in symptomatic and asymptomatic patients. J Nucl Med. 2008 Oct;49(10):1601-5
151. Spacek M, Belohlavek O, Votrubova J, Sebesta P, Stadler P. Diagnostics of "non-acute" vascular prosthesis infection using 18F-FDG PET/CT: our experience with 96 prostheses. Eur J Nucl Med Mol Imaging. 2009 May;36(5):850-8
152. Wiseman J, Rolueau J, Rigo P, Strauss HW, Pitt B. Gallium-67 myocardial imaging for the detection of bacterial endocarditis. Radiology 1976; 135-138
153. Melvin ET, Berger M, Lutzker LG, Goldberg E, Mildvan D. Noninvasive methods for detection of valve vegetations in infective endocarditis. Am J Cardiol 1981; 47:271-278
154. Martin P, Devriendt J, Goffin Y, Verhas M. Gallium-67 scintigraphy in fibrinous pericarditis associated with bacterial endocarditis. Eur J Nucl Med. 1982;7:192-193
155. Miller SW, Palmer EL, Dinsmore RE, Brady TJ. Gallium-67 and Magnetic resonance imaging in aortic root abscess. J Nucl Med, 1987;28:1616-1619
156. Hardoff R, Luder AS, Lorber A, Dembo L. Early detection of infantile endocarditis by gallium-67 scintigraphy. Eur J Nucl Med. 1989;15:219-221
157. Desai SP, Yuille DL. The unsuspected complication of bactrerial endocarditis imaged by gallium-67 scanning. J Nucl Med. 1993; 34:955-957
158. Vandenbos F, Roger PM, Mondain-Miton V, Dunais B, Fouché R, Kreitmann P, Carles D, Migneco O, Dellamonica P. Ventricular patch endocarditis caused by Propionibacterium acnes: adcantages of gallium scanning. J Infect 2001; 43:249-251.
159. Pena FJ, Banzo I, Quirce R, Vallina NK, Hernandez A, Gaude C, Carril JM. Clin Nucl med 2002 Jun; 27(6): 401-404

160. Yavari A, Ayoub T, Livieratos L, Raman V, McWilliams Et. Diagnosis of prosthetic aortic valve endocarditis with gallium-67 citrate single-photon emission computed tomography/computed tomography hybrid imaging using software registration. Circ Cardiovasc Imaging, 2009 Nov;2:e41-3
161. McWilliams ET, J Cardiovascu Comput Tomogr 2011;5:122-124
162. Bair HJ, Becker W, Volkholz HJ, Wolf F. ^{99m}Tc-labelled anti NCA-95 antibodies in prosthetic heart valve endocarditis.Nuklearmedizin. 1991;30:149-50.
163. O'Doherty MJ, Page C, Croft D. 111In-leukocyte imaging: intrasplenic abscesses. Eur J Nucl Med 1985; 11:141-142 (44)
164. Oated E, Sarno RC. Detection of bacterial endocarditis with indium-111 labelled leukocytes. Clin Nucl Med 1988; 13:691-693
165. Borst U, et al. [Indium-111 or Tc-99m-HMPAO marked granulocytes as specific markers of florid stage endocarditis--results comparing clinical, histological and scintigraphic findings in 30 patients with suspected endocarditis]. ZKardiol. 1992;81:432-7
166. Ramackers JM, et al. The use of technetium-99m hexamethylpropylene amine oxime labelled granulocytes with single-photon emission tomography imaging in the detection and follow-up of recurrence of infective endocarditis complicating transvenous endocardial pacemaker. Eur J Nucl Med. 1995;22:1351-4
167. Adams BK. Tc-99m leukocyte scintigraphy in infective endocarditis. Clin Nucl Med 1995; 20:395-397
168. Campeau RJ, Ingram C. Perivalvular abscess complicating infective endocarditis: complementary role of echocardiography and indium-111-labeled-leukocytes. Clin Nucl Med 1998; 23:582-584.
169. Ellemann A, Rubow S, Erlank P, Reuter H. Is there a role for 99mTc-HMPAO leukocyte scintigraphy in infective endocarditis? Cardiovasc J S Afr 2003; 14:199-203
170. McDermott BP, Mohan S, Thermidor M, Parchuri S, Poulose J, Cunha BA. The lack of diagnostic value of indium scan in acute bacterial endocarditis. Am J Med 2004; 17:621-623
171. Yen RF, Chen YC, Wu YW, et al. Using 18-fluoro-2-deoxyglucose positron emission tomography in detecting infectious endocarditis/endoarteritis: a preliminary report. Acad Radiol 2004; 11:316-321
172. Ho HH, Cheung CW, Yeung CK. Septic peripheral embolization from Haemophilus parainfluenzae endocarditis. Eur Heart J 2006; 27:1009
173. Vind SH, Hess S. Possible role of PET/CT in infective endocarditis. J Nucl Cardiol 2010; 17:516-9
174. Sankatsing SU, Kolader ME, Bouma BJ, et al. 18F-fluoro-2-deoxyglucose positron emission tomography-negative endocarditis lenta caused by Bartonella henselae. J Heart Valve Dis 2011; 20:100-102
175. Yeh CL, Liou JY, Chen SW, et al. Infective endocarditis detected by ^{1}F-fluoro-2 deoxy-D-glucose positron emission tomography/computed tomography in a patient with occult infection. Kaohsiung J Med Sci 2011; 27:528-531
176. Gheysens O, Lips N, Adriaenssens T, et al. Septic pulmonary embolisms and metastatic infections from methicillin-resistant Staphylococcus aureus endocarditis on FDG PET/CT. Eur J Nucl Med Mol Imaging 2012; 39:183

177. Belohlavek O, Votrubova J, Skopalova M, et al.The detection of aortic valve infection by FDG-PET/CT in a patient with infection following total knee replacement. Eur J Nucl Med Mol Imaging 2005; 32:518
178. Love C, Tomas MB, Tronco GG, et al. FDG PET of infection and inflammation. Radiographics 2005; 25:1357-1368
179. Klingensmith WC 3rd, Perlman D, Baum K. Intrapatient comparison of 2-deoxy-2-[F 18]fluoro-D-glucose with positron emissiontomography/computed tomography to Tc-99m fanolesomab (NeutroSpec) for localization of infection. Mol Imaging Biol 2007; 9:295-299
180. Moghadam-Kia S, Nawaz A, Millar BC, et al. Imaging with (18)F-FDG-PET in infective endocarditis: promising role in difficult diagnosis and treatment monitoring. Hell J Nucl Med 2009; 12:165-167
181. Huyge V, Unger P, Goldman S. Images in radiology. A bright spot. Am J Med 2010; 123:37-39
182. Kenzaka T, Shimoshikiryo M, Kitao A, et al. Positron emission tomography scan can be a reassuring tool to treat difficult cases of infective endocarditis. J Nucl Cardiol 2011; 18:741-743
183. Plank F, Mueller S, Uprimny C, et al. Detection of bioprosthetic valve infection by image fusion of (18)fluorodeoxyglucose-positron emission tomography and computed tomography. Interact Cardiovasc Thorac Surg 2012; 14:364-366
184. Yedidya I, Stein GY, Vaturi M, et al. Positron emission tomography/computed tomography for the diagnosis of endocarditis in patients with pulmonic stented valve/pulmonic stent. Ann Thorac Surg 2011; 91:287-289
185. Wallner M, Steyer G, Krause R, et al: Fungal endocarditis of a bioprosthetic aortic valve: Pharmacologic treatment of a Candida parapsilosis endocarditis. Herz 2013; 38:431-434
186. Feuchtner G, Plank F, Uprimny C, et al. Paravalvular prosthetic valve abscess detected with 18FDG-PET/128-slice CT image fusion. Eur Heart J Cardiovasc Imaging 2012; 13:276- 277
187. Klaipetch A, Manabe O, Oyama-Manabe N, et al. Cardiac (18)F-FDG PET/CT with heparin detects infective vegetation in a patient with mechanical valve replacement. Clin Nucl Med 2012; 37:1184-1185ù
188. Pons J, Morin F, Bernier M, et al. Diagnostic challenge of annular abscess in a patient with prosthetic aortic valve: can F-fluorodeoxyglucose positron emission tomography be helpful? Rev Esp Cardiol (Engl Ed) 2012; 65:296-298
189. Gouriet F, Bayle S, le Dolley, Y, et al: Infectious endocarditis detected by PET/CT in a patient with a prosthetic knee infection: Case report and review of the literature. Scand J Infect Dis 2013; 45:570-574
190. El Hajjaji I, Mansencal N, Dubourg O. Diagnosis of Cardiobacterium hominis endocarditis: usefulness of positron emission tomography. Int J Cardiol 2012; 160:e3-4
191. Vos FJ, Bleeker-Rovers CP, van Dijk AP, et al. Detection of pacemaker and lead infection with FDG-PET. Eur J Nucl Med Mol Imaging 2006; 33:1245
192. Miura T, Kinoshita O, Horigome M, et al. Detection of pacemaker lead infection by Fluorodeoxyglucose positron emission tomography. J Arrhythmia 2006; 22:242–4

193. Khamaisi M, Medina A, Mazouz B, et al. Imaging coronary sinus infection in pacemaker electrode with [18F]-fluorodeoxyglucose positron emission tomography. J Cardiovasc Electrophysiol 2008; 19:1327-1328
194. Abikhzer G, Turpin S, Bigras JL. Infected pacemaker causing septic lung emboli detected on FDG PET/CT. J Nucl Cardiol 2010; 17:514-515
195. Turpin S, Lambert R, Poirier N. An unusual looking pacemaker infection imaged with 18F-FDG PET/CT. Eur J Nucl Med Mol Imaging. 2010; 37:1438
196. Bensimhon L, Lavergne T, Hugonnet F, et al. Whole body [(18) F]fluorodeoxyglucose positron emission tomography imaging for the diagnosis of pacemaker or implantable cardioverter defibrillator infection: a preliminary prospective study. Clin Microbiol Infect 2011; 17:836-844
197. Mehta PA, Zuberi Z, Rinaldi CA. The use of positron emission tomography in the diagnosis of pacemaker related infection. Heart 2012; 98:376
198. Kluge S, Braune S, Nierhaus A, et al. Diagnostic value of positron emission tomography combined with computed tomography for evaluating patients with septic shock of unknown origin. J Crit Care 2012; 27:316.e1-7
199. Amraoui S, Texier-Maugein J, Bordachar P. PET scan in suspected but unproven pacemaker endocarditis. Arch Cardiovasc Dis 2012; 105:125-126
200. van Oostrom AJ, Wijffels MC, van Boven WJ, et al. Positron emission tomography in a complex case of cardiac device-related infection. Europace 2012; 14:1806
201. Sarrazin JF, Philippon F, Tessier M, et al. Usefulness of fluorine-18 positron emission tomography/computed tomography for identification of cardiovascular implantable electronic device infections. J Am Coll Cardiol 2012; 59:1616-1625
202. Costo S, Hourna E, Massetti M, et al. Impact of F-18 FDG PET-CT for the diagnosis and management of infection in JARVIK 2000 device. Clin Nucl Med 2011; 36:e188-191
203. Causey DA, Fajman WA, Perdue GD, Constantino MJ, Sones PJ, Tarcan YA. 67Ga scintigraphy in postoperative synthetic graft infection. AJR Am J Roentgenol 1980;134:1041–5
204. Lawrence FP, Dries DJ, Alazraki N, Albo D Jr. Indium 111-labeled leucocyte scanning for detection of prosthetic vascular graft infection. J Vasc Surg 1985;2:165–73.
205. Williamson MR, Boyd CM, Read RC et al. 111In-labeled leukocytes in the detection of prosthetic vascular graft infection. Am J Roentgenol 1986; 147:173-6
206. Brunner MC, Mitchell RS, Baldwin JC et al.Prosthetic graft infection: limitations of indium white blood cell scanning. J Vasc Surg 1986; 3:42-48 1986
207. Sedwitz MM, Davies RJ, Pretorius HT, Vasquez TE. Indium 111-labeled white blood cell scans after vascular prosthetic reconstruction. J Vasc Surg 1987;6:476-81
208. Vorne M, Soini I, Lantto T, Paakkinen S. Technetim-99m HM-PAO-labeled lekocyte in detetction of inflammatory lesions: comparison with gallium-67 citrate. J Nucl Med 1989;30:1332-6
209. Reilly DT, Grigg MJ, Cunningham DA, Thomas EJ, Mansfield AO. Vascular graft infection: the role of indium scanning. Eur J Vasc Surg. 1989;3:393-397
210. Johnson KK, Russ PD, Bair JH, Friefeld GD. Diagnosis of synthetic vascular graft infection: comparison of CT and gallium scans. Am J Roentgenol 1990;154:405–9
211. Thomas P, Forstrom L. In-111 Labeled purified granulocytes in the diagnosis of synthetic vascular graft infections. Clin Nucle Med 1994; 19:1075-1078

212. Fiorani P. Speziale F. Rizzo L, De Santis F, Massimi GJ, Taurino M, Faraglia V, Fiorani L, Baiocchi P, Santini C et al. et al. Detection of aortic graft infection with leucocytes labeled with technetium 99m-hexametazime. J Vasc Surg 1993;17:87–95
213. Prats E, Banzo J, Abos MD, Garcia-Lopez F, Escalera T, Garcia-Miralles M, Gaston R, Asenjo MJ. Diagnosis of prosthetic vascular graft infection by technetium-99m-HMPAO labeled leucocytes. J Nucl Med 1994;35:1303-1307
214. Krznaric E, Nevelsteen A, van Hoe L, de Roo M, Schiepers C, Verbruggen A, Mortelmans L. Diagnostic value of 99Tc-HMPAO labelled leucocyte scintigraphy in the detection of vascular graft infections. Nucl Med Commun 1994;15:953–960.
215. Liberatore M, Iurilli AP, Ponzo F, Prosperi D, Santini C, Baiocchi P, Serra P, Rizzo L, Speziale F, Fiorani P, Centi Colella A. Eur J Vacs Endovasc Surgery 1997; 14:27-29
216. Liberatore M, Iurilli AP, Ponzo F, Prosperi D, Santini C, Baiocchi P, Rizzo L, Speziale F, Fiorani P, Colella CA. Clinical usefulness of technetium-99m-HMPAO labeled leucocyte scans in prosthetic vascular graft infection. J Nucl Med 1998;39:875–9.
217. Lee A, Biggs H, Chen S, Urriola N, Aggarwal S, Al-Gailani H, Mansberg R. SPECT/CT of Axillofemoral Graft Infection. Clin Nucl Med 2008;33:333-334
218. Khaja MS, Sildiroglu O, Hagspiel K, Rehm PK, Cherry KJ, Turba UC. Clin Imaging 2013; 37:239-244
219. Krupnick AS et l. 18-fluorodeoxyglucose positron emission tomography as a novel imaging tool for the diagnosis of aortoenteric fistula and aortic graft infection-a case report. Vasc Endovascular Surg 2003;37:363–366.
220. Stadler P. Bilohlavek O, Spacek M, Michalek P. Diagnosis of vascular prosthesis infection with FDG-PET/CT. J Vasc Surg 2004;40:1246–1247
221. Tsunekawa T, Ogino H, Minatoya K, Matsuda H, Sasaki H, Fukuchi K. Masked prosthetic graft to sigmoid colon fistula diagnosed by 18-fluorodeoxyglucose positron emission tomography. Eur J Vasc Endovasc Surg 2007;33:187-189
222. Lauwers P, Van den Broeck S, Carp L, Hendriks J, Van Schil P, Blockx P. The use of positron emission tomography with (18)F-fluorodeoxyglucose for the diagnosis of vascular graft infection. Angiology 2007;58:717–722
223. Balink H, Reijnen MM. Diagnosis of abdominal aortic prosthesis infection with FDG-PET/CT. Vasc Endovascular Surg 2007;41:428–433
224. Tegler G, Sorensen J, Bjorck M, Savitcheva I, Wanhainen A. Detection of aortic graft infection by 18-fluorodeoxyglucose positron emission tomography combined with computed tomography. J Vasc Surg 2007;45:828–30
225. Keidar Z, Engel A, Nitecki S, Bar Shalom R, Hoffman A, Israel O. PET/CT using 2-deoxy-2-[18F]fluoro-D-glucose for the evaluation of suspected infected vascular graft. Mol Imaging Biol 2003;5:23–5
226. Jaruskova M, Belohlavek O. Role of FDG-PET and PET/CT in the diagnosis of prolonged febrile states. Eur J Nucl Med Mol Imaging 2006;33:913–8
227. Van Assen S, Houwerzijl EJ, van den Dungen JJ, Koopmans KP. Vascular graft infection due to chronic Q fever diagnosed with fusion positron emission tomography/computed tomography J Vasc Surg 2007;46:372
228. Zimmerman PM, Cherr GS, Angelo GC, Gona J, Dosluoglu HH. Is F 18 fluorodeoxyglucose positron emission tomography too sensitive fro the diagnosis of vascular endograft infection?. Vascular 2008;16:346-349

229. Marion MD, Swanson MK, Spellman J, Spieth ME. Femoropopliteal prosthetic bypass graft infection due to Mycobacterium abscessus localized by FDG-PET/CT scan. J Vasc Surg 2009;50:907-909
230. Makis W, Stern J Chronic vascular graft infection with fistula to bone causing vertebral osteomyelitis, imaged with F-18 FDG PET/CT. 2010;35:794-796
231. Gardet E, Addas R, Monteil J, Le Guyader A. Comparison of detection of F-18 fluorodeoxyglucose positron emission tomography and 99mTc-hexamethylpropylrnr amine oxime labelled leukocyte scintigraphy for an aortic graft infection. Interact Cardiovasc Thorsc Surg 2010;10:142-143
232. Merhej V, Camilleri S, Piquet P, Casalta JP, Raolt D. Relevance of the positron emission tomography in thr diagnosis of vascular graft infection with Coxiella burnetii. Comp Immunol Microbiol Infect Dis 2012, 35:45-49
233. Motloch L, Rottlaender D, Darabi T, Joost I, Erdmann E, Hoppe UC. Conservative management of Candida infection of prosthetic aortic graft by means of caspofungin and fluconazole alone. Tex Heart Inst J 2011;38:197-200

Chapter 2

Added value of ^{99m}Tc-HMPAO-labeled leukocyte SPECT/CT imaging in the characterization and management of patients with infectious endocarditis

Paola A. Erba[1], Umberto Conti[2], Elena Lazzeri[1], Martina Sollini[1], Roberta Doria[3], Salvatore M. De Tommasi[4], Francesco Bandera[5], Carlo Tascini[3], Francesco Menichetti[3], Rudi A.J.O. Dierckx[6], Alberto Signore[6,7] and Giuliano Mariani[1]

[1]Regional Center of Nuclear Medicine, University of Pisa Medical School, Pisa, Italy;
[2]Laboratory of Echocardiography, Cardiology Unit, Azianda Ospaedaliero-Universitaria Pisana, Pisa, Italy;
[3]Infectious Disease Department, Azienda Ospedaliero Universitaria Pisana, Pisa, Italy;
[4]Cardiology Department, Azienda Ospedaliero Universitaria Pisana, Pisa, Italy;
[5]Cardiovascular Department "Malan", IRCCS Policlinico San Donato Milanese, Milan, Italy;
[6]Nuclear Medicine and Molecular Imaging Dept, University Medical Center Groningen, The Netherland;
[7]Nuclear Medicine Unit, S. Andrea Hosp, University of Rome.

J Nucl Med 2012; 53:1235–1243

Clinical performance of the Duke Endocarditis Service criteria to establish the diagnosis of infectious endocarditis (IE) can be improved through functional imaging procedures such as radiolabeled leukocytes (^{99m}Tc-HMPAO-WBC). Methods: We assessed the value of ^{99m}Tc-HMPAO-WBC scintigraphy including SPECT/CT acquisitions in a series of 131 consecutive patients with suspected IE. Patients with permanent cardiac devices were excluded. ^{99m}Tc-HMPAO-WBC scintigraphy results were correlated with transthoracic (TTE) or transesophageal (TEE) echocardiography, blood culture and the Duke criteria. Results: Scintigraphy was true positive in 46/51 and false negative in 5/51 cases (90% sensitivity, 94% NPV, 100% specificity and PPV). No false positive results were found, even in patients with early IE evaluated within the first two months from the surgical procedure. In 24/51 patients with IE we also found extracardiac uptake, indicating septic embolism in 21/24. Despite septic embolism was found in 11/18 cases of Duke “definite IE”, most of the added value from the ^{99m}Tc-HMPAO-WBC scan for decision-making was seen in patients in whom the Duke criteria yielded "possible" IE. The scan was particularly valuable in patients with negative and/or difficult-to-interpret echocardiographic findings since it correctly classified 11/88 of these patients as having IE. Furthermore, 3 patients were falsely positive at echocardiography but correctly negative at ^{99m}Tc-HMPAO-WBC scintigraphy: these patients had marantic vegetations. Conclusions: Our results demonstrate ^{99m}Tc-HMPAO-WBC scintigraphy ability to reduce the rate of misdiagnosed IE when combined to the standard diagnostic tests (a) in patients with high clinical suspicion but inconclusive echocardiographic findings; (b) for the differential diagnosis between septic and sterile vegetations detected at echocardiography; (c) when echocardiographic, laboratory and clinical data are contradictory, as also to exclude valve involvement (especially of a prosthetic valve) during febrile episodes, sepsis or post-surgical infections.

Key words: infectious endocarditis, ^{99m}Tc-HMPAO-WBC, SPECT/CT, septic embolism.

Introduction

The incidence of infectious endocarditis (IE), is approximately 2-4 cases per 100,000 persons/year (*1*). At present, 25-50% of the cases occur in patients older than 60 years (*2*).
The diagnosis of IE, first suspected on clinical ground, is further supported either by detecting a vegetation at transthoracic (TTE) or transesophageal (TEE) echocardiography, and/or by positive blood culture (*3*). In most institutions the final diagnosis is established using the Duke Endocarditis Service criteria (*4*), which also entail echocardiographic findings. Overall sensitivity is about 80% (*5*). However, in some instances blood culture or echocardiography are inconclusive, thus leading to a high proportion of unconfirmed cases of suspected IE. Indeed, up to 24% of the patients with pathologically proven endocarditis were misclassified as "possible" IE based on Duke criteria alone (*5*).
Attempts have been made at improving the diagnostic performance of the above criteria, and modifications that consider several additional clinical and microbiological parameters have been proposed (*6*). The so-called modified Duke criteria are now recommended for diagnostic classification (*7*). Traditional diagnostic criteria may also be integrated with information derived from radionuclide imaging, given the ability to localize functional hallmark of infection as represented by increased radiolabeled leukocytes recruitment. Using three-dimensional reconstruction of hybrid SPECT/CT or PET/CT images it's possible to detect and precisely localized throughout the body all the sites of infections represented by areas of radiopharmaceutical uptake. In association with echocardiography, this imaging technique can be employed to confirm or rule out IE in equivocal and/or difficult-to-explore situations (i.e., marantic vegetations, artefacts caused by mechanical prosthesis). Furthermore, scintigraphy can also reveal the presence of extra-cardiac infection sites as the consequence of septic embolism originated from IE (*8*). In this study we assessed the added value(s) of SPECT/CT with ^{99m}Tc-HMPAO-labeled autologous leukocyte (^{99m}T-HMPAO-WBC) in the characterization of patients with suspected or established IE, as defined according to Duke criteria.

Materials and methods

Patient Population

Between October 2005 and December 2010, a total of 185 consecutive patients were referred for scintigraphy with ^{99m}T-HMPAO-WBC for suspected IE. Fifty-four of these patients were excluded from the present analysis because they were bearing permanent cardiac devices, a condition that might introduce confounding factors linked to the different mechanism of infection (*9*). Therefore, the population for the present work included the remaining 131 patients (45 women and 86 men, mean age 62.8±16.6 years), in whom IE was suspected, or established as definite according to the Duke criteria; in the latter case, scintigraphy was performed to exclude septic embolism. All patients had undergone clinical examination, blood tests including WBC counts, CRP, ESR, acute phase proteins, electrophoresis, urinalysis and echocardiography (either TTE, TEE or both). Three sets of blood cultures including at least one aerobic and one anaerobic from a peripheral vein were performed for all patients (*10*). The main clinical features and risk factors of the patients are summarized in Table 2.1.

Final diagnosis of IE, or exclusion of this condition and identification of an alternative cause of disease was defined based on the final microbiological (n=20) or clinical diagnosis (n=31), with clinical follow-up of 12 months for all patients. Based on these combined parameters, IE was confirmed in 51 out of the 131 patients, that is, in 24/28, 25/55 and 2/48 of the cases in which IE had been classified as definite, possible, or rejected, respectively, according to Duke criteria.

In the 51 patients who were eventually diagnosed as having IE, infection involved more frequently the aortic valve and affected almost equally native valves either biological or mechanical prosthetic implants (Table 2). In patients with prosthetic valves early IE (< 2 months from valve replacement) was present in 9/35 patients, semi-late IE (between 2 and 12 months) in 11/35 and late-onset IE in 15/35 (Table 2.2).

Staphylococcus spp. was the microorganism more frequently responsible for the infection (24/51), followed by *Enterococcus* spp. (11/51), *Streptococcus* spp. (10/51), and *P. aeruginosa* (4/51). *Haemophilus* and *Candida* were found in 2/51 patients each.

Table 2.1: Main features of the 131 patients included in the study.

Age (years)	Mean ± SD 62.8 ± 16.6	Median 66	Range 19-89
Sex	Women 45/131 (34%)	Men 86/131 (66%)	
Risk factors	Diabetes 20/131 (15%)	Renal failure 24/131 (18%)	Cutaneous lesions 10/131 (8%)
Blood tests	ESR 110/131 (84%)	CR 78/131 (60%)	Leukocytosis 55/131 (42%)
Blood culture	Positive 67/131 (51%)	Negative 64/131 (49%)	
Duke criteria	Definite 28/131	Possible 55/131	Rejected 48/131

Table 2.2: Site of IE, type of valve and time of infection onset.

Type of valve	Native	Biological prosthesis	Mechanical prosthesis	
	116/51 (31%)	19/51 (38%)	16/51 (31%)	
Site of IE	Aortic	Mitral	Tricuspid	Aortic + mitral
Native	9/30 (30%)	6/19 (32%)	1/1 (100%)	-
Biological prosthesis	10/30 (33%)	8/19 (42%)	-	1/1 (100%)
Mechanical prosthesis	11/30 (37%)	5/19 (26%)*	-	-
Type of infection	Early IE	Semi-late IE	Late IE	
	9/35 (26%)	11 (31%)	15 (43%)	
Time from valve replacement (months)	mean 1.39 range 0.5-2	mean 6 range 3-10	mean 51.4 range 6-204	

(*) including 2 patients with anuloplasty.

Radiolabelling of Autologous Leukocytes and Image Acquisition Protocol

Autologous radiolabeled WBCs were prepared according to the EANM Guidelines for the labeling of leukocytes with ^{99m}Tc-HMPAO (*11*,*12*). Radiolabelling efficiency was always between 70-85%, and viability of the radiolabeled leukocytes was always tested by the Tripan blue exclusion test before reinfusion.

Whole body and spot planar images were obtained after 30 minutes (early), then 4-6 and 20-24 hours (delayed images) after reinfusion of 370-555 MBq of ^{99m}Tc-HMPAO-WBC. SPECT/CT of the chest was performed in all patients at 6 hours and repeated at 24 hours in case of negative or doubtful

imaging at 6 hours. Images were acquired using a dual-head, variable-angle SPECT/CT gamma camera (Hawkeye, GE Healthcare). The low-dose CT transmission scan was acquired for 16 seconds over 220° for each transaxial slice. The full FOV consisting of 40 slices was completed in 10 minutes. The transmission data were reconstructed using filtered back-projection to produce cross-sectional images. Resolution of the CT scan was 2.2 mm and localization images were produced with a 4.5-mm pixel size, similar to the nuclear medicine emission images. The CT scans were reconstructed into a 256×256 matrix. The SPECT component of the same FOV was acquired using a 128×128 matrix, 360° rotation, 6° angle step, and 40/60-sec-per-frame acquisition time at 6 and at 24 hours, respectively. Both CT-attenuation corrected and non-corrected SPECT images were evaluated in the coronal, transaxial, and sagittal planes, as well as in tridimensional maximum intensity projection (MIP) cine mode. Matching pairs of x-ray transmission and radionuclide emission images were fused using the Xeleris software, and hybrid images of overlying transmission and emission data were generated.

Interpretation Criteria

Two experienced nuclear physicians aware of the patients' clinical history and of the results of prior conventional imaging tests reviewed independently the planar scans and the SPECT/CT images, with regard to the presence and location of any focus of abnormal radioactivity accumulation indicating infection. Preliminary analysis of the SPECT/CT images included visual inspection to exclude misregistration between the SPECT and the CT components.

The scintigraphic studies were classified as negative when no sites of abnormal uptake were observed at SPECT/CT images, or positive for infection when at least one focus of abnormal uptake characterized by time-dependent increase in radioactivity from early planar to delayed images was observed (*13*). This time-dependent pattern of uptake is especially relevant for the cardiac region, considering that physiologic accumulation of radiolabeled leukocytes in the bone marrow (as in the sternum, overlying the heart) early after reinfusion can interfere with interpretation of the planar images. When present, focal uptake indicating infection was further classified as pertaining to the heart and/or to extracardiac sites.

The contribution of SPECT/CT was considered with special attention to the possibility of anatomically localizing the exact site of infection, particularly for the heart region. In fact, neither the planar nor the stand-alone

SPECT images allow to localize areas of focal uptake of the radiolabeled leukocytes in the cardiac region as pertaining or not to endocardium.

Data Analysis

Results of ^{99m}Tc-HMPAO-WBC scintigraphy were correlated with those of TTE, TEE, blood culture and the Duke criteria. The ability to detect or to exclude the presence of IE was defined based on the final microbiological or clinical diagnosis. Furthermore, in patients with known IE the ability to identify septic emboli and metastatic sites of infection was considered, in order to assess the ability of ^{99m}Tc-HMPAO-WBC scintigraphy to define disease burden.

No comparative analysis was performed between the stand-alone SPECT and the SPECT/CT findings concerning intracardiac location of infection, because in case of focal uptake in the cardiac region no further topographic localization is possible with the former sets of images, considering that the mitral valve and, i.e., the aortic valve (the most frequent site of IE) are <1 cm apart one from each other.

Statistical Analysis

All values are expressed as median and range, as customary for nonparametric data.

Results

By adopting the interpretation criteria described above for scintigraphic detection of infection, it was possible to classify all the scans as either frankly positive or frankly negative, therefore without any equivocal result at scintigraphy. With these criteria, ^{99m}Tc-HMPAO-WBC scintigraphy was totally negative in 34/131 patients for either cardiac and/or extracardiac sites of focal uptake indicating infection, without any discordant results between planar and SPECT/CT acquisitions. At least one abnormal area with focal uptake of the radiolabeled leukocytes was detected in 97 out of the 131 patients included in this study. When considering the 51 patients with final diagnosis of IE, the uptake was either limited to the heart only (n=23; Figures 2.1, 2.2 and 2.3), both at the heart and at extracardiac sites (n=23), or at extracardiac sites only (1 case with septic embolism in the spleen, which was therefore considered as a false negative scan for IE).

^{99m}Tc-HMPAO-WBC SPECT/CT was therefore true positive in 46/51 and false negative in 5/51 cases. The 5 false negative findings for IE at ^{99m}Tc-

HMPAO-WBC scintigraphy occurred in patients with small valve vegetations (<6 mm) and in the presence of infection from *Enterococcus* (n=4) or *Candida* (n=1); all such patients were under high-dose antimicrobial therapy at the time of scintigraphy. There were no false positive scans for infection of the cardiac valves.

Although both planar and stand-alone SPECT images were sufficiently accurate to detect the presence of infection involving the heart in the majority of the patients (there were in fact only 4 false negative planar scans due to accumulation of the radiolabeled leukocytes hidden by the sternum or the ribs), only after co-registration with CT it was possible to precisely discriminate the localization of ^{99m}Tc-HMPAO-WBC uptake (i.e. especially mitral *versus* aortic valves, given their proximity, metal devices, or surgical stitches/clips) from any non-cardiac site of infection in the mediastinal space. Out of the total 89 sites of increased ^{99m}Tc-HMPAO-WBC uptake in the chest, fused SPECT/CT imaging demonstrated heart valve localization in 44 cases, as opposed to non-cardiac-valve localizations due to infection of aortic graft (n=11), sternum osteomyelitis (n=13), mediastinitis (n=3), and lung infection (n=17). For areas with focal ^{99m}Tc-HMPAO-WBC uptake located outside the thorax, major impact of the SPECT/CT findings was observed for infection sites in the CNS and head-and-neck lesions, as well as to discriminate between bone infection and soft tissue infection. In particular, the exact sites of ^{99m}Tc-HMPAO-WBC accumulation were diagnosed as CNS, nasal and maxillary sinus infections (in 3 and 5 cases, respectively), spleen embolism (n=4) or bone, soft tissue or prosthetic joint infections (22 cases overall, involving spine in 10 cases).

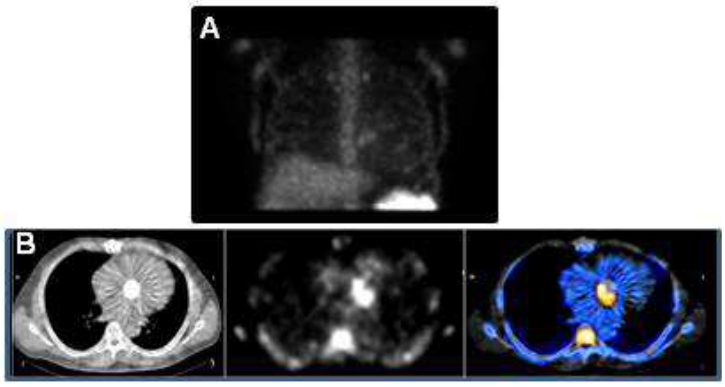

Figure 2.1 - ^{99m}Tc-HMPAO-WBC scintigraphic images in a patient with aortic endocarditis. The MIP image (A) demonstrates focal increase of radiolabeled WBCs in the heart region. Transiaxial SPECT/CT images (panel B) show that such focal uptake is localized at the mechanical prosthesis of the aortic valve (CT section in left panel, fused SPECT/CT section in center panel, SPECT right panel).

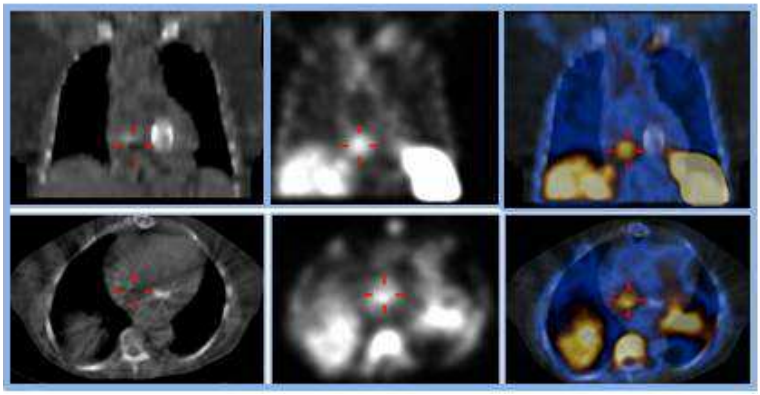

Figure 2.2 - ^{99m}Tc-HMPAO-WBC SPECT/CT images obtained in a patient with positive blood culture and fever arose few months after substitution of the mitral valve with a mechanical prosthesis (coronal sections in upper panel, transaxial sections in lower panel; CT images in left panels, SPECT/CT images in central panels, SPECT images in right panels). SPECT images demonstrate a clear focus of uptake in the right heart, identified as endocarditis of the native tricuspid valve by the superimposed SPECT/CT images (central panels). Endocarditis of the mechanical prosthesis, the expected site of infection before performing ^{99m}Tc-HMPAO-WBC, was therefore excluded.

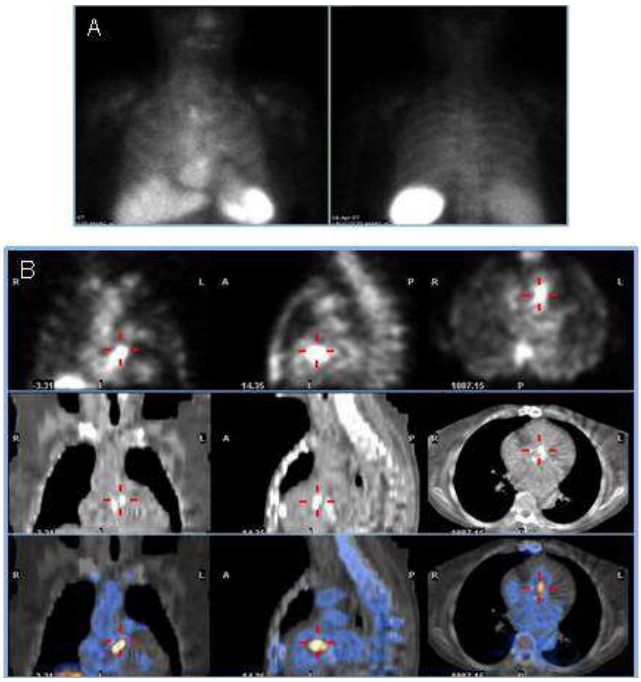

Figure 2.3 - ^{99m}Tc-HMPAO-WBC scintigraphy demonstrating the value of SPECT/CT for precisely localizing the site of infection. (A) Planar anterior and posterior views (anterior in left panel, posterior in right panel), where focal uptake of radiolabeled WBCs mimic sternal osteomyelitis. (B) Coronal, sagittal, and transaxial CT sections in left panels, fused SPECT/CT sections in middle panels and SPECT sections in right panels. The tomographic images correctly localize uptake of ^{99m}Tc-HMPAO-WBCs at the mitral valve prosthesis.

Septic embolism was detected in 41% of patients (Figure 2.4). Three cases interpreted as septic embolism at ^{99m}Tc-HMPAO-WBC scintigraphy were instead false-positive, due to active vasculitis of the aortic arch, an isolated vertebral metastasis from prostate cancer, and an osteoporotic vertebral crush, respectively. There were 8 false negative scans for extracardiac infection, due to kidney (n=3) or cerebral septic embolism (n=5) (all detected by the CT or MRI imaging).

Table 2.3 correlates the SPECT/CT results and the Duke classification in the 51 patients with final diagnosis of IE. Most of the added value from the ^{99m}Tc-HMPAO-WBC scan for decision-making was seen in patients in whom the Duke criteria yielded "possible" IE. Furthermore, 3 patients were falsely positive at echocardiography but correctly negative at ^{99m}Tc-HMPAO-WBC scintigraphy: these patients had marantic vegetations.

Table 2.4 shows the correlation between echocardiographic and ^{99m}Tc-HMPAO-WBC scintigraphic findings. The scan was particularly valuable in patients with negative and/or difficult-to-interpret echocardiographic findings due to several circumstances, such as mechanical valve implants or the presence of huge calcifications (in a diabetic patient undergoing dialysis).

Table 2.5 correlates the results of ^{99m}Tc-HMPAO-WBC scintigraphy and blood culture. The most striking result was a positive scan observed in patients with negative blood culture; such high negative fraction of false-negative result of the blood culture could be linked to high-dose antibiotic therapy.

Table 2.3: Results of ^{99m}Tc-HMPAO-WBC scintigraphy in patients with final diagnosis of IE, stratified according to Duke criteria.

		Positive scan			Negative scan
		cardiac only	cardiac and extracardiac	extracardiac only	
Duke criteria	Definite IE (24/51)	9	11*	0	4
	Possible IE (25/51)	13	11$^{\#}$	1*	0
	Rejected IE (2/51)	1	1*	0	0

(*) with septic embolism consequent to IE
($^{\#}$) 8 patients with septic embolism, 1 with vasculitis, and two false-positive scans due to vertebral crush and metastasis from prostate cancer

Table 2.4 - Results of ^{99m}Tc-HMPAO-WBC scintigraphy in patients with final diagnosis of IE, stratified according to echocardiography (ECHO).

		Positive scan	Negative scan
ECHO	positive (40/51)	35	5
	negative (11/51)	11	0

Table 2.6 shows results of all the diagnostic procedures in patients without IE. Out of the 50/80 patients without IE who exhibited a positive ^{99m}Tc-HMPAO-WBC scintigraphy (only at extracardiac sites), the scan correctly classified such patients as having either osteomyelitis (n=22), peripheral vascular graft infection (n=12), lung infection (n=7), mediastinitis (n=5), or cholecystitis (n=2). In 2 cases focal uptake of the radiolabeled leukocytes in the spine was falsely positive for infection, as it was due to vertebral crush caused by osteoporosis in one case, by metastasis from a melanoma with unknown primary site in the other case.

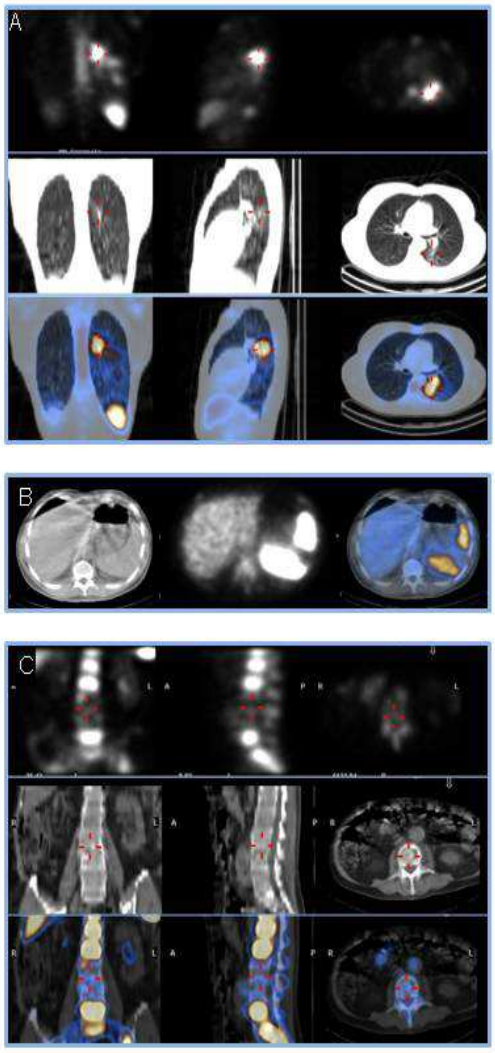

Figure 2.4 - Examples of septic embolism at different sites as detected by ^{99m}Tc-HMPAO-WBC SPECT/CT. (A) Patient with septic embolism in the left lung (coronal, sagittal and transaxial CT sections in left panels, fused SPECT/CT sections in middle panels, and SPECT sections in right panels). (B). Patient with spetic embolism in the spleen, where infection shows as a photopenic area in the splenic parenchyma (transaxial CT section in left panel, fused SPECT/CT section in center panel, SPECT in right panel). (C) Patient with septic embolism in the spine (coronal, sagittal and transaxial CT sections in left panels, fused SPECT/CT sections in middle panels, and SPECT sections in right panels). Similarly as in the case of the spleen, infection shows as a photopenic area which in this patient involves two vertebral bodies.

Table 2.5 - Results of ^{99m}Tc-HMPAO-WBC scintigraphy in patients with final diagnosis of IE, stratified according to blood culture.

		Positive scan			Negative scan
		cardiac only	cardiac and extracardiac	extracardiac only	
Blood culture	positive (32/51)	15	14*	0	3
	negative (19$^{\#}$/51)	8	9§	1	1

(*) 11/14 with septic embolism consequent to IE and two false-positive scans due to vertebral crush
($^{\#}$) during antibiotic therapy in 44/64 patients
(§) 8/9 with septic embolism consequent to IE and one false-positive scan due to vasculitis

Table 2.6: Results of all the diagnostic procedures in the 80 patients without IE (ECHO = echocardiography).

		^{99m}Tc-HMPAO-WBC scintigraphy	
		Positive scan*	Negative scan
ECHO	positive (n = 3/80)	0	3
	negative (n = 77/80)	0	77
Blood culture	positive (n = 35/80)	26	9
	negative (n = 45/80)	24	21
Dukes criteria	Definitive IE (n = 4)	4	0
	Possible IE (n =30)	19	11
	Rejected IE (n =46)	27	19

*all patients presented only with extracardiac sites of radiopharmaceutical uptake

Discussion

The diagnosis of IE is becoming progressively more challenging due to a variety of factors. These include the indiscriminate use of antimicrobial agents in some clinical settings, the increased proportion of individuals with predisposing and/or underlying conditions (i.e., frail and elderly, immunosuppressed persons), as well the increasing number of interventional cardiovascular procedures and placement of valve prosthesis, intravascular, or cardiac devices. Mortality of IE remains high when this condition is undiagnosed, therefore not adequately treated (*14*). Early diagnosis and prompt institution of appropriate antibiotic therapy reduce septic embolism

and mortality (*15*); therefore, the identification of patients at highest risk of death may offer the opportunity to change the course of the disease and improve prognosis.

Because of the ability to detect endocardial vegetations (*16*), abscess (*17*) as well as intra-cardiac complications (i.e., valve perforation and chordal rupture) (*18*), echocardiography is the indirect method of choice for investigating patients with clinical suspicion of IE (*19,20*). Furthermore, some echocardiographic features such as vegetation size (higher risk for lesions >10 mm in diameter and for vegetations that are increasing in size), number (multiple) and features (mobile but pedunculated, noncalcified, prolapsing) (*20*) may be also used to predict the potential embolic burden of IE. However, the presence of prosthetic valves consistently decreases sensitivity and specificity of echocardiography, to about 20% for TTE and around 90% (in the hands of an experienced operator) for TEE (*8*). In approximately 15% of the cases, echocardiography can be false positive (because thickened valves, nodules, or valvular calcifications are misinterpreted as vegetations) (*4*), while a similar proportion can be false negative (*4*). Thus, echocardiographic findings alone cannot always definitely confirm nor exclude the clinical suspicion of IE. Since echocardiography represent the backbone of Duke criteria, this suboptimal diagnostic accuracy translates into a relatively high proportion of the cases classified as "possible" IE; yet, about 24% of such cases are eventually diagnosed to have indeed IE (*5*).

Additional potentially misleading factors in the Duke's classification include some well-known pitfalls in blood culture (antimicrobial treatment, subacute right-sided and mural endocarditis (*21*), fungi, slow-growing and difficult to identify organisms) (*22*), and ambiguous symptoms without any of the classical stigmata of valvular infection.

A functional imaging modality such as radionuclide imaging, capable of characterizing specific features of the endocardial vegetations, may contribute to solve clinical dilemmas in such conditions. In our experience, when the results of ^{99m}Tc-HMPAO-WBC scintigraphy were associated with either a positive echocardiography or a positive blood culture no cases of IE went undiagnosed. In particular, the radiolabeled leukocyte scan facilitated the diagnosis of IE in challenging situations for echocardiography, as in the presence of mechanical prosthetic valve, anuloplasty rings, calcifications, and/or nonbacterial thrombotic vegetations. Furthermore, ^{99m}Tc-HMPAO-WBC scintigraphy allowed to exclude valve infection in patients with concomitant risk factors, non-diagnostic echocardiographic findings, positive

blood cultures (37% of the cases in our series), or to identify other focal infections different from IE (as occurred in 38% of the overall 131 patients). ^{99m}Tc-HMPAO-WBC scintigraphy can therefore be considered as the second-line test of choice in patients with prosthetic valve/device, fever, positive blood cultures and equivocal TTE/TEE findings.

This study confirms that ^{99m}Tc-HMPAO-WBC scintigraphy is a crucial imaging modality also for localizing sites of infection in patients with symptoms and signs and laboratory findings of sepsis (increased ESR, CRP, and WBC count) (*12*) with either a positive or a negative blood culture. In these patients generally neither TEE nor TTE are used for screening purposes (*4*) and, therefore, the heart region should always be carefully evaluated when analysing the ^{99m}Tc-HMPAO-WBC scan.

The possibility of acquiring whole-body images and additional planar and SPECT/CT spot images constitutes an invaluable aid for detecting septic embolism and metastatic sites of infection, as observed in our patients population. In particular, septic embolism was detected even in the absence of the typical echocardiographic predictors of systemic embolism (*8,20*).

These results refer only to patients with IE arising on native and prosthetic valves since we intentionally excluded patients with device related infection. In fact, we consider not possible to apply the same diagnostic algorithm intended for IE to this different clinical entity.

Specific methodology-related issues must be properly addressed in order to ensure adequate scintigraphic acquisitions. Images should be acquired in time-mode, compensating for isotope decay at each time point. In case of equivocal findings at 6 hours SPECT/CT imaging of the thorax, images should be repeated also at 24 hours. Images should be analysed using the same scale frame to easily identify any focal area of activity that increases over time or modifies its shape from early to late images. Both CT-attenuation corrected and non-corrected images should be always inspected side by side, to minimise metal-related artefacts. Quantitative analysis of target/background (T/B) ratios was not necessary in these patients. SPECT/CT is mandatory to correctly interpret and localize sites and extension of radiolabeled leukocyte uptake indicating infection (*23*), to discriminate involvement of the heart valve or prosthesis from uptake around the prosthesis. Furthermore, in cases with positive scintigraphy in the cardiac region SPECT/CT imaging can discriminate endocardial infections from all other possible causes of post-surgical fever, i.e., mediastinitis, osteomyelytis of the sternum or ribs, wound infections.

No false positive findings were found, particularly in patients with early IE evaluated within the first two months from the surgical procedure, suggesting that adequate acquisition protocol and interpretation criteria can optimize specificity of the scan also in this clinical setting. On the other hand, the false negative scans observed in presence of IE sustained by *Candida* spp. or *Enterococcus* spp. may be explained by the ability of these micro-organisms (as well as others such as *S. epidermis*) of forming a "biofilm" that results in resistance to antimicrobial treatment and escape from the host defence mechanisms (*24*). Additionally, altered neutrophil recruitment at the primary site of IE by *E. faecalis* extracellular proteases constitute a further mechanism of innate immune response impairment (*25*). Such mechanisms might reduce sensitivity of scintigraphy with radiolabeled leukocytes in patients with IE. However, in our experience the reduced sensitivity of ^{99m}Tc-HMPAO-WBC scintigraphy was counterbalanced by the association with echocardiography.

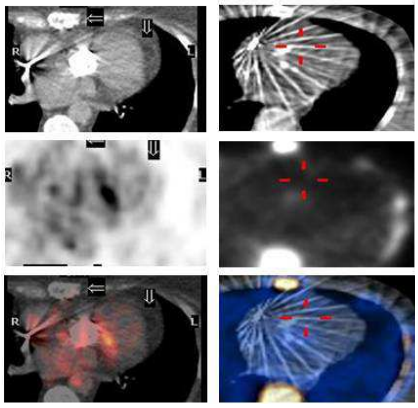

Figure 2.5 - False positive [^{18}F]FDG PET/CT result in a patient with fever. The area of increased [^{18}F]FDG uptake suspected for endocarditis at a mitral valve mechanical prosthesis (A, central panel fused transaxial PET/CT and right panel PET stand alone) turned out to be negative in the ^{99m}Tc-HMPAO-WBC SPECT/CT (B; central panel fused transaxial SPECT/CT and right panel SPECT) clinical follow-up confirmed the absence of infection. Left column, CT transaxial image.

Both false negative and false positive findings were also observed in our patients' group regarding distant septic embolism. In particular, the typical ^{99m}Tc-HMPAO-WBC scintigraphic pattern of spleen embolism and spondilodiscitis represented by a cold spot (*26*) may be also present in other benign or malignant conditions. Thus, despite highly suggestive for septic embolism, such finding in patients with IE should be confirmed with additional diagnostic imaging, as MRI. Finally, it is reasonable to assume that the availability of new generation SPECT/CT scanners with a more advanced CT component will further increase diagnostic accuracy, particularly when evaluating the CNS and bone. Alternatively, PET/CT imaging may be proposed to improve spatial resolution. In this regard, preliminary data have

demonstrated significant uptake of [^{18}F]FDG both in infected endocardial vegetations and at metastatic sites of infection (*27-30*). However, [^{18}F]FDG uptake is observed in a variety of benign and malignant conditions such as inflammation or tumours (*31*), thus reducing its specificity. Moreover, special caution should be employed when interpreting of [^{18}F]FDG uptake in the cardiac region, due to the high number of possible causes other than IE for a positive scan: recent thrombi (*32*), soft atherosclerotic plaques (*33*), vasculitis (*34*), primary and metastatic cardiac tumors (*35,36*), or simply post-surgical inflammatory reaction (*37*). In the clinical routine, focal areas of [^{18}F]FDG uptake at heart site in the absence of IE are quite commonly observed (unpublished data, see Figure 2.5). The possibility of efficient radiolabelling of autologous leukocytes with positron emitting radionuclides can be expected to change the whole scenario of PET imaging for patients with suspected IE. In this regard, intense [^{18}F]FDG-WBC uptake at the valve site has been described for the only patient with IE ever reported up to now (*38*). Unfortunately, the physical half-life of ^{18}F is too short to encompass the whole kinetics of leukocyte migration into sites of infection, thus making a major limit for the use of this method in this clinical setting.

Conclusion

In conclusion, our experience supports the use of scintigraphy with ^{99m}Tc-HMPAO-WBC in patients with high clinical suspicion of IE, in order to confirm the diagnosis in doubtful circumstances and/or to detect sites of septic embolism. The rate of misdiagnosed IE can be reduced with the use of ^{99m}Tc-HMPAO-WBC (a) in patients with high clinical suspicion but inconclusive echocardiographic findings; (b) for the differential diagnosis between septic and sterile vegetations detected at echocardiography; (c) when echocardiographic, laboratory and clinical data are contradictory, as also to exclude valve involvement (especially of a prosthetic valve) during febrile episodes, sepsis or post-surgical infections.
SPECT/CT is necessary to demonstrate and localize ^{99m}Tc-HMPAO-WBCs at native or prosthetic valves, thus confirming the diagnosis of IE. Furthermore, whole-body images followed by additional planar and SPECT/CT spot images allow to detect distant sites of septic embolism, thus constituting an invaluable aid of this scintigraphic procedure. Negative results in presence of a typical echocardiographic pattern for IE should be carefully evaluated, since false negative findings due to limited spatial resolution or non-leukocyte recruiting microorganisms can be encountered.

References

1. Tleyjeh IM, Steckelberg JM, Murad HS, et al. Temporal trends in infective endocarditis: a population-based study in Olmsted Country, Minnesota. JAMA 2005;293:3022-3028.
2. Durante-Mangoni E, Bradley S, Selton-Suty C, et al. Current features of infective endocarditis in elderly patients: results of the International Collaboration on Endocarditis Prospective Cohort Study. Arch Intern Med. 2008;168:2095-2103.
3. Bayer AS, Bolger AF, Taubert KA, et al. Diagnosis and management of infective endocarditis and its complications. Circulation. 1998;98:2936-2948.
4. Durack DT, Lukes AS, Bright DK. New criteria for diagnosis of infective endocarditis: utilization of specific echocardiographic findings. Duke endocarditis service. Am J Med. 1994;96:200-209.
5. Habib G, Derumeaux G, Avierinos JF, et al. Value and limitations of the Duke criteria for the diagnosis of infective endocarditis. J Am Coll Cardiol. 1999;33:2023-2029.
6. Li JS, Sexton DJ, Mick N, et al. Proposed modifications to the Duke criteria for the diagnosis of infective endocarditis. Clin Infect Dis. 2000;30:633-638.
7. Habib G, Hoen B, Tornos P, et al. Guidelines on the prevention, diagnosis, and treatment of infective endocarditis (new version 2009): the Task Force on the Prevention, Diagnosis, and Treatment of Infective Endocarditis of the European Society of Cardiology (ESC). Endorsed by the European Society of Clinical Microbiology and Infectious Diseases (ESCMID) and the International Society of Chemotherapy (ISC) for Infection and Cancer. Eur Heart J. 2009;30:2369-2413.
8. Cahn-Hidalgo DG, Cappuccio JD. Infective endocarditis. In: Edgar R. Black, eds, Diagnostic Strategies for Common Medical Problems. East Pretoria, IL: Versa Press Inc: 1999:280-290.
9. Chelazzi C, Selmi V, Vitali L, De Gaudio AR. Infections of cardiac implantable electronic devices: etiology, prevention and treatment. In: Vonend O, Eckert S, eds. Aspects of Pacemakers – Functions and Interactions in Cardiac and Non-Cardiac Indications. Rijeka, Croatia: InTech: 2011: 127-141.
10. Raoult D, Casalta JP, Richet H, et al. Contribution of systematic serological testing in diagnosis of infective endocarditis. J Clin Microbiol 2005;43:5238-5242.
11. Roca M, Martín-Comín J, Becker W, et al. A consensus protocol for white blood cells labelling with technetium-99m hexamethylpropylene amine oxime. International Society of Radiolabeled Blood Elements (ISORBE). Eur J Nucl Med. 1998 Jul;25:797-799.
12. de Vries EF, Roca M, Jamar F, Israel O, Signore A. Guidelines for the labelling of leucocytes with 99mTc-HMPAO. Inflammation/Infection Taskgroup of the European Association of Nuclear Medicine. Eur J Nucl Med Mol Imaging. 2010;37:842-848.
13. Palestro CJ, Brown ML, Forstrom LA, et al. Society of Nuclear Medicine Procedure Guideline for 99mTc-exametazime (HMPAO)-labeled leukocyte scintigraphy for

suspected infection/ inflammation, version 3.0, 2004, http://interactive.snm.org/docs/HMPAO_v3.pdf.
14. Baddour LM, Wilson WR, Bayer AS, et al. Infective endocarditis: diagnosis, antimicrobial therapy, and management of complications: a statement for healthcare professionals from the Committee on Rheumatic Fever, Endocarditis, and Kawasaki Disease, Council on Cardiovascular Disease in the Young, and the Councils on Clinical Cardiology, Stroke, and Cardiovascular Surgery and Anesthesia, American Heart Association: endorsed by the Infectious Disease Society of America. Circulation. 2005;111:e394-434.
15. Vilacosta I, Graupner C, San Roman JA, et al. Risk of embolization after institution of antibiotic therapy for infective endocarditis. J Am Coll Cardiol. 2002;39:1489-1495.
16. Evangelista A, Gonzalez-Alujas MT. Echocardiography in infective endocarditis. Heart 2004;90:614-617.
17. Hill EE, Herijgers P, Claus P, Vanderschueren S, Peetermans WE, Herregods MC. Abscess in infective endocarditis: the value of transesophageal echocardiography and outcome: a 5-year study. Am Heart J. 2007;154:923-928.
18. Murphy JG, Foster-Smith K. Management of complications of infective endocarditis with emphasis on echocardiographic findings. Infect Dis Clin North Am. 1993;7:153-165.
19. Habib G, Badano L, Tribouilloy C, et al. Recommendations for the practice of echocardiography in infective endocarditis. Eur J Echocardiogr. 2010;11:202-219.
20. Di Salvo G, Habib G, Pergola V, et al. Echocardiography predicts embolic events in infective endocarditis. J Am Coll Cardiol. 2001;37:1069-1076.
21. Brouqui P, Raoult D. Endocarditis due to rare and fastidious bacteria. Clin Microbiol Rev. 2001;14:177-207.
22. Lamas CC, Eykyn SJ. Blood culture negative endocarditis: analysis of 63 cases presenting over 25 years. Heart. 2003;89:258-262.
23. Ingui CJ, Shah NP, Oates ME. Infection scintigraphy: added value of single-photon emission computed tomography/computed tomography fusion compared with traditional analysis. J Comput Assist Tomogr. 2007;31:375-380.
24. Cheung GY, Rigby K, Wang R, Queck SY, et al. Staphylococcus epidermidis strategies to avoid killing by human neutrophils. PLoS Pathog. 2010;6:e1001133.
25. Thurlow LR, Thomas VC, Narayanan S, et al. Gelatinase contributes to the pathogenesis of endocarditis caused by Enterococcus faecalis. Infect Immun. 2010; 11:4936-4943.
26. Love C, Palestro CJ. Radionuclide imaging of infection. J Nucl Med Technol. 2004;32:47-57.
27. Vind SH, Hess S. Possible role of PET/CT in infective endocarditis. J Nucl Cardiol. 2010;17:516-519.

28. Yeh CL, Liou JY, Chen SW, Chen YK. Infective endocarditis detected by ^{18}F-fluoro-2-deoxy-D-glucose positron emission tomography/computed tomography in a patient with occult infection. Kaohsiung J Med Sci. 2011;27:528-531.
29. Bertagna F, Bisleri G, Motta F, et al. Possible role of F18-FDG-PET/CT in the diagnosis of endocarditis: preliminary evidence from a review of the literature. Int J Cardiovasc Imaging. Nov 26, 2011 [Epub ahead of print].
30. Gheysens O, Lips N, Adriaenssens T, et al. Septic pulmonary embolisms and metastatic infections from methicillin-resistant Staphylococcus aureus endocarditis on FDG PET/CT. Eur J Nucl Med Mol Imaging. 2012;39:183.
31. Maurer AH, Burshteyn M, Adler LP, Steiner RM. How to differentiate benign versus malignant cardiac and paracardiac 18F FDG uptake at oncologic PET/CT. Radiographics. 2011;31:1287-1305.
32. Shreve PD, Anzai Y, Wahl RL. Pitfalls in oncologic diagnosis with FDG PET imaging: physiologic and benign variants. Radiographics. 1999;19:61-77.
33. Williams G, Kolodny GM. Retrospective study of coronary uptake of 18F-fluorodeoxyglucose in association with calcification and coronary artery disease: a preliminary study. Nucl Med Commun. 2009;30:287-291.
34. Kobayashi Y, Ishii K, Oda K, et al. Aortic wall inflammation due to Takayasu arteritis imaged with 18F-FDG PET coregistered with enhanced CT. J Nucl Med. 2005;46:917-922.
35. Kaderli AA, Baran I, Aydin O, et al. Diffuse involvement of the heart and great vessels in primary cardiac lymphoma. Eur J Echocardiogr. 2010;11:74-76.
36. García JR, Simo M, Huguet M, Ysamat M, Lomeña F. Usefulness of 18-fluorodeoxyglucose positron emission tomography in the evaluation of tumor cardiac thrombus from renal cell carcinoma. Clin Transl Oncol. 2006;8:124-128.
37. Abidov A, D'agnolo A, Hayes SW, Berman DS, Waxman AD. Uptake of FDG in the area of a recently implanted bioprosthetic mitral valve. Clin Nucl Med. 2004;29:848.
38. Dumarey N, Egrise D, Blocklet D, et al. Imaging infection with 18F-FDG-labeled leukocyte PET/CT: initial experience in 21 patients. J Nucl Med. 2006;47:625-632.

Chapter 3

Radiolabeled leukocyte scintigraphy in the diagnostic workup of patients with suspected cardiac device-related infections

Paola A. Erba[1,2], MD, Martina Sollini[2*], MD, Umberto Conti[3], MD, Francesco Bandera,[4**] MD, Carlo Tascini[5], MD, Salvatore M. De Tommasi[**], MD, Giulio Zucchelli[3], MD, Roberta Doria[5], MD, Francesco Menichetti[5], MD, MariaGrazia Bongiorni[3], Elena Lazzeri[1], MD and PhD and Giuliano Mariani[1], MD

[1] Regional Center of Nuclear Medicine, Department of Translational Research and Advanced Technologies in Medicine, University of Pisa, Pisa, Italy
[2] Nuclear Medicine Unit, Department of Oncology and Advanced Technology, Arcispedale S. Maria Nuova – IRCCS, Reggio Emilia, Reggio Emilia, Italy
[3] Division of Cardiology, University Hospital of Pisa, Pisa, Italy
[4] Heart Failure Unit, IRCCS Policlinico San Donato, Milano
[5] Division of Infectious Diseases, University Hospital of Pisa, Pisa, Italy
* Formerly with the Regional Center of Nuclear Medicine, University of Pisa, Pisa, Italy
** Formerly with the Division of Cardiology, University Hospital of Pisa, Pisa, Italy

J Am Coll Cardiol Img. 2013; 6:1075-1086

Abstract

Objectives: We investigated the diagnostic performance of ^{99m}Tc-HMPAO-labeled autologous leukocyte (^{99m}Tc-HMPAO-WBC) scintigraphy in patients with suspected infections of cardiovascular implantable electronic devices (CIED). Background: Early, definite recognition of CIED infections combined with accurate localization and quantification of disease burden is a prerequisite for optimal treatment strategies. Methods All 63 consecutive patients underwent clinical examination, blood chemistry, microbiology and echography of the cardiac region/venous pathway of the device. Final diagnosis of infection was established in 32/63 patients, in 23/32 by microbiology. Results: ^{99m}Tc-HMPAO-WBC SPECT/CT had 94% sensitivity for both detection and localization of CIED-associated infection. SPECT/CT imaging had a definite added diagnostic value over both planar and stand-alone SPECT. Pocket infection was often associated with lead(s) involvement; the intracardiac portion of the lead(s) more frequently exhibited ^{99m}Tc-HMPAO-WBC accumulation and presented the highest rate of complications, infectious endocarditis and septic embolism. Two false-negative cases and no false positive results were observed. None of the patients with negative ^{99m}Tc-HMPAO-WBC scintigraphy develop CIED infection during follow-up until 12 months. Echography of the cardiac region/venous pathway of the device had 90% specificity, but low sensitivity (81%, when considering only intracardiac lead(s) infection). The Duke criteria had 31% sensitivity for the “definite” category (100% specificity) and 81% for the “definite+possible” categories (77% specificity). Conclusions: ^{99m}Tc-HMPAO-WBC scintigraphy enabled to confirm the presence of CIED-associated infection, to define the extent of device involvement, and to detect associated complications. Moreover, ^{99m}Tc-HMPAO-WBC scintigraphy reliably excluded device-associated infection during a febrile episode and sepsis, with 95% negative predictive value.

Key words: cardiac device infection, ^{99m}Tc-HMPAO-WBC, SPECT/CT, disease burden.

Introduction

Use of cardiovascular implantable electronic devices (CIED) has increased significantly over the last decade due to growing evidence of improved quality of life and survival among certain groups of patient (1); such devices include permanent pacemakers (PM), the implantable cardioverter/defibrillators (ICD), and cardiac resynchronization therapy devices. Associated complications, particularly infections, have risen disproportionally higher than the growth of newly implanted devices (2). The rate of CIED infections varies widely between 1% and 7% (3), with significant morbidity and mortality especially in case of delayed diagnosis (4). Therefore, strategies to facilitate early diagnosis are crucial for favorable clinical outcome.

Diagnostic workup of CIED infections is problematic, since patients can present with a variety of manifestations including subtle signs of systemic or local infection (5). The decision whether to medically treat or to remove the device represents a further crucial point, also because it implies evaluation of response to antimicrobial therapy and selection of the optimal time to re-implant (6).

Final diagnosis of CIED infection is generally based on microbiological tests (blood cultures and culture of material from exposed sites of implantation) and ultrasound evaluation of the cardiac region (either transthoracic and transesophageal) and of the venous pathway of the device. The above tests constitute the basis for defining the patients' likelihood to have CIED according to the Duke criteria (7). However, in case of CIED infections the Duke criteria, originally developed for the diagnosis of infectious endocarditis, may be inadequate; even with the addition of clinical parameters (8), the possibility remains high of missing the presence and/or underestimating the extent of infection (5).

Evidence is growing that positron emission tomography co-registered with computed tomography using ^{18}F-labelled fluorodeoxyglucose ([^{18}F]FDG PET/CT) improves the diagnosis of CIED infections (9-11). On the other hand, in the era of high spatial resolution hybrid systems for single photon emission tomography co-registered with computed tomography (SPECT/CT), scintigraphy with radiolabeled autologous leukocytes represents a valuable option for imaging patients with suspected CIED infections, as already demonstrated in a number of other clinical conditions such as native and prosthetic valve endocarditis (12). These functional imaging modalities are based on the ability to detect and localize metabolically active cells, such as

those involved in inflammation and infection. By following the pattern of radiolabeled leukocyte accumulation over time and by using well-defined interpretation criteria (13), it is possible to discriminate active infection from inflammatory changes (e.g., post-surgical changes, foreign body reactions) and to define the extent of active infection.

In this study we investigated the diagnostic performances of radiolabeled leukocyte scintigraphy in suspected CIED infection, by evaluating with ^{99m}Tc-hexamethypropylene amine oxime labeled autologous leukocytes (^{99m}Tc-HMPAO-WBC) SPECT/CT all consecutive patients referred to the Division of Cardiology or Infectious Diseases of our hospital because of such condition.

Material and methods

Study design and patient population

Between June 2007 and June 2011 a total of 63 consecutive patients (47 men and 16 women with mean age 68.6±13.9 years, median age 70, range 27-87) were referred for scintigraphy with radiolabeled autologous leukocytes (^{99m}Tc-HMPAO-WBC), recording both planar and SPECT/CT acquisitions and results were retrospectively evaluated. All patients provided informed consent to the procedure. Patients workout consisted of clinical examination, blood chemistry including WBC counts, C-reactive protein, erythrocyte sedimentation rate, acute phase proteins, electrophoresis, urine-analysis, transthoracic and transesophageal echocardiography (TTE and TEE, respectively), and ultrasound evaluation of the venous pathway. Three sets of peripheral venous blood samples were obtained for cultures, including at least one aerobic and one anaerobic (14). Scintigraphy was performed in all cases of unconfirmed diagnosis of CIED-infection at the end of the described conventional procedures. After ^{99m}Tc-HMPAO-WBC, treatment was decided on the basis of the degree of certainty of the CIED infection diagnosis as results of conventional tests and clinical guidelines: 35 patients were treated with either device extraction followed by antimicrobial therapy as previously described (15) , 9 patients with antimicrobial therapy alone, 11 patients with other disease-specific surgical procedures. Eight patients received no treatment. Results of ^{99m}Tc-HMPAO-WBC was not used to guide the final decision on the management of patients when a high clinical suspicion of CIED-infection based on either a diagnostic echocardiography (n=7) or a positive blood-culture (n=12) was present since these patients underwent

device extraction followed by antimicrobial therapy (see Figure 3.1). In cases of antimicrobial therapy alone or no treatment, clinical follow-up of at least 12 months was available for final classification. All 9 patients undergoing antimicrobial therapy alone repeat 99mTc-HMPAO-WBC scintigraphy at the end of the standard antimicrobial therapy. A total of 75 exams were therefore performed, 63 baseline and 12 follow-up studies; in particular, 9 patients had repeat studies (6 with one follow-up scan 6 months apart, 3 with two follow-up scans at 6-9 and 12 months apart).

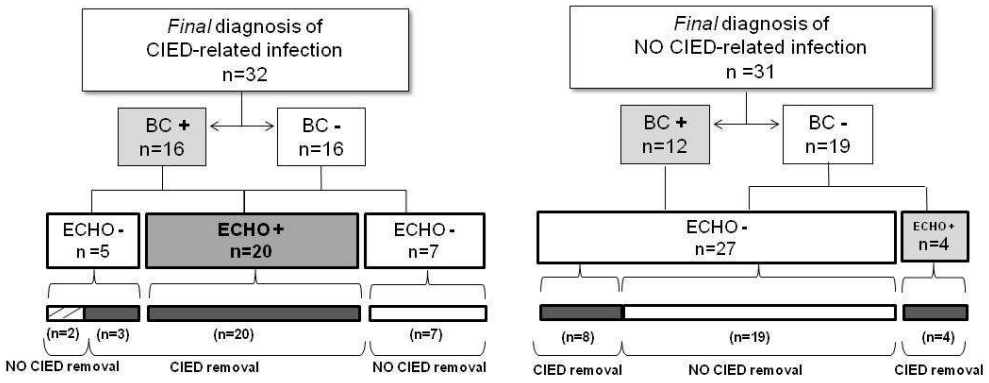

Figure 3.1 – Schematic representation of the clinical management of patients included in the study according to the final diagnosis of CIED-related infection (left panel) or exclusion of CIED-related infection (right panel). BC = blood culture; ECHO = echocardiography.

The main clinical features of patients and type of devices implanted are reported in Table 3.1.

Final diagnosis of CIED-associated infection was established in 32/63 patients (see Table 3.2); in 23 of these 32 patients diagnosis was confirmed by microbiology after extraction of the device. In the remaining 9/32 cases the diagnosis was obtained with clinical follow-up of at least 12 months based on negative finding at clinical examination, sequential blood tests, TTE/TEE, ultrasound evaluation of the venous pathway and ^{99m}Tc-HMPAO-WBC scintigraphy following antimicrobial treatment.

Staphylococcus spp. was the microorganism more frequently responsible for CIED-associated infection (12/32), followed by Streptococcus spp. (8/32), Enterococcus spp. (3/32), Enterobacteriaceae spp., Micrococcus and Candida (2 each); P. aeruginosa, Acinetobacter baumanni, Propionibacter Acnes were identified in 1 patient each.

Infection occurred most frequently early after implant (6/8 of patients evaluated <1 month and 5/13 cases evaluated 1-3 months after implantation). Semi-late and late infections were observed in 8/18 and in 13/22 patients, respectively (see Table 1). Nineteen out of the 32 infections occurred after the second implantation procedure.

Table 3.1 – Type of cardiac devices and main clinical features of the patients included in the study (PM = pace-maker; ICD = implantable cardioverter defibrillator; ESR = erythrocyte sedimentation rate; CRP = C-reactive protein).

Type of device	single-chamber PM	dual-chamber PM	temporary PM	single-chamber ICDs	dual-chamber ICDs
	30/63 (48%)	17/63 (27%)	2/63 (3%)	9/63 (14%)	5/63 (8%)
Infection rate	12/30 (40%)	7/17 (41%)	1/2 (50%)	7/9 (78%)	3/5 (60%)
Risk factors	Diabetes	Renal failure	Long term corticoid	Previous infection	Recent invasive procedures
	17/63 (27%)	11/63 (17%)	7/63 (11%)	8/63 (13%)	30/63 (48%)
Fever	Present	Absent			
	35/63 (55%)	28/63 (45%)			
Time from device implant (months)	≤ 1	1-3	4-12	> 12	
	10/63 (16%)	13/63 (21%)	18/63 (28%)	22/63 (35%)	
Infection rate	6/8 (75%)	5/13 (38%)	8/18 (44%)	13/22 (59%)	
Local inflammation signs/symptoms	Pain	Tenderness	Erythema	Purulent drainage	
	16/63 (25%)	14/63 (22%)	8/63 (13%)	3/63 (5%)	
Blood tests	ESR	PCR	Leukocytosis		
	49/63 (77%)	42/63 (67%)	29/63 (46%)		
Microbiological results		Positive	Negative		
	Blood culture	28/63 (44%)	37/63 (56%)*		

* during antibiotic therapy in 29/63 patients; 5 patients presented either positive EC or pocket culture

Table 3.2 - Results of microbiological evaluation/culture in the 32 patients with CIED-associated infections

Microbiological results		
	Positive	Negative
Blood culture	16/32 (50%)	16/32 (50%)*
Microbiology after device removal**	23/32 (74%)	-

* during antibiotic therapy in 8/16 patients
** extraction was performed in a total of 35 patients including 11 resulting without CIED associated infection; 9/32 patients with CIED infection did not undergo extraction

Radiolabeling and acquisition protocol

Autologous radiolabelled WBCs were prepared according to the EANM Guidelines for labeling leukocytes with 99mTc-HMPAO (16, 17). Radiolabelling efficiency was always between 70-85%;viability of the radiolabelled leukocytes was always evaluated by the Tripan blue exclusion test before reinfusion. Radiolabelling of leukocytes with ^{99m}Tc was preferred over the radiolabelling with 111In for both radiation safety (0.017 mSv/MBq with a recommended administered activity of 185-370 Mbq for ^{99m}Tc versus 0.59 mSv/MBq with a recommended administered activity of 10-18.5 Mbq for 111In) (13,18) and imaging quality when performing SPECT/CT.

Whole body and spot planar images were obtained after 30 minutes, then 4-6 (early images) and 20-24 hours (delayed images) after reinfusion of 370-555 MBq of ^{99m}Tc-HMPAO-WBC. SPECT/CT of the chest was performed in all patients at 6 hours and repeated at 24 hours in case of negative or doubtful imaging at 6 hours. Images were acquired using a dual-head, variable-angle SPECT/CT gamma camera (Hawkeye and Discovery 670, GE Healthcare) as previously reported (12). Both CT-attenuation corrected and non-corrected SPECT images were evaluated in the coronal, transaxial, and sagittal planes, as well as in tridimensional maximum intensity projection (MIP) cine mode. Matching pairs of x-ray transmission and radionuclide emission images were fused using the Xeleris software, and hybrid images of overlying transmission and emission data were generated.

Interpretation criteria

All images were re-evaluated, independently, by two experienced nuclear physicians aware of the patients' clinical history and of the results of prior conventional imaging. Images were first visual inspected to exclude misregistration between the SPECT and the CT components. Thereafter, for all sets of images the presence and location of any focus of abnormal radioactivity accumulation indicating infection was evaluated. The scintigraphic studies were classified as negative when no sites of abnormal uptake were observed in the SPECT/CT images, or positive for infection when at least one focus of abnormal uptake characterized by time-dependent increase in radioactivity between early and delayed images was observed (13). When present, focal uptake indicating infection was further classified as: a) isolated pocket infection; b) isolated lead infection at either the intravascular or the intracardiac portion of the lead; c) pocket and lead infection (either intravascular or intracardiac portion); d) concomitant endocarditis; e) extracardiac sites of infection consistent with embolism; f) other infections.

Data Analysis

Results of ^{99m}Tc-HMPAO-WBC scintigraphy were correlated with those of ultrasonography (echocardiography + soft tissue/venous ultrasound), with the Duke criteria classification and with final microbiological or clinical diagnosis. Furthermore, the ability to identify concomitant endocarditis as well septic emboli was considered, in order to assess the ability of ^{99m}Tc - HMPAO-WBC scintigraphy to define disease burden.
For the site-based analysis, results of the planar, stand-alone SPECT and SPECT/CT images were compared. Stand-alone SPECT and SPECT/CT were considered to have a definite added value when they provided data that could not be obtained from planar imaging concerning the presence of infection or its precise location. The contribution of SPECT/CT was considered with special attention to the possibility of anatomically localizing the exact site of infection.

Statistical analysis

All values are expressed as median and range, as customary for nonparametric data. The Pearson's $\chi 2$ test was employed for comparing

nominal data between groups. The interobserver agreement was determined and expressed in a weighted kappa which corrects for agreement by chance. The higher the kappa, the higher the agreement, with a maximum of 1.0: <0 = no agreement, 0.0–0.19 = poor agreement, 0.20–0.39 = fair agreement, 0.40–0.59 = moderate agreement, 0.60–0.79 = substantial agreement, 0.80–1.00 = almost perfect agreement (19). In case of disagreement between the two observers a final consensus reading was performed. Sensitivity, specificity, accuracy, positive predictive value and negative predictive values of echocardiography, Duke's criteria and ^{99m}Tc-HMPAO-WBC planar, stand-alone SPECT, and SPECT/CT imaging were calculated based on the final diagnosis with 95% confidence intervals and compared using the McNemar test.

Results

^{99m}Tc-HMPAO-WBC scintigraphy in patients with CIED related infections

By adopting the interpretation criteria described above for scintigraphic detection of infection evaluating the best-performing imaging, i.e., SPECT/CT, it was possible to classify all the scans as either frankly positive or frankly negative, therefore without any equivocal result. The kappa value for interobserver agreement was 0.951 (95% CI; 0.909–1.000).
The ^{99m}Tc-HMPAO-WBC scans were totally negative in 22/63 cases. At least one area with focal accumulation of the radiolabeled leukocytes was detected in the remaining 41 patients.
^{99m}Tc-HMPAO-WBC scintigraphy was true positive in 30/32 patients with final diagnosis of CIED-associated infection (94%). The two false negative scans were observed in patients with CIED infections caused by Candida and Enterococcus (final diagnosis obtained by culture of the leads). One of these two patients also had false negative echocardiography and was classified as "rejected" infection according to the Duke criteria; the second false-negative scintigraphy case was true positive at echocardiography and classified as "definite" infection according to the Duke criteria. Both the latter patients were under antimicrobial therapy at the time of scintigraphy. There were no false positive scans for CIED infection. Figure 3.2 shows an example of positive ^{99m}Tc-HMPAO-WBC scintigraphy for infection localized at the pocket. Figures 3.3 and Figure 3.4 show the scintigrafic pattern of infection localized at the intravascular and intracardiac portion of the leads, respectively.

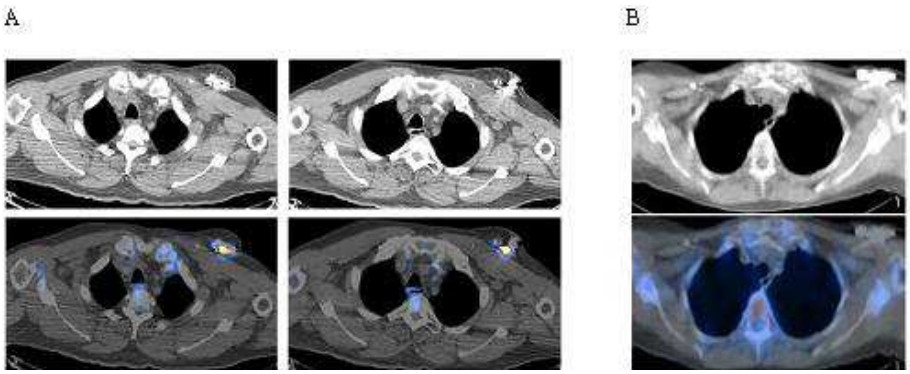

Figure 3.2 - (A) 99mTc-HMPAO-WBC scintigraphy in a patient with localized pocket infection, with transaxial slices shown at different levels (CT sections in upper panel, corresponding fused SPECT/CT sections in lower panel). Obvious focal accumulation of radiolabelled leukocytes at the pocket. (B) A normal scintigraphic pattern is shown for comparison.

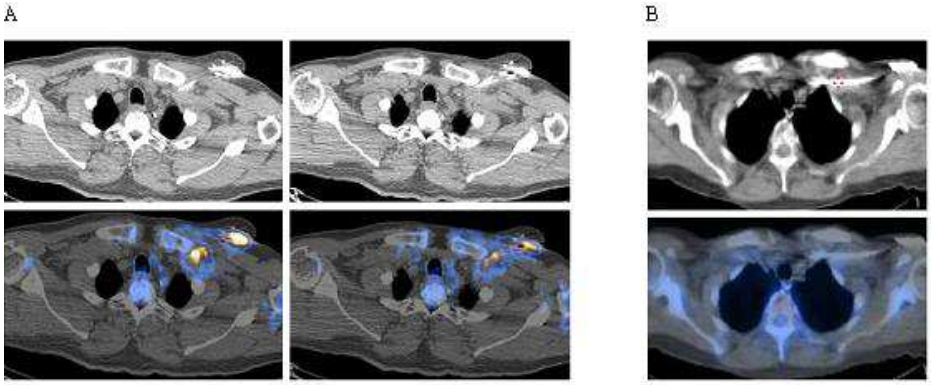

Figure 3.3 - (A) ^{99m}Tc-HMPAO-WBC scintigraphy in a patient with clinically ascertained pocket infection with transaxial slices shown at different levels (CT sections in upper panel, corresponding fused SPECT/CT sections in lower panel). Obvious focal accumulation of radiolabelled leukocytes involving both the pocket and the intravascular portion of the lead. (B) A normal scintigraphic pattern is shown for comparison.

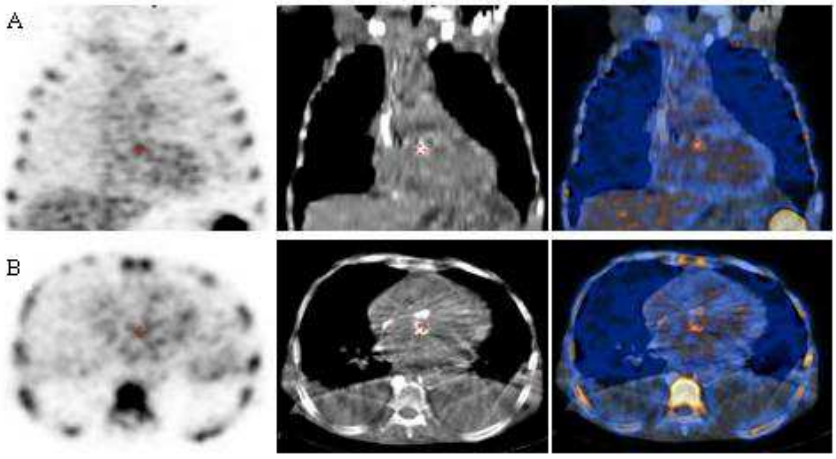

Figure 3.4 - ^{99m}Tc-HMPAO-WBC scintigraphy in a patient with suspected CIED infection. Obvious focal accumulation of radiolabelled leukocytes at the heart region in the SPECT coronal (A left panel) and transaxial images (B left panel); fused SPECT/CT sections exactly localized the focus of infection at the intracardiac lead (right panels). CT images are shown in middle panels.

SPECT/CT acquisition provided higher accuracy both for detecting infection and for localizing ^{99m}Tc-HMPAO-WBC accumulation at any portion of the device, the heart valves or other non-cardiac sites of infection in the thoracic and mediastinal space. SPECT/CT acquisitions changed the final classification of the scan from negative to positive for CIED-associated infection in 15/32 of the cases as compared to the standard planar and 9/32 as compared SPECT-alone acquisition ($\chi^2 = 4.5$, $p = 0.03$, Table 3.3). It should also be noted that no false positive findings due to artifacts were detected in both the attenuation-corrected and the non-attenuation corrected images.
Table 3.4 summarizes the results of ^{99m}Tc-HMPAO-WBC scintigraphy (considering the best nuclear imaging technique i.e. SPECT/CT), of echocardiography and of classification according to Duke criteria in the cases with final diagnosis of CIED infection. Table 3.5 correlates the results of ^{99m}Tc-HMPAO-WBC scintigraphy with the results of echocardiography and with the Duke classification, stratifying the patients according to the site of radiolabeled leukocyte accumulation, as follows: at the pocket, at the intravascular and/or intracardiac portion of the lead(s), at both the pocket and the lead(s). Sites of ^{99m}Tc-HMPAO-WBC accumulation consistent with additional infections (n=38) are also indicated.

Particular attention was paid to identification of concomitant infectious endocarditis (6 cases, see Figure 3.5) and distant septic embolism (osteomyelitis n= 6, vascular graft infection and lung infection n= 4 each, spetic embolism in the spleen n= 1). Septic embolism causing ophtalmitis or cerebral infection (one case each), detected by CT, remained undiagnosed on the radiolabeled leukocyte scan.

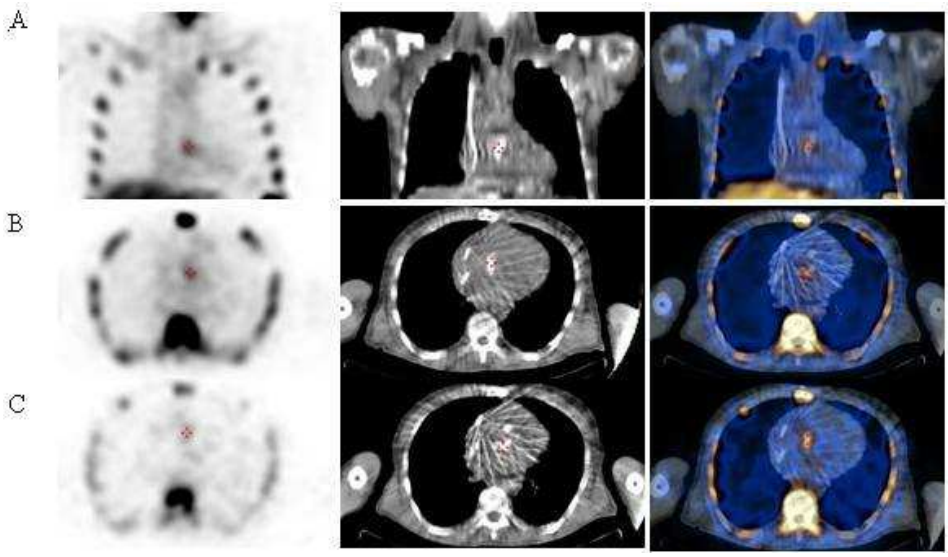

Figure 3.5 - ^{99m}Tc-HMPAO-WBC coronal images (A) and transaxial images at different levels (B and C) in a patient with CIED presenting with positive blood culture and fever three months after mitral valve replacement. SPECT images (left panels) depict focal accumulation of ^{99m}Tc-HMPAO-WBC at both the intracardiac leads (A and B) and the mitral valve mechanical prosthesis (C). SPECT/CT images are shown at right panels and CT images in middle panels.

Table 3.3a: Results of ^{99m}Tc-HMPAO-WBC planar, SPECT and SPECT/CT acquisitions in patients with CIED-associated infection

	Positive for CIED	Doubtful for CIED infection	Negative for CIED infection	Correct extent for device infection	Correct exclusion device involvement	Correct detection of embolism	Correct detection of IE	Positive for other infections	Correct extent for other sites of infection
Planar images	15/32	11/32	6/32	12/32	36/43*	12/18†	3/6	9/15	7/15
SPECT	21/32	9/32	2/32	21/32	42/43	13/18†	4/6	13/15	11/15
SPECT/CT	30/32	-	2/32	30/32	43/43	15/18†	6/6	15/15	15/15

* Including 5 false positive cases due to sternal osteomyelitis and mediastinitis
† Including 3 false negative cases due to ophtalmitis and cerebral infection

Table 3.3b: Diagnostic performances of ^{99m}Tc-HMPAO-WBC planar, SPECT and SPECT/CT acquisitions for the diagnosis of CIED-associated infection.

	Sensitivity	Specificity	Accuracy	Positive Predictive Value	Negative Predictive Value
^{99m}Tc-HMPAO-WBC, planar images*	53.1% (40.2%-65.6%)	83.9% (72%-91.5%)	68.3% (55.2%-79.1%)	77.3% (64.7%-86.5%)	63.4% (50.3%-74.9%)
^{99m}Tc-HMPAO-WBC SPECT images	71.9% (58.9%-82.1%)	96.8% (87.9%-99.4%)	84.1% (72.3%-91.7%)	95.8% (86.6%-99%)	76.9% (64.3%-86.2%)
^{99m}Tc-HMPAO-WBC SPECT/CT images$^{\#}$	93.7% (83.9%-98%)	100% (92.8%-100%)	96.8% (88%-99.4%)	100% (92.8%-100%)	93.9% (84.1%-98.1%)

* planar images *versus* SPECT images $\chi^2 = 0.4$, $p = 0.5$; planar images *versus* SPECT/CT images $\chi^2 = 3.5$, $p = 0.06$, by McNemar test
$^{\#}$ SPECT images *versus* SPECT/CT images $\chi^2 = 4.5$, $p = 0.03$ by McNemar test

Table 3.4: Results of ^{99m}Tc-HMPAO-WBC scintigraphy, echocardiography and Duke criteria according to the final diagnosis of CIED infection or no infection for all the exams performed at baseline (by McNemar test ^{99m}Tc-HMPAO-WBC images *versus* echocardiography $\chi^2 = 2.6$, $p = 0.1$; ^{99m}Tc-HMPAO-WBCimages *versus* Duke Criteria considering as positive for IE the only "Definite" category $\chi^2 = 20$, $p < 0.001$ and *versus* Duke Criteria considering as positive for IE both the "Definite" and "Possible" categories $\chi^2 = 1.3$, $p = 0.25$).

		CIED infection (n =32)	No CIED infection (n =31)	Sensitivity	Specificity	Accuracy	Positive Predictive Value	Negative Predictive Value
^{99m}Tc-HMPAO-WBC	Positive	30/32	0/31	93.7% (83.9%-98%)	100% (92.8%-100%)	96.8% (88%-99.4%)	100% (92.8%-100%)	93.9% (84.1%-98.1%)
	Negative	2/32	31/31					
Echocardiography	Positive	20/32	4/31	62.5% (49.4%-74.1%)	87.1% (75.7%-93.8%)	74.6% (61.8%-84.4%)	83.3% (71.4%-91.1%)	69.2% (56.2%-79.9%
	Negative	12/32	27/31					
Duke Criteria	Definite	10/32	0/31	31.3%* (20.5%-44.3%)	100%* (92.8%-100%)	65.1%* (51.9%-76.4%)	100%* (92.8%-100%)	58.5%* (45.4%-70.5%)
	Possible	16/32	8/31	81.3%# (69%-89.6%)	74.2%# (61.4%-84%)	52.4%# (65.2%-86.9%)	76.5%# (63.8%-85.9%)	79.3%# (66.9%-88.1%)
	Rejected	6/32	23/31					

* Considering as positive for IE the only "Definite" category
# considering as positive for IE both the "Definite" and "Possible" categories.

Table 3.5: Results of ^{99m}Tc-HMPAO-WBC scintigraphy, echocardiography and Duke criteria according to the final diagnosis for all the exams performed at baseline, classified according to the site of radiolabelled leukocytes accumulation at scintigraphy.

		Pocket infection	Leads infection			Pocket + lead infection			
			Intravascular	Intracardiac	Both leads	Intravascular	Intracardiac	Both leads	Other infections
CEID infections (n=32)		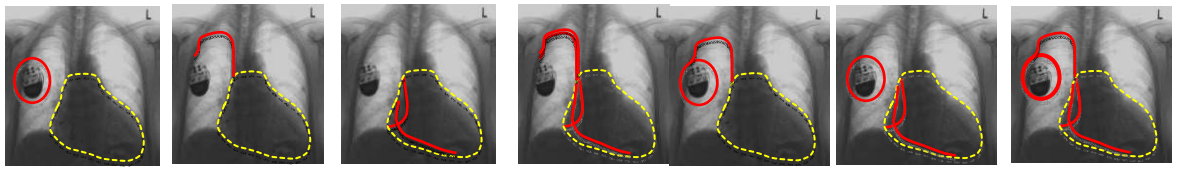							
^{99m}Tc-HMPAO-WBC accumulation		1	1	18*†	2	2	4*	2	15
Echo	pos			14‡	2		2	2	3
	neg	1	1	8‡		2	2		12
Duke criteria	Definite			8			3		
	Possible			13			3		3
	Rejected	1		2			2		12

* with concomitant IE and/or extracardiac localization for a total of 6 cases* and 15 cases †

‡ including one cases of FN at WBC scan

Blood cultures

Blood cultures were positive in only 28/63 of the patients (16/32 of the cases with confirmed CIED infection); 28/35 of the blood-culture negative patients with CIED infection were under antimicrobial treatment at the time of assessment. All the 5 cases of CIED infection with positive blood culture and negative TEE and intact pocket, had a true positive ^{99m}Tc-HMPAO-WBC SPECT/CT examination.
^{99m}Tc-HMPAO-WBC SPECT/CT ruled out device involvement during a febrile episode and sepsis (20/63 with positive blood culture), correctly excluding the presence of device involvement in 31/63 of cases.

^{99m}Tc-HMPAO-WBC scintigraphy in patients without CIED infections

As to the 11 baseline scans showing focal accumulation of radiolabeled leukocytes in patients without CIED infection, scintigraphy actually detected alternative sites of infection occurring in the patients (with sensitivity and specificity of 93% and 91%, respectively, Table 3.6). These patients was subsequently treated according to standard procedures as indicated for the each clinical condition and none of them, including patients with positive blood culture, developed CIED infection during follow-up.

Table 3 6: results of the ^{99m}Tc-HMPAO-WBC scintigraphy in patients with suspected CIED infection where scintigraphy actually detected alternative sites of infection.

Type of infections	
osteomyelitis*	**5**
vascular graft infection	**2**
mediastinitis	**2**
lung infection	**2**
cholecystitis	**2**

* including two spondilodiscitis

Follow-up studies

Follow-up studies performed 6-9 months after the baseline scintigraphy showed the disappearance of all the sites of radiolabeled leukocyte accumulation in 7/9 patients, thus allowing to discontinue antimicrobial treatment in these patients. In the remaining 2 patients ^{99m}Tc-HMPAO-WBC positivity resulted in prolonged medical treatment, that was stopped only

after normalization of a third ^{99m}Tc-HMPAO-WBC scintigraphy performed 6 months later. CIED infection did not recur in any of these patients during subsequent follow-up.

DISCUSSION

Infections of CIEDs are associated with significant morbidity and high death rate, particularly in presence of endovascular infection (20%) (6, 20). The incremental cost for managing CIED infection has been estimated to be about $ 28,676 to $ 53,349 (21), nearly half of this amount being due to intensive care procedures (4). Furthermore, device replacement procedures that are periodically necessary for battery depletion or for upgrading are associated with infection rates higher than those occurring after initial implantation (3).
Early, definite recognition of CIED infection combined with accurate localization and quantification of disease burden could provide a rational basis for adopting optimal treatment strategies, that have so far not been sufficiently defined.
In this work we evaluated a consecutive series of patients in whom the suspicion of CIED infection had been raised on clinical ground. All patients underwent ^{99m}Tc-HMPAO-WBC scintigraphy with the purpose of validating the use of this procedure to confirm CIED infection and to define disease burden, the final diagnosis being obtained either by microbiology in 23/32 or with clinical follow-up of at least 12 months in the remaining cases.
^{99m}Tc-HMPAO-WBC scintigraphy had 94% sensitivity and no false positive results were found, thus confirming the validity of the interpretation criteria adopted (increasing radiolabeled leukocyte recruitment over time at infection sites) as a diagnostic parameter enhancing specificity (16). Conversely, the two false negative cases of ^{99m}Tc-HMPAO-WBC scintigraphy observed in our series were most likely due to infection caused by low-leukocyte recruiting microorganisms (22-24) as are the Candida spp. and Enterococcus spp. strains isolated in the two patients with confirmed CIED infection in whom ^{99m}Tc-HMPAO-WBC scintigraphy was negative. Therefore, when infections sustained by such microorganisms are suspected discontinuation of antimicrobial treatment should be considered to enhance diagnostic performances of ^{99m}Tc-HMPAO-WBC scintigraphy.
The ^{99m}Tc-HMPAO-WBC SPECT/CT images aided not only in diagnosing infection, but also in defining the infection burden, in particular by distinguishing patients with infection limited to either the pocket or the

lead(s) from patients with more severe infection involving both the pocket and the lead(s), or other sites of infection in some patients.
The intracardiac portion of the lead(s) was the site more frequently exhibiting radiolabeled WBC accumulation (n=18); these cases were also more frequently associated with complications such as either infectious endocarditis (n=6) and/or septic embolism (n=15). The higher prevalence of infection of the intracardiac portion of the lead(s) over the surgical pocket is consistent with the relatively high prevalence of semi-late and late infections in our patients' population, similarly to data reported in literature due to slowly progressing, implant-related infection (25). Indeed, localized pocket infection was found in just one of our patients, while in all the other cases infection of the pocket was associated with lead(s)' involvement. An important feature of ^{99m}Tc-HMPAO-WBC scintigraphy is therefore its unique ability, shared only with PET/CT, to detect all sites of infection with a single examination, considering the frequent underestimation of the infection burden based on clinical signs alone (26).
As customary in case of suspected CIED-associated infection, all patients included in this study underwent echography of the cardiac region and of the venous pathway of the device as a first-line diagnostic test. In this group of patients, echocardiography had high specificity (90%), but relatively low sensitivity for diagnosing CIECD infection (63%). The echocardiographic finding of vegetations at the distal part of the lead typical for infection (27) was detected in 9/32 patients with confirmed infection. On the other hand, in 4/31 patients who were eventually classified as not having infection, a lead-associated mass, possibly of thrombotic nature, was also detected, in line with a previous report (28). Moreover, in 12/32 patients with final diagnosis of CIED infection TEE failed to visualize a mass adherent to the intracardiac lead, thus confirming that a negative echocardiography does not exclude lead infection (29). In 6 out of these 12 cases with negative echocardiography, ^{99m}Tc-HMPAO-WBC SPECT/CT detected infection, which was localized either at the intravascular portion of the lead(s) and/or at the surgical pocket (Table 4). Therefore, when considering the echocardiographic findings in patients with intracardiac infection (n=26), sensitivity increased to 81%.
Sensitivity of the Duke criteria was 31% for the patients classified in the “definite” category (with 100% specificity), increasing to 81% when considering both the “definite” and the “possible” categories (with 74% specificity). This relatively low sensitivity is not surprising, since the Duke criteria have originally been developed for infectious endocarditis and that several of the minor Duke criteria are not applicable in this setting.

The results obtained in this study demonstrate that SPECT/CT imaging with radiolabeled leukocytes in patients with suspected CIED infection increases the detection rate of infection and allows accurate assessment of disease burden. In patients with left-ventricular-assist device and valve infections radiolabeled leukocyte SPECT/CT has been shown to determine the precise anatomic location and extension of a suspected infection, thus impacting on patients' management (12, 30). High diagnostic accuracy in such condition has been observed also with the use of PET/CT with [18F]FDG, particularly for ruling out involvement of the devices during febrile episodes (31) or for defining the embolic burden in presence of ascertained infection (32). A more recent report encourages the use of [18F]FDG PET/CT also in case of early device infection (10). However, despite its high resolution, this technique is still limited by the lack of a suitable infection-specific radiopharmaceutical. In fact, the enhanced glucose consumption that causes increased [18F]FDG uptake at infectious sites (for the presence of activated leukocytes, monocyte-macrophages (33, 34), and CD4+ T-lymphocytes (35)), can also occur in a number of non-infectious, inflammatory conditions (36) and in post-surgical changes (37).

The higher specificity of ^{99m}Tc-HMPAO-WBC scintigraphy observed in our study when employing SPECT/CT imaging (with the associated better spatial resolution than planar and stand-alone SPECT) enabled to precisely define the disease burden, therefore allowing patients risk stratification and decision-making. In fact, similarly as observed with [18F]FDG PET/CT, a negative scan has consistently been associated with a favourable clinical outcome when antimicrobial therapy alone is initiated. Indeed, a negative ^{99m}Tc-HMPAO-WBC SPECT/CT might be used as a guide to clinicians for choosing the most suitable treatment, i.e., conservative treatment (antimicrobic agents alone, or removal of just the generator) versus full hardware extraction. Despite leukocyte imaging is a relative more complex procedure as compared to [18F]FDG PET/CT both in terms of radiopharmaceutical preparation that include blood manipulation, and imaging acquisition that require multiple scans at different time points , we believe that when differentiation between active infection and inflammation is crucial, ^{99m}Tc-HMPAO-WBC should be considered the method of choice.

In conclusion, ^{99m}Tc-HMPAO-WBC scintigraphy with SPECT/CT acquisition of the chest in patients with high clinical suspicion of CIED infection enabled to confirm the presence of infection, to define the extent of device involvement, and to detect associated complications such as infectious endocarditis and septic embolism. In addition, ^{99m}Tc-HMPAO-WBC

scintigraphy was helpful to exclude the presence of device infection during a febrile episode and sepsis, with 95% negative predictive value. Demonstration of the impact of functional imaging on the overall healthcare costs of the clinical management of CIED on large scale will represents the next challenge.

REFERENCES

1. Uslan DZ, Tleyjeh IM, Baddour LM, et al. Temporal trends in permanent pacemaker implantation: a population-based study. Am Heart J. 2008;155:896-903.
2. Voigt A, Shalaby A, Saba S. Continued rise in rates of cardiovascular implantable electronic device infections in the United States: temporal trends and causative insights. Pacing Clin Electrophysiol. 2010;33:414-419.
3. Klug D, Balde M, Pavin D, et al. Risk factors related to infections of implanted pacemakers and cardioverter-defibrillators: results of a large prospective study. Circulation. 2007;116:1349-1355.
4. Sohail MR, Henrikson CA, Braid-Forbes MJ, Forbes KF, Lerner DJ. Mortality and cost associated with cardiovascular implantable electronic device infections. Arch Intern Med. 2011;171:1821-1828.
5. Gandhi T, Crawford T, Riddell J 4th. Cardiovascular implantable electronic device associated infections. Infect Dis Clin North Am. 2012;26:57-76
6. Sohail MR, Uslan DZ, Khan AH, et. al. Management and outcome of permanent pacemaker and implantable cardioverter-defibrillator infections, J Am Coll Cardiol. 2007;49:1851–1859.
7. Durack DT, Lukes AS, Bright DK. New criteria for diagnosis of infective endocarditis: utilization of specific echocardiographic findings. Duke endocarditis service. Am J Med. 1994;96:200-209
8. Cacoub P, Leprince P, Nataf P,et al. Pacemaker infective endocarditis. Am J Cardiol. 1998;82:480-484.
9. Ploux S, Riviere A, Amraoui S, et al. Positron emission tomography in patients with suspected pacing system infections may play a critical role in difficult cases. Heart Rhythm. 2011;8:1478-1481.
10. Sarrazin JF, Philippon F, Tessier M, et. al. Usefulness of fluorine-18 positron emission tomography/computed tomography for identification of cardiovascular implantable electronic device infections. J Am Coll Cardiol. 2012;59:1616-1625.
11. Millar BC, Prendergast BD, Alavi A, Moore JE. 18FDG-positron emission tomography (PET) has a role to play in the diagnosis and therapy of infective endocarditis and cardiac device infection. Int J Cardiol 2013. Jan [E-pub ahead of print]. doi: pii: S0167-5273(12)01633-6. 10.1016/j.ijcard.2012.12.005.
12. Erba PA, Conti U, Lazzeri E, et al. Added value of ^{99m}Tc-HMPAO-labeled leukocyte SPECT/CT in the characterization and management of patients with infectious endocarditis. J Nucl Med. 2012;53:1235-1243.
13. Palestro CJ, Brown ML, Forstrom LA, et al. Society of Nuclear Medicine Procedure Guideline for ^{99m}Tc-exametazime (HMPAO)-labeled leukocyte scintigraphy for suspected infection/ inflammation, version 3.0, 2004, http://interactive.snm.org/docs/ HMPAO_v3.pdf. (last accessed 14/01/2013).
14. Tascini C, Bongiorni MG, Gemignani G, et al. Management of cardiac device infections: A retrospective survey of a non-surgical approach combining antibiotic therapy with transvenous removal. J Chemother. 2006;18:157-163.
15. Raoult D, Casalta JP, Richet H, et al. Contribution of systematic serological testing in diagnosis of infective endocarditis. J Clin Microbiol. 2005;43:5238-5242.

16. Roca M, Martín-Comín J, Becker W, et al. A consensus protocol for white blood cells labelling with technetium-^{99m} hexamethylpropylene amine oxime. International Society of Radiolabeled Blood Elements (ISORBE) Eur J Nucl Med. 1998;25:797-799.
17. de Vries EF, Roca M, Jamar F, Israel O, Signore A. Guidelines for the labelling of leucocytes with ^{99m}Tc-HMPAO. Inflammation/Infection Taskgroup of the European Association of Nuclear Medicine. Eur J Nucl Med Mol Imaging. 2010;37:842-848.
18. International Commission on Radiological Protection. Annals of the ICRP, Publication 53, Radiation Dose to Patients from Radiopharmaceuticals. Pergamon, Elsevier Science, London; 1988, pp. 255-256
19. Landis JR, Koch GG. The measurement of observer agreement for categorical data. Biometrics 1977; 33:159 -174.
20.Le KY, Sohail MR, Friedman PA, et al. Clinical predictors of cardiovascular implantable electronic device-related infective endocarditis. Pacing Clin Electrophysiol. 2011;34:450-459.
21Ferguson TB Jr, Ferguson CL, Crites K, Crimmins-Reda P. The additional hospital costs generated in the management of complications of pacemaker and defibrillator implantations. J Thorac Cardiovasc Surg. 1996;111:742-751.
22. Cheung GY, Rigby K, Wang R, et. al. Staphylococcus epidermidis strategies to avoid killing by human neutrophils. PLoS Pathog. 2010;6:e1001133.
23. Thurlow LR, Thomas VC, Narayanan S, Olson S, Fleming SD, Hancock LE. Gelatinase contributes to the pathogenesis of endocarditis caused by Enterococcus faecalis. Infect Immun. 2010; 11:4936-4943.
24. Arruda MA, Barja-Fidalgo C. NADPH oxidase activity: In the crossroad of neutrophil life and death. Front Biosci. 2009;14:4546-4556
25. Uslan DZ. Infections of electrophysiologic cardiac devices. Expert Rev Med Devices 2008;5:183-195.
26. Sexton DJ, Spelman D. Current best practices and guidelines. Assessment and management of complications in infective endocarditis. Cardiol Clin 2003;21:273-282
27. Victor F, De Place C, Camus C, et. al. Pacemaker lead infection: echocardiographic features, management, and outcome. Heart. 1999;81:82-87.
28. Downey BC, Juselius WE, Pandian NG, Estes NA 3rd, Link MS. Incidence and significance of pacemaker and implantable cardioverter-defibrillator lead masses discovered during transesophageal echocardiography. Pacing Clin Electrophysiol. 2011;34:679-683.
29. Sohail MR, Uslan DZ, Khan AH, et. al. Infective endocarditis complicating permanent pacemaker and implantable cardioverter-defibrillator infection. Mayo Clin Proc. 2008;83:46-53.
30. Litzler PY, Manrique A, Etienne M, et. al. Leukocyte SPECT/CT for detecting infection of left-ventricular-assist devices: preliminary results. J Nucl Med. 2010;51:1044-1048.
31. Vos FJ, Bleeker-Rovers CP, Kullberg BJ, Adang EM, Oyen WJ. Cost-effectiveness of routine 18F-FDG PET/CT in high-risk patients with gram-positive bacteremia. J Nucl Med. 2011;52:1673-1678.
32. Van Riet J, Hill EE, Gheysens O, et. al. 18F-FDG PET/CT for early detection of embolism and metastatic infection in patients with infective endocarditis. Eur J Nucl Med Mol Imaging. 2010;37:1189-1197.
33. Kaim AH, Weber B, Kurrer MO, et. al. 18F-FDG and 18F-FET uptake in experimental soft tissue infection. Eur J Nucl Med Mol Imaging. 2002;29:648-654.

34. Ogawa M, Ishino S, Mukai T, et. al. 18F-FDG accumulation in atherosclerotic plaques: immunohistochemical and PET imaging study. J Nucl Med. 2004;45:1245-1250.
35. Brewer S, McPherson M, Fujiwara D, et. al. Molecular imaging of murine intestinal inflammation with 2-deoxy-2-[18F]fluoro-D-glucose and positron emission tomography. Gastroenterology. 2008;135:744-55.
36. Blockmans D. PET in vasculitis. Ann N Y Acad Sci. 2011;1228:64-70.
37. Abidov A, D'agnolo A, Hayes SW, Berman DS, Waxman AD. Uptake of FDG in the area of a recently implanted bioprosthetic mitral valve. Clin Nucl Med. 2004;29:848.

Chapter 4

Radiolabelled leukocyte scintigraphy versus conventional radiological imaging for the management of late, low grade vascular prosthesis infections

P. A. Erba[1], G. Leo[2], M. Sollini[3], C. Tascini[4], R. Boni[1], R. N. Berchiolli[2], F. Menichetti[3], M. Ferrari[2], E. Lazzeri[1], and G. Mariani[1]

[1] Regional Center of Nuclear Medicine, Department of Translational Research and Advanced Technology in Medicine, University of Pisa, and University Hospital of Pisa, Pisa, Italy
[2] Division of Vascular Surgery, Department of Translational Research and Advanced Technology in Medicine, University of Pisa, and University Hospital of Pisa, Pisa, Italy
[3] Nuclear Medicine Unit, Department of Oncology and Advanced Technology, Az. Osp. S.Maria Nuova -IRCCS Reggio Emilia, Via Risorgimento 80, 42123 Reggio Emilia, Italy
[4] Division of Infectious Diseases, University Hospital of Pisa, Pisa, Italy

European Journal of Nuclear Medicine Molecular Imaging, in press
doi.org/10.1007/s00259-013-2582-9

Abstract

Purpose: In this study we evaluated the diagnostic performance of ^{99m}Tc-HMPAO-leukocyte scintigraphy (WBC) in a consecutive series of 55 patients (46 men and 9 women, mean age 71±9 yrs, range 50-88 yrs) with suspected late and low-grade late vascular prosthesis infections (VPI) comparing moreover the diagnostic accuracy of WBC to other radiological imaging. **Methods**: All patients suspected to have VPI underwent clinical examination, blood tests, microbiology, US and CT and were classified according to Fitzgerald. Final diagnosis of VPI was established in 47/55 patients, with microbiological confirmation after surgical removal of the prosthesis in 36/47. In the 11 patients presenting major contraindications for surgery, the final diagnosis was based on microbiology and clinical follow-up of at least 18 months. **Results:** ^{99m}Tc-HMPAO-WBC planar, SPECT and SPECT/CT imaging identified VPI in 43/47 patients (16 of these showed also extra-VPI). In the remaining 8 patients without VPI different sites of infections were found. Using SPECT/CT images we obtained a significant reduction of the false positive findings in 37% of patients (sensitivity and specificity 100% versus 85.1% and 62.5% of SPECT stand-alone). Sensitivity and specificity were 34% and 75% for US, 48.9% and 83.3% for CT and 68.1% and 62.5% for Fitzgerald classification. Perioperative mortality was 5.5%, mid-term mortality 12%, and long term-mortality was 27%. Survival rates were similar in patients treated with surgery and antimicrobial therapy as compared to patients treated with antimicrobial therapy alone (61% *versus* 63%), while infection eradication at 12 months was significantly higher when surgery was performed (83.3% *versus* 45.5%). **Conclusions:** ^{99m}Tc-HMPAO-WBC SPECT/CT is useful to detect, localize and define the extent of graft infection in patients with late and low-grade late VPI with inconclusive radiological findings. ^{99m}Tc-HMPAO-WBC SPECT/CT might be used to optimize patients' management.

Introduction

Prosthetic graft infections are uncommon complications of vascular surgical procedures that are reported in up to 6% of cases [1]. However, infection rates vary significantly according to location of the vascular bypass, being less than 1% in case of aorto-iliac graft, increasing to about 2% in case of aorto-femoral bypass, and to 6% in case of infra-inguinal bypass [2, 3].

While in presence of early infection (i.e., earlier than 4 months after graft implantation), and in case of infections of the femoral component the clinical presentation may be straightforward, intracavitary graft infection often presents with nonspecific signs and may appear up to 10 years after surgery. Indeed, late infections (i.e., all infections appearing over 4 months after surgery) are less frequently characterized by fever as compared with the early form [4], and patients may present with general malaise. These patients are more likely to present with complications, such as false aneurysm, intermittent lumbar pain, or an intermittent fistula that can result in gastrointestinal bleeding in case of aortic localization, hydronephrosis, or osteomyelitis [5]. From a microbiological standpoint, blood culture is positive in approximately 35% of the cases, higher in aortic and early VPI [4] since bacteria adhering to the vascular graft are organized in a biofilm, confining to a quiescent state [6, 7]. Such nonspecific presentation makes the diagnosis and treatment of these infections a real challenge, and success of surgical intervention is closely dependent on an early diagnosis.

Polymicrobial etiology is often present [4, 8] with similar distribution of bacteria for early and late infection and for aortic or peripheral localization, except for an increased incidence of *Staphylococci* spp in peripheral VPIs [4, 9]. Even though rates vary in different reported series, the predominance of *Staphylococcus* spp is invariable [4, 8]. *Enterococcus* spp and Gram-negative bacilli being less predominant [2].

Based on the experience with infection of orthopedic prosthetic implants [10, 11] and of endocarditis associated with cardiovascular implantable electronic devices [12], several classification systems have been developed to facilitate the diagnosis of VPI [2], taking into account significant clinical, biological, microbiological, and radiological data. The routine approach to the diagnosis of VPI is often somewhat *ad hoc* and can vary from centre to centre [2]. In general, contrast-enhanced computerized tomography (CT) is the technique of choice for the diagnosis of infection and its complications. CT has over 95% sensitivity, and specificity around 85% when the criteria of perigraft fluid, perigraft soft tissue attenuation, ectopic

gas, pseudoaneurysm, or focal bowel wall thickening are considered [13]. However, in the immediate postoperative period and in case of late/chronic infection the sensitivity of CT decreases to 55% due to the drawback of differentiating between the stigmas of VPI and signs of usual posteoperative outcome [13, 14-20]. Furthermore, the frequently impaired renal function of these patients does not always allow injecting iodinated contrast agents. Doppler ultrasonography (US) may prove useful in case of peripheral bypass [21], but the absence of periprosthetic fluid collections on US does not invariably rule out VPI [4]. Finally, magnetic resonance angiography did not prove superior to CT for diagnosins early VPI [22, 23].

^{99m}Tc-HPMAO-labeled autologous leukocyte (^{99m}Tc-HPMAO-WBC) scintigraphy has shown clear advantages over other methods [20]. Single photon emission tomography co-registered with computed tomography (SPECT/CT) has further enhanced the specificity of ^{99m}Tc-HPMAO-WBC scintigraphy [24-26] both by decreasing false positive findings and by improving the characterization of pathological foci of radiolabeled leukocyte accumulation. However, the clinical application of this diagnostic approach is still limited.

In this study we investigated the diagnostic performances of radiolabeled leukocyte scintigraphy in patients with suspected VPI or suspected infection of abdominal aneurysmatic dilatation. All patients, referred to the Divisions of Vascular Surgery, or Infectious Diseases of Pisa hospital with inconclusive diagnosis after first-line diagnostic tests (clinical examination, ultrasound and contrast-enhanced CT), were evaluated with ^{99m}Tc-HMPAO-leukocyte SPECT/CT.

Material and methods

Patients

Between 2005 and 2011, 55 patients (46 men and 9 women, mean age 71±9 yrs, range 50-88 yrs) were referred for ^{99m}Tc-HMPAO-WBC scintigraphy because of suspected VPI. Thirty-seven patients had aortic graft replacement (aorto-aortic n=6, aorto-iliac n=20, aorto-femoral n=11), 2/55 had vascular prosthesis of iliac-femoral vessels, 16/55 had peripheral by passes using synthetic grafts, and 3/55 had carotid Dacron patches; there were a total of 58 vascular grafts, since 3 patients had more than one vascular graft. The mean interval between surgery and symptoms was 52±74 months (range 0-372 months), suspicion of VPI being raised within 1 month post-surgery in 6/55

cases and between 1 to 3 months in 10/55. In 12/55 cases late VPI was suspected and very late account for 27/55. The main clinical features of patients, including significant comorbidities, are reported in Table 4.1.

Infection was suspected based on clinical examination and on blood tests including WBC counts, C-reactive protein, erythrocyte sedimentation rate, and at least three sets of blood cultures from a peripheral vein (at least one aerobic and one anaerobic) [27]. US and contrast-enhanced CT were performed in all patients.

Clinical signs and symptoms including the presence of fever, shaking chills, inflammatory or disjoined scar, serous and purulent discharge, superinfected lymphocele, local pain, and radiological results were considered to stratify patients according to Fitzgerald classification [2] (see below) before ^{99m}Tc-HMPAO WBC baseline scintigraphy. In all patients, scintigraphy was performed within 24 hrs from the clinical request.

Final diagnosis of VPI was established in 47/55 patients, microbiological confirmation being obtained after surgical removal of the prosthesis in 36/47. In the remaining 11/47 patients, all presenting with major contraindications for surgery, the final diagnosis was obtained either by blood culture or by culture of infected fluid. Therefore, all such patients were treated with antimicrobial agents and clinically followed for at least 18 months. Sequential US, contrast-enhanced CT and ^{99m}Tc-HMPAO-WBC scintigraphy to monitor antimicrobial treatment were performed. During follow-up, ^{99m}Tc-HMPAO-WBC scintigraphy (n=18) was performed in case of negative clinical examination, no symptoms/signs of persistent infection, negative blood tests, negative echocardiography and negative blood cultures. Therefore, a total of 73 scans were available for the final analysis.

Staphylococcus spp. was the microorganism more frequently responsible for the infection (12/47), followed by *Candida* (10/47), *Streptococcus* spp. and *Escherichia Coli* (5/47 each), and finally *Aspergillus*, *P. aeruginosa* and *Salmonella* spp. (2 cases each). Polymicrobial etiology was found in the other 9/47 patients.

Infection occurred most frequently in carotid patches (3/3), aorto-aortic grafts (6/6) and iliac-femoral grafts (2/2), followed by aorto-iliac (18/20), aorto-femoral prosthesis (8/11) and femoro-popliteal-tibial (10/16). Late and very late infections were prevalent (see Table 4.1).

Duplex Ultrasound

Color-coded duplex ultrasound (AU5; Esaote Biomedica, Genoa, Italy) included the vascular region of the graft. Cross-sectional views were recorded with an abdominal phased-array transducer (2.5–3.5 MHz) to visualize pseudoaneurysms, sustained gas, anechoic fluid collections, abscess [28] using color Doppler and power Doppler US imaging. Spectral Doppler waveform analysis was made of the detected leaks.

CT scanning

Whole-body CT scanning included the thorax, abdomen and aorto-iliofemoral tract. Unenhanced scan, followed by acquisitions in the arterial phase after intravenous iodinated contrast administration (120 mL) with a flow rate of 3 to 4 mL/s. (delay calculated by bolus test) and delayed phases (80- to 100-second delay), using 3-mm collimation and 1-mm reconstruction spacing with the single-row equipment or 2.5-mm collimation and a 1.25-mm reconstruction interval with the multidetector scanner (Light Speed Plus; GE Medical Systems) was performed. Images were processed with a dedicated software package on an independent workstation (Advantage Windows 3.1 or 4.1; Sun Microsystems, Mountain View, CA, USA) to generate multiplanar reformations, maximum intensity projections, and volume renderings. The following findings were considered predictive for VPI: presence of aortoenteric fistula, pseudo-aneurysm, intergraft thrombus, hydronephrosis, perigraftic fluid, perigraft air, perigraft soft tissue attenuation, focal bowel wall thickening, discontinuity of the aneurysmal wrap [13].

Fitzgerald classification

According to Fitzgerald criteria [4], a patient was considered positive or VPI if fulfilling at least two criteria among the following: i) positive intra-operative samples and/or blood cultures; ii) local or general clinical signs related to the infection of a vascular site (fever, shaking chills, severe sepsis, septic or hemhorrhagic shock due to an aorto-digestive fistula or to anastomotic rupture of the bypass, local pain, erythema, local swelling, suppurative fistula, abscess, lack of vascular material integration); iii) biological or radiological signs related to the vascular site (C-reactive protein > 10 mg/L, hyperleucocytosis > 10,000/mm3, presence or persistence of collections/periprosthetic air bubbles/abscess/ false aneurysm).

^{99m}Tc-HMPAO-WBC radiolabeling, imaging and data interpretation

Autologous radiolabelled WBCs were prepared according to the EANM Guidelines for the labeling of leukocytes with ^{99m}Tc-HMPAO [29, 30]. Radiolabelling efficiency was always between 70-85%, and viability of the radiolabelled leukocytes was always tested by the Trypan blue exclusion test before reinfusion.

Whole body and spot planar images were obtained after 30 minutes, then 2 or 4-6 (delayed images) and 20-24 hours (late images) after reinfusion of 370-555 MBq of ^{99m}Tc-HMPAO-WBC. Images at 2 hrs were acquired in patients with aorto-aortic, aorto-iliac, aorto-femoral grafts whereas images at 4-6 hrs were registered in case of iliac-femoral peripheral by passes and carotid Dacron patches. SPECT/CT of the region of interest was performed in all patients at 2 or 4-6 hours and repeated at 24 hours in case of negative or doubtful imaging at delayed images. Images were acquired using a dual-head, variable-angle SPECT/CT gamma camera (Hawkeye and Discovery ST, GE Healthcare). The low-dose CT transmission scan was acquired for 16 seconds over 220° for each transaxial slice. The full FOV consisting of 40 slices was completed in 10 minutes. The transmission data were reconstructed using filtered back-projection to produce cross-sectional images. Resolution of the CT scan was 2.2 mm and localization images were produced with a 4.5-mm pixel size, similar to the nuclear medicine emission images. The CT scans were reconstructed into a 256×256 matrix. The SPECT component of the same FOV was acquired using a 128×128 matrix, 360° rotation, 6° angle step, and 40/60-sec-per-frame acquisition time at 2-4 and at 24 hours, respectively. Both CT-attenuation corrected and non-corrected SPECT images were evaluated in the coronal, transaxial, and sagittal planes, as well as in tridimensional maximum intensity projection (MIP) cine mode. Matching pairs of x-ray transmission and radionuclide emission images were fused using the Xeleris software, and hybrid images of overlying transmission and emission data were generated.

All scintigraphic images were evaluated, independently, by two experienced nuclear medicine physicians aware of the patients' clinical history and of the results of prior conventional imaging, by reviewing the planar scans and the SPECT/CT images, with regard to the presence and location of any focus of abnormal radioactivity accumulation indicating infection. Preliminary analysis of the SPECT/CT images included visual inspection to exclude misregistration between the SPECT and the CT

components. The scintigraphic studies were classified as negative when no sites of abnormal uptake were observed in the SPECT/CT images, or positive for infection when at least one focal abnormal accumulation, characterized by time-dependent increase in radioactivity from early to delayed images, was observed [31]. When present, focal accumulation indicating infection was further classified as pertaining to the vascular grafts and/or to extra-prosthetis sites (extra-VPI). Positive scans were categorized as follow: a) isolated VPI; b) isolated extra-VPI; c) VPI and extra-VPI; d) other infections.

Patients treatment

In 36 patients with VPI, combined radical surgical explantation and antimicrobial therapy were carried out, the surgical procedure being performed within 72 hours from scintigraphy. The surgical procedure consisted in debridement of the infected prosthesis with in situ replacement using homograft (n=17) or with an autologous vein (n=13). Complete removal of the infected prosthesis followed by immediate vascular reconstruction with axillo-bifemoral bypass was performed in 2 patients, whereas rifampicin-bounded dacron prosthesis was used in the other 4 cases. Table 4.2 reports the specific surgical treatment for all patients based on the site of the prosthesis. Eleven of the patients with VPI (8 aorto-iliac-femoral and 3 periferal femoro-popliteal-tibial prosthesis) underwent conservative medical therapy alone, because of major contraindications to surgery. The remaining 8 patients without VPI were treated with disease-specific medical and surgical procedures, according to standard procedures as indicated for each clinical condition.

Data analysis

Results of ^{99m}Tc-HMPAO-WBC scintigraphy were correlated with those of US/CT, blood culture, and Fitzgerald classification (the latter only for the baseline scans). The ability to detect or to exclude the presence of VPI was based on the final microbiological or clinical diagnosis. Furthermore, the ability to identify peri-prosthetic infections as well as alternative cause of infections were considered, in order to assess the ability of ^{99m}Tc-HMPAO-WBC scintigraphy to exclude VPI.

For site-based analysis, results of the planar, stand-alone SPECT and SPECT/CT images were compared. Stand-alone SPECT and SPECT/CT were considered contributory when they provided data that could not be

obtained from the assessment of planar images concerning the presence of infection or its precise location. The contribution of SPECT/CT was considered with special attention to the possibility of anatomically localizing

Table 4.1 – Type of vascular prosthesis and main clinical features of the patients included in the study (CAD =; BPCO =; ESR = erythrocyte sedimentation rate; CRP = C-reactive protein).

Primary vascular reconstruction (n=58)	abdominal aorta	peripheral lower limb vessels	iliac-femoral	carotid patches			
	37/58 (64%)	16/58 (28%)	2/58 (3%)	3/58 (5%)			
Infection rate	32/37 (86%)	10/16 (63%)	2/2 (100%)	3/3 (100%)			
Risk factors	Diabetes	Renal failure	CAD	BPCO	Hyperthension	Long term corticoid use	Recent major surgery
	25/55 (45%)	3/55 (5%)	8/55 (15%)	4/55 (7%)	33/55 (60%)	5/55 (9%)	38/55 (69%)
Fever	Present	Absent					
	21/55 (38%)	34/55 (62%)					
Time from device implant (last procedure, months)	≤ 1	1-3	4-12	> 12			
	6/55 (16%)	10/55 (21%)	12/55 (28%)	27/55 (35%)			
	5/6 (%)	7/10 (%)	10/12 (%)	25/27 (%)			
Local inflammation signs/symptoms	Pain	Wound inflammation	Abscess	Fistula	Bleeding	Purulent drainage/ lymphorrhagia	Atypical presentation (dyspesia, pain, fatigue, weight loss)
	11/55 (20%)	5/55 (9%)	2/55 (4%)	2/55 (4%)	2/55 (4%)	5/55 (9%)	21/55 (38%)
Blood tests	ESR	PCR	Leukocytosis				
	22/55 (40%)	18/55 (33%)	17/55 (31%)				
Microbiological results		Positive	Negative				
	Blood culture*	16/55 (29%)	39/55 (71%)				

* during antibiotic therapy in 33/55 patients

Table 4.2: Type of surgical treatment for patients with VPI and infection of abdominal aneurysmatic dilatation.

Site of the vascular prosthesis	Type of surgical treatment
carotid patch (n=3)	autogenous veins (n=3)
aorto-aortic prostheis (n=6)	homograft (n=5) orthotopic rifampicin-bounded dacron graft (n=1)
aorto-iliac prosthesis (n=14)	axillo-bifemoral bypass (n=2) homograft (n=9) orthotopic rifampicin-bounded dacron graft (n=3)
aorto-femoral (n= 4)	autogenous veins (n=2) homograft (n=2)
iliac-femoral (n=2)	autogenous veins (n=2)
femoro-popliteal-tibial (n=7)	autogenous veins (n=6) homograft (n=1)

the exact site of infection, particularly for vessels and the heart region. Interpretation of the images obtained at 2-4 and 24 hours were also compared, to define the most suitable protocol to image patients.

For each patients we recorded the type of surgical treatment of VPI after considering the results of ^{99m}Tc-HMPAO-WBC scintigraphy. We also evaluated peri-operative and long-term mortality of such surgical treatments, as well as infection eradication at 1 year both for patients treated with removal of the surgical graft followed by antimicrobial therapy and for patients treated with antimicrobial therapy alone. VPI eradication was defined in case of negative clinical examination, negative blood tests (including microbiology), negative US/CT, and negative ^{99m}Tc-HMPAO-WBC scan (the latter when performed).

Statistical analysis

All values are expressed as median and range, as customary for nonparametric data. The Pearson's χ^2 test was employed for comparing parametric data between groups. Sensitivity and specificity of US, CT, the Fitzgerald classification and ^{99m}Tc-HMPAO-WBC planar, stand-alone SPECT and SPECT/CT imaging were calculated based on the final diagnosis with 95% confidence intervals and compared using the McNemar test.

R**esults**

^{99m}Tc-HMPAO-WBC scintigraphy was positive in all the patients referred for the baseline scan, confirming VPI in 47/55 patients. Positive scans identified isolated VPI 27/47 patients. VPI and extra-VPI infection was detected in 16/47 patients, with local complications of VPI represented by involvement of perivascular graft tissues in the majority of the cases (n=7) and/or fistulas (n=5); VPI and distant sites of infections were detected in 4 patients. No case of isolated extra-VPI was detected.

In the remaining 8/55 basal scans showing focal accumulation of labeled leukocytes in patients without VPI, scintigraphy detected alternative sites of infections in all such patients. In particular, osteomyelitis was detected in 4 cases, inflammatory bowel disease in 3, whereas the last case had infection of an artero-venous fistula for hemodialysis access. These patients with alternative causes of infection were therefore treated according to standard procedures, as indicated for the each clinical condition. None of

the 8/55 patients with a negative ^{99m}Tc-HMPAO-WBC developed infection during follow-up.

Diagnostic performances of ^{99m}Tc-HMPAO-WBC scintigraphy versus US, CT and Fitzgerald classification

US was positive for VPI in 16/47 patients (33% sensitivity in the whole population, but 68% for peripheral VPI; specificity 69%). Contrast-enhanced CT was positive in 26/55 patients, being true-positive in 23/47 cases of VPI. Whereas, CT was inconclusive in 15/47 cases. Major CT findings were peri-graft fluid and collections (n=14), pseudoaneurysms (n=19) and peri-graft gas bubbles (n=9), focal bowel wall thickening (n=4), increased soft tissue between the graft and surrounding wrap (n=2), disruption of the aneurysmal wrap (n=1).
According to Fitzgerald classification, our patients were classified as positive for VPI in 35/55 (32 true positives, 3 false positives), and negative for VPI in 20/55 (15 true negatives, 5 false negatives).
Table 4.3 summarizes the results of ^{99m}Tc-HMPAO-WBC scintigraphy, of US and contrast-enhanced CT and of stratification according to Fitzgerald classification in the cases with final diagnosis of VIP infection. Table 4.4 directly compares the results of ^{99m}Tc-HMPAO-WBC scintigraphy and contrast-enhanced CT according to the type of VPI (i.e., early *versus* late). Blood cultures were positive in only 16/55 patients, 14 out of such 16 cases with confirmed VPI; however, 29/39 of the blood-culture negative patients were under antimicrobial treatment at the time of assessment.

^{99m}Tc-HMPAO-WBC scintigraphy and patients' clinical management

In 36 patients with positive ^{99m}Tc-HMPAO-WBC scintigraphy for VPI, combined radical surgical explantation and antimicrobial therapy were carried out. In 34/36 patients demonstration at ^{99m}Tc-HMPAO-WBC scintigraphy of infection of the whole vascular prosthesis resulted in complete removal of the infected prosthesis. The 2 patients in whom accumulation of radiolabelled leukocytes limited only at the distal portion of the aorto-iliac grafts was detected, were treated with partial removal and replacement of the prosthesis; follow-up demonstrated eradication of infection in both cases.

In patients undergoing combined surgical and medical treatment perioperative mortality was 5.5%, mid-term mortality (within 1 month) was 12% (all deaths being associated with infective complications), and long term-mortality was 27% (mainly unrelated to infection). Survival rate was 61%, whereas the rate of infection eradication at 12 months was 83.3%.

Eleven of the patients with VPI (8 aorto-iliac-femoral and 3 periferal femoro-popliteal-tibial prosthesis) underwent conservative medical therapy alone, because of major contraindications to surgery. In these patients infection was sustained by *Staphylococcus* spp, *Candida* in 3/11 each, *Escherichia Coli* and *Aspergillus* in 1 case each; the other 3 VPI was of polymicrobial origin. Follow-up examination performed in these patients 6-9 months after the baseline scan showed the disappearance of the pathologic accumulation of radiolabelled leukocytes in only 3/11 cases. In 2/8 of the remaining patients medical therapy was discontinued after normalization observed in a third ^{99m}Tc-HMPAO-WBC scan (at 6 months), whereas the other 6 patients had persistent abnormal scintigraphy despite the prolonged medical treatment; Survival rates of these patients treated with antimicrobial therapy alone was 63% and the corresponding infection eradication rate was 45.5%.

Four major contributions of ^{99m}Tc-HMPAO-WBC scintigraphy on patients' management have been identified: i) saving the prosthesis after identification of an alternative site of infection; ii) identifying VPI and concomitant distant sites of infections; iii) selecting the most suitable surgical timing; iv) aiding in the selection of the optimal surgical planning (complete *versus* partial prosthesis removal).

Comparison of ^{99m}Tc-HMPAO-WBC planar, stand-alone SPECT and SPECT/CT images

Table 4.5 compares the results of scintigraphic findings based on interpretation of planar, stand-alone SPECT and SPECT/CT images. SPECT/CT acquisition provided higher accuracy both for the detection of infection and for localization of ^{99m}Tc-HMPAO-WBC accumulation at specific portions of the graft, distinguishing soft tissue and cutaneous involvement from infection localized at the vascular prosthesis. Additionally, SPECT/CT allowed to recognize false positive results at planar imaging (n=9) as well as at stand-alone SPECT imaging (n=7), by identifying either blood-pool activity in the vascular bed and in the bone marrow (vertebral bodies) and/or nonspecific radioactivity accumulation in the bowel. Overall,

SPECT/CT imaging changed the final classification of the scan from negative to positive for infection in 14/57 cases as compared to planar imaging and in 9/57 cases as compared to stand-alone SPECT imaging. Figures 4.1, 4.2, 4.3 and 4.4 show examples od radiolabelled WBC imaging in our patients.

Table 4.3: Results of ^{99m}Tc-HMPAO-WBC scintigraphy, US, contrast-enhanced CT and the Fitzgerald classification according to the final diagnosis of VPI, other concomitant infections or no infection for all the exams performed at baseline. By McNemar test ^{99m}Tc-HMPAO WBC SPECT/CT performed significantly better as compared to US($\chi^2 = 25.48$, $p < 0.0001$), contrast-enhanced TC ($\chi^2 = 16.33$, $p < 0.0001$) and Fitzgerald classification ($\chi^2 = 8$, $p = 0.004$).

		VPI (n=47)	Other infections (n=8)	Sensitivity	Specificity	Accuracy	Positive Predictive Value	Negative Predictive Value
^{99m}Tc-HMPAO WBC	Positive	47/47	8/8	100% (91.9%-100%)	100% (91.9%-100%)	100% (91.9%-100%)	100% (91.9%-100%)	100% (91.9%-100%)
	Negative	0/47	0/8					
US	Positive	16/47	2/8	34% (22.2%-48.2%)	75% (70.1%-91.7%)	40% (27.3%-54.1%)	88.9% (76.8%-95.4%)	16.2% (8.1%-29.1%)
	Negative	31/47	6/8					
TC	Positive	23/47	3/8	48.9% (35.1%-62.9%)	83.3% (70.1%-91.7%)	52.8% (38.8%-66.5%)	95.8% (85.4%-99.2%)	17.2% (8.7%-30.6%)
	Negative	9/47	1/8					
	Non-diagnostic	15/47	4/8					
Fitzgerald classification	Positive	32/47	3/8	68.1% (54%-79.6%)	62.5% (48.4%-74.9%)	67.3% (72.8%-93.1%)	91.4% (79.9%-96.9%)	25% (14.7%-38.8%)
	Negative	15/47	5/8					

Table 4.4: Results of ^{99m}Tc-HMPAO-WBC scintigraphy and contrast-enhanced CT for all the exams performed at baseline, classified according to the time of suspected VPI onset.

	Very early VP (n=6)		Early VP (n=10)		Late VP (n=12)		Very late VP (n=27)	
	^{99m}Tc-HMPAO-WBC							
Contrast enhanced CT	pos (n=5)	neg (n=1)	pos (n=7)	Neg (n=3)	Pos (n=10)	Neg (n=2)	Pos (n=25)	Neg (n=2)
positive (n=26)	4	1	5	2	4	0	10	0
non diagnostic (n=19)	1	0	2	1	3	1	9	2
negative (n=10)	0	0	0	0	3	1	6	0

Table 4.5: Results of ^{99m}Tc-HMPAO-WBC planar, SPECT and SPECT/CT acquisitions in the 55 patients evaluated with a baseline scintigraphy for suspected VPI. (SPECT images *versus* planar images $\chi^2 = 1.8$, p = 0.179; SPECT/CT images *versus* planar images $\chi^2 = 3.26$, p = 0.07 and SPECT/CT *versus* SPECT images $\chi^2 = 1.6$, p = 0.2, by McNemar test)

	Positive for VPI	Doubtful for VPI	Negative for VPI	Correct extent of VPI	Correct extent for peri-graft infection and local complications	Correct exclusion VPI	Positive for other infections	Correct extent for other sites of infection	Sensitivity	Specificity	Accuracy	Positive Predictive Value	Negative Predictive Value
Planar images	40/55*	0/55	15/55**	20/47	0/15	4/8	5/8	4/8	76.6% (62.9%-96.5%)	50% (36.5%-63.6%)	72.7% (58.8%-83.5%)	90% (78.2%-96.1%)	26.7% (16.1%-40.6%)
SPECT	43/55[$]	9/55[#]	3/47	23/47	8/15	5/8	8/8	5/8	85.1% (72.4%-92.8%)	62.5% (48.4%-74.9%)	81.8% (68.6%-90.5%)	93% (81.9%-97.8%)	41.7% (28.8%-55.7%)
SPECT/ CT	47/55	0/55	8/55	47/47	15/15	8/8	8/8	8/8	100% (91.9%-100%)	100% (91.9%-100%)	100% (91.9%-100%)	100% (91.9%-100%)	100% (91.9%-100%)

*including 4 FP results due to bowel and bone marrow uptake, soft tissue and cutaneous infections
** including 9 FN results because of overlapping of the abdominal aorta and bone marrow-uptake at the vertebral bodies
[#] all 9 inconclusive findings because of the lack on anatomical landmarks
[$] including 3 FP results due to bowel and bone marrow uptake

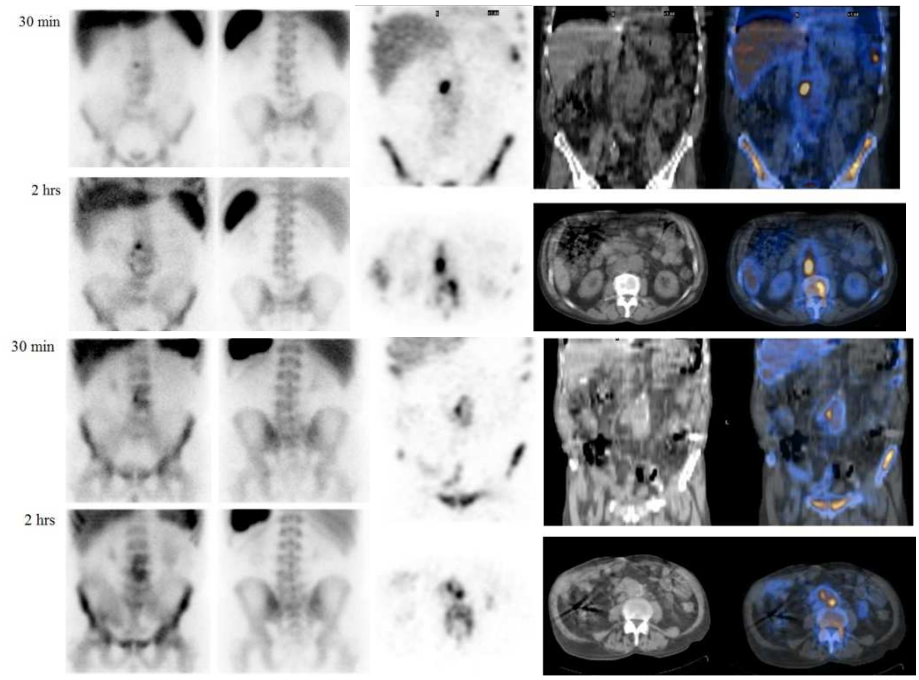

Figure 4.1: ^{99m}Tc-HMPAO-WBC scintigraphy in a patient with suspected late infection of an aorto-bisiliac vascular prosthesis presenting with cellulitis and erysipelas of the left lower leg and fever. Blood culture was negative and swab culture isolate *Enterobacter sakazakii and Escherichia Coli*. Anterior (left panel) and posterior (right panel) planar images of the abdominal region at 30 min and 2 hrs at baseline (A) and follow-up studies (C). Coronal and transaxial slices: CT (left panel) and corresponding fused SPECT/CT sections (right panel) at baseline (B) and follow-up studies (D). Baseline planar images show increased WBC accumulation at the level of L1-L3 corresponding to vascular graft in the SPECT/CT images. The patient was first treated with antimicrobial therapy and repeated ^{99m}Tc-HMPAO-WBC scintigraphy that showed persistence of uptake at the vascular prosthesis, less intense as compared to baseline. After the follow-up study, the patient was treated with debridement of the prosthesis with in situ replacement with autologous femoral veins and microbiology confirms infection sustained by *Candida albicans*.

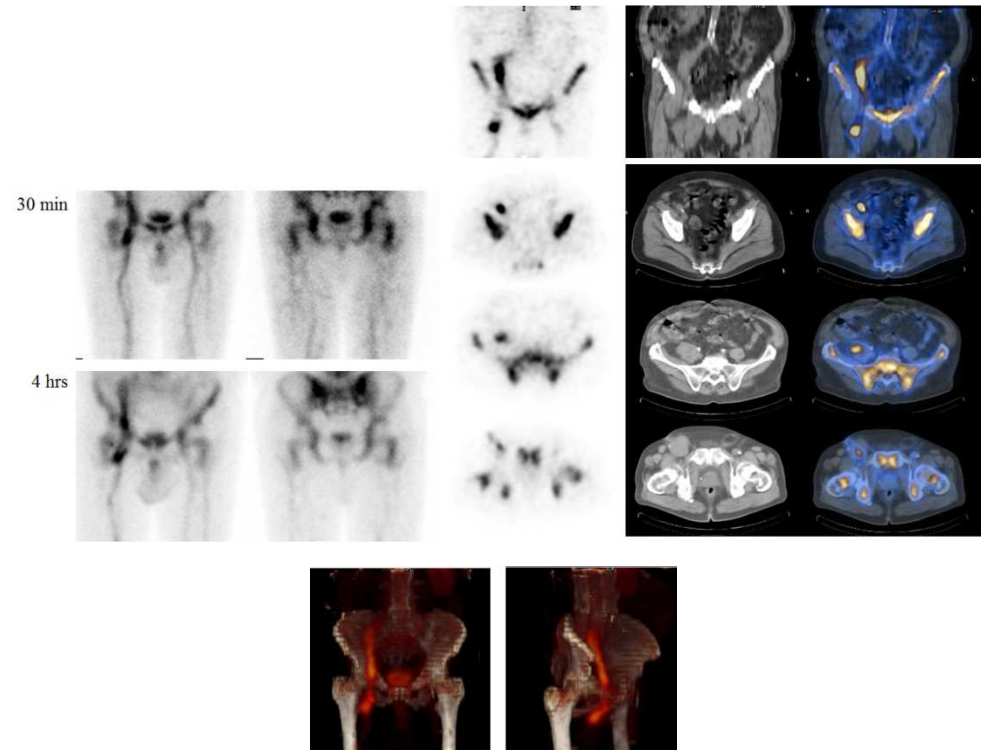

Figure 4.2: ^{99m}Tc-HMPAO-WBC scintigraphy in a patient with suspected late infection of right iliac-femoral and femoro-popliteal vascular prosthesis. The patient presented a peri-prosthetic collection extending surrounding the whole prosthesis and negative blood culture. (A) Anterior (left panel) and posterior (right panel) planar images of the region extending from the iliac crest to the knee at 30 min and 4 hrs, showing increased WBC uptake at the inguinal region. (B) Coronal and transaxial slices (emission images in left panel, corresponding CT sections in the middle panel and fused SPECT/CT sections in right panel) localized the focal accumulation of radiolabelled leukocytes at the vascular graft, at both the iliac and the femoral portions. Microbiology confirms infection sustained by poly-microbial agents. (C) 3D images showing the uptake of WBC all along the vascular graft.

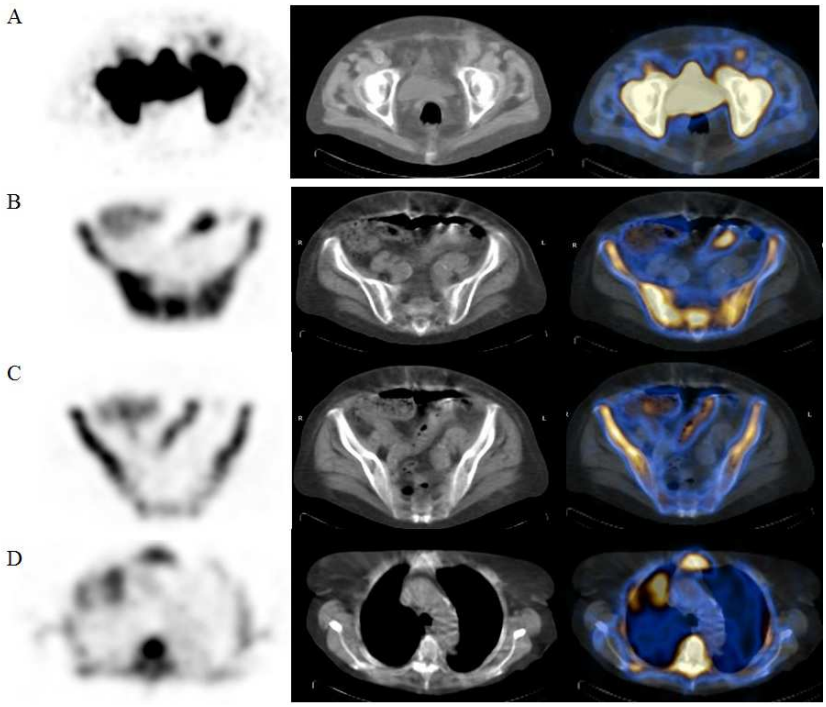

Figure 4.3: ^{99m}Tc-HMPAO-WBC scintigraphy in a patient with suspected very early infection of aorto-bifemoral vascular prosthesis. The patient presented a left lower limb lymphedema, lymphocele with isolation of *Enterococcus faecalis* at microbiology of the aspirate. Transaxial slices at different levels (emission images in left panel, corresponding CT sections in the middle panel and fused SPECT/CT sections in right panel) showing multiple sites of radiolabelled leukocytes uptake at the vascular graft at the femoral left branch (A), at the intestine (B and C) and at the right lung/costal pleura (D). Microbiology after debridement of the prosthesis with in situ replacement with homograft confirms infection sustained by poly-microbial agents.

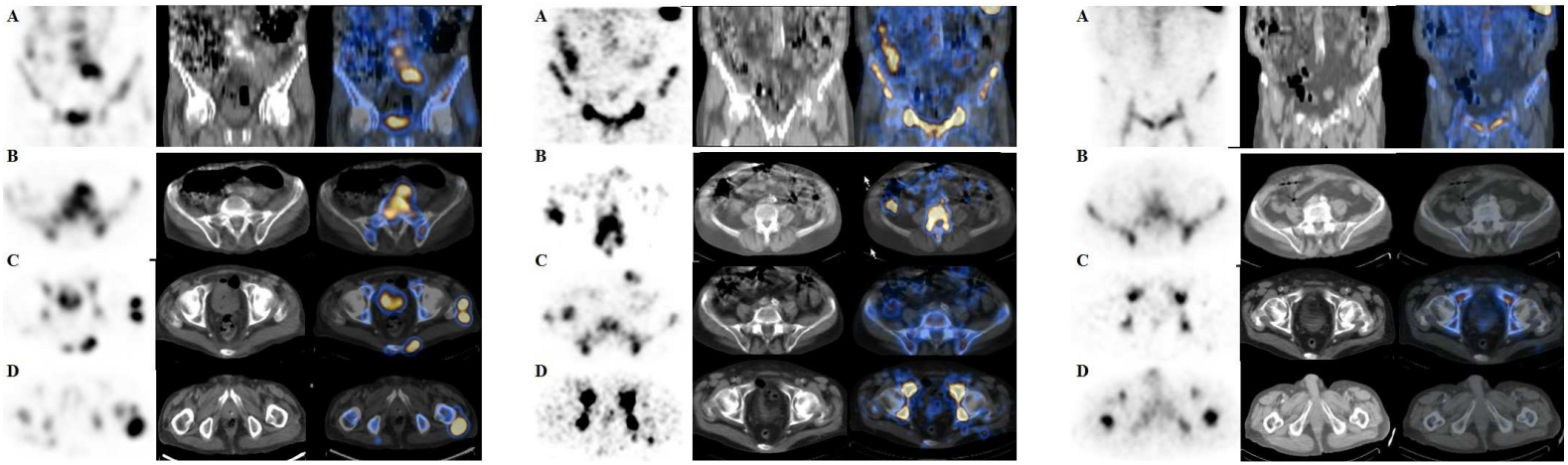

Figure 4.4: ^{99m}Tc-HMPAO-WBC scintigraphy basal (left panel) and follow-up studies at 6 (middle panel) and 12 months (right panel) in a patient with suspected late infection of aorto-bisiliac vascular prosthesis. The patient presented fever, positive blood culture for Methicillin-resistant *Staphylococcus Aureus* and CT finding of 20mm pseudoaneurysm at the left iliac anastomosis. Coronal (A) and transaxial emission images (left panel), corresponding CT sections (middle panel) and fused SPECT/CT sections (right panel) at different levels (B, C, D) showing WBC uptake at the distal portion of the prosthesis, at the level of the left iliac branch extending into muscles and soft tissue very intense at baseline (right panel), decreasing both in intensity and extension at the first follow-up scan (middle panel) and almost disappeared at the second follow-up scan (left panel).

Discussion

VPI are associated with significant morbidity, including major amputation [4, 19, 32] and death. Overall cost of VPI combined medical and surgical treatment as well as of associated morbidities in the US has estimated to amount annually to 720,000,000 US $ [33]. Furthermore, reinfection after abdominal aortic graft re-implantation remains a risk, particularly during treatment of an extra-anatomic bypass graft infection [34]. The success of surgical treatment is closely dependent on early diagnosis, which however may be hampered by nonspecific presentation such as in case of low-grade late infections. Indeed, in this condition as in the case of very early infections, sensitivity of contrast-enhanced CT, that is considered the imaging method of choice for VPI diagnosis, significantly decreases [17]. Therefore, search for alternative imaging modalities is needed to expedite diagnosis.

In this study we evaluated a consecutive series of patients with suspected VPI that remained unconfirmed after standard diagnostic tests, including blood chemistry, US and contrast-enhanced CT. All patients underwent ^{99m}Tc-HMPAO-WBC scintigraphy with the purpose of confirming or excluding VPI. VPI was eventually confirmed in 47/55 of the patients, being mainly represented by low grade late VPI (51%). Most of the infections were sustained by *Staphylococcus* spp. (26%). Patients were treated either with combined radical surgical explantation and antimicrobial therapy (36/47 patients) or with conservative medical treatment alone (11/47 patients) in case of major contraindications for surgery.

^{99m}Tc-HMPAO-WBC scintigraphy identified isolated VPI in 57% patients, and VPI associated with extra-VPI in 43% of the cases, including distant site of infections. No cases of isolated extra-VPI were detected. No false positive or false negative results were observed, irrespective of the strain of sustaining microrganisms or of concomitant administration of antimicrobial agents. High specificity was achieved even when scintigraphy was performed within few months after surgery, in line with previous findings [35]. Furthermore, ^{99m}Tc-HMPAO-WBC scintigraphy excluded VPI and identified instead alternative sites of infection (such as osteomyelitis, inflammatory bowel disease and infection of a hemodialysis fistula). An important advantage of SPECT/CT imaging was the resulting significant reduction of the false positive findings in 37% of patients as compared to stand-alone SPECT (i.e., vascular pool, nonspecific abdominal accumulation), accurate characterization of the site and extension of

abnormal accumulation, even in presence of post-surgical distortions and in complex anatomical sites, supporting previous similar findings [26]. Therefore, SPECT/CT further enhanced the high values of sensitivity (82-100%) and specificity (85-100%) already reported in the literature for ^{99m}Tc-HMPAO-WBC scintigraphy in patients with suspected VPI.

Sub-optimal diagnostic performance of contrast-enhanced CT in this series of patients with predominant very late infections is not surprising. In fact, it is well known that CT might fail to distinguish the stigmas of periprosthetic infection from normal postoperative changes [16, 17] and might be false-negative in chronic low-grade infections [36]. Indeed, in our patients more than 80% of the inconclusive findings at CT were found in case of late and very late infection.

From a surgical perspective, major contributions of ^{99m}Tc-HMPAO-WBC scintigraphy on patients' management have been identified. In fact, based on ^{99m}Tc-HMPAO-WBC imaging, patients with VPI without major surgical contraindications were treated within 72 hours with a surgical approach that include the information of ^{99m}Tc-HMPAO-WBC scintigraphy. Therefore, while in 34/36 patients complete debridement of infected tissues, complete exeresis of the prosthesis and adjacent arterial area maintaining or restoring the arterial flux was performed, the 2 cases with accumulation of radiolabelled leukocytes limited only at the proximal portion of the aorto-iliac graft were treated with partial removal and replacement of the prosthesis. Infection eradication was obtained in both such cases. Furthermore, in the patients with concomitant distant sites of infections at ^{99m}Tc-HMPAO-WBC scintigraphy, treatment was multimodal and included treatment for the VPI followed by surgical debridement and long-lasting antimicrobial therapy.

Perioperative mortality of our patients was 6%, higher in the group with aorto-iliac VPI. Despite explantation of the graft and reperfusion of the area is considered the gold standard for treatment of an infected prosthetic graft [37] to avoid infection chronicization [38] we observed similar survival rates in patients treated with combined surgical and medical treatment as compared to those treated with conservative medical treatment alone (61% versus 63%). However, infection eradication at 12 months was significantly higher in VPI patients treated with combined surgical and medical treatment as compared to patients treated with conservative medical treatment alone (83.3% versus 45%). In patients with persistent infection, the ^{99m}Tc-HMPAO-WBC follow-up scans clearly depicted the sites of persistent

infection, thus demonstrating the reliability of this imaging modality when used to monitor treatment response.

Therefore, we believe that our results constitute the basis for a more extensive application of ^{99m}Tc-HMPAO-WBC not only for the diagnosis of VPI or to exclude graft involvement, but for providing to the surgeon complementary information useful for the choice of alternative surgical procedures, such as complete or partial graft preservation in high-risk patients in whom conventional management is precluded because of severe co-morbid illness or a hostile abdomen. Furthermore, ^{99m}Tc-HMPAO-WBC scintigraphy enables to monitor response to antimicrobial treatment, by distinguishing patients who respond favourably from those who require intensified administration or alternative treatment options.

Conclusions

^{99m}Tc-HMPAO-WBC scintigraphy with SPECT/CT acquisition in patients with clinical suspicion of VPI enabled to confirm the presence of infection and to define the extent of graft infection, thus impacting on subsequent planning of surgical management. In addition, ^{99m}Tc-HMPAO-WBC scintigraphy was helpful in identifying concomitant distant sites of infection, in excluding graft infection during a febrile episode and sepsis and in monitoring response to antimicrobial treatment.

Our results demonstrated that ^{99m}Tc-HMPAO-WBC scintigraphy with SPECT/CT acquisition is to be considered in patients with suspected VPI and inconclusive radiological imaging to optimize patients' management.

Acknowledgments

The authors thank G. A. Cataldi for her assistance in radiolabelling and quality controls of ^{99m}Tc-HMPAO-WBC.

References

1. Lorentzen JE, Nielsen OM, Arendrup H, Kimose HH, Bille S, Andersen J, et al. Vascular graft infection: an analysis of 62 graft infections in 2411 consecutively implanted synthetic vascular grafts. Surgery. 1985; 98(1):81-86.
2. FitzGerald SF, Kelly C, Humphreys H. Diagnosis and treatment of prosthetic aortic graft infections: confusion and inconsistency in the absence of evidence or consensus. J Antimicrob Chemother. 2005;56(6):996–9.
3. Antonios VS, Noel AA, Steckelberg JM, Wilson WR, Mandrekar JN, Harmsen WS, et al. Prosthetic vascular graft infection: a risk factor analysis using a case-control study. J Infect. 2006;53(1):49–55
4. Legout L, Sarraz-Bournet B, D'Elia PV, Devos P, Pasquet A, Caillaux M, et al. Characteristics and prognosis in patients with prosthetic vascular graft infection: a prospective observational cohort study. Clin Microbiol Infect. 2012 Apr;18(4):352-8.
5. Valentine RJ. Diagnosis and management of aortic graft infection. Semin Vasc Surg. 2001; 14(4): 292–301.
6. Lorenz U, Schäfer T, Ohlsen K, Tiurbe GC, Bühler C, Germer CT, et al. In vivo detection of Staphylococcus aureus in biofilm on vascular prostheses using non-invasive biophotonic imaging. Eur J Vasc Endovasc Surg. 2011;41(1):68–75.
7. Hicks RC, Greenhalgh RM. The pathogenesis of vascular graft infection. Eur J Vasc Endovasc Surg. 1997;14(Suppl. A):5–9
8. Calligaro KD, Veith FJ, Schwartz ML, Dougherty MJ, DeLaurentis DA. Differences in early versus late extracavitary arterial graft infections. J Vasc Surg. 1995;22(6):680–5 [discussion 5–8].
9. Szczot M, Meybeck A, Legout L, Pasquet A, Van Grunderbeeck N, Langlois J. Vascular graft infections in the intensive care unit: clinical spectrum and prognostic factors. J Infect. 2011;62(3):204–11.
10. Recommendations for bone and joint prosthetic device infections in clinical practice (prosthesis, implants, osteosynthesis). Société de pathologie infectieuse de langue francaise. Med Mal Infect. 2010;40(4):185–211.
11. Zimmerli W, Trampuz A, Ochsner PE. Prosthetic-joint infections. N Engl J Med 2004;351(16):1645–54.
12. Taylor J. The 2009 ESC Guidelines for management of infective endocarditis reviewed. Eur Heart J. 2009;30(19):2185–6.
13. Low RN, Wall SD, Jeffrey Jr RB, Sollitto RA, Reilly LM, Tierney Jr LM. Aortoenteric fistula and perigraft infection: evaluation with CT. Radiology. 1990;175(1):157–62.
14. Orton DF, LeVeen RF, Saigh JA, et al. Aortic prosthetic graft infections: radiologic manifestations and implications for management. Radiographics 2000;20(4):977–93.
15. Haaga JR, Baldwin GN, Reich NE, Beven E, Kramer A, Weinstein A, et al. CT detection of infected synthetic grafts: preliminary report of a new sign. AJR Am J Roentgenol. 1978;131(2):317–20.
16. O'Hara PJ, Borkowski GP, Hertzer NR, O'Donovan PB, Brigham SL, Beven EG. Natural history of periprosthetic air on computerized axial tomographic examination of the abdomen following abdominal aortic aneurysm repair. J Vasc Surg. 1984;1(3):429–33
17. Qvarfordt PG, Reilly LM, Mark AS, Goldstone J, Wall SD, Ehrenfeld WK, et al. Computerized tomographic assessment of graft incorporation after aortic reconstruction. Am J Surg 1985;150(2):227–31

18. Bruggink JL, Glaudemans AW, Saleem BR, Meerwaldt R, Alkefaji H, Prins TR, et al. Accuracy of FDG-PETCT in the diagnostic work-up of vascular prosthetic graft infection. Eur J Vasc Endovasc Surg. 2010;40(3):348–54.
19. Fukuchi K, Ishida Y, Higashi M, Tsunekawa T, Ogino H, Minatoya K, et al. Detection of aortic graft infection by fluorodeoxyglucose positron emission tomography: comparison with computed tomographic findings. J Vasc Surg. 2005;42(5):919–25.
20. Fiorani P, Speziale F, Rizzo L, De Santis F, Massimi GJ, Taurino M, et al. Detection of aortic graft infection with leukocytes labeled with technetium 99m-hexametazime. J Vasc Surg. 1993;17(1):87–95 [discussion -6].
21. Bruggink JL, Slart RH, Pol JA, Reijnen MM, Zeebregts CJ. Current role of imaging in diagnosing aortic graft infections. Semin Vasc Surg. 2011 Dec;24(4):182-90.
22. Olofsson PA, Auffermann W, Higgins CB, Rabahie GN, Tavares N, Stoney RJ. Diagnosis of prosthetic aortic graft infection by magnetic resonance imaging. J Vasc Surg.1988;8(2):99–105.
23. Spartera C, Morettini G, Petrassi C, Marino G, Minuti U, Pavone P, et al. Role of magnetic resonance imaging in the evaluation of aortic graft healing, perigraft fluid collection, and graft infection. Eur J Vasc Surg. 1990;4(1):69–73.
24. Bar-Shalom R, Yefremov N, Guralnik L, Keidar Z, Engel A, Nitecki S, et al. SPECT/CT using 67Ga and 111In-labeled leukocyte scintigraphy for diagnosis of infection. J Nucl Med. 2006; 47(4):587-594.
25. Djekidel M, Brown RK, Piert M. Benefits of hybrid SPECT/CT for (111)In-oxine- and Tc-99m-hexamethylpropylene amine oxime-labeled leukocyte imaging. Clin Nucl Med. 2011; 36(7):e50-56.
26. Lou L, Alibhai KN, Winkelaar GB, Turnbull RG, Hoskinson ME, Warshawski R, et al. 99mTc-WBC scintigraphy with SPECT/CT in the evaluation of arterial graft infection. Nucl Med Commun. 2010 May;31(5):411-6
27. Raoult D, Casalta JP, Richet H, Khan M, Bernit E, Rovery C, et al. Contribution of systematic serological testing in diagnosis of infective endocarditis. J Clin Microbiol. 2005;43(10):5238-5242.
28. G.B. Perera, R.M. Fujitani, S.M. Kubaska. Aortic graft infection: update on management and treatment options. Vasc Endovascular Surg. 2006;40(1):1–10
29. Roca M, Martín-Comín J, Becker W, Bernardo-Filho M, Gutfilen B, Moisan A, et al. A consensus protocol for white blood cells labelling with technetium-99m hexamethylpropylene amine oxime. International Society of Radiolabeled Blood Elements (ISORBE). Eur J Nucl Med. 1998 Jul;25(7):797-9.
30. de Vries EF, Roca M, Jamar F, Israel O, Signore A. Guidelines for the labelling of leucocytes with ^{99m}Tc-HMPAO. Inflammation/Infection Taskgroup of the European Association of Nuclear Medicine. Eur J Nucl Med Mol Imaging. 2010;37:842-848.
31. Palestro CJ, Brown ML, Forstrom LA, Greenspanet BS, McAfee JG, Royal HD, et al. Society of Nuclear Medicine Procedure Guideline for ^{99m}Tc-exametazime (HMPAO)-labeled leukocyte scintigraphy for suspected infection/ inflammation, version 3.0, 2004, http://interactive.snm.org/docs/ HMPAO_v3.pdf.
32. O'Connor S, Andrew P, Batt M, Becquemin JP. A systematic review and meta-analysis of treatments for aortic graft infection. J Vasc Surg 2006;44(1):38–45.
33. Darouiche RO. Treatment of infections associated with surgical implants. N Engl J Med. 2004 Apr 1;350(14):1422-9.

34. Munzio PJ, Reilly LM, Stoney RJ. Redo aortic grafting after treatment of aortic graft infection.J Vasc Surg1996; 24(3):328-335
35. Liberatore M, Misuraca M, Calandri E, Rizzo L, Speziale F, Iurilli AP, et al. White blood cell scintigraphy in the diagnosis of infection of endovascular prostheses within the first month after implantation. Med Sci Monit. 2006 Mar;12(3):MT5-9
36. Keidar Z, Nitecki S. FDG-PET for the detection of infected vascular grafts. Q J Nucl Med Mol Imaging. 2009;53(1):35–50.
37. Bunt TJ. Vascular graft infections: an update. Cardiovasc Surg. 2001; 9(3): 225–33.
38. Maze MJ, Laws P, Buckenham T, Pithie A, Gallagher K, Metcalf S, et al. Outcomes of infected abdominal aortic grafts managed with antimicrobial therapy and graft retention in an unselected cohort. Eur J Vasc Endovasc Surg. 2013 Apr;45(4):373-80.

Chapter 5

Image acquisition and interpretation criteria for ^{99m}Tc-HMPAO labelled white blood cell scintigraphy: results of a multicenter study

Paola A. Erba[1]*, Andor W.J.M. Glaudemans[2]*, Niels C. Veltman[3], Martina Sollini[4], Marta Pacilio[5], Filippo Galli[5], Rudi A.J.O. Dierckx[2], Alberto Signore[2,5]

*authors equally contributed

[1] Regional Center of Nuclear Medicine, Department of Translational Research and Advanced Technologies in Medicine University of Pisa Medical School, Pisa, Italy
[2] Department of Nuclear Medicine and Molecular Imaging, University of Groningen, University Medical Center Groningen, Groningen, the Netherlands
[3] Department of Nuclear Medicine, Jeroen Bosch Hospital, 's-Hertogenbosch, the Netherlands
[4] Nuclear Medicine Unit, Department of Oncology and Advanced Technology, Arcispedale S. Maria Nuova – IRCCS, Reggio Emilia, Reggio Emilia, Italy
[5]Nuclear Medicine Unit, Department of Medical-Surgical Sciences and of Translational Medicine, Faculty of Medicine and Psychology, "Sapienza" University, Rome, Italy

Eur J Nucl med Mol Imaging, under revision

Abstract

There is no consensus yet on the best protocol for planar image acquisition and interpretation of radiolabelled white blood cell (WBC) scintigraphy. This may account for differences in reported diagnostic accuracy amongst different centers. Here we report the results of a multicentre retrospectively study performed by analysing 235 WBC scans divided in 2 groups. First group (105 patients) acquired with a fixed-time acquisition protocol and second group (130 patients) acquired with a time-decay corrected acquisition protocol. Image interpretation was performed on planar images both qualitatively and semi-quantitatively. Three different blind readers analysed the images.

Results showed that the most accurate imaging acquisition protocol is to acquire images at 3-4h and at 20-24h in time mode with acquisition times corrected for isotope decay. When using this protocol, visual analysis leads to high sensitivity and specificity for diagnosis of infection. Semi-quantitative analysis might be used in doubtful cases, using no cut-off for the percentage of increase in radiolabelled WBC over time, as a criteria to define a positive scan.

Keywords: White Blood Cells, Scintigraphy, Infection imaging

Introduction

The use of ^{99m}Tc-HMPAO or ^{111}In-oxine labelled white blood cells (WBC) is still considered the gold standard nuclear imaging technique to diagnose infections in the bone and soft tissue, except for spondylodiscitis [1, 2]. For acute osteomyelitis and for prosthetic joint infections, reported diagnostic accuracy is approximately 90% [3-5]. However, there are also various reports that mention lower rates for sensitivity and specificity. These differences in diagnostic accuracy reported for WBC scintigraphy may be related to different image acquisition protocols and different interpretation criteria [6, 7]. To strengthen the clinical use of WBC scintigraphy, procedures and protocols are being standardized throughout the world. To this aim, the recent published guidelines by the Infection Committee of the European Association of Nuclear Medicine (EANM) provide indications, practical aspects, quality controls and safety procedures of this technique [8, 9]. Guidelines that describe the correct image acquisition and interpretation criteria for labelled WBC are also under preparation. Accurate acquisition protocols and interpretation criteria require knowledge of the normal radiolabelled WBC biodistribution (ie. blood and bone marrow) and pathological variants of WBC localization in different tissues and organs [2]. The general agreement for osteo-muscular infections and soft tissue infections is that at least two imaging time points are necessary, delayed (3-4 h after re-injection) and late (20-24 h). Early imaging (30 min-1 h after re-injection), which may be a surrogate for bone marrow uptake, is optional. Image interpretation can be made qualitatively (visual) or semi-quantitatively (calculation). In case of doubtful planar images with suspected bone marrow expansion, bone marrow imaging with ^{99m}Tc-colloids is currently performed to reduce the false positive rate [5, 10]. For exact localization of the infection SPECT/CT may have added value [11].

In this article, we retrospectively compared in a large series of ^{99m}Tc-HMPAO-WBC planar scintigraphies in different types of infections, two different acquisition protocols (time decay corrected *versus* fixed-time acquisition) and two different interpretation criteria (visual *versus* semi-quantitative evaluation), to determine which is the best combination to obtain the highest diagnostic accuracy for infection versus sterile inflammation. The hypothesis is that a sterile inflammation will not show an increase focal uptake with time, differently from an infection, and that this trend of increase/decrease in time is better detectable by acquiring time decay corrected images than fixed-time acquired images.

Methods

Patient population

This is a retrospective study analysing patients that were referred for scintigraphy with ^{99m}Tc-HMPAO labelled WBC from January 2009 to December 2011, in three University centers (University Medical Center Groningen, University of Pisa Medical School, and Sapienza University of Rome). Ethic Committee approved the study in all centers. We therefore analyzed 235 patients with suspected osteomyelitis suspected prosthesis infection and suspected soft tissue infection as shown in Table 5.1. Infection was suspected based on clinical examination, blood tests (including WBC counts, C-reactive protein, erythrocyte sedimentation rate, acute phase proteins), urine-analysis, three sets of blood cultures including at least one aerobic and one anaerobic from a peripheral vein [12], and/or conventional radiology, e.g. plain X-ray, ultrasound and/or contrast-enhanced computed tomography (CT).
Final diagnosis of an infection or exclusion of an infection was defined on the basis of pathological, microbiological, or clinical diagnosis, with clinical follow-up of more than 6 months for all patients. Overall, 109 patients were diagnosed with an infection and 126 were negative for infection (see Table 5.2).

^{99m}Tc-HMPAO WBC preparation and imaging protocol

Preparation and labelling of WBC were performed according to the guidelines for the labelling of leukocytes with ^{99m}Tc-HMPAO from the European Association of Nuclear Medicine [13]. Radiolabelling efficiency was always between 70-85%.
In 105 patients, we used the fixed-time (FT) acquisition protocol by acquiring planar delayed and late images for 600 seconds each. In 130 patients, we used the time-decay corrected (TDC) acquisition protocol by acquiring planar (static) images at 30 min-1 h (optional “early images”, 100-200 sec), at 3-4 h (“delayed images”, 133-300 sec) and at 20-24 h (“late images”, 951-2396 sec) after reinjection of 370-555 MBq ^{99m}Tc-HMPAO labelled WBC (see Table 5.3).

Table 5.1 Patient characteristics (n = 235)

Age	
Mean	61
Median	63
Range	16-93
SD	17
Sex	
Female	131 (56%)
Male	104 (44%)
Type of suspected infection	
Osteomyelitis	80 (34%)
Hip prosthesis	63 (27%)
Knee prosthesis	66 (28%)
Shoulder prosthesis	3 (1%)
Soft tissue	23 (10%)
Blood tests	
WBC counts	
Increased	13 (5%)
Normal	134 (57%)
C-reactive protein	
Increased	74 (31%)
Normal	69 (29%)
Erythrocyte Sedimentation Rate	
Increased	69 (29%)
Normal	69 (29%)

Table 5. 2 Final diagnosis in all patients and divided in the two groups studied with fixed time acquisition (FT) and time-decay corrected acquisition (TDC).

Diagnosis	n (%)	FT (%)	TDC (%)
Infection			
Osteomyelitis	35 (32)	24 (69)	11 (31)
Infected hip prosthesis	23 (21)	8 (35)	15 (65)
Infected knee prosthesis	31 (28.4)	16 (52)	15 (48)
Infected shoulder prosthesis	3 (3)	3 (100)	0
Soft tissue infection	17 (15.6)	7 (41)	10 (59)
Total	109 (46.4)	58 (53)	51 (47)
No infection	126 (53.6)	48 (38)	78 (62)

Table 5.3: Examples of acquisition times for the time-decay corrected images with ^{99m}Tc-HMPAO-WBC.

	Hours after the 1st acquisition	Corrected acquisition time (seconds) if early images were acquired for 100 seconds	Corrected acquisition time (seconds) if early images were acquired for 200 seconds
Delayed images	1.5	119	238
	2	126	252
	2.5	133	267
	3	141	283
	3.5	150	300
Late images	19.5	951	1902
	20	1007	2015
	20.5	1067	2135
	21	1131	2262
	21.5	1198	2396

All images (128×128 matrix size or 256x256 matrix size depending on centers) were acquired on a SPECT gamma camera system (Siemens Symbia T, Siemens Medical Systems (Groningen), Hawkeye, GE Healthcare (Pisa) or SkyLight, Philips (Rome)) equipped with low-energy high resolution collimators with energy window centred at the 140 keV photo-peak of ^{99m}Tc using a width of 20%.

All images were displayed and analysed using the same workstation (Osiris), to avoid differences in display of different camera systems. TDC images were displayed in number of counts, using the same intensity scale both for delayed and late images, thereby avoiding operator-bias in changing the intensity scale. This is essential when interpreting time-decay corrected images but it is not possible when images are acquired with a fixed-time protocol. Therefore, FT images were displayed in % of maximum counts as they usually appear in automatic mode on both Siemens, GE and Philips workstations.

SPECT/CT was performed for precise location of the infectious focus. In these cases, the low-dose CT transmission scan was acquired for 16 seconds over 220° for each transaxial slice. The full FOV consisting of 40 slices was completed in 10 minutes. The transmission data were reconstructed using filtered back-projection to produce cross-sectional images. Resolution of the CT scan was 2.2 mm and localization images were produced with a 4.5-mm pixel size, similar to the nuclear medicine emission images. The CT scans

were reconstructed into a 256×256 matrix. The SPECT component of the same FOV was acquired using a 128×128 matrix, 360° rotation, 6° angle step, and 40/60-sec-per-frame acquisition time at 4 and at 24 hours, respectively. Both CT-attenuation corrected and non-corrected SPECT images were evaluated in the coronal, transaxial, and sagittal planes, as well as in three-dimensional maximum intensity projection (MIP) cine mode. Matching pairs of x-ray transmission and radionuclide emission images were fused using the Xeleris workstation (Pisa), and hybrid images of overlying transmission and emission data were generated.

Visual and semi-quantitative image interpretation

The planar scintigraphic images were visually analysed separately by two experienced nuclear medicine physicians (PE, AG); in case of disagreement by the two observers a third reader (AS) reviewed the images and his decision was considered as for the final classification. The studies were classified (a) “negative for infection” if no uptake was seen in both delayed and late planar images or when the uptake was the same or decreasing in time, and (b) “positive for infection” when at least one focus of abnormal uptake characterized by time-dependent increase in radioactivity or increase in size from delayed to late planar images was observed. In some positive patients with peripheral osteomyelitis, when differential diagnosis between bone and soft tissue involvement was not ascertained at planar images, we did perform SPECT/CT for exact localization.
The visual analysis was performed using the same criteria for the non-decay corrected and the decay corrected images. For semi-quantitative analysis, in all images a ROI was drawn over the area suspected for infection and copied to presumed normal reference tissue (e.g. anterior-superior iliac crest, unaffected contralateral bone, etc.) The mean counts per pixel in these ROIs were recorded to calculate Target/Background (T/B) ratios both in delayed and late images. When the T/B was similar or decreased with time the scan was considered negative for infection; when the T/B increased with time, the scan was considered positive. Images were classified using different thresholds of increase of T/B ratio over time: ≤ 5, ≤ 10, ≤ 20, and ≤ 25 %.

Data analysis and statistics

Results of ^{99m}Tc-HMPAO-WBC scintigraphy were correlated with those of conventional radiologic imaging and with the final microbiological,

pathological or clinical diagnosis. For each patient results of visual and semi-quantitative interpretation were compared to the final diagnosis. Semi-quantitative analysis using < 5, < 10, < 20, and < 25% of increase in time, were calculated.
All values are expressed as median and range, as customary for nonparametric data. Comparison of the two groups for clinical and demographic factors was performed by Pearson's χ^2. The readers inter-observer agreement rates were also evaluated and expressed in weighted kappa which corrects for agreement by chance. The sensitivity, specificity, diagnostic accuracy, negative predictive value and positive predictive value were calculated and differences between groups compared by Chi-squared test. All statistical evaluations were performed using the STATA Statistical Software package, Release 10-2010 (STATA Corporation, College Station, Texas, USA).

Results

No significant difference in age distribution or any other clinical parameters between the two groups was observed.
By adopting the interpretation criteria described above for scintigraphic detection of infection, it was possible to classify all the scans as either frankly positive or frankly negative, therefore without any equivocal result. ^{99m}Tc-HMPAO-WBC scans were totally negative in 121 cases (47/105 FT acquisition and 74/130 TDC acquisition; p=ns). At least one abnormal area with focal accumulation of the radiolabelled leukocytes with increase of radioactivity over time, or size, was detected in the remaining 114 patients (58/105 FT acquisition and 56/130 TDC acquisition; p=ns). Table 5.4 shows the results of ^{99m}Tc-HMPAO-WBC at visual analysis, in all patients and according to the specific clinical indication. Overall, TDC acquired images, as compared to the FT acquired images, showed comparable sensitivity (94.1% *versus* 94.8%; p=ns) and NPV (96.3% *versus* 93.3%; p=ns), but better specificity (100% *versus* 89.4%; p=0.006), accuracy (97.7% *versus* 92.4%; p=0.05) and PPV (100% *versus* 91.6%; p=0.05). Figures 5.1 shows examples of positive and negative radiolabelled WBC scan at the visual analysis. Even though numbers vary according to the specific clinical indication, the better performances for the TDC acquired images at the visual analysis are invariable with the exception of soft tissue infections (Table 5.4).

For the semi-quantitative analysis we found best accuracy, sensitivity and NPV when considering any percentage of increase of radioactivity in the suspected lesion over time, for both FT and TDC acquired images. By contrast, specificity and PPV increase by increasing the threshold of percentage increase (Table 5.5).
Furthermore, accuracy, specificity and PPV are generally higher in the semi-quantitative analysis when images are acquired with FT method, whereas sensitivity and NPV are higher when images are acquired with TDC method (Table 5.6). This is particularly true for osteomyelitis and hip prosthesis, but not for soft tissue infections and knee prosthesis. Figure 5.2 provides examples of visual and semi-quantitative interpretation of images.
Inter-observer agreement rates for the interpretation of ^{99m}Tc-HMPAO-WBC images were higher for TDC acquired images as compared to the FT acquired images (lack of consensus in 11% and 19% of cases, respectively, with the lower agreement for hip and knee prosthesis infections).
The rate of concordance between the visual and the semi-quantitative analysis was better considering any % of increase of radioactivity in time and for the TDC images (200/235) either considering all patients together or considering osteomyelitis and prosthetic infections alone. In case of soft tissue infection, the best agreement was obtained comparing the visual and the semi-quantitative analysis considering 5% of increase of radioactivity in time (always better for the TDC images).

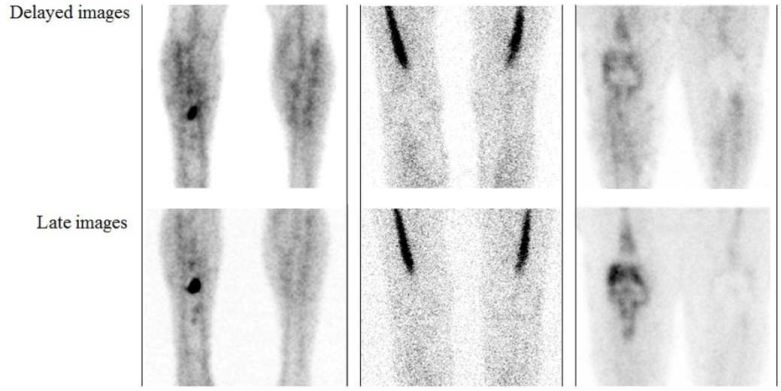

Figure 5.1: ^{99m}Tc-HMPAO-WBC scintigraphy in patients with suspected bone and knee prosthesis infections acquired after 4h (delayed images) and 20h (late images) with either fixed time acquisition modality (left and middle panels) or time-decay corrected modality (right panels). In all cases the visual analysis correctly diagnosed osteomyelitis (left panel), aseptic bone marrow expansion (middle panel) and right knee infected prosthesis vs non-infected left knee prosthesis (right panel).

Table 5.4: Results of qualitative (visual) analysis of ^{99m}Tc-HMPAO-WBC scintigraphy as compared to final diagnosis

	Visual *vs* final diagnosis									
	Osteomyelitis		Prosthesis hip		Prosthesis knee		Soft tissue		Total	
	FT	TDC	FT	TDC	FT	TDC	FT	TDC	FT	TDC
TP	23	11	7	14	15	14	7	9	55*	48
TN	23	20	10	29	8	25	1	5	42	79
FP	2	0	1	0	2	0	0	0	5	0
FN	1	0	1	1	1	1	0	1	3	3
Sensitivity	96%	100%	87%	93%	94%	93%	100%	90%	95%	94%
Specificity	92%	100%	91%	100%	80%	100%$^{\#}$	100%	100%	89%	100%$^{\#}$
Accuracy	94%	100%	89%	98%	88%	98%$^{\#}$	100%	93%	92%	98%$^{\#}$
PPV	92%	100%	87%	100%	88%	100%$^{\#}$	100%	100%	92%	100%$^{\#}$
NPV	96%	100%	90%	93%	89%	93%	100%	83%	93%	96%

TP, TN, FP and FN are numbers of patients. FT = fixed time acquisition, TDC = time-decay corrected acquisition. *includes 3 cases of shoulder prosthesis. $^{\#}$ $p<0.05$ *versus* FT.

Table 5.5: Results of semi-quantitative analysis of ^{99m}Tc-HMPAO-WBC scintigraphy compared to final diagnosis, specified for both acquisition protocols

	Semi-quantitative vs final diagnosis									
	Any T/B increase		Increase >5%		Increase >10%		Increase >20%		Increase >25%	
	FT	TDC	FT	TDC	FT	TDC	FT	TDC	FT	TDC
TP	56	48	46	38	41	34	30	24	26	18
TN	34	59	40	65	45	69	45	69	45	69
FP	13	20	6	15	2	10	2	10	2	10
FN	2	3	13	12	17	17	28	27	32	33
Sensitivity	97%	94%	78%	76%	71%	67%	52%	47%	45%	35%
Specificity	72%	75%	87%	81%	96%	87%	96%	87%	93%	87%
Accuracy	86%	82%	82%	79%	82%	79%	71%	72%	68%	67%
PPV	81%	70%	87%	72%$^{\#}$	95%	77%$^{\#}$	94%	71%$^{\#}$	96%	64%$^{\#}$
NPV	94%	95%	75%	84%	73%	80%	62%	72%	58%	68%

TP, TN, FP and FN are numbers of patients. FT = fixed time acquisition, TDC = time-decay corrected acquisition. $^{\#}$ $p < 0.05$ *versus* FT.

Table 5.6: Results of semi-quantitative analysis of ^{99m}Tc-HMPAO-WBC scintigraphy, defined for each specific indication and compared to final diagnosis, specified for both acquisition protocols

	Semi-quantitative vs final diagnosis (any T/B increase)							
	Osteomyelitis		Prosthesis hip		Prosthesis knee		Soft tissue	
	FT	TDC	FT	TDC	FT	TDC	FT	TDC
TP	23	11	7	14	16	14	7	9
TN	23	17	9	20	6	17	1	5
FP	2	3	2	9	4	8	0	0
FN	1	0	1	1	0	1	0	1
Sensitivity	96%	100%	88%	93%	100%	93%	100%	90%
Specificity	92%	85%	82%	69%	60%	68%	100%	100%
Accuracy	94%	90%	84%	77%	85%	78%	100%	93%
PPV	92%	79%	78%	61%	80%	64%$^{\#}$	100%	100%
NPV	96%	100%	90%	95%	100%	94%	100%	83%

TP, TN, FP and FN are numbers of patients. FT = fixed time acquisition, TDC = time-decay corrected acquisition. $^{\#}$ $p < 0.05$ *versus* FT.

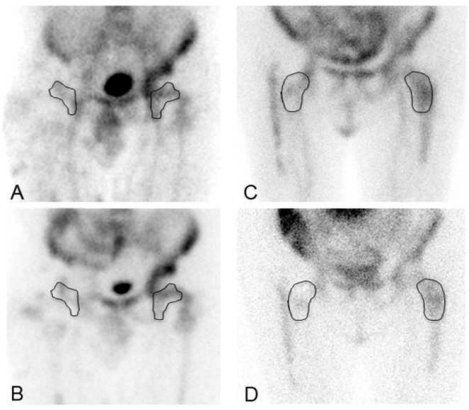

Figure 5.2: ^{99m}Tc-HMPAO-WBC scintigraphy in two different patients with suspected low grade infection of the right hip prosthesis acquired after 4h (upper panels) and 20h (lower panels) with either fixed time acquisition modality (left panels) or time-decay corrected modality (right panels). Images A and B at visual analysis were judged negative and semi-quantitative analysis showed a stable T/B over time (equivocal for infection). After prosthesis removal microbiology showed the presence of infection. Images C and D at visual analysis were judged negative and semi-quantitative analysis showed a stable T/B over time (equivocal for infection). After prosthesis removal microbiology confirmed the absence of infection. These two examples highlights how TDC acquisition allows accurate and easier visual interpretation of images.

Discussion

It is commonly accepted that WBC images are visually classified as (i) negative if no uptake or a decrease in uptake from delayed to late images is present, (ii) positive when uptake is seen in both delayed and late images with increase in activity or size in time, and (iii) equivocal when uptake in delayed and late images is the same or slightly decreasing. However, a general criticism to the visual analysis is that it is strictly operator dependent and that the final results may differ significantly when images are acquired and displayed, using
different ways with different contrast and background. Acquisition protocols are variable. Some author acquire, early, delayed and late images, with a fixed constant time for all images; others acquire all images with a fixed number of counts, but both methods are not corrected for isotope decay, are influenced by variations of background activity and are operator dependent. To reduce variability some authors suggest, after acquisition, to display images equalizing bone marrow activity, as reference. However, also bone marrow activity may change in time, therefore this modality of displaying images does not improve accuracy and is limited to expert readers and some regions of the body with a good bone-marrow activity. We suggest here to acquire images at different time points with different acquisition times, starting from a settled amount of time in the early images and deriving the corresponding acquisition time for delayed and late images by correction due to isotope decay (as shown in Table 5.3). As a result, delayed and late images have the same counting statistics of early images and comparison is possible reducing the operator bias [14-16]. It is of course mandatory to display all images with same intensity scale in counts units and not in percentage of max counts per pixels that is another common display error. If images are correctly acquired and displayed, they are operator independent, reproducible, comparable and easy to interpret.
We used the same software system (Osirix) for all patients, in order to avoid differences in display of different software systems between the centers. However, we want to state that all data are reproducible on all three systems (GE, Philips and Siemens) by displaying images in count units with the same intensity scale.
Semi-quantitative analysis may also be helpful when visual interpretation is doubtful. Regions of interest (ROIs) can be drawn over the part of the presumed infected focus, copied to presumed normal reference tissue (e.g. anterior-superior iliac crest, contralateral bone), and target-to-background

(T/B) ratios can be calculated. However, location of ROIs in lesion and reference tissue is operator dependent. Additionally, the level of significance of the T/B ratios is arbitrarily decided and no studies have yet defined the threshold of increase of radiolabelled WBC over time to be considered positive.

In this study, we retrospectively compared two different acquisition protocols for planar images (TDC vs. FT) and two different interpretation criteria (visually vs. semi-quantitatively) to determine the criteria that allow highest diagnostic performances.

Best results were obtained with TDC acquired images and visual analysis for bone associated infections but not for soft tissue infections. Despite statistical significance is reached only when considering the whole group of patients, for each bone indication a consistent improvement of the diagnostic performances was always achieved by acquiring TDC images. The add value of the TDC acquisition is more evident in patients with bone and prosthetic infections, hereby potentially limiting the need for bone marrow imaging with colloids. The FT acquired images possibly have an advantage in term of sensitivity, but lead to a significant drop in specificity and diagnostic accuracy. On the other hand, when soft tissue infections were considered, the advantage of TDC acquisition was not evident. This may have several explanations. First, there might be different kinetics of migration of radiolabelled WBC in bones and soft tissues. Additionally, soft tissue infections includes muscular, brain, abdominal, heart, lung or dermal infections, thus being a very heterogeneous group with possible different behavior in terms of leukocyte recruitment and may need “ad hoc” interpretation criteria as already demonstrated for dermal filler infections and dermal infections in diabetic foot [14, 15]. In our study the 7 cases of soft tissue infections acquired with FT modality were mainly muscular infections, whereas the 10 soft tissue infections acquired with TDC modality were all dermal infections and this difference may account for the different accuracy in our results.

Overall, the main advantage of TDC acquisition protocol is represented by the absence of operator interference and bias, that, by contrast, can strongly affect the results of FT acquired images. In this study there was little but significant difference in global diagnostic accuracy between FT and TDC acquired images (92.4% versus 97.7%; $p<0.05$) but we should consider that readers were experts also in FT acquired images. Indeed we can expect that a lower diagnostic accuracy of FT acquired images can be observed for less expert readers thus being TDC acquired images even more relevant.

Our results indicate that any percentage of radioactivity increase over time leads to high sensitivity (Table 5.5). Increasing the threshold to i.e. 20% radioactivity increase over time improves specificity, but lowers sensitivity.
The threshold of the percentage of T/B increase over time may be affected by several parameters such as the type of infection (acute *versus* chronic), the type of disease (osteomyelitis *versus* soft tissue infections), the sustaining microorganisms and the presence of concomitant antimicrobial treatment. Since all these factors can significantly modify the intensity and the pattern of radiolabelled WBC over time, further studies are warrant to give clinical validation to this approach.
Another point of discussion is the placement of the ROIs, which can differ between operators (contralateral, bone marrow, etc.). Despite a recent study from our group showed that the contralateral region is the most accurate for positioning the ROI for the background semi-quantitative calculation [17], in this study it was not possible to apply this criteria and background ROIs were positioned either on ipsilateral bone marrow or muscle when contralateral bone marrow was not available.
To better localize the site and extent of infection, SPECT/CT images may be used. If sequential SPECT images are acquired, acquisition times for SPECT can also be normalized according to isotope decay using the same decay formula shown in Table 5.3. SPECT/CT is invaluable to better identify the site and delineate the extent of ^{99m}Tc-HMPAO-WBC uptake (i.e. bone or soft tissue) as compared to the planar and stand-alone SPECT images due to the easy identification of either blood-pool activity at the vascular bed or at bone marrow or e.g. non specific accumulation of ^{99m}Tc-HMPAO in the bowel. In this study, however, SPECT/CT was not used for diagnosing infection but for determining its extent in positive planar images.
The role of SPECT/CT has been established for soft tissue infections [15] and endocarditis, cardiac devices, vascular prosthesis infections [11] and diabetic foot [18] when the need of anatomical landmarks is relevant. However, in some circumstances attention should be paid since intense uptake of the radiolabelled WBC localized close to the bone may lead to false positive results for osteomyelitis (see Figure 5.3).
When evaluating bone/prosthesis infection and soft tissue infections, whole body imaging is mostly not necessary. However, such images allowed the check for the normal biodistribution of the radiolabelled autologous leukocytes and also the detection of distant sites of infection when suspected. In cases of sequential whole body imaging, acquisition times can also be normalized.

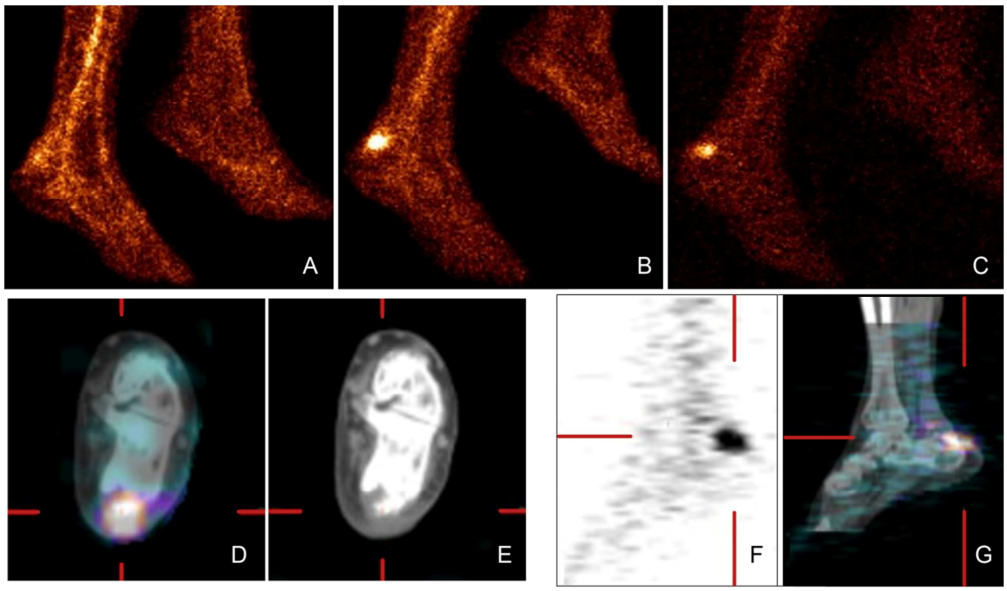

Figure 5.3: Planar images of feet of a patient with a suspected osteomyelitis consequent to a fracture of the calcaneus bone with a cutaneous wound. At 30 min post-injection (first image, "early image") image was acquired for 100 sec/frame (61,269 counts) (A). At 3 hrs post-injection ("delayed image", 2.5 hrs after first image) image was acquired for 133 sec/frame (52,274 counts) (B). At 20 hrs post-injection ("late image", 19.5 hrs after first image) image was acquired for 951 sec/frame (52,212 counts) (C) showing evident decrease of activity at visual analysis, sign of no osteomyelitis. At 3 hrs semi-quantitative analysis showed T/B=2.2 and at 20 hrs T/B=1.8 confirming a decrease with time, sign of no infection but just wound inflammation. The SPECT/CT at 20 hrs (D-G) however, does not allow to clearly identify the origin of uptake (cutaneous *vs* bone surface), thus being the visual analysis of planar imaging more accurate. Patient was operated to remove the bone fragment and no sign of osteomyelitis was confirmed at histology.

Conclusions

When having a suspicion of a prosthetic joint infection or osteomyelitis, WBC scintigraphy should be performed by acquiring images at least at two time points, one at 3-4 hours (delayed images) and one at 20-24 hours (late images). Early images (at 30min-1h post-injection) may also be performed to have an early map of bone marrow distribution, but are not strictly necessary.
The most reproducible and accurate acquisition protocol in musculoskeletal infections is using time-decay corrected acquisitions.
Images must then be displayed using the same intensity scale in count units and not in percentage of max counts per pixel.

When these methodological considerations are fulfilled, visual analysis of images is operator-independent and is enough for high diagnostic accuracy of infection, thus avoiding semi-quantitative analysis.

References

1. Van der Bruggen W, Bleeker-Rovers CP, Boerman OC, Gotthardt M, Oyen WJ. PET and SPECT in osteomyelitis and prosthetic bone and joint infections: a systematic review. *Semin Nucl Med.* 2010;40:3-15.
2. Signore A, Glaudemans AW. The molecular imaging approach to image infections and inflammation by nuclear medicine techniques. Ann Nucl Med. 2011;25:681-700.
3. Palestro CJ, Love C, Bhargava KK. Labeled leukocyte imaging: current status and future directions. Q J Nucl Med Mol Imaging. 2009;53:105-123.
4. Love C, Marwin SE, Palestro CJ. Nuclear medicine and the infected joint replacement. Semin Nucl Med. 2009;39:66-78.
5. Gemmel F, Van den Wyngaert H, Love C, Welling MM, Gemmel P, Palestro CJ. Prosthetic joint infections: radionuclide state-of-the-art imaging. Eur J Nucl Med Mol Imaging. 2012;39:892-909.
6. Tondeur MC, Sand A, Ham HH. Interobserver reproducibility in the interpretation of ^{99m}Tc-labelled white blood cell scintigraphic images. Nucl Med Commun. 2008;29:1093-1099.
7. Glaudemans AW, Galli F, Pacilio M, Signore A. Leukocyte and bacteria imaging in prosthetic joint infections. Eur Cell Mater. 2013;25:61-77.
8. De Vries EF, Roca M, Jamar F, Israel O, Signore A. Guidelines for the labelling of leucocytes with (99m)Tc-HMPAO. Inflammation/infection Taskgroup of the European Association of Nuclear Medicine. Eur J Nucl Med Mol Imaging. 2010;37:842-848.
9. Roca M, De Vries EF, Jamar F, Israel O, Signore A. Guidelines for the labelling of leucocytes with (111)In-oxine. Inflammation/infection Taskgroup of the European Association of Nuclear Medicine. Eur J Nucl Med Mol Imaging. 2010;37:835-841.
10. Gotthardt M, Bleeker-Rovers CP, Boerman, OC, Oyen WJ. Imaging of inflammation by PET, conventional scintigraphy, and other imaging techniques. J Nucl Med. 2010;51:1937-49.
11. Erba PA, Conti U, Lazzeri E, Sollini M, Doria R, De Tommasi SM, et al. Added value of ^{99m}Tc-HMPAO labeled leukocyte SPECT/CT in the characterization and management of patients with infectious endocarditis. J Nucl Med. *2012*;53:1235-1243.
12. Raoult D, Casalta JP, Richet H, et al. Contribution of systematic serological testing in diagnosis of infective endocarditis. J Clin Microbiol. 2005;43:5238-5242.
13. de Vries EF, Roca M, Jamar F, Israel O, Signore A. Guidelines for the labelling of leucocytes with (99m)Tc-HMPAO. Inflammation/Infection Taskgroup of the European Association of Nuclear Medicine. Eur J Nucl Med Mol Imaging. 2010;37:842-848.
14. Familiari D, Glaudemans AW, Vitale V, Prosperi D, Bagni O, Lenza A, et al. Can sequential 18F-FDG PET/CT replace WBC imaging in the diabetic foot? J Nucl Med. 2011;52:1012-1019.
15. Grippaudo FR, Pacilio M, Di Girolamo M, Dierckx RA, Signore A. Radiolabelled white blood cells in the work out of dermal filler complications. Eur J Nucl Med Mol Imaging. 2013;40:418-425.
16. Signore A. Techniques, image acquisition and interpretation criteria. In: A. Signore and AM Quintero, eds. Diagnostic imaging of infections and inflammatory diseases: a multidisciplinary approach. New York, NY: J. Wiley Pbl; 2013:149-167.
17. Glaudemans AW, De Vries EF, Vermeulen LE, Slart RH, Dierckx RA, Signore A. A large retrospective single-centre study to define the best image acquisition protocols

and interpretation criteria for white blood cell scintigraphy with ^{99m}Tc-HMPAO-labelled leucoyctes in musculoskeletal infections. Eur J Nucl Med Mol Imaging. 2013.
18. Schillaci O. Hybrid imaging systems in the diagnosis of osteomyelitis and prosthetic joint infection. Q J Nucl Med Mol Imaging. 2009;53:95-104.

Chapter 6

^{111}In-DTPA-Biotin uptake by Staphylococcus aureus

Paola Anna Erba[1], Angela G. Cataldi[1], Carlo Tascini[2], Alessandro Leonildi[2], Chiara Manfredi[1], Giuliano Mariani[1] and Elena Lazzeri[1]

[1]Regional Center of Nuclear Medicine, University of Pisa Medical School
[2]Infective and Tropical Diseases Division, University Hospital of Pisa, Pisa, Italy

Nuclear Medicine Communications 2010, 31:994–997

Abstract

The potential of indium-111 labelled diethylene- triaminepentaacetic acid a,o-bis(biocytinamide) (^{111}In-DTPA-Biotin) as a specific tracer in nuclear medicine imaging of vertebral osteomyelitis has been shown in a large series of consecutive patients. Biocytin is known to serve as a biotin source for a number of different microorganisms and quantitative studies on staphylococci indicated that on a molar basis biocytin seemed to have an activity equal to that of biotin. In this study, we evaluated the possibility of an illicit transport of ^{111}In-DTPA-Biotin in cultures of Staphylococcus aureus on continued incubation for 24 h. Radiolabelled biocytin was prepared as described earlier and the stability and radiochemical purity was assessed in vitro for 24 h after labelling. Our data seem to demonstrate a passive transport of ^{111}In-DTPA -Biotin into the cells of the microrganisms.

Introduction

Staphylococcus aureus is the bacterium most frequently isolated (55–80%) in infections (especially in spondilo- discitis), followed by coagulase-negative staphylococcus and enterobacteriaceae (Salmonella spp., Escherichia coli, Klebsiella spp.) [1–5]. Several radiopharmaceuticals have been developed for the scintigraphic imaging of infection/inflammation [6,7], aiming in particular at discriminating infection from ster- ile inflammation. However, none of the agents nowadays available are completely infection-specific. Indium-111 labelled diethylenetriaminepentaacetic acid a,o-bis(biocytinamide) (^{111}In-DTPA-Biotin) has been used in a two-step approach to infection imaging (the avidin/^{111}In-DTPA-Biotin technique) [8–12]; neverthe- less, the potential of radiolabelled biotin as an infec- tion-imaging agent per se has already been shown in an experimental animal model of infection using biotin labelled with fluorine-18 [13] and in a large series of consecutive patients with vertebral osteomyelitis using ^{111}In-DTPA-Biotin [14,15]. A possible pathophysiologic basis for such an observation is that biotin accumulates at the sites of infection not only because of passive local dif- fusion on account of abnormally increased capillary perme- ability, but also because of some incorporation of the radiolabelled agent into the bacteria; this consideration is based on the ascertained function of biotin itself as a growth factor for several bacteria (including staphylococ- ci) [16–19]. Such early observations emphasize the need to take into account several parameters when evaluating the biotin requirement of staphylococci (especially S. aureus). In particular, attention must be paid to avoid the inhibitory effect of biotin excess on the synthesis of the transport system; furthermore, it should be con- sidered that some bacterial strains that require biotin for growth, can actually synthesize such a compound starting from the constituents of the culture medium. The aim of this study, to further validate the clinical relevance of labelled biotin, particularly in spine infec- tion, was to assess the extent, stability and mechanism of ^{111}In-DTPA-Biotin incorporation by S. aureus on contin- ued incubation for 24 h in simply saline solution under aerobic conditions and adding known amounts of radio-labelled biotin.

Materials and methods

Radiopharmaceutical

One milligram of DTPA-Biotin, purchased from Sigma (St Louis, Missouri, USA), was diluted in 20 ml of sterile acetate buffer 0.05 mol/l, pH 5.5. Aliquots containing 500 mg/ml of DTPA-Biotin were then prepared and stored at 41C for subsequent labelling with indium-111. Just before use, each 500 mg aliquot of DTPA-Biotin was labelled with 111 MBq of ^{111}In-chloride (Mallinckrodt Inc., St Louis, Missouri, USA) by incubation at room tem- perature for 15 min; labelling efficiency was assessed by instant thin-layer chromatography-silica gel (Pall, New York, USA) using bicarbonate buffer 0.05 mol/l as the mobile phase. In this chromatographic system, ^{111}In-chloride remains at the origin, whereas 111In-DTPA-Biotin migrates with the solvent with an RF of 0.7. Radioactivity in the chromatographic strips was measured both by counting with a g-counter and by imaging with a phos-phor imager (Perkin-Elmer, Monza, Milan, Italy).

Microorganisms and growth conditions

Clinical isolates of S. aureus supplied by the Infection Disease Unit of the University Hospital of Pisa were inoculated into vials containing 50 ml of Mu¨ller–Hinton broth (Biomerieux, Bagno a Ripoli, Firenze, Italy) and stored overnight at 351C in a rotating incubator (Bactec 9240; Becton Dickinson, Franklin Lakes, New Jersey, USA). Microbial growth was quantified by sequential dilutions and subcultures on selective agar plates (Mannitol Salt Agar; Becton Dickinson), and also tested on permissive agar plates (Chocolate Agar; Becton Dickinson) as a con- trol for contaminating bacteria (that were always absent).

Incorporation assay

Suspensions of S. aureus were washed twice with saline, resuspended in distilled water and standardized turbidi- metrically so that each suspension tube would contain 4 x 1010 colony-forming units per millilitre equivalent to 0.2 mg of dry cells per millilitre. A total of 84 incubation tubes were prepared for each experiment: 61 tubes with viable bacteria and 21 tubes with killed staphylococci (boiled for 20 min). Viable microorganisms were incu- bated at 37 and 41#C for different incubation times (30 min, 1, 2, 4, 6, and 24 h) with 200 ml of both a 3.5 nmol/l (approximately 4 ng/ml) ^{111}In-

DTPA-Biotin solution in sterile saline (corresponding to 0.7 pmol of radiolabelled biotin per tube, or 0.8 ng of the compound) and a 3.5 mmol/l (approximately 4 mg/ml) ^{111}In-DTPA- Biotin solution. To explore possible active uptake, in one set of experiments, 0.01 mol/l glucose was added to the viable staphylococci incubation tubes. The viable count of staphylococci was also monitored for all time periods by the standard-agar plating technique. At the end of the incubation, microorganisms were recovered by centrifugation at 4500 g for 10 min. The bacterial pellets were washed three times with 1 ml of sterile saline to remove free ^{111}In-DTPA-Biotin, and radio- activity retained in the bacterial pellet was measured in a well-type gamma-counter (LKB Wallac, Turku, Finland). Background radioactivity possibly because of adsorption onto the incubation tubes was assessed using ^{111}In-DTPA- Biotin in sterile saline, without microorganisms, in the same incubation times and conditions described above. Radioactive counts were used to determine the amount of ^{111}In- DTPA-Biotin incorporated by bacterial suspensions, ex- pressed as nanograms of ^{111}In-DTPA-Biotin per milligram of dry cells. The experiments were carried out using sets of 3–6 tubes per incubation time and condition, and the results reported here represent the average of two separate experiments performed on different days.

Results

Radiochemical purity and stability of ^{111}In-DTPA-Biotin

Radiolabelling efficiency was consistently greater than 99% in all the experiments performed (n = 4). Stability of ^{111}In-DTPA-Biotin, assessed by evaluating radioche- mical purity at 2, 4, 6 and 24 h after labelling, was remark- ably high with radiochemical purity greater than 99% at all time points up to 24 h of incubation at room tempera- ture in the labelling reaction mixture (Fig. 6.1), which depicts a typical output of phosphor-imager analysis. Agree- ment between the strip cut-and-count technique and phosphor-imager analysis was 99%.

Incorporation assay

After thorough washing, the residual radioactivity because of ^{111}In-DTPA-Biotin adsorbed to the incubation tubes without adding bacteria was always much less than 0.005% of the total added radiolabelled biotin. No radioactivity was found associated with the bacterial pellet at all incubation

times and conditions in the experiments performed with the lower concentration of ^{111}In-DTPA-Biotin (3.5 nmol/l, data not shown).
In contrast, in the experiments performed with the higher concentration (3.5 mmol/l), a stable association of ^{111}In-DTPA-Biotin with the cell pellets of

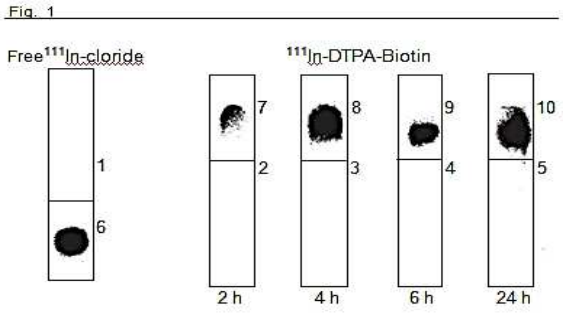

Figure 6.1: Radiopharmaceutical stability of indium-111 labelled diethylenetriaminepentaacetic acid a,o-bis(biocytinmaide) (^{111}In-DTPA-Biotin) in vitro. Chromatographic strips images generate on a phosphor screen at different time points.

viable S. aureus was observed, with an incorporation curve rising until 6 h of incubation and then plateauing until 24 h at approxi- mately 0.95 ng/mg of dry cells (corresponding to approxi- mately 0.86 pmol); the addition of glucose did not change such a time-pattern of incorporation (data not shown). Similarly, the incorporation curves obtained when in- cubating at 41°C were nearly identical to those obtained at 37°C (Fig. 6.2). The count of viable cells was found to be constant over the 24 h of incubation. In contrast, the microorganisms killed by boiling for 20 min showed an incorporation pattern characterized by the continuous rise of the curve, with values that were significantly higher than those observed with viable staphylococci (P = 0.02). In particular, the incorporation of ^{111}In-DTPA-Biotin by the killed bacteria at 6 and 24 h was approximately two-fold and four-fold the correspond- ing values observed with the viable bacteria, respectively

Discussion

Little is known about the conditions that affect the accumulation of native biotin into S. aureus. Hugo and Davidson [20] observed that S. aureus growing under limited biotin supply (if compared with the standard glucose meat-infusion broth, Müller–Hinton broth) slight- ly reduced their growth rate. Biotin transport into bacterial cells has been extensively investigated in

Lactobacillus by Waller and Lichstein [21], who showed that biotin transport occurred by two mechanisms: one process was dependent on temperature, pH and active cellular metabolism (Michaelis–Menten constant of 31.5 nmol/l), whereas the other one was inde- pendent of these.

Fig. 2

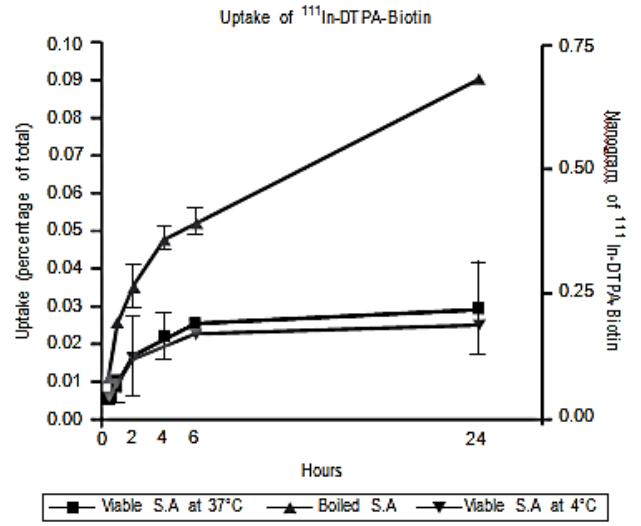

Figure 6.2: Comparison of the time-pattern of indium-111 labelled diethylenetriaminepentaacetic acid a,o-bis(biocytinamide) (^{111}In-DTPA- Biotin) uptake by suspensions of Staphylococcus aureus (S.A) in different experimental conditions. Each point represents the mean ± 1 SD of two independent experiments with triplicate tubes.

According to Rogers and Lichstein [22,23], the apparent Km for active transport of ^{14}C-biotin in yeast cultures of Saccaromyces cerevisiae was 0.03 nmol/l and the presence of glucose caused a 13-fold increase in the amount of biotin uptake after 30 min of incubation: 13 ng (0.05 nmol) versus 0.99 ng (0.004 nmol) of d-biotin (20 ng/ml) per milligram of dry cells. These investigators evaluated the inhibition of the active transport system of 14C-biotin in yeast cells grown in biotin excess (25 ng/ml, 100 nmol/l) medium, and they observed a mild uptake of biotin (less than 10 ng of biotin/mg of dry cells), with many features suggesting passive diffusion.

The possibility that biotin and biocytin could have, on a molar basis, the same activity [24] prompted us to evaluate the possible occurrence of an illicit transport when the larger ^{11}1In-DTPA-Biotin complex is available to S. aureus cells.

Nevertheless, there is still some contradictory evidence about the specific portion of biotin's structure affecting its ability to be taken up by bacterial cells; Prakash and Eisenberg [25] showed that the ureido ring of biotin must be intact for its uptake by bacteria, and that modifying the side chain does not reduce its uptake, whereas Gretler et al. [18] suggested that modifications of the side chain of biotin could reduce its transport across cell membranes.

We evaluated the ^{111}In-DTPA-Biotin incorporation into viable and killed S. aureus over the 24 h of incubation in a growth-limiting medium consisting of saline, but added with two different levels (4 ng/ml and 4 mg/ml, respec- tively) of radiolabelled biotin. Viable S. aureus cells show a slight uptake of radiolabelled biocytin (0.2 ng/mg of dry cells) as early as after 1 h of incubation in a medium containing excess (4 mg/ml) of radiolabelled biocytin, with a mechanism independent of glucose and temperature. ^{111}In-DTPA-Biotin has two biotin carboxyl groups joined to the DTPA through an amide bond and two intact ureido rings. Our data are consistent with the hypothesis that modifications of only the side chain (leaving the ureido rings intact) do not affect the uptake of ^{111}In- DTPA-Biotin.

The effect of the absence of glucose and temperature on radiolabelled DTPA-biotin uptake suggests that there is passive diffusion of approximately 0.2 pmol of labelled biocytin from the surrounding fluid into viable S. aureus, similar to that shown in the yeast cells grown in biotin excess medium (that still exhibited an ability to take up 4 pmol of ^{14}C-biotin even in the absence of glucose). On continued incubation for 24 h, the ^{111}In-DTPA-Biotin intracellular content reaches a steady state level of 0.95 ng (or 0.86 nmol) per milligram of dry cells within 6 h. The viable cell count and the level of incorporated ^{111}In-DTPA-Biotin then remain constant, suggesting that there is a stable association of ^{111}In-DTPA-Biotin with the cells. Several factors might be responsible for the saturation kinetics of this process. For instance, cells might be capable of taking up radiolabelled biotin by a mediated carrier transport system displaying saturation kinetics, or alternatively, synthesis of the transport system might be inhibited in such aging cells. Further- more, some saturation of the outer binding sites for 111In- Biotin in the absence of growth might occur as well.

On the other hand, killed staphylococci show a substan- tially higher uptake of ^{111}In-DTPA-Biotin, continuing for 24 h apparently without saturation. This finding supports the hypothesis that radiolabelled biocytin is normally able to pass the viable cell membrane probably through a faci-

litated diffusion process displaying a saturation kinetic pattern; on the contrary, ^{111}In-DTPA-Biotin can freely enter into the cells if the membrane has been damaged (killed staphylococci). Nevertheless, whichever is the mechanism of ^{111}In-DTPA-Biotin uptake under the con- ditions described here, it seems to be a passive process in which the radiolabelled biotin is presumably taken from the environment and stored, rather than destroyed by nonproliferating living organisms Further research is in progress to elucidate the fraction of ^{111}In-DTPA-Biotin that remains in the membrane and the fraction that completely passes inside the viable bacterial cells.

References

1. Carragee EJ. Pyogenic vertebral osteomyelitis. J Bone Joint Surg Am 1997; 79:874-880.
2. Torda AJ, Gottlieb T, Bradbury R. Pyogenic vertebral osteomyelitis: analysis of 20 cases and review. Clin Infect Dis 1995; 20:320-328.
3. Honan M, White GW, Eisenberg GM. Spontaneous infectious discitis in adults. Am J Med 1996; 100:85-89.
4. Carragee EJ, Kim D, Van der Vlugt T, Vittum D. The clinical use of erythrocyte sedimentation rate in pyogenic vertebral osteomyelitis. Spine 1997; 22:2089-2093.
5. Chen HC, Tzaan WC, Lui TN. Spinal epidural abscesses: a retrospective analysis of clinical manifestations, sources of infection, and outcomes. Chang Gung Med J 2004; 27:351-358.
6. Welling MM, Paulusma-Annema A, Balter HS, Pauwels EK, Nibbering PH. Technetium-99m labelled antimicrobial peptides discriminate between bacterial infections and sterile inflammations. Eur J Nucl Med 2000; 27:292-301.
7. Lupetti A, Welling MM, Pauwels EK, Nibbering PH. Radiolabelled antimicrobial peptides for infection detection. Lancet Infect Dis 2003; 3:223-229.
8. Chiesa R, Melissano G, Castellano R, Fernandez Zamora C, Astore D, Samuel A, et al. Avidin and 111In-labelled biotin scan: a new radioisotopic method for localising vascular graft infection. Eur J Vasc Endovasc Surg 1995; 10:405-414.
9. Rusckowski M, Paganelli G, Hnatowich DJ, Magnani P, Virzi F, Fogarasi M, et al. Imaging osteomyelitis with streptavidin and indium-111-labeled biotin. J Nucl Med 1996; 37:1655-1662.
10. Samuel A, Paganelli G, Chiesa R, Sudati F, Calvitto M, Melissano G, et al. Detection of prosthetic vascular graft infection using avidin/indium-111- biotin scintigraphy. J Nucl Med 1996; 37:55-61.
11. Lazzeri E, Manca M, Molea N, Marchetti S, Consoli V, Bodei L, et al. Clinical validation of the avidin/indium-111 biotin approach for imaging infection/inflammation in orthopaedic patients. Eur J Nucl Med 1999; 26:606-614.
12. Lazzeri E, Pauwels EKJ, Erba P, Volterrani D, Manca M, Bodei L, et al. Clinical feasibility of two-step streptavidin/In-biotin scintigraphy in patients with suspected vertebral osteomyelitis. Eur J Nucl Med 2004; 31:1505-1511.
13. Shoup TM, Fischman AJ, Jaywook S, Babich JW, Strauss HW, Elmaleh DR. Synthesis of fluorine-18-labeled biotin derivatives: biodistribution and infection localization. J Nucl Med 1994; 35:1685-1690.
14. Lazzeri E, Erba P, Perri M, Tascini C, Doria R, Giorgetti J, et al. Scintigraphic imaging of vertebral osteomyelitis with 111In-biotin. Spine (Phila Pa 1976) 2008; 33:E198-E204.
15. Lazzeri E, Erba P, Perri M, Doria R, Tascini C, Mariani G. Clinical impact of SPECT/CT with In-111 biotin on the management of patients with suspected spine infection. Clin Nucl Med 2010; 35:12-17.
16. Wright LD, Cresson EL, Valentick K, Skeggs HR. Microbiological characterization of biocytin. Federation Proc 1950; 9:374.
17. Broquist HP, Snell EE. Biotin and bacterial growth I. Relation to aspartate, oleate, and carbon dioxide. J Biol Chem 1951; 188:431-444.
18. Gretler CA, Mucciolo P, Evans JB, Niven CF. Vitamin nutrition of the staphylococci with special reference to their biotin requirements. J Bacteriol 1955;70:44-49.

19. Piffeteau A, Gaudry M. Biotin uptake: influx, efflux, and countertransport in Escherichia coli. Biochim Biophys Acta 1985; 816:77-82.
20. Hugo WB, Davidson JR. Effect of cell lipid depletion in Staphylococcus aureus upon its resistance to antimicrobial agents. Microbios 1973; 8:43-51.
21. Waller JR, Lichstein HC. Factors affecting the accumulation of biotin by Lactobacillus arabinosus. J Bacteriol 1961; 81:65–69.
22. Rogers TO, Lichstein HC. Characterization of the biotin transport system in Saccharomyces cerevisiae. J Bacteriol 1969; 100:557-564.
23. Rogers TO, Lichstein HC. Regulation of biotin transport in Saccharomyces cerevisiae. J Bacteriol 1969; 100:565-572.
24. Wright LD, Cresson EL, Skeggs HR. Biocytin in bacterial deamination of aspartic acid. Proc Soc Exp Biol Med 1950; 74:334-335.
25. Prakash OM, Eisenberg MA. Active transport of biotin in Escherichia coli K-12. J Bacteriol 1974; 120:785-791.

Chapter 7

Radiosynthesis of ^{68}Ga-labelled DOTA–biocytin (^{68}Ga-r-BHD) and assessment of its pharmaceutical quality for clinical use

Mattia Asti[1], Michele Iori[1], Paola A. Erba[2], Giulia Atti[1], Daniela Farioli[1], Claudio Guidotti[1] and Annibale Versari[1]

[1]Nuclear Medicine Unit, Advanced Technology Department, Santa Maria Nuova Hospital-IRCCS, Reggio Emilia
[2]Regional Center of Nuclear Medicine, University of Pisa Medical School, Pisa, Italy

Nuclear Medicine Communications, 2012 Nov; 33 (11): 1179-1187

Abstract

Objectives Biocytin analogues labelled with indium-111, yttrium-90 and lutetium-177 have shown their effectiveness in the imaging of infections/inflammation in patients with osteomyelitis and function as efficient tools in pretargeted antibody-guided radioimmunotherapy. In this study, the labelling of a biocytin analogue coupled with DOTA (1,4,7,10-tetraazacyclododecane-1,4,7,10-tetraacetic acid), namely, r-BHD, with gallium-68 (^{68}Ga) was optimized, and the quality and stability of the preparations were assessed for clinical use. Materials and methods Synthesis of ^{68}Ga-r-BHD was carried out by heating a fraction of the ^{68}Ge/^{68}Ga eluate in a reactor containing the biocytin analogue with the appropriate buffer. The influence of the precursor amount (from 2.5 to 140 nmol), the pH of the reaction (from 2 to 5.5) and the buffer species (1.5 mol/l sodium acetate, 1.5 mol/l sodium formate, 4.5 mol/l HEPES) on radiochemical yield and radiochemical purity was assessed. Studies on stability and binding to avidin (Av) were also conducted in different media. Results Under the best labelling condition (56 nmol of precursor, 3.8 pH, sodium formate buffer) synthesis of ^{68}Ga-r-BHD resulted in a yield of 64±3% (not decay corrected). Radiochemical purity was around 95% because a 68Ga-coordinated sulphoxide form of the ligand was detected as a by-product of the reaction (68Ga-r-SBHD). The by-product was identified and characterized by liquid chromatography–electrospray ionization tandem mass spectrometry. At the natural 1:4 Av/^{68}Ga-r-BHD molar ratio, affinity results were 62±2 and 80±2% in saline and human serum, respectively. Stability of ^{68}Ga-r-BHD and of the radiotracer/Av complex remains almost constant over 180 min. ^{68}Ga-r-BHD appears to be a good candidate for clinical applications.

Introduction

Biotin (5-[(3aR,4R,6aS)-2-oxohexahydro-1H-thieno[3,4-d]imidazol-4yl]pentanoic acid) is a natural vitamin that acts as a coenzyme in the metabolism of fatty acids, isoleucine and valine and plays a role in gluconeogenesis. Biotin has a strong binding affinity for avidin (Av) and streptavidin, and this binding property can be exploited to develop tracers for a number of applications on the basis of a pretargeting concept. Biocytin is an amide derived from the condensation between the biotin carbo- xylic moiety and the amino acid L-lysine that acts as a biotin source for a number of different microorganisms in vitro. For this reason an indium-111 (^{111}In)-labelled DTPA-biocytin analogue [^{111}In -diethylenetriaminepen-taacetic acid a,o-bis(biocytinamide)] has been used along with preinjection of Av or per se as an infection/ inflammation imaging agent and has shown its effective- ness in a large number of patients with vertebral osteomyelitis [1–3]. Recently, the infection specificity of ^{111}In –DTPA-biocytin with respect to inflammation was postulated [4]. Nevertheless, DTPA-biocytin adducts show relatively low stability in human serum mainly because of the susceptibility to hydrolysis of the amide bond between biotin and the L-lysine linked to the chelating moiety by the serum biotinidase [5,6]. More- over, in recent years, the use of DTPA itself as a chelator of metal radionuclides in bioconjugate molecules has been replaced by the use of macrocyclic chelating agents such as 1,4,7,10-tetraazacyclododecane-1,4,7,10-tetraacetic acid (DOTA), providing kinetically more stable complexes in human serum [7,8]. Both chemical drawbacks were overcome by Sabatino et al. [9], who reported the preparation of a CO-reduced N-aminoexylbiotinamido derivative conjugated to DOTA (r-BHD). This biocytin analogue showed improved stability in human serum and retained a high binding affinity for Av r-BHD, labelled with yttrium-90 (^{90}Y) and lutetium-177 (^{177}Lu), was used in a number of clinical studies to facilitate efficient pretargeted antibody guided radioimmunotherapy (PAGRIT) [10,11]. PET has shown a large number of advantages with respect to single photon emission tomography in terms of spatial resolution and target background ratio. However, even if the labelling of r-BHD with a positron emitter radionuclide such as ^{68}Ga could improve the imaging of both inflammation/infection and the pretargeting approach, limited data are available for the preparation and quality assessment of the ^{68}Ga-labelled r-BHD biocytin analogue [12]. The present study aimed at optimizing the radiolabelling of the biocytin

r-BHD derivative with the positron emitter ^{68}Ga radionuclide in order to yield a well-characterized product of high purity. Herein, the effect of some reaction parameters such as precursor and buffer amounts, buffer species and the stabilizers used on the radiochemical yield (RCY) and radiochemical purity (RCP) was investigated. Further, a full set of analyse was developed in order to achieve a pharmaceutical grade of the preparation and allow its safe use in clinical trials.

Materials and methods

Reagents and instrumentation

4-(2-hydroxyethyl)-1-piperazineethanesulphonic acid (HEPES), sodium acetate, sodium formate, Av (M_W 66 kDa), biotin and gallium(III) chloride (purity > 99.999%) were purchased from Sigma-Aldrich (Milan, Italy). A 3 mg/ml solution of r-BHD (ST2210-DP) was obtained from Sigma-Tau (Pomezia, Italy). A 1850 MBq IGG100 ^{68}Ge/^{68}Gagenerator and a Modular Lab automatic synthesizer were purchased from Eckert & Ziegler (Berlin, Germany). Metal-free hydrochloric acid (0.1 mol/l) was purchased from Carlo Erba (Milan, Italy), whereas 10 ml of disposable 95% ethanol, 0.9% sodium chloride and injectable water solu- tions were purchased from SALF (Bergamo, Italy) and B. Braun (Milano, Italy). Human albumin solution (20%) was obtained from Kedrion Biopharmaceuticals (Lucca, Italy). All reagents were used without further purification. When needed, milliQ water (resistivity 18.2 MO·cm) was used for preparing reagent solutions. Radiochemical and chemical analyses were carried out by ultrahigh-performance liquid chromatography (UHPLC) using an Acquity system with a binary solvent, a BEH C-18 1.7-mm column (2.1 x 150 mm) and autosampler manager modules (Waters, Milan, Italy). The instrument was equipped with an Acquity TUV detector (Waters) and a Herm LB 500 radiochemical detector (Berthold Technologies, Milan, Italy). RCP was also assessed by thin-layer chromatography (TLC) using an AR 2000 Imaging Scanner device (Bioscan, Washington, District of Columbia, USA). Liquid chromatography-electrospray ionization tandem mass spectrometry (LC-ESI-MS) was performed using an Ultimate 3000 HPLC chromatographic system (Dionex, Sunnyvale, California, USA) equipped with a Luna C-18 100-A column (4.6x50 mm; Phenomenex, Bologna,

Italy). The eluted samples were analysed using an LTQ Orbitrap XL instrument (Thermo Scientific, Waltham, Massachu- setts, USA) equipped with an electronspray ion source. The pH of the samples was assessed using a pH 213 Microprocessor pH-meter (Hanna Instruments, Milan, Italy). For the stability and Av affinity studies, samples were prepared using 10 kDa molecular weight cut-off Amicon Ultra-4 centrifugal filter devices (Millipore, Milan, Italy) and centrifuged at 6000 RCF for 60 min using an SL16 centrifuge (Thermo Fisher, Milan, Italy). All the activity measures described in this study were performed using an Aktivimeter ISOMED 2000 dose calibrator (MED Nuklear-Medizintechnik, Dresden, Germany).

Radiosynthesis of 68Ga--r-BHD

The radiolabelling of Ga-r-BHD was performed with a Modular Lab synthesizer using the fractionating method as already described by Decristoforo et al. [13] for the radiolabelling of Ga-DOTATATE. The software sequence was modified to allow the operator to manually select the eluate fraction to be collected, obtaining more than 80% of the Ga activity in an B2 ml 0.1 mol/l HCl fraction. The selected fraction was transferred into a reactor vial containing varying amounts of a 1 mg/ml r-BHD water solution (corresponding to a range from 2.5 to 140 nmol) and varying amounts of different buffer solutions in order to study the effect of the pH (ranging from 2 to 5.5) and the buffer species (1.5 mol/l sodium formate, 1.5mol/l sodium acetate, 4.5 mol/l HEPES solutions) on the RCY and RCP. The mixture was heated to 1001C for 5 min and then passed through a light C-18 cartridge (Waters) preconditioned manually with 3 ml of a 50% EtOH solution and 3 ml of a 0.9% sodium chloride solution. The product was retained in the cartridge, and the solution was collected separately in order to measure the pH of the reaction precisely. Ga-r-BHD was eluted with 0.5-1 ml of a 50% ethanol solution and diluted with 8 ml of a 0.9% sodium chloride solution. Before being collected into the final vial the solution was passed through a sterile 0.22 mm filter (Waters). In the second step of the experiments, varying amounts of EtOH (50, 100 and 200 ml) were directly added to the reactor before the labelling reaction in order to assess the effect of the radical scavenger on the RCP. The synthesis time was about 14 min and every preparation was performed in triplicate. None of the radiochemical yields reported in the results of this study are corrected for decay and are referred to the radioactivity of Ga-r-BHD at the end of synthesis with respect to the total ^{68}Ga activity eluted from

the generator. The yield was calculated considering the RCP obtained from UHPLC analyses. Preparation of free $^{68}Ga^{3+}$ and the ^{68}Ga-hydrolysed product as a reference standard.
To develop a reliable set of quality controls and to identify the chromatographic peaks during the analyses, free $^{68}Ga^{3+}$ was obtained directly by collecting a 100 ml aliquot (B10 MBq) of the 0.1 mol/l HCl generator eluate. ^{68}Ga-hydrolysed products were obtained at varying pH values (5,7 and 10) by adding varying aliquots of a 1 mol/l NaOH solution to 100 ml of the generator eluate. All the mixtures were incubated for 5 min at room temperature.

Synthesis of ^{nat}Ga-r-BHD as a reference standard

A measure of 12.40 mg of GaCl3 (70 nmol) was dissolved in 1.8 ml of 0.1 mol/l HCl, and then a solution of 170 ml of 1.5 mol/l sodium formate containing 50 mg (70 nmol) of r-BHD was added to obtain a solution of pH 3. The mixture was heated for 10 min at 1001C on a heater block and then passed through a C-18 cartridge (precondi- tioned with 3 ml of a 50% EtOH solution and 3 ml of a 0.9% sodium chloride solution). The products were eluted with 1 ml of 50% EtOH and diluted with 2 ml of water.

Quality controls

Quality control of the ^{nat}Ga-r-BHD solution as performed by LC–ESI-MS. The chromatographic part was carried out with a constant 0.2-ml/min flow using a 0.2% formic acid–water solution (A) and a 0.2% formic acid-acetonitrile (ACN) solution (B) as the mobile phase, with the following gradient: 0-9 min, 6-8% B; 9-12 min, 8% B; 12–15 min, 8–15% B; and finally 15-24 min, 15% B. Analysis was carried out by ESI-MS using the following parameters: source voltage of 3.3 kV and capillary and tube lens voltages of 13 and 85 V, respectively. The source was heated at 2751C with a 20 sheath gas flow rate and five sweep gas flow rate. The acquisition was carried out by full mass spectroscopy in the FT mode (R's = 60 000). Quality controls on every radioactive preparation were performed by chromatographic methods. UHPLC was the preferred procedure; however, as this technology is not routinely available in every laboratory, a radio-TLC method was also applied. The UHPLC analyses were carried out at a flow rate of 0.35 ml/min using ACN and a 0.1% v/v trifluoroacetic acid-water solution as the mobile phase, with the following gradient: 0-3 min, 6-

8% ACN and 4–5 min, 8–15% ACN. The wavelength of the ultraviolet detector was set to 220 nm and the column temperature was fixed at 301C. To verify the effectiveness of the purification through the C-18 cartridge, the UHPLC analysis was carried out both on the crude product of the reaction and on the final product. The identity of the products was confirmed by coinjection of the ^{nat}Ga-r-BHD standard or by injection of the free $^{68}Ga^{3+}$ or the ^{68}Ga -hydrolysed products obtained as described before. A 100 ppm r-BHD solution was also used to determine the retention time of the free ligand. The RCP of ^{68}Ga-r-BHD solutions was also assessed by TLC with RP-18F plates (Merck, Whitehouse Station, New Jersey, USA) as the stationary phase and a solution with 97% 0.1 mol/l sodium citrate and 3% 1 mol/l HCl as the mobile phase.
As various buffers were used and their eligibility for human use is, in some cases, debated, the presence of buffer residues in the final ^{68}Ga-r-BHD solutions was assessed by a second UHPLC analysis under the following conditions: use BEH C-18 1.7mm column (2.1 x 150 mm), 0.35 ml/min flow rate using ACN and a 17 mmol/l H_3PO_4 water solution (pH 2.5) as the mobile phase, with a gradient of 0–15% ACN from 0 to 15 min, and an ultraviolet detector set at 210 nm. The sterility and absence of bacterial endotoxins were tested for according to European Pharmacopeia standards.

Stability of ^{68}Ga -r-BHD

For stability studies, ^{68}Ga-r-BHD was synthesized by reacting 56 nmol of the precursor at pH 3.8 obtained using sodium formate as the buffer. Different aliquots of the ^{68}Ga-r-BHD solution (0.75 ml, 45 MBq) were alter- natively mixed with 0.75 ml of a 0.9% NaCl, 4% human albumin (pH = 7) or healthy human serum solution. The mixtures were incubated at 371C, and after 10, 30, 60, 120 and 180 min, a 10 ml aliquot of each solution was injected into the UHPLC. Analyses were carried out by the method described before. All tests were performed in triplicate.

Avidin binding reactions

To obtain ^{68}Ga-r-BHD to Av molar ratios of 2:1, 4:1, 8:1, 16:1 and 32:1, a fixed amount of ^{68}Ga-labelled r-BHD solution (1.4 nmol, 13

MBq) was added to 1.5 ml of a 0.9% NaCl solution or to healthy human serum containing decreasing amounts of Av. For separating the activity bound to Av from the bulk solution, the mixtures were incubated at 371C for 5 min and centrifuged using Amicon Ultra-4 devices. The top and bottom parts of the Amicon were measured using a dose calibrator. The amount of Ga-r-BHD that aspecifically bound to the filter membrane was evaluated by incubating and centrifuging aliquots of the radiotracer under the same conditions described above but in the absence of Av. All tests were conducted in triplicate.

Blocking experiments

A 100-fold molar excess of natural biotin was added to 1.5 ml of a 0.9% NaCl solution or human serum containing 0.35 nmol of Av solution. The mixture was incubated at 371C for 5 min and an aliquot of Ga-r-BHD solution (1.4 nmol, 13 MBq) was added. Thereafter, the solutions were freshly incubated for 5 min and then centrifuged in an Amicon Ultra-4 centrifuge. The top and bottom parts were measured in a dose calibrator.

Stability of the avidin/ Ga-r-BHD complex

Solutions containing an aliquot of Ga-labelled r-BHD (1.4 nmol, 13 MBq) and Av in a 4:1 molar ratio were incubated in Amicon Ultra-4 devices with 1.5 ml of a 0.9% NaCl solution or human serum at 371C for 0, 30, 60, 120 and 180 min, respectively. After incubation, centrifugation was performed on the Amicon Ultra-4 centrifuge and the top and bottom parts were measured using a dose calibrator. All tests were conducted in triplicate.

Results

Radiosynthesis of ^{68}Ga-r-BHD

Figure 7.1a shows the dependence of the radiolabelling yield on the precursor amount. Although the highest yield was obtained with 140 nmol of precursor (68±1%), a substantial plateau was observed at 56 nmol of r-BHD, corresponding to a 64±3% RCY. Therefore, this amount was used in the subsequent labelling reactions, being considered a good compromise between high yield and high specific activity. Figure 7.1b shows the

dependence of the RCY on the pH and on different buffer species. On using sodium acetate buffer, the best yield was 58±2% and was achieved at a pH of 4.6. Both sodium formate and HEPES buffers gave better RCY values than did sodium acetate, although the best results were obtained at different pH values (64±3% RCY at pH 3.8 and 64±4% RCY at pH 2.8 for formate and HEPES, respectively).

Quality controls

RCP and chemical purity of the product were assessed by UHPLC before and after the final purification through the C-18 cartridge. A comparison of the two chromatograms of a typical preparation is shown in Fig. 7.2 and the following retention times can be observed: free $^{68}Ga^{3+}$,1.14 min; ^{68}Ga-hydrolysed products, 1.35 min; ^{68}Ga-r-SBHD, 3.33 min; and ^{68}Ga-r-BHD, 6.80 min. When the radiosynthesis was performed under the best conditions (56 nmol of r-BHD, pH = 3.8, sodium formate buffer), but in the absence of EtOH as a stabilizer, an RCP of 95±1% was achieved. The addition of varying amounts of EtOH to the reactor before the labelling has a strong impact on the RCP of the preparation and also affects the RCY. The best conditions were found when 50 ml of EtOH was added to the reactor. In this case RCP was improved to 98% and RCY was comparable to that achieved under the same reaction conditions but in the absence of EtOH (64%). If a higher amount of EtOH was added, the RCY markedly decreased to 45% (100 ml) and 8% (200 ml). Radio-TLC analyses were carried out on the final solutions only and the following R_f values were obtained: ^{68}Ga -r-BHD and ^{68}Ga -r-SBHD, 0.0-0.2; free $^{68}Ga^{3+}$ and hydrolysed products, 0.9-1.0. The amount of free ligands was under the limit of detection (0.1 mg/ml) despite the total amount used for the labelling. The second set of UHPLC analyses for determining the amount of buffers in the final solutions gave the following results: 20±5 mg/ml (R_t = 1.2 min) for HEPES, 36±4 mg/ml (R_t = 1.3 min) for sodium formate and 33±3 mg/ml (R_t = 1.9) for sodium acetate. Every preparation was sterile and pyrogen free.

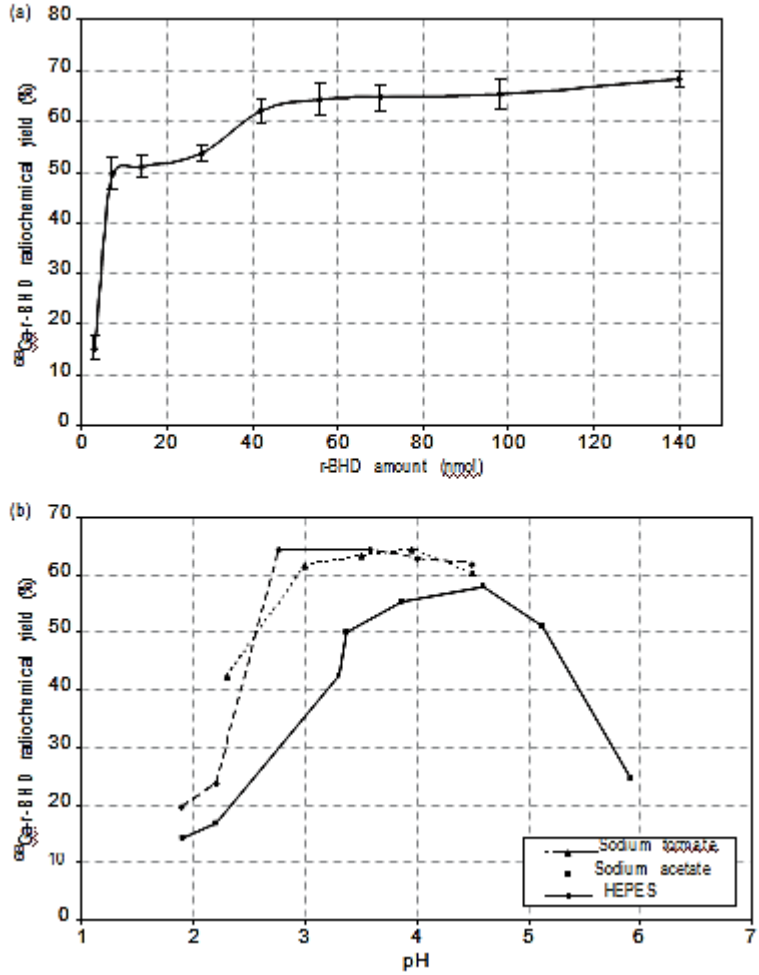

Figure 7.1: (a) ^{68}Ga-r-BHD radiochemical yield as a function of precursor amount (sodium formate buffer, pH = 3.8). (b) ^{68}Ga-r-BHD radiochemical yield as a function of pH and buffer species (56 nmol of r-BHD). Error bars have been omitted for clarity.

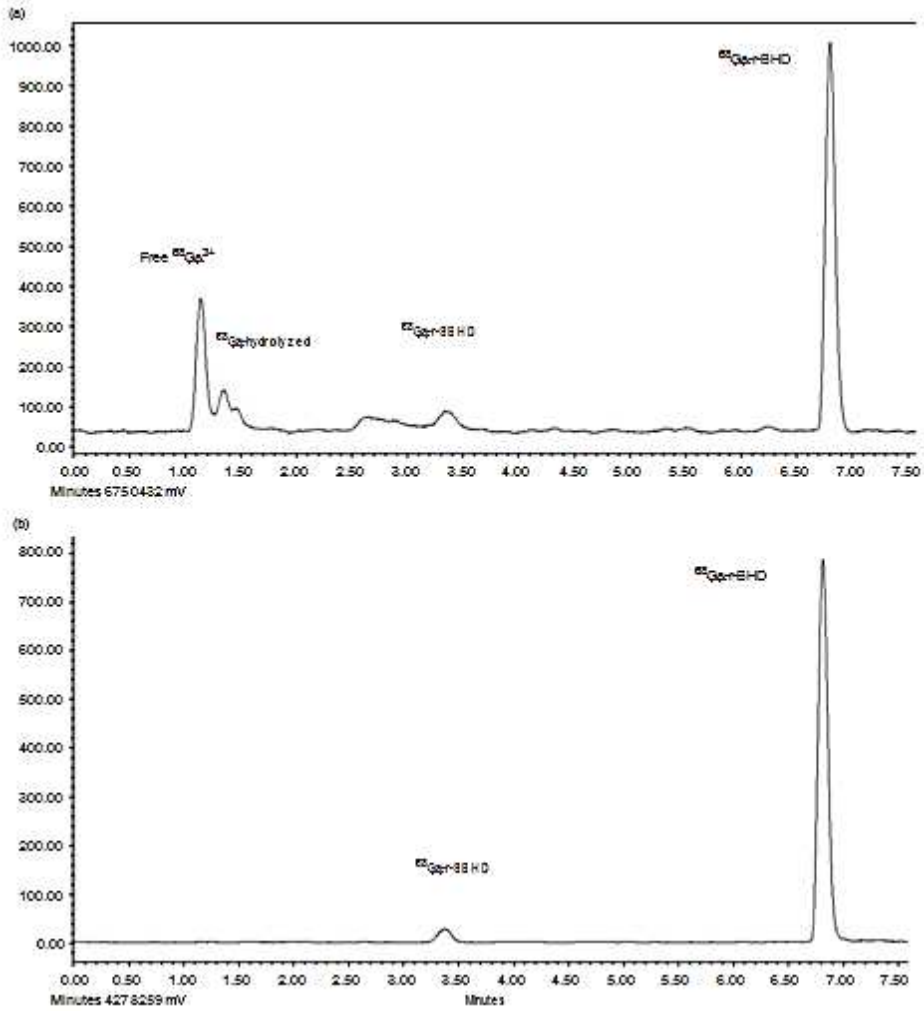

Figure 7.2: UHPLC chromatogram (radiochemical detector) of a typical ^{68}Ga-r-BHD preparation before (a) and after (b) purification through a C-18 cartridge

Stability of ^{68}Ga-r-BHD

Stability of ^{68}Ga-r-BHD in different media is shown in Fig. 7.3a. Considering the fact that the initial RCP was 95±1%, a high stability of the radiotracer in 0.9% NaCl and albumin solutions can be observed within the assessed time. In addition, after 180 min at 37°C the percentage of ^{68}Ga bound to the r-BHD analogue remained greater

than 94±1 and 93±1% for 0.9% NaCl and albumin solutions, respectively. The stability in human serum is slightly lower (a decrease from 95±1 to 90±1% after 180 min was observed) and it was likely because of the presence of serum enzymes, proteins and metal competitors in the solution.

Binding to avidin and blocking experiments

Results of the study on ^{68}Ga-r-BHD affinity for decreasing amounts of Av in a 0.9% NaCl solution and in healthy human serum are shown in Fig. 7.3b. In the 0.9% NaCl solution, when the molar ratio between r-BHD and Av was 2:1, the amount of radiotracer bound to Av was about 70%; however, at the natural 4:1 molar ratio, it decreased to about 62%. These results are comparable to the findings obtained for ^{90}Y-r-BHD by Sabatino et al. [9]. In human serum, the amount of radiotracer bound to Av was notably higher than that in saline and was about 95 and 80% for 2:1 and 4:1 molar ratios, respectively. For all the calculations, the average percentage of radiotracer that aspecifically bound to the Amicon was subtracted by the amount measured in the top part of the device. In the blocking experiments performed by adding a 100-fold excess of natural biotin for saturating the Av binding sites, the percentages of ^{68}Ga-r-BHD still binding Av were about 5 and 20% for the 0.9% NaCl solution and human serum, respectively.

Stability of the avidin/^{68}Ga-r-BHD complex

Stability of the Av/^{68}Ga-r-BHD complex in the 0.9% NaCl solution and in human serum is shown in Fig. 7.3c. The study was conducted using a 1:4 Av/r-BHD molar ratio. In both media the stability of the complex remains almost constant for the duration of the study. In the 0.9% NaCl solution, the amount of ^{68}Ga-r-BHD bound to Av started from 62% and decreased to about 54% after 180 min. For the experiments performed in human serum the percentage started from 80% and decreased to about 77% after 180 min.

Discussion

The labelling of r-BHD with a positron emitter radionuclide such as ^{68}Ga can potentially lead to an improvement both in the localization of small foci of avidinated cells in the pretargeting approach and in the per-se

injection of the radiotracer as an infection/inflammation imaging agent. Moreover, ^{68}Ga is produced by means of a ^{68}Ge/^{68}Ga generator from the long-lived parent ^{68}Ga ($t_{1/2}$ = 270 days) and can also be utilized in facilities without a cyclotron in situ. ^{68}Ge/^{68}Ga generators are widely used in many nuclear medicine departments nowadays and ^{68}Ga labelled radiopharmaceuticals are recognized as effective tools for clinical trials [14,15].

The ^{68}Ga –DOTA-biocytin analogue was prepared using a commercial automatic synthesizer. Similar to the proce- dure adopted for the synthesis of ^{68}Ga labelled somatostatin analogues already described in the literature [13,16], a fraction of the ^{68}Ge /^{68}Ga generator eluate was transferred into a reactor and labelled with bioconju-gates at high temperature for 3-10 min in the presence of a buffer. On the basis of this procedure, synthesis of ^{68}Ga-r-BHD was optimized for pH, buffer species and precursor amount in order to obtain the most reliable and highest yielding procedure. The feasibility of labelling biotin analogues with ^{68}Ga has already been explored by Bloom et al. [17]. In their study three analogues linked to DOTA by different alkyland polyethylenglycol chains were manually labelled with ^{68}Ga for monitoring the graft survival during islet transplantation. However, these derivatives are still in a preclinical phase of evaluation [18]. In contrast, the use of the r-BHD analogue labelled with ^{90}Y and ^{177}Lu has already been reported in a large number of human applications [10,11].

In our study, the labelling yield of the reaction between $^{68}Ga^{3+}$ and 2.5-140 nmol of the DOTA-conjugated biocytin analogue r-BHD was investigated (Fig. 7.1a). As the RCY did not markedly improve when more than 56 nmol of the ligand was reacted, we decided to use this amount for the rest of the study. Using 56 nmol of r-BHD and starting from 962 MBq of ^{68}Ga(III), the specific activity was 11 MBq/nmol. These results can be compared with the results obtained by Bloom and colleagues on the labelling of DOTA-pegylated biocytin analogues. In their study, the plateau of $^{68}Ga^{3+}$ incorporation was reached at 10 nmol, but chemical concentration/purification of the ^{68}Ga eluate through an anion exchange cartridge was performed instead of simple fractionation [17].

$^{68}Ga^{3+}$ incorporation in r-BHD was also notably influenced by the pH of the reaction and by the nature of the buffer used during labelling. In an analogue study on the radiosynthesis of ^{68}Ga -DOTATOC, Bauwens et al. [19] reported that the use of HEPES, sodium acetate and sodium succinate as buffering agents yielded comparable results. However, the researchers concluded that only sodium acetate should

be applied in clinical ^{68}Ga-DOTATOC labelling as it is the only buffer among the three to be recognized as a substance for pharmaceutical and human use in the European legislation. Herein, the RCY and RCP obtained using 1.5 mol/l sodium acetate were compared with those obtained with 4.5 mol/l HEPES and 1.5 mol/l sodium formate, and an B10% higher RCY was achieved when both HEPES and sodium formate were used instead of sodium acetate (Fig. 7.1b). It appears complicated to explain this difference because both thermodynamic and kinetic factors may influence the trend of the reaction, and the constants for all the processes are not available yet. Reasoning on the mechanism, we suppose that the $^{68}Ga^{3+}$ in solution is rapidly coordinated by the donor atoms of the buffers and then these complexes are slowly converted to the DOTA bioconjugates during heating. As the constant for forma- tion for Ga–acetate complexes (log K = 3.68) is almost two orders of magnitude greater than that for Ga–HEPES (log K = 1.99), we surmised that the conversion to Ga-r- BHD is better promoted starting from the HEPES complexes than from the acetate ones [20,21]. Thermo- dynamic data for Ga-formate complex formation are not available; hence, a direct comparison between acetate and formate buffers is not yet possible. However, it is likely to suppose analogous reasons for the higher RCY compared with that for HEPES when formate instead of acetate is used, as the log K values of the metal-formate complexes (i.e. ^{90}Y or ^{177}Lu) are normally two to three orders of magnitude lower than the log K values of the corresponding metal-acetate complexes [22]. As the use of sodium formate or HEPES as an additive for injectable prepara- tions is not universally accepted, a UHPLC method for assessing the buffer amount was developed. The amount of residues detected in the final solutions was very low when compared with the reported LD_{50} sodium acetate, 3530 mg/kg (mouse); sodium formate, 11200 mg/kg (mouse); HEPES, 316 mg/kg (quail). However, as a really concen- trated HEPES solution was needed to buffer the reaction solution to the optimal pH, we decided to use sodium formate for the rest of the study.

In contrast to that reported in the study by Blom et al. [17], in which purification after a labelling reaction was not considered necessary, we observed considerable improvement in the RCP after purification by solid phase extraction of the crude labelled Ga-r-BHD solution through the C-18 cartridge, as demonstrated by UHPLC analysis. However, as shown in Fig. 7.2b, it was not possible to achieve an RCP of greater than 95% as a radioactive by-product (Rt = 3.33 min) was still present in the solution after

purification by solid phase extraction. The LC-ESI-MS analysis of the natGa-r-BHD preparation allowed the separation of the impurity and the acquisition of its mass spectra. The m/z pattern was ascribed to the ^{68}Ga-coordinated r-BHD sulphoxide. Although the formation of D-biotin and L-biotin sulphoxides as intermediate products of the biotin oxidation to the sulphone was already reported [23], the UHPLC analysis of the r-BHD ligand did not show the presence of by-products in the solution. Hence, the formation of D-CO-reduced and L-CO-reduced N-aminoexyl sulphoxide biotinamido-DOTA (r-SBHD) by oxidation of r-BHD was supposed to occur during the labelling reactions. Structures of ^{68}Ga-r- BHD and ^{68}Ga-r-SBHD are shown in Fig. 7.4. In addition, under the best reaction conditions (56 nmol r-BHD, pH = 3.8, sodium formate buffer) it was not possible to fully eliminate this byproduct from the final solution, and the best RCP achieved was 95%. In contrast to that reported on the preparation of ^{68}Ga-labelled somatostatin analogues [24], the use of HEPES as buffer did not significantly improve the RCP of ^{68}Ga-r-BHD preparations, as the results are comparable to those obtained using sodium formate and acetate.

Biotin sulphoxide is a product of the catabolic pathway of biotin in mammals and is commonly found in urine and plasma of rats, pigs and humans [25–28]. However, ^{68}Ga-r-SBHD may affect image quality because of its possible metabolization by liver or kidney enzymes. In our study, the formation of ^{68}Ga-r-SBHD was partially avoided by adding 50 ml of EtOH to the reaction solution [29]. The use of different antioxidants such as sodium ascorbate, selenomethionine or sodium thiosulphate is currently under investigation in our laboratory.

Because of the short half-life of ^{68}Ga, the stability of ^{68}Ga-r-BHD was assessed by UHPLC after a maximum of 180 min from preparation. As shown in Fig. 7.3a, when the preparation was mixed with a 0.9% NaCl or a 4% albumin solution, ^{68}Ga (III) remained almost completely in the coordinated form during the assessment period, whereas the RCP decreases to 90±1% after 180 min when tested in human serum. Under this condition, the activity dissociated from ^{68}Ga-r-BHD corresponded to about 6.2% and could be attributed to ^{68}Ga-hydrolysed by-products obtained under physiological conditions (UHPLC-ob- served retention time was 1.35 min). The formation of these by-products can be because of the suboptimal properties of DOTA chelator in the context of ^{68}Ga a coordination with respect to larger cations such as ^{90}Y or ^{177}Lu. Decomplexation and transchelation from DOTA to competitor serum

proteins, such as transferrin, can bring about rapid hydrolysis of ^{68}Ga a(III) at human serum pH.
As radiolabelled biocytin analogues were used in clinical trials not only per se but also coupled with a preinjection of Av [2,3,10,11], we tested the binding of ^{68}Ga-r-BHD and Av at varying Av/radiotracer molar ratios and for the specificity of the bindings itself. The studies were conducted in a 0.9% NaCl solution and in healthy human serum to mimic the behaviour of the Ga-r-BHD *in vivo* (Fig. 7.3b). At the natural 1:4 molar ratio, 62±2% of Ga-r-BHD was bound to Av in saline, whereas the percentage was 80±2% in serum. Comparing these findings, we concluded that some proteins present in high concentra- tion in human serum, such as albumin or transferrin, can aspecifically bind Ga-r-BHD and de-facto decrease the calculated 4:1 radiotracer/Av molar ratio. As a result, an increase in the radioactivity amount measured in the top part of the Amicon devices in serum with respect to saline solution was found. The contribution of these proteins to the total activity with respect to Av itself is evaluated to be around 20%. This conclusion is also supported by the experiments performed with a 100-fold excess of natural biotin, in which a percentage of only 5% ^{68}Ga-r-BHD bound to Av was found in the 0.9% NaCl solution, whereas the percentage in serum remained around 20%. The amount of ^{68}Ga-r-BHD bound to Av remained almost constant over 180 min from the incubation both in the 0.9% NaCl solution and in human serum (Fig. 7.3c).

Conclusion

The feasibility of labelling a reduced biocytin derivative coupled with DOTA, namely, r-BHD, with ^{68}Ga has been investigated in depth. The safety of the preparation has been assessed and the products obtained have been characterized by developing a complete set of quality controls. The high affinity of ^{68}Ga -r-BHD to Av and the stability of both the ^{68}Ga-r-BHD/Av complex and ^{68}Ga-r-BHD itself make the radiopharmaceutical suitable for acquiring PET images. ^{68}Ga-r-BHD per se or with preinjection of Av appears to be a good candidate for preclinical and clinical applications.

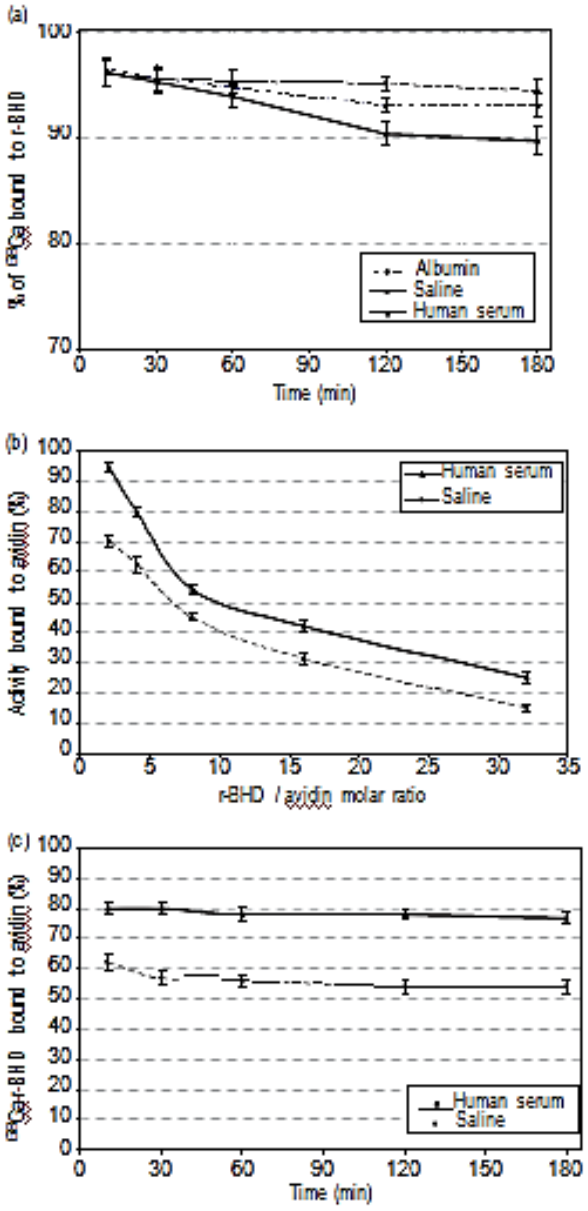

Figure 7.3: (a) Stability of Ga-r-BHD in different media at 37°C (56 nmol of r- BHD, sodium formate buffer, pH = 3.8). (b) Percentage of ^{68}Ga-r-BHD bound to Av as a function of the r-BHD/Av molar ratio in different media. (c) Stability of the Ga-r-BHD/Av complex at 37°C as a function of time (a 4:1 r-BHD/Av molar ratio was used) in different media.

(a)

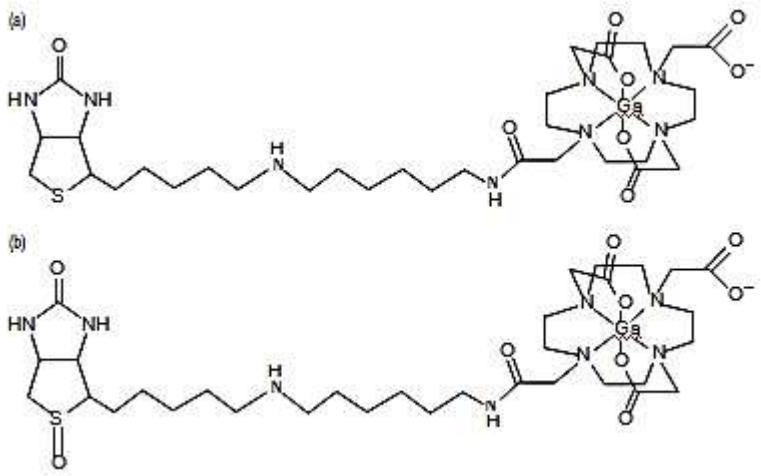

Figure 7.4: Structures of ^{68}Ga-r-BHD (a) and ^{68}Ga-r-SBHD (b).

References

1. Lazzeri E, Pauwels EK, Erba PA, Volterrani D, Manca M, Bodei L, et al. Clinical feasibility of two-step streptavidin/111In-biotin scintigraphy in patients with suspected vertebral osteomyelitis. Eur J Nucl Med Mol Imaging 2004; 31:1505-1511.
2. Lazzeri E, Erba PA, Perri M, Tascini C, Doria R, Giorgetti J, Mariani G. Scintigraphic imaging of vertebral osteomyelitis with 111In-biotin. Spine 2008; 33:198-204.
3. Lazzeri E, Erba PA, Perri M, Doria R, Tascini C, Mariani G. Clinical impact of SPECT/CT with In-111 Biotin on the management of patients with suspected spine infection. Clin Nucl Med 2010; 35: 12-17.
4. Erba PA, Cataldi AG, Tascini C, Leonildi A, Manfredi C, Mariani G, Lazzeri E. 111In-DTPA–biotin uptake by Staphylococcus aureus. Nucl Med Commun 2010; 31:994-997.
5. Pispa J. Animal biotinidase. Ann Med Exp Biol Fenn 1965; 43 (Suppl 5): 1-39.
6. Hymes J, Wolf B. Biotinidase and its roles in biotin metabolism. Clin Chim Acta 1996; 255:1-11.
7. Stimmel JB, Stockstill ME, Kull FC. Yttrium-90 chelation properties of tetraazatetraacetic acid macrocycles, diethylenetriaminepentaacetic acid analogues, and a novel terpyridine acyclic chelator. Bioconjug Chem 1995; 6:219-225.
8. Stimmel JB, Kull FC. Samarium-153 and lutetium-177 chelation properties of selected macrocyclic and acyclic ligands. Nucl Med Biol 1998; 25: 117-125.
9. Sabatino G, Chinol M, Paganelli G, Papi S, Chelli M, Leone G, et al. A new biotin derivative–DOTA conjugate as a candidate for pretargeted diagnosis and therapy of tumors. J Med Chem 2003; 46: 3170-3173.
10. Urbano N, Papi S, Ginanneschi M, De Santis R, Pace S, Lindsteadt R, et al. Evaluation of a new biotin–DOTA conjugate for pretargeted antibody-guided radioimmunotherapy (PAGRITs). Eur J Nucl Med Mol Imaging 2007; 34:68-77.
11. Paganelli G, De Cicco C, Ferrari ME, Carbone G, Pagani G, Leonardi MC, et al. Intraoperative avidination for radionuclide treatment as a radiotherapy boost in breast cancer: results of a phase II study with 90Y-labeled biotin. Eur J Nucl Med Mol Imaging 2010; 37:203-211.
12. Chinol M, Papi S, Garaboldi L, Martano L, Paganelli G. Automated synthesis of 68Ga-DOTA–biotin derivative to detect targeted avidin by PET. Q J Nucl Med Mol Imaging 2010; 54 (Suppl1):8.
13. Decristoforo C, Knopp R, Von Guggenberg E, Rupprich M, Dreger T, Hess A, et al. A fully automated synthesis for the preparation of 68Ga-labelled peptides. Nucl Med Commun 2007; 28:870-875.
14. Fani M, Andre´ JP, Maecke HR. 68Ga-PET: a powerful generator-based alternative to cyclotron-based PET radiopharmaceuticals. Contrast Media Mol Imaging 2008; 3:53-63.
15. Asti M, De Pietri G, Fraternali A, Grassi E, Sghedoni R, Fioroni F, et al. Validation of 68Ge/68Ga generator processing by chemical purification for routine clinical application of Ga-DOTATOC. Nucl Med Biol 2008; 35:721-725.
16. Breeman WAP, de Jong M, de Blois E, Bernard BF, Konijnenberg M, Krenning EP. Radiolabelling DOTA-peptides with Imaging 2005; 32:478-485.
17. Blom E, Langstrom B, Velikyan I. 68Ga-Labeling of biotin analogues and their characterization. Bioconjug Chem 2009; 20:1146-1151.
18. Eriksson O, Carlsson F, Blom E, Sundin A, Langstrom B, Korsgren O, Irina V. Preclinical evaluation of a 68Ga-labeled biotin analogue for applications in islet

transplantation. Nucl Med Biol 2012; 39:415-421.
19. Bauwens M, Chekol R, Vanbilloen H, Bormans G, Verbruggen A. Optimal buffer choice of the radiosynthesis of 68Ga-DOTATOC for clinical application. Nucl Med Commun 2010; 31:753-758.
20. Skorik NA, Artish AS. The stability of the complexes of scandium, gallium, indium and thorium with the anions of various organic acids. Russ J Inorg Chem 1985; 30:1130.
21. Hassan AA, Kholoud M, Abou EN, Sherif HS. Metal ion complexes containing dipeptides, tripeptides, and biologically important zwitterionic buffers. J Chem Eng Data 2007; 52:381-390.
22. Kovar LE, Powell JE. Stability constants of rare earth with some weak carboxylic acids. Technical report. IS-1450. Report TID-4500, Ames Laboratory, Iowa State University; 1966. pp. 54.
23. Melville DB. Biotin sulfoxide. J Biol Chem 1954; 208:495-501.
24. Sasson R, Vaknin D, Bross A, Lavie E. Determination of HEPES in 68Ga-labeled peptide solutions. J Radioanal Nucl Chem 2010; 283: 753-756.
25. Mock DM, Lankford GL, Cazin J. Biotin and biotin analogs in human urine: biotin accounts for only half the total. J Nutr 1993; 123: 1844-1851.
26. Mock DM, Lankford GL, Mock NI. Biotin accounts for only half of the total avidin binding substances in human serum. J Nutr 1995; 125: 941-946.
27. Wang KS, Patel A, Mock DM. The metabolite profile of radioisotope-labeled biotin in rats indicates that rat biotin metabolism is similar to that in humans. J Nutr 1996; 126:1852-1857.
28. Zempleni J, McCormick DB, Mock DM. Identification of biotin sulfone, bisnorbiotin methyl ketone and tetranorbiotin-L-sulfoxide in human urine. Am J Clin Nutr 1997; 65:508-511.
29. Hasselman R, Johayem A, Ozdemir U, Dragic M, Blainc A, Mu L, Schibli R. Improving radiochemical purity and quality controls of 68Ga-DOTATATE. J Nucl Med 2011; 10:P020.

Chapter 8

Conclusions and future perspectives

In conclusion, we demonstrate that the use of ^{99m}Tc-HMPAO-WBC scintigraphy is beneficial in patients with a high clinical probability of infected endocarditis and suspected infections of cardiovascular implantable electronic devices or vascular grafts. The main indications of ^{99m}Tc-HMPAO-WBC scintigraphy are the confirmation of diagnosis in doubtful circumstances, defining the extent of device involvement, and the detection of associated complications and septic embolisms, thus potentially determining treatment strategy. SPECT/CT combined technology is preferred to visulaize infection by ^{99m}Tc-HMPAO-WBCs, confirming or excluding the diagnosis of infection. In addition, ^{99m}Tc-HMPAO-WBC scintigraphy might be used to monitor the response to antimicrobial treatment. Whole-body images followed by additional planar spot and SPECT/CT images allow to detect distant sites of septic embolism, constituting an invaluable aid of this scintigraphic procedure in the management of patients with IE, CIED or VPI.

The next step to complete the process of validation of scintigraphy with ^{99m}Tc-HMPAO-WBC is to introduce this diagnostic procedure within the clinical guideline. To this aim, within the European Association of Nuclear Medicine (EANM) we have started the discussion together with the European Society of Cardiology, Thoracic Surgery and Vascular Surgery trying to design the most suitable diagnostic clinical algoritm that include ^{99m}Tc-HMPAO-WBC and [^{18}F]FDG PET/CT. Indeed, the first results of this collaboration will soon be published containing a proposed diagnostic flow-chart for patients with endocarditis and suspected vascular graft infections. The proposed diagnostic flow-chart are shown in Figure 8.1, 8.2 and 8.3.

Before completing the clinical validation of ^{99m}Tc-HMPAO-WBCs SPECT/CT and [^{18}F]FDG PET/CT it is still need to identify advantages and limitations of each diagnostic technique. To this regard a well designed multicentre prospective clinical trial, that will compare the diagnostic performances of each method using the final microbiological and histological diagnosis as gold standard, will provide the answer to these open questions. Such clinical trial will also give the possibility to better investigate and understand which paramether can significantly affect the scintigraphic results as the type of microorganism, the effect of prolonged antimicrobial teraphy with new moleculesactive on biofilm, etc.

In addition, continuous efforts are required to make new radiopharmaceuticals for PET/CT to image infectious processes. Indeed, besides well established limitations, [^{18}F]FDG is the only PET radiopharmaceutical commercially available for imaging infections. Therefore, the development of efficient radiolabelling procedures of WBCs with long-lived positron emitter isotopes and labelling new small molecules specific for bacterial imaging, will represent a fundamental step to further increase the use of molecular imaging in all patients suffering from infections. In this view we are preparing the first clinical application of ^{68}Ga-DOTA-Biotin in human with the aim of defining the biodistribution proprieties and the diagnostic performances of this new radiopharmaceutical. Furthermore, we are also working at the possible development of new biotin-derivatives suitable for the radiolabelling with ^{99m}Tc-pertecnetate that, in case of success, will allow cheaper and wider use.

When suitable PET radiopharmaceuticals will be available, this will eventually translate in improvements in the diagnosis and management of infectious diseases. In addition, it would also open new perspective for investigating a promising hybrid technology where PET is combined with MRI (PET/MRI). Indeed, nearly a decade after the introduction of PET/CT, combined PET/MRI systems have become available first in the pre-clinical settings and subsequently for clinical applications. PET/MRI scanners have been technically developed ahead of detailed considerations for many important pratical issues including clinical applications that would benefit exclusively from simultaneous imaging acquisition or dual-modality imaging probes, as in the case of heart and vessels. One of the great advantage of MRI over CT is its excellent soft-tissue contrast in combination with high spatial resolution along with absence of radiation burden. Therefore the use of PET/MRI in combination with specific infection tracking radiopharmaceuticals could significantly improve the sensitivity and specificity for diagnosing inflammatory and infectious, allowing more accurate assessment of sites of infection/inflammation as weel as of their extent rather than PET-CT expecially in case of soft tissues, cardiac and vascular structures. Furthermore, multiparametric and functional imaging such as dynamic contrast enhancement (DCE), diffusion weighted imaging (DWI) and spectroscopy as well as combined new paramagnetic nano-cell-contrast agent with radiolabelled probes could be used for histological characterization of tissues in vivo and could provide more insight into the dynamics and characteristics of the inflammatory/infectious processes.

The pivotal questions are whether simultaneous PET/MRI may provide a competitive advantage over separate clinical examinations and whether such advantages will translate into significant clinical benefit.

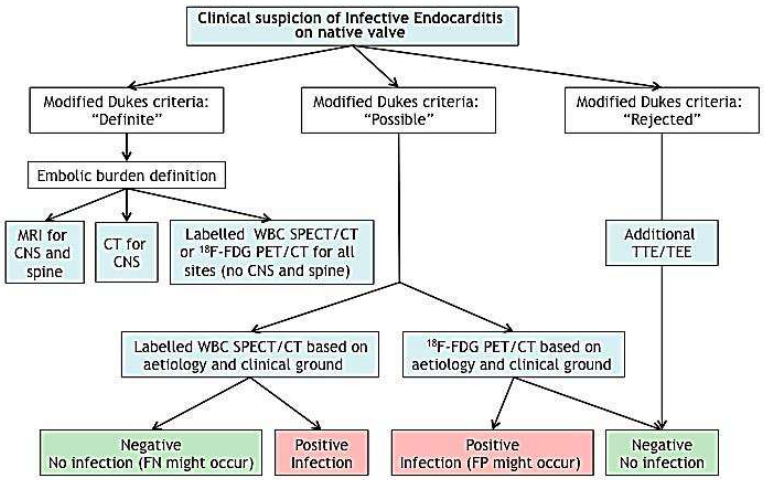

Figure 8.1: diagnostic flow-chart for native valve IE proposed by the Infection and Inflammation Committee of the European Association of Nuclear Medicine and shared with the European Society of Cardiology and the European Society of Clinical Microbiology and Infectious Diseases.

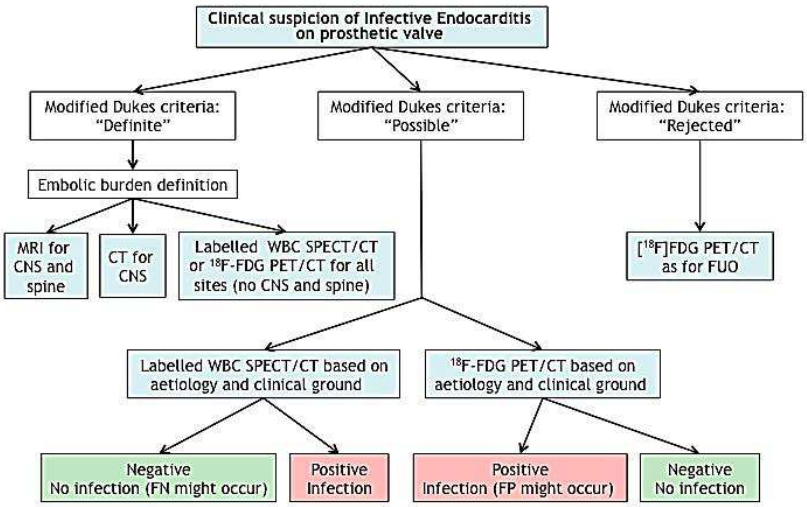

Figure 8.2: diagnostic flow-chart for prosthetic valve IE proposed by the Infection and Inflammation Committee of the European Association of Nuclear Medicine and shared with the European Society of Cardiology and the European Society of Clinical Microbiology and Infectious Diseases

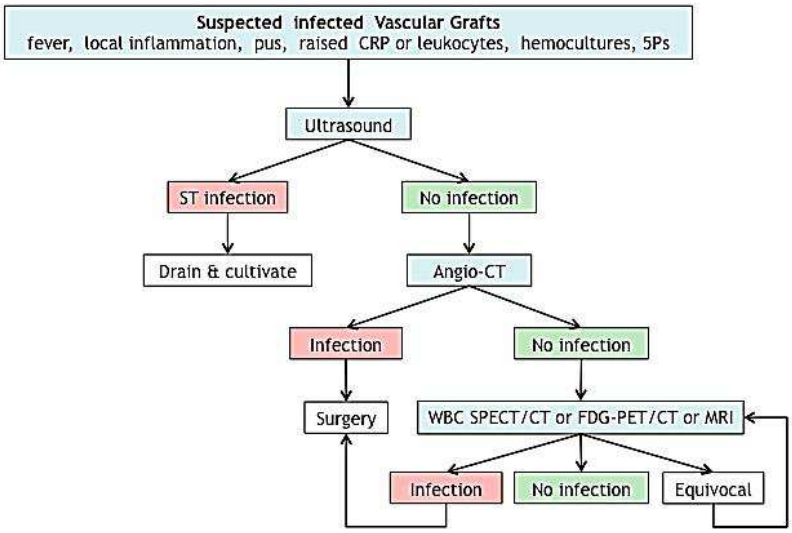

Figure 8.3: diagnostic flow-chart for prosthetic valve IE proposed by the Infection and Inflammation Committee of the European Association of Nuclear Medicine and shared with the European Society for Vascular Surgery and the European Society of Clinical Microbiology and Infectious Diseases.

Chapter 9

Summary

In the beginning of the project, the main indication for imaging of infection using scintigraphy with ^{99m}Tc-HMPAO radiolabelled leukocytes, musculoskeletal infections. In fact, despite the enormous potential of the techniques very few patients were referred for the evaluation of infections of other tissues or devices.

In 2005 the first SPECT/CT hybrid scanner (Infinia, GE) was introduced in our center followed just after the installation of a PET/CT system (Discovery ST, GE). This was the opportunity to start expanding our clinical experience in the field of infectious disease. In particular, infections of the cardiovascular system were a challenge. There was a clinical need of identifying patients with a high probability of infection, but undetermined results after a first line clinical management that include blood chemistry, echocardiography and blood culture as well as for antimicrobial treatment evaluation during ascertained infection. In addition, the widespread use of PET/CT and [^{18}F]FDG have created the need of a comparative evaluation of the two procedures. Using ^{99m}Tc-HMPAO radiolabelled leukocytes scintigraphy enhanced specificity is expected, whereas a higher sensitivity is expected using [^{18}F]FDG PET/CT imaging.

Therefore, in this work we applied ^{99m}Tc-HMPAO radiolabelled leukocytes in patients with infective endocarditis (chapter 2). Clinical performance of the Duke Endocarditis Service criteria to establish the diagnosis of infectious endocarditis can be improved through molecular imaging procedures as ^{99m}Tc-HMPAO-WBC SPECT. Therefore we assessed the value of ^{99m}Tc-HMPAO-WBC with SPECT/CT in a cohort of 131 patients with suspected IE. No false positive results were found, even in patients with early IE, whom were evaluated within the first two months after the surgical procedure. Most of the added value from the ^{99m}Tc-HMPAO-WBC scan for decision-making was seen in patients of whom the Duke criteria indicated "possible" IE. The scan was also valuable in patients with negative and/or difficult-to-interpret echocardiographic findings. Our results demonstrate the ability of ^{99m}Tc-HMPAO-WBC to reduce the rate of misdiagnosed IE, when combined with the standard diagnostic tests, (a) in patients with a high clinical

probability but inconclusive echocardiographic findings; (b) for the differential diagnosis of septic and sterile vegetations detected by echocardiography; (c) when echocardiographic, laboratory and clinical data are contradictory; (d) to exclude valve infection (especially of a prosthetic valve) during febrile episodes, sepsis or post-surgical infections.

Cardiovascular device related infections are discussed in chapter 3. ^{99m}Tc-HMPAO-WBC SPECT/CT had a 94% sensitivity for both detection and localization of CIED-associated infection. SPECT/CT imaging had a definite added diagnostic value over both planar and stand-alone SPECT. Pocket infection was often associated with infections of the lead(s).The intracardiac portion of the lead(s) more frequently exhibited ^{99m}Tc-HMPAO-WBC accumulation and presented the highest rate of complications, infectious endocarditis and septic embolism. None of the patients with negative ^{99m}Tc-HMPAO-WBC scintigraphy develop CIED infection during follow-up until after 12 months. ^{99m}Tc-HMPAO-WBC scintigraphy was able to confirm the presence of CIED-associated infection, to define the extent of device involvement, and to detect associated complications. Moreover, ^{99m}Tc-HMPAO-WBC scintigraphy reliably excluded device-associated infection during a febrile episode and sepsis, with a 95% negative predictive value.

Vascular graft prosthesis are discussed in chapter 4. In patients with suspected late and low-grade late vascular prosthesis infections ^{99m}Tc-HMPAO-WBC using SPECT/CT demonstrated a significant reduction of false positive findings in 37% of patients (sensitivity and specificity were both 100% of SPECT/CT versus 85.1% and 62.5% of SPECT stand-alone). ^{99m}Tc-HMPAO-WBC SPECT/CT is useful to detect, localize and define the extent of graft infection in patients with late and low-grade late VPI with inconclusive radiological findings. ^{99m}Tc-HMPAO-WBC SPECT/CT might be used to optimize treatment decisions. In fact, perioperative mortality was 5.5%, mid-term mortality 12%, and long term-mortality 27%. Survival rates were similar in patients treated with surgery and antimicrobial therapy, as compared to patients treated with antimicrobial therapy alone (61% versus 63%), while infection eradication at 12 months was significantly higher when surgery was performed (83.3% versus 45.5%).

In addition to these investigations, we tried to established how the use of standardized imaging acquisition protocols (Chapter 5) and

new, bacterial specific, radiopharmaceuticals may improve the accuracy of scintigraphy (Chapter 6 and 7).

In Chapter 5 we compared the analysis of ^{99m}Tc-HMPAO-WBC scans in patients using a fixed-time acquisition protocol with a time-decay corrected acquisition protocol.The most accurate imaging acquisition protocol is scanning at 3-4h and at 20-24h after radiolabelled leukocyte injection, corrected for isotope decay. When using this protocol, visual analysis of the scans leads to high sensitivity and specificity for diagnosis of infection. Semi-quantitative analysis might be used in doubtful cases, without using a cut-off for the percentage of increase in radiolabelled WBC as a criteria to define a positive scan.

In chapter 6, we evaluated the possibility of an illicit transport of indium-111 labelled diethylene- triaminepentaacetic acid a,o-bis(biocytinamide) (^{111}In-DTPA-Biotin), already shown as a specific tracer in nuclear medicine imaging of vertebral osteomyelitis. To this aim we evaluated 111In-DTPA-Biotin was evaluated in cultures of Staphylococcus aureus on continued incubation for 24 h. Our results seem to demonstrate the mechanism of 111In-DTPA-Biotin uptake seems to be a passive process in which the radiolabelled biotin is presumably taken from the environment and stored, rather than destroyed by nonproliferating living organisms.

In Chapter 7 the labelling of a biocytin analogue, coupled to DOTA, with gallium-68 (^{68}Ga-r-BHD) was optimized, and the quality and stability of the preparations were assessed for clinical use. In addition, the influence of the precursor amount (from 2.5 to 140 nmol), the pH of the reaction (from 2 to 5.5) and the buffer species (1.5 mol/l sodium acetate, 1.5 mol/l sodium formate, 4.5 mol/l HEPES) on radiochemical yield and radiochemical purity were assessed. Studies on the stability and binding of the ^{68}Ga-DOTA-Biotin to avidin (Av) in different media were also conducted. Under the best labelling condition (56 nmol of precursor, 3.8 pH, sodium formate buffer) synthesis of ^{68}Ga-DOTA-Biotin resulted in a yield of 64±3% (not decay corrected). Radiochemical purity was around 95% because a ^{68}Ga-coordinated sulphoxide form of the ligand was detected as a by-product of the reaction (68Ga-r-SBHD). The by-product was identified and characterized by liquid chromatography–electrospray ionization tandem mass spectrometry. At the natural 1:4 Av/^{68}Ga-r-BHD molar ratio, affinity results were 62±2 and 80±2% in saline and human serum, respectively. Stability of ^{68}Ga-r-BHD and of the radiotracer/Av complex

remains almost constant over 180 min. ^{68}Ga-r-BHD appears to be a good candidate for clinical applications.

Chapter 10

Curriculum Vitae

Paola Anna Erba, Gallarate (VA), 12.6.1973. Nationality: Italian

Present address: Nuclear Medicine, Department of Oncology, University of Pisa Medical School, Via Roma 55, 56125 Pisa (Italy)

Education	1992: High School Degree
	1998 M.D. Graduation University of Insubria, Varese Title of the thesis "*Extracorporeal circulation (ECC) induced brain damage: 99mTc-ECD-SPECT, S-100 and NSE kinetic, neurological and neuropsychological assessment "*, Promoter Prof. Bellotti S.
	2002: Postgraduate specialties: Nuclear Medicine, University of Pisa, Title of the thesis "*Comparative Diagnostic Accuracy of Whole-Body [18 F]FDG-PET and 99mTc-MDP Bone Scintigraphy in the Identification of Bone Metastasis*", Promoter Prof. Bianchi R.
	2009: Starting postgraduate specialty in Clinical Biochemistry, University of Rome Tor Vergata
Accademic career	1995-1998: Fellow at Nuclear Medicine Department, Ospedale di Circolo e Fondazione Macchi, Varese.
	2000: "Visiting Fellow" at Nuclear Medicine Division del Dana Farber Cancer Institute Harvard Medical School, Boston (Feb-Mar).
	2002: Assistant Professor since 2002 at the University of Pisa Medical School, Pisa

Main Research topics: development of new radiopharmaceutical from the laboratory to early human application for both diagnostic purpose and therapy; biological markers of disease; imaging infection with new molecular imaging agents; development of new radioimmunoconjugates for molecular radiotherapy; development and optimization of a small animal PET/SPECT scanner YAP-(S)PET for preclinical imaging.

International and national research activity

2003: “Co-Investigator” of the governmental research project “Development of A Combined Nuclear Medicine Diagnostic and Therapeutic Approach to Patients With Breast Cancer” .

2005: “Co-Investigator” of the governmental research project “Molecular targeting and development of a new radioreceptor therapeutic strategy for non-iodophil epithelial follicular thyroid tumor”.

2005: “Co-Investigator” for the clinical study: Effectiveness of Zometa treatment for the prevention of bone metastasis in high risk prostate cancer patients. A randomized, open label, mlticenter study of the European Association of Urology (EAU) in cooperation with the Scandinavian Prostate cancer Group (SPCG) and the Arbeitsgemeinschaft Urologische Onkologie (AOU)

2006: “Co-Investigator” for the clinical study “Phase I dosimteric study of ^{131}I-L19SIP in solid tumors and lymphoproliferative diseases”.

2007 Fondazione Cassa di Risparmio, Pisa, Italy (Private Funding). “Construction of a PEM prototype” - Group leader: A. Del Guerra (ongoing).

2007: Tutor of the Research Doctorate School in BIOmolecular Sciences, Course of Molecular and experimental Oncology for the program “Molecular targeting and development of a new radioreceptor therapeutic strategy for non-iodophil epithelial follicular thyroid and neuroendocrine-like tumors.”2008: “Co-Investigator” for the clinical study “ A phase I/II dose finding and efficacy study of the tumor targeting human ^{131}I-F16 monoclonal antibody in patients with cancer”.

2008: “Co-Investigator” for the clinical study “ A phase I/II dose finding and efficacy study
of the tumor targeting human ^{131}I-L19SIP monoclonal antibody in patients with cancer”.

2009: “Principal-Investigator” for the clinical study “MyDySyA Study, Myocardial Dyssynchrony and Sympathetic activity by cardiac gated -SPECT in patients with heart failure treated with cardiac resynchronyzation”.

2009: “Co-Investigator” for the clinical study *BO21003 (GAUSS)* On open-label, multi-centre, dose escalating, phase I/randomized phase II study to investigate the safety and tolerability of RO 5072759 given as monotherapy in patients with CD20+ malignant disease.

2009: “Co-Investigator” for the clinical study *Novartis CRAD001N2301,* A Randomized, open, multi-center phase I/II study of Ro5072759 with a adjuvant therapy in poor risk patients with Diffuse Large B-Cell Lymphoma (DLCBL)

of RAD001 versus matching placebo after patients have achieved complete response with first-line rituximan-chemotherapy.
2009: “Co-Investigator” for the clinical study *Novartis CHCD122* A Phase IA/II, Multi-center, Open-label Study of HCD122 Administered Intravenously Once Weekly for Four Weeks in Adult Patients With Advanced Non-Hodgkin's or Hodgkin's Lymphoma Who Have Progressed After at Least Two Prior Therapies”.
2010: “Co-Investigator” for the clinical study “A prospective non-randomized study of ^{131}I-L19SIP Radioimmunotherapy (RIT) in combination with External Beam Radiotherapy (EBRT) and concurrent Chemotherapy in patients with inoperable, locally-advanced (Stage III) NSCLC”
2010: “Co-Investigator” for the clinical study VEG113046 “A randomised double-blind cross-over patient preference study of pazopanib versus sunitinib in treatment naïve locally advanced or metastatic renal cell carcinoma”.
2010: “Co-Investigator” for the clinical study “A randomized, open-label, multi-center phase II study to compare AUY922 with docetaxel or irinotecan in adult patients with advanced gastric cancer, who have progressed after one line of chemotherapy”
2010: “Co-Investigator” for the clinical study CA033 “An Open-Label, Multicenter, Phase III Trial of ABI-007 vs Dacarbazine in Previously Untreated Patients with Metastatic Malignant Melanoma”.
2010: “Co-Investigator” for the clinical study “Phase 3, Randomized, Open-Label, Two-Arm Study of Neratinib Plus Paclitaxel Versus Trastuzumab Plus Paclitaxel as First-Line Treatment for ErbB-2-Positive Locally Recurrent or Metastatic Breast Cancer”.
2011: “Co-Investigator” for the clinical study “A prospective non-randomized study of ^{131}I-L19SIP Radioimmunotherapy (RIT) in combination with Whole Brain Radiotherapy (WBRT) in patients with multiple brain metastases from solid tumors”.
2011 Bando Ricerca finalizzata e Giovani Ricercatori 2010, “Principal-Investigator” for the Project GR-2010-2318367 "Biomarkers and functional imaging guided treatment decision making in recurrent prostate cancer"
2011: Bando ERA-net TRANSCAN JTC 2011 “Principal-Investigator” for the project: "GRANT-T-MTC. Phase I clinical trial of the novel biomarker based on CCK-2/gastrin receptor-binding radiolabelled analogue for personalized cancer diagnostic and therapy and optimization of the treatment strategy for patients with progressive or metastatic medullary thyroid carcinoma"

Scientific papers: author/coauthor of more than 30 papers on international journals demonstrating the professional potential of growth as independent investigator with a total IF of 93.7, contributors at different books writing autonomously a number of chapters and co-editing a recent book on the field.

- Giovanella L, La Rosa S, Ceriani L, Uccella S, Erba P, Garancini S. Chromogranin-A as a serum marker for neuroendocrine tumors: comparison with neuron-specific enolase and correlation with immunohistochemical findings. Int J Biol Markers. 1999 Jul-Sep;14(3):160-6.
- dell'Erba L, Baldari S, Borsato N, Bruno G, Calò-Gabrieli G, Carletto M, Ciampolillo A, Dondi M, Erba P, Gerundini P, Lastoria S, Marinelli P, Santoro M, Scarano B, Zagni P, Bagnasco M, Mariani G. Retrospective analysis of the association of nodular goiter with primary and secondary hyperparathyroidism. Eur J Endocrinol. 2001 Oct;145(4):429-34.
- Mariani G, Gulec SA, Rubello D, Boni G, Puccini M, Pelizzo MR, Manca G, Casara D, Sotti G, Erba P, Volterrani D, Giuliano AE. Preoperative localization and radioguided parathyroid surgery. J Nucl Med. 2003 Sep;44(9):1443-58.
- Mariani G, Filocamo M, Giona F, Villa G, Amendola A, Erba P, Buffoni F, Copello F, Pierini A, Minichilli F, Gatti R, Brady RO. Severity of bone marrow involvement in patients with Gaucher's disease evaluated by scintigraphy with 99mTc-sestamibi. J Nucl Med. 2003 Aug;44(8):1253-62.
- Mariani G, Erba P, Manca G, Villa G, Gipponi M, Boni G, Buffoni F, Suriano S, Castagnola F, Bartolomei M, Strauss HW. Radioguided sentinel lymph node biopsy in patients with malignant cutaneous melanoma: the nuclear medicine contribution. J Surg Oncol. 2004 Mar;85(3):141-51.
- Mariani G, Erba P, Villa G, Gipponi M, Manca G, Boni G, Buffoni F, Castagnola F, Paganelli G, Strauss HW. Lymphoscintigraphic and intraoperative detection of the sentinel lymph node in breast cancer patients: the nuclear medicine perspective. J Surg Oncol. 2004 Mar;85(3):112-22.
- Lazzeri E, Pauwels EK, Erba PA, Volterrani D, Manca M, Bodei L, Trippi D, Bottoni A, Cristofani R, Consoli V, Palestro CJ, Mariani G. Clinical feasibility of two-step streptavidin/111In-biotin scintigraphy in patients with suspected vertebral osteomyelitis. Eur J Nucl Med Mol Imaging. 2004 Nov;31(11):1505-11.

- Rubello D, Piotto A, Medi F, Gross MD, Shapiro B, Erba P, Mariani G, Pelizzo MR; Italian Study Group on Radioguided Surgery and ImmunoScintigraphy. 'Low dose' 99mTc-Sestamibi for radioguided surgery of primary hyperparathyroidism. Eur J Surg Oncol. 2005 Mar;31(2):191-6.
- Nanni C, Rubello D, Farsad M, De Iaco P, Sansovini M, Erba P, Rampin L, Mariani G, Fanti S. (18)F-FDG PET/CT in the evaluation of recurrent ovarian cancer: a prospective study on forty-one patients. Eur J Surg Oncol. 2005 Sep;31(7):792-7.
- Prandini N, Lazzeri E, Rossi B, Erba P, Parisella MG, Signore A. Nuclear medicine imaging of bone infections. Nucl Med Commun. 2006 Aug;27(8):633-44.
- Manassero Francesca, Erba Paola Anna, Lazzeri Paolo, Evangelisti Silvia, Mariani Giuliano, Selli Cesare. Somastostatin receptor scintigraphy for neuroendocrine pattern in patients with hormone-refractory prostate cancer: preliminary experience, European Urology Supplements, 2006, vol. 52, pp 93.
- Manassero F, Erba P, Mariani G, Mogorovich A, Giannarini G, Selli C. Metastatic prostate cancer after orchiectomy, radiotherapy, and testosterone replacement in a patient with bilateral seminoma.J Androl. 2007 Jan-Feb;28(1):10-2.
- Mariani G, Erba PA, Signore A. Receptor-mediated tumor targeting with radiolabeled peptides: there is more to it than somatostatin analogs. J Nucl Med. 2006 Dec;47(12):1904-7.
- Eckelman WC, Erba PA, Schwaiger M, Wagner HN Jr, Alberto R, Mazzi U. Postmeeting summary on the round table discussion at the Seventh International Symposium on Technetium in Chemistry and Nuclear Medicine held in Bressanone, Italy on Sept 6-9, 2006. Nucl Med Biol. 2007 Jan;34(1):1-4.
- Pauwels EK, Erba P. Radioimmunotherapy of non-Hodgkin's lymphoma: molecular targeting and novel agents. Drug News Perspect. 2007 Mar;20(2):87-93.
- Capirci C, Rampin L, Erba PA, Galeotti F, Crepaldi G, Banti E, Gava M, Fanti S, Mariani G, Muzzio PC, Rubello D. Sequential FDG-PET/CT reliably predicts response of locally advanced rectal cancer to neo-adjuvant chemo-radiation therapy. Eur J Nucl Med Mol Imaging. 2007 Oct;34(10):1583-93.
- Pauwels EK, Erba P. Towards the use of nanoparticles in cancer therapy and imaging. Drug News Perspect. 2007 May;20(4):213-20.

- Pauwels EK, Erba P, Mariani G, Gomes CM. Multidrug resistance in cancer: its mechanism and its modulation. Drug News Perspect. 2007 Jul-Aug;20(6):371-7
- Pauwels EK, Erba PA, Kostkiewicz M. Antioxidants: a tale of two stories. Drug News Perspect. 2007 Nov;20(9):579-85.
- Mariani Giuliano, Erba Paola Anna, Radionuclide evaluation of Gaucher disease in Gaucher Disease ed. Futerman AH and Zimran A. 2007, Taylor and Francis, Chapter 16 pag 287-319
- Mariani Giuliano, Erba Paola Anna. Bone metabolism: implications for Gaucher disease. Clinical Terapeutics, 2008**,** 30 suppl C: S81-S83.
- Lazzeri E, Erba P, Perri M, Tascini C, Doria R, Giorgetti J, Mariani G. Scintigraphic imaging of vertebral osteomyelitis with 111In-biotin. Spine. 2008 Apr 1;33(7):E198-204.
- Perri M, Erba P, Volterrani D, Lazzeri E, Boni G, Grosso M, Mariani G. Octreo-SPECT/CT imaging for accurate detection and localization of suspected neuroendocrine tumors. Q J Nucl Med Mol Imaging. 2008 Dec;52(4):323-33.
- Sauer S, Erba PA, Petrini M, Menrad A, Giovannoni L, Grana C, Hirsch B, Zardi L, Paganelli G, Mariani G, Neri D, Durkop H, Menssen HD. Expression of the oncofetal ED-B containing fibronectin isoform in hematologic tumors enables ED-B targeted 131I-L19SIP radioimmunotherapy in Hodgkin lymphoma patients. Blood. 2009 Jan 8
- Dati E, Baroncelli GI, Mora S, Russo G, Baldinotti F, Parrini D, Erba P, Simi P, Bertelloni S. Body composition and metabolic profile in women with complete androgen insensitivity syndrome. Sex Dev. 2009;3(4):188-93.
- Chiocca E, Dati E, Baroncelli GI, Mora S, Parrini D, Erba P, Bertelloni. Body mass index and body composition in adolescents treated with gonadotropin-releasing hormone analogue triptorelin depot for central precocious puberty: data at near final height. Neuroendocrinology. 2009;89(4):441-7.
- Benedetti E, Proietti A, Miccoli P, Basolo F., Ciancia E, ERBA P, Galimberti S, Orsitto E, Petrini M. Contrast-enhanced ultrasonography in nodular splenomegaly associated with type B Niemann-Pick disease: an atypical hemangioma enhancement pattern. Journal of Ultrasound 2009; 12: 85-92.
- Mariani G, Perri M, Erba P (2009). Bone disease scoring and managment of Gaucher disease. Clinical Therapeutics, vol. 31, p. S188-S190

- Lazzeri E, Erba P, Perri M, Doria R, Tascini C, Mariani G. Clinical impact of SPECT/CT with In-111 biotin on the management of patients with suspected spine infection. Clin Nucl Med. 2010 Jan;35(1):12-7.
- Erba PA, Manfredi C, Lazzeri E, Minichilli F, Pauwels EK, Sbrana A, Strauss HW, Mariani G. Time course of Paclitaxel-induced apoptosis in an experimental model of virus-induced breast cancer. J Nucl Med. 2010 May;51(5):775-81.
- Lupetti A, De Boer MG, Erba P, Campa M, Nibbering PH. Radiotracers for fungal infection imaging. Med Mycol. 2010 Aug 26
- Erba PA, Cataldi AG, Tascini C, Leonildi A, Manfredi C, Mariani G, Lazzeri E. 111In-DTPA-Biotin uptake by Staphylococcus aureus. Nucl Med Commun. 2010 Nov;31(11):994-7.
- Greco C, Forte L, Erba P, Mariani G. Bone metastases, general and clinical issues. Q J Nucl Med Mol Imaging. 2011 Aug;55(4):337-52
- Perri M, Erba P, Volterrani D, Guidoccio F, Lazzeri E, Caramella D, Mariani G. Adrenal masses in patients with cancer: PET/CT characterization with combined CT histogram and standardized uptake value PET analysis. AJR Am J Roentgenol. 2011 Jul;197(1):209-16
- Erba PA, Sollini M, Orciuolo E, Traino C, Petrini M, Paganelli G, Bombardieri E, Grana C, Giovannoni L, Neri D, Menssen HD, Mariani G.Radioimmunotherapy with radretumab in patients with relapsed hematologic malignancies. J Nucl Med. 2012 Jun;53(6):922-7. Epub 2012 May
- Chiellini G, Erba P, Carnicelli V, Manfredi C, Frascarelli S, Ghelardoni S, Mariani G, Zucchi R. Distribution of exogenous [125I]-3-iodothyronamine in mouse in vivo: relationship with trace amine-associated receptors. J Endocrinol. 2012 Jun;213(3):223-30.
- Erba PA, Conti U, Lazzeri E, Sollini M, Doria R, De Tommasi SM, Bandera F, Tascini C, Menichetti F, Dierckx RA, Signore A, Mariani G. Added Value of 99mTc-HMPAO-Labeled Leukocyte SPECT/CT in the Characterization and Management of Patients with Infectious Endocarditis. J Nucl Med. 2012 Jul 11.
- Erba PA, Bandera F, Sollini M, Tascini C. The Use of (18)F-FDG-PET/CT in the Diagnostic Workup of CIED Infections: Another Perspective. Journal of The American College of Cardiology, 2012, 9: 1435-1436.
- Filice A, Fraternali A, Frasoldati A, Asti M, Grassi E, Massi L, Sollini M, Froio A, Erba PA, Versari A. Radiolabeled somatostatin analogues

therapy in advanced neuroendocrine tumors: a single centre experience. Journal of Oncology, 2012 vol. 320198.
- Asti M, Iori M, Erba PA, Atti G, Farioli D, Guidotti C, Versari A. Radiosynthesis of 68Ga-labelled DOTA-biocytin (68Ga-r-BHD) and assessment of its pharmaceutical quality for clinical use. Nuclear Medicine Communications 2012, 33: 1179-1187.
- Del Guerra A, Bardies M, Belcari N, Caruana CJ, Christofides S, Erba PA, Gori C, Lassmann M, Lonsdale MN, Sattler B, Waddington W. (2012). Curriculum for education and training of Medical Physicists in Nuclear Medicine: Recommendations from the EANM Physics Committee, the EANM Dosimetry Committee and EFOMP. Medical Physics, 2012; 17: 1-24.
- Baroncelli GI, Vierucci F, Bertelloni S, Erba P, Zampollo E, Giuca MR. Pamidronate treatment stimulates the onset of recovery phase reducing fracture rate and skeletal deformities in patients with idiopathic juvenile osteoporosis: comparison with untreated patients. J Bone Miner Metab. 2013 Apr 3. [Epub ahead of print]
- Traino AC, Marcatili S, Avigo C, Sollini M, Erba PA, Mariani G. Dosimetry for nonuniform activity distributions: a method for the calculation of 3D absorbed-dose distribution without the use of voxel S-values, point kernels, or Monte Carlo simulations. Med Phys. 2013 Apr;40(4):042505.
- Sollini M, Farioli D, Froio A, Chella A, Asti M, Boni R, Grassi E, Roncali M, Versari A, Erba PA. Brief report on the use of radiolabeled somatostatin analogs for the diagnosis and treatment of metastatic small-cell lung cancer patients. J Thorac Oncol. 2013 Aug;8(8):1095-101.
- Erba PA, Sollini M, Lazzeri E, Mariani G. FDG-PET in Cardiac Infections. Semin Nucl Med. 2013 Sep;43(5):377-95.
- Erba PA, Sollini M, Conti U, Bandera F, Tascini C, De Tommasi SM, Zucchelli G, Doria R, Menichetti F, Bongiorni MG, Lazzeri , Mariani G. Radiolabeled leukocyte scintigraphy in the diagnostic workup of patients with suspected cardiac device-related infections. *J Am Coll Cardiol Img.* 2013, *Published online September 4*
- Vierucci F, Del Pistoia M, FanosM, Gori M, Carlone G, Erba PA, Massimetti G, Federico G, Saggese G. Vitamin D Status and Predictors of Hypovitaminosis D in Italian Children and Adolescents: a Cross Sectional Study. Eur J Pediatr 2013, *in press*
- Erba PA, Minichilli F, Giona F, Linari S, Dambrosia J, Pierini A, Filocamo M, Di Rocco M, Buffoni F, Brady RO, Mariani G. ^{99m}Tc-

Sestamibi Scintigraphy to Monitor the Long-Term Efficacy of Enzyme Replacement Therapy on Bone Marrow Infiltration in Patients with Gaucher Disease. J Nucl Med. 2013 Aug 29

Books:

- Giovanella L, Ceriani L, Erba P, Bandera M.,Prognostic significance of tissue polipeptide-specific antigen (TPS) in patients with small and non-small cell lung cancer., Pandora,vol. 10,pp 29-34, 1998
- G. Panattoni, P. Erba, F. Matteucci, L. Bruschini, E. Lazzeri, Scintigrafia e fisiopatologia delle ghiandole salivari in La scintigrafia in Otorinolaringoiatria,pp 167, 176, 2003
- Volterrani D, Giorgetti A, Erba P, Chiacchio S, Mariani G. La Tomografia ad Emissione di Positroni. in La Scintigrafia in Otorinolaringoiatria,pp 33, 44, Associazione Otorinolaringologi Ospedalieri Italiani, 2003
- Volterrani D, Erba P, Grosso M, Mariani G, Medicina nucleare: concetti generali, i radio-isotopi, i radiofarmaci, gli strumenti di rilevazione della radioattività in La Scintigrafia in Otorinolaringoiatria, pp 11, 32, Associazione Otorinolaringologi Ospedalieri Italiani, 2003
- Mariani G. and Erba PA. Gaucher Disease in Radionuclide evaluation of Gaucher disease., pp 283, 315, 2007
- Obenaus E, Erba P, Chinol M, Van de Wiele C, Gyozo AJ, Dierckx AJ, Scopinaro F, Signore A. Radiopharmaceuticals for Radioguided Surgery . In: Mariani, Giuliano; Giuliano, Armando E.; Strauss H. William . Radioguided Surgery Springer Verlag 2008
- Volterrani D, Erba P, Mariani G. Fondamenti di Medicina Nucleare, Springer 2010
- Erba PA SPECT-CT for Tumor imaging: new tracers . In: Fanti S, Mohsen F, Mansi L. Atlas of SPECT-CT. Springer Verlag 2012 p. 96-104
- Erba PA, Sollini M, Boni R. Lymphoscintigraphy for the Differential Diagnosis of Peripheral Edema and Intracavitary Lymph Effusion. In: Mariani, G.; Manca, G.; Valdés Olmos, R.A.; Orsini, F.; Vidal-Sicart,. Atlas of Lymphoscintigraphy and Sentinel Node Mapping A Pictorial Case-Based Approach. Springer 2012
- Erba PA, Bisogni G, Del Guerra A, Mariani G. Methodological Aspects of Lymphoscintigraphy: Radiopharmaceuticals and Instrumentation. In: Mariani, G.; Manca, G.; Valdés Olmos, R.A.; Orsini, F.; Vidal-Sicart,.

Atlas of Lymphoscintigraphy and Sentinel Node Mapping Atlas of Lymphoscintigraphy and Sentinel Node Mapping A Pictorial Case-Based Approac . Springer 2012

- Di Stefano R, Erba PA, D'Errico G. Pathophysiology of lymphatic circulation in different disease conditions. In: Mariani, G.; Manca, G.; Valdés Olmos, R.A.; Orsini, F.; Vidal-Sicart, S. Atlas of Lymphoscintigraphy and Sentinel Node Mapping Atlas of Lymphoscintigraphy and Sentinel Node Mapping A Pictorial Case-Based Approach. Springer 2012
- Lazzeri E, Signore A, Erba PA, Prandini N, Versari A, D'Errico G, Mariani G. Radionuclide Imaging of Infection and Inflammation Radionuclide Imaging of Infection and Inflammation. Springer Verlag 2012
- Erba PA . Nonorthopedic or Cardiovascular Implantable Device Infection. In: Lazzeri, E., Signore, A., Erba, P.A., Prandini, N., Versari, A., D'Errico, G., Mariani, G.. Radionuclide Imaging of Infection and Inflammation Radionuclide Imaging of Infection and Inflammation A Pictorial Case-Based Atlas. Springer 2012
- Erba PA. Infective Endocarditis and Cardiovascular Implantable Electronic Device Infection. In: Lazzeri, E., Signore, A., Erba, P.A., Prandini, N., Versari, A., D'Errico, G., Mariani, G. Radionuclide Imaging of Infection and Inflammation Radionuclide Imaging of Infection and Inflammation A Pictorial Case-Based Atlas. Springer 2012

Awards

2004: Primo premio per il migliore poster VII Congresso AIMN Palermo, Ottobre 2004 (Titolo: " La scintigrafia con leucociti autologhi marcati con 99mTc-HMPAO in pazienti ricoverati in UO di Terapia Intensiva con FUO")
2011: "Masaoka Prize" dell'International Thymic Malignancy Intereste Group per la migliore presentazione orale (Titolo: Radioimmunotherapy with 131I-L19SIP in thymoma: first clinical data)
2011: "Lights in Arrhythmology Award" per il migliore poster (Titolo: "Myocardial dyssynchrony, Myocardia Perfusion and Sympathetic activity in patients with heart failure treated with cardiac resynchronyzation")
2011: "Premio Barani per l'innovazione e la ricerca" (Zonta Club)

2012: "IRIST Award" per la migliore presentazione orale (Titolo:"68Ga-peptide and [18F]FDG-PET/CT in thymic malignancies")

Other:

- Member of the Task Group on “Infection and Inflammation” of the AIMN, Italian National Association of Nuclear Medicine
- Member of the Task Group on “PET and PET-CT application” of the AIMN, Italian National Association of Nuclear Medicine
- Member of COST action BM0607, Targeted Radionuclide Therapy (TRNT)
- Member of COST action D38, Metal-Based Systems for Molecular Imaging Application
- Core Lab responsible for the IAEA project CRP E1.30.35, Longitudinal monitoring of complicated osteomyelitis by SPECT/CT
- IAEA consultant and web page contributor
- Reviewer for the European Journal of Nuclear Medicine and Molecular Imaging; Current Radiopharmaceuticals; Journal of Nuclear Medicine Technology; European Heart Journal.

Teaching:

- Tutor of the Research Doctorate School in BIOmolecular Sciences, Course of Molecular and experimental Oncology and of the Research Doctorate School of “Neuroscience and Endocrino-metabolic science” .
- Responsible for the following teaching courses:
  - Diagnostica per immagini, Laurea in Medicina e Chirurgia (2003-2012);
  - Radiofarmaci, Tecniche di Radiologia Medica, per Immagini e Radioterapia (2002-2012);
  - Radiofarmaci/Farmacologia dei mezzi di contrasto (2011 ongoing)
  - Tecniche di Medicina Nucleare, Tecniche di Radiologia Medica, per Immagini e Radioterapia (2002-2010);
  - Scienze applicate ai processi organizzativi in diagnostica per immagine, Scienze delle Professioni Sanitarie (2009-2011);
  - Diagnostica per immagini e Radioterapia, Diagnostica clinica radio-isotopica I e IX della Scuola di Specializzazione in Medicina Nucleare (2002-2012)

Chapter 11

Acknowledgements

At the beginning of this long list, I first wish to acknowledge my Promoters, Prof. Giuliano Mariani, Prof. Alberto Signore and Prof. Rudi A.J.O. Dierckx.
My first remembering of Prof. Giuliano Mariani is back in July 1998, two weeks before my graduation in medicine when speaking at the phone he kindly gave me direction how to reach him in Genoa for our first meeting. Since that time, first as Director of the Nuclear Medicine Department in Genoa and then of the Nuclear Medicine Regional Center in Pisa where we moved in 2001, he became my invaluable chief and tutor. He has countinuosly encouraged my research, stimulating my critical thinking, always being positive torward every single new idea I proposed him.
A special remark is for Prof. Alberto Signore, for his significant contribution to my PhD research. He was the one that introduced me to Groningen. Throught his criticisms and his continuous support that extended over the professional perspective he became a key person during my research.
A very special thanks is deserved for Prof. Rudi Dierckx who accept and host my PhD at the prestigious University of Groningen. Together with all the team of the Nuclear Medicine Department in Groningen, he always friendly welcome every my staying.
I also wish to address a very special thank to Prof. Giuseppina Roncari and all the team of the Nuclear Medicine department of Ospedale di Circolo in Varese where I first got involved into nuclear medicine and make me love the discipline. A special remark is for Dr. Luca Giovanella, the very first person whom I share with the enjoiment of research.
A distinctive mention is for Dr. Mario De Tommasi, whom I'm grateful for his valued teachings on infective endocarditis and for trusting and encouraging my investigations from the very fist.
I also wish to thank Dr. Umberto Conti, not only for the effective participation in the clinical work of this thesis, but also for his collaborative attitude and his emotional support. Together with him, I wish to thanks several colleagues that have participated and contributed to my research during the years, in particular Dr. Carlo Tascini and Prof. Francesco Menichetti for their precious remarks.

I also would like to express my gratitude to Prof. Mario Petrini and Prof. Mauro Ferrari, invaluable mentors, whose encouragements represent a significant motivation for continuing my work.
A special thanks to Dr. Arturo Chiti for his friendship and closeness as to Dr. Massimo Salvadori for his experienced and sharp advices.
It's very hard to find the right words to thank my colleagues and friends Dr. Rossella Di Stefano and Dr. Francesco Bandera, Dr. Francesco Pasqualetti and Dr. Lisa Bodei for their professional and effective assistance to my work during all the years of this research is inseparable from their emotional contribution and support.
Many thanks are also due to Dr. Roberto Boni, Dr.ssa Gabriella Cataldi, Dr.ssa Letizia Modeo, all the people from the Laboratory of Radioimmunoassay, the technologists of the Nuclear Medicine Regional Center, in particular Dr.ssa Roberta Cantini, all the team in Reggio Emilia, in particular Dr. Diana Salvo, Dr. Annibale Versari and Dr. Mattia Asti for their help in the research and their friendship.
I would also like to thank all the co-authors of the manuscripts that have contributed to this research. Some of them reserve a special mention because they are not just colleagues, but invaluable friends: Dr. Martina Sollini and Dr. Roberta Doria.
A spetial word of gratitude is for Dr.ssa Elena Lazzeri, my paranynph, that has adopted me and to her husband Carlo and their son Lorenzo that have feed me since my arrival in Pisa every Wednesday night.
Lastly, I wish to thank all my big family to whom this thesis is dedicated: Simo, Roby, Tino and Antonella, Mari, my sweet nephews Alice and Renato, my grannies Gianna and Piero, my brother Giobi, my mum Gina and my father Renato that would have been proud of this achievement.